GMe

Gesellschaft für Mikroelektronik

The Society for Microelectronics

Annual Report

1996

Vienna, April 1997

GMe

Gesellschaft für Mikroelektronik

The Society for Microelectronics

Annual Report

1996

Gesellschaft für Mikroelektronik
c/o Technische Universität Wien
Institut für Allgemeine Elektrotechnik und Elektronik
Gußhausstraße 27-29/359, A-1040 Wien

Vienna, April 1997

Editor: Karl Riedling

Layout: Claudia Ritter
Karl Riedling

c/o Technische Universität Wien
Institut für Allgemeine Elektrotechnik und Elektronik
Gußhausstraße 27-29/359, A-1040 Wien

The Society for Microelectronics (GMe — Gesellschaft für Mikroelektronik)

E. Gornik, K. Riedling

Gesellschaft für Mikroelektronik,
c/o Institut für Allgemeine Elektrotechnik und Elektronik, TU Wien
Gußhausstraße 27 – 29, A-1040 Wien

1. Goals of the Society for Microelectronics

The Society for Microelectronics (GMe) was founded in 1985 with the aim to "*support microelectronics technology and its applications in an interdisciplinary way*". The GMe defines its tasks as follows:

- Support of university-based high-technology research in the areas of microelectronics, semiconductor technology, sensors, and opto-electronics;
- Construction and operation of research facilities;
- Support and consulting for industry, in particular, for small and medium enterprises, within the area of microelectronics.

The central task of the GMe is the creation and maintenance of *infra-structure* for an internationally competitive microelectronics technology. The funds provided by the GMe support a variety of projects and activities in the fields of semiconductor technology, sensors, and opto-electronics. One of the criteria for the support of an activity by the GMe is a project area that needs seed money for infra-structure to obtain funding by other sources.

2. Activities of the Society

Currently, the GMe recognizes three focal points for its activities. In general, projects that expect support by the GMe must pertain to at least one of these areas. Other microelectronics-related projects may receive occasional support by the GMe, for example, for infra-structure that is a prerequisite to a funding by other sources, or in the case of an emergency. The current focal points of the GMe activities are:

- Construction and operation of university-based laboratories for microelectronics technology;
- Design of application specific integrated circuits (ASICs) — UNICHIP;
- Microsensors.

2.1 Microelectronics Technology — Cleanrooms Vienna and Linz

The currently most important task of the GMe is closely linked to the construction and the operation of technological installations, in particular, of the cleanroom laboratories in Vienna and Linz. In 1992, the Austrian Federal Ministry of Science and Research invited the GMe to act as a coordinator for the construction of the Microstructure Center (MISZ — Mikrostrukturzentrum) in Vienna. The MISZ Vienna finished construction by the end of 1993 and went into operation in June 1994. The GMe now provides with its funds a significant part of the operation costs for the cleanroom laboratories in Vienna and Linz.

The following university institutes are supported within this focal point activity:

- TU Wien:
  - Institut für Festkörperelektronik
  - Institut für Allgemeine Elektrotechnik und Elektronik
- Johannes Kepler Universität Linz:
  - Institut für Halbleiterphysik
  - Institut für Experimentalphysik
  - Institut für Mikroelektronik

The results of these activities are outlined in this report beginning with page 9 (for the groups at the TU Wien) and page 71 (for the groups at the Johannes Kepler Universität Linz), respectively. The first of the reports in either section summarizes the work that benefited from the general GMe contribution to the basic laboratory operation; the subsequent reports pertain to projects specifically supported by the GMe.

2.2 Application Specific Integrated Circuits (ASICs) — UNICHIP

The UNICHIP activities of the GMe are closely linked to the requirements of the Austrian industry: Based on groups at the Technical Universities in Graz and Vienna, and using equipment and software which were purchased from GMe funding, two major actions are pursued: (1) ASIC projects for partners in the Austrian industry, ranging from feasibility studies to the design of ASICs that are commercially produced; and (2) the education and training of engineers in the area of ASIC design. Due to its close links to industrial requirements, UNICHIP played a leading role in Austria. The UNICHIP groups also have a long-standing tradition in European cooperation; many years before Austria joined the EU, they participated in the "EUROCHIP" European project; currently, they are involved in the "EUROPRACTICE" program.

During 1996, the UNICHIP activities were merged into an Austria-wide activity that comprises all university-based competence centers for ASIC design, the *Technologieverbund Mikroelektronik Österreich* (TMÖ). The TMÖ includes the following university institutes:

- TU Wien:
  - Institut für Allgemeine Elektrotechnik und Elektronik (*)
  - Institut für Computertechnik

  - Institut für Technische Informatik
- TU Graz:
  - Institut für Angewandte Informationsverarbeitung und Kommunikationstechnologie
  - Institut für Elektronik (*)
- Johannes Kepler Universität Linz:
  - Institut für Systemwissenschaften

Since only the original UNICHIP institutes marked with "*" in the list above received funding from the GMe, the other institutes included the TMÖ activity are out of the scope of this report. The results achieved by the UNICHIP groups are presented beginning with page 137.

2.3 Microsensors

One of the most rewarding potentials of microelectronics technology is related to applications in sensors: A large variety of possible sensors can be realized with comparatively modest technological resources, which makes them commercially quite interesting. In recent years, the GMe supported activities, mainly at the Technical University in Vienna, that led to sensors for medical, environmental, and technical applications, many of which could meanwhile be commercialized or have, at least, found commercial interest. Examples for such sensors are biosensors for metabolic parameters such as the concentrations of glucose and lactate, or temperature sensors that can be inserted into the combustion chamber of a Diesel engine.

The following university institute participates in this focal point activity:

- TU Wien:
  - Institut für Allgemeine Elektrotechnik und Elektronik

The current work done within the microsensors focal point activity of the GMe is disclosed from page 155 on.

2.4 Other Projects

Projects that are closely linked to microelectronics but do not belong to one of the above focal points have been supported on a smaller scale at the following institutes in 1996:

- TU Wien:
  - Institut für Allgemeine Elektrotechnik und Elektronik
  - Institut für Analytische Chemie
- Montanuniversität Leoben:
  - Institut für Physik

This report presents these supplementary projects of the GMe in 1996 beginning with page 163.

3. Other Activities of the Society

One of the declared tasks of the GMe is to provide information on current Austrian academic activities in the field of microelectronics to industry, in particular to Austrian small- and medium enterprises (SMEs). This will improve the transfer of knowledge between Austrian universities and industry. During 1996, the GMe began to supply editorial articles to an Austrian publishing house that targets its magazines on the management and technical staff of Austrian industrial enterprises. The articles presented some of those projects supported by the GMe that had a direct impact on Austrian industry. As an additional approach, the GMe installed a Web server in December 1996, which provides general information on the GMe and a collection of research reports. It is also planned to add the contents of this report to the GMe's Web server. The GMe Web server is available under the URL:

http://www.iaee.tuwien.ac.at/gme/

Finally, the GMe prepared the biennial seminar "*Grundlagen und Technologie elektronischer Bauelemente*" in Großarl, Salzburg, which took place in March 1997. The seminar has first been held in 1977; since 1987, the GMe contributes financial support, and since 1993, the Society acts as its main organizer. The 11th Großarl seminar presented seven main lectures given by international experts, and 20 short contributions, most of which resulted from work supported by the GMe.

Contents

Microelectronics Technology — Cleanroom Vienna

Microstructure Research: Cleanroom Vienna

E. Gornik, G. Strasser

Institute of Solid State Electronics &
Center of Microstructure Research (MISZ), TU Wien,
A-1040 Vienna, Austria

In this paper, the main activities in the cleanroom of the MISZ are described. The cleanroom of the MISZ was opened 1993; during 1994, most of the equipment for the production of semiconductor devices was installed. Since 1995, state of the art growth of III-V compounds as well as the production of patterned masks used in lithography is done on a regular basis. One of the main research areas of our institute is the preparation and characterization of III-V devices. Therefore the fke maintains several collaborations with national and international research institutions and companies by providing them with epitaxial layers (III-V-compounds). A second main research topic is the production of micron and sub-micron devices down to nanometer scale. Patterned masks for optical lithography are also provided to different institutions.

1. Introduction

Since 1995, the cleanroom of the MISZ is operated and maintained on a regular basis. Main research areas are the state of the art growth of III-V compounds and the processing of these layers resulting in transport and optical devices. Processing steps are lithography, structuring (different etching techniques), planarization, and metallization of the different layers. A production of patterned masks is part of the cleanroom facility as well as the deposition of dielectric material by chemical vapor deposition. Supplementary to the normal operation and maintenance of the cleanroom and the cleanroom equipment, additional equipment was installed. Testing of the cleanroom quality and adjustment (laminar air flow, filters, cooling, humidity…) if necessary is done periodically.

During 1996, various new equipment was installed in the cleanroom of the MISZ. In detail, an Oxford Plasmalab 80+ system was installed in a two chamber master-slave configuration. One chamber is equipped for RIE processes, the second chamber is a plasma CVD system.

The RIE system has two main applications in the MISZ: First, almost all grating couplers for the GaAs-AlGaAs surface emitting lasers are fabricated on this machine. Second, all samples fabricated by electron beam lithography are processed in this machine. As a first result, a single quantum dot was fabricated on a high mesa, which was subsequently used as tip on a scanning tunneling microscope.

The CVD machine is used for the deposition of insulating Si-nitride and Si-oxide films. Insulating layers are necessary for the fabrication of multi layer device structures, such as the 3-terminal devices for ballistic electron spectroscopy and also for MOS-device structures. Furthermore, dielectric laser mirrors are fabricated with this machine.

As second major installation, a Süß MJB3 UV mask aligner was brought into the cleanroom. The main purpose of this machine is to guarantee an industrial standard in optical lithography. The new mask aligner is capable to transfer patterns down to 0.5 μm, which is the limit of our CGA machine for mask fabrication. The new mask aligner is used for GaAs lasers with surface grating couplers and also for the fabrication of sub-μm tunneling diodes and the 3- and 4-terminal devices used in ballistic electron spectroscopy.

2. Research Activities

2.1 Reactive Ion Etching

A new type of surface-emitting laser diode has been developed, which is based on a Surface-Mode-Emission-(SME)-technique. This technique utilizes an interactive coupling process between the laser mode propagating in the cavity and a TE_0-surface mode in a waveguide structure on top of the laser diode. This technique has been successfully applied to GaAs/AlGaAs-laser diodes to achieve a single-mode emission and a single, surface emitted beam with a beam divergence as low as 0.15°. Presently a power up to 4 mW (which is 20 % of the total emitted power) is emitted into the single beam.

Usually laser diodes are cleaved to single devices out of the chip. For the fabrication of 2-dimensional arrays of laser diodes, which is of high importance for coherent high-power application, the mirror facets have to be etched by a proper etching technique. High-reflecting coatings on the etched mirrors suppress the edge emission of SME-laser diodes and should therefore result in a strongly increased surface emission.

Laser mirrors make high demands on the etching technique. The etched facets have to be perfectly vertical and the roughness has to be less than $\lambda/(10 \cdot n_{GaAs})$, which requires at an emission wavelength of 880 nm a smoothness of less than 20 nm. As a wet-chemical etching process is not suitable to achieve vertical facets, a Reactive-Ion-Etching-(RIE)-technique has been used. Photoresist, metal and dielectric layers of SiO and SiN were used as etching masks. The best results have been achieved with photoresist-masks removable by a solvent instead of etchants necessary for metal- and dielectric-masks, which can corrode the GaAs/AlGaAs-samples. $SiCl_4$ was used as etching gas. The angle of the etched sidewalls depends strongly on the etching parameters and can be adjusted via the pressure and the RF-power. The etching results have been controlled with help of a Dektak-profiler and the SEM-system. Figure 1 shows a SEM-photograph of an etching facet achieved in a GaAs-sample at a pressure of 100 mTorr and a power of 150 W ($SiCl_4$-flow 15 sccm, duration 10 min, self bias 300 V). The sidewalls are only a few degrees off the vertical. Figure 2 shows a result achieved at a pressure of 4 mTorr and a power of 100 W ($SiCl_4$-flow 15 sccm, duration 7 min, self bias 500 V). Here the sidewalls are even overhanging, while Fig. 3 shows a result achieved at a pressure of 50 mTorr and a power of 75 W ($SiCl_4$-flow 15 sccm, duration 30 min, self bias 250 V), where the sidewalls are vertical. The slight roughness in longitudinal direction is due to the photomask used for the exposure. Figure 4 finally shows a perfect result with roughness less than 10 nm.

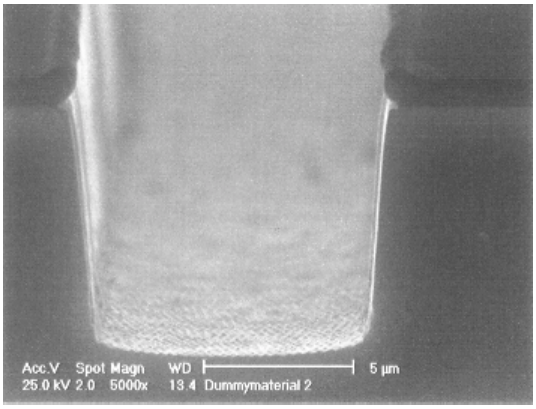

Fig. 1: SEM photograph of RIE etched GaAs (Photoresist not removed)

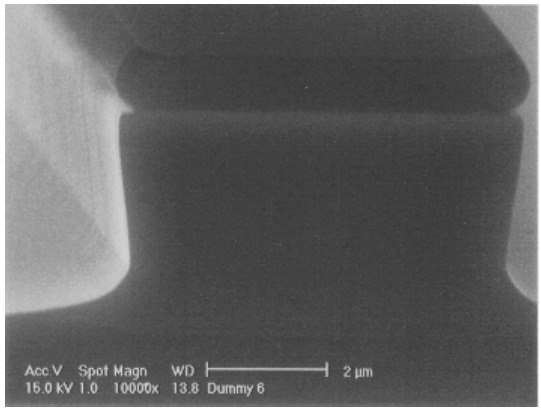

Fig. 2: SEM photograph of RIE etched GaAs (Photoresist not removed)

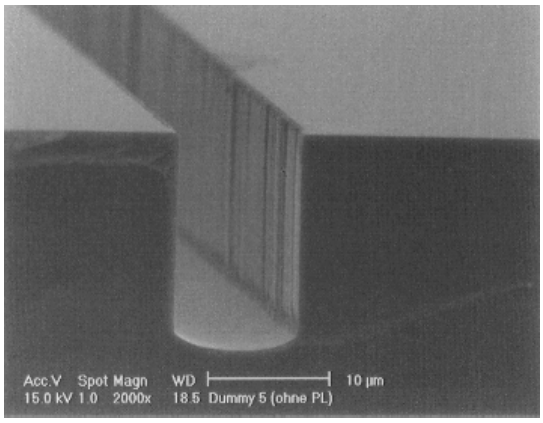

Fig. 3: SEM photograph of RIE etched GaAs (Photoresist removed)

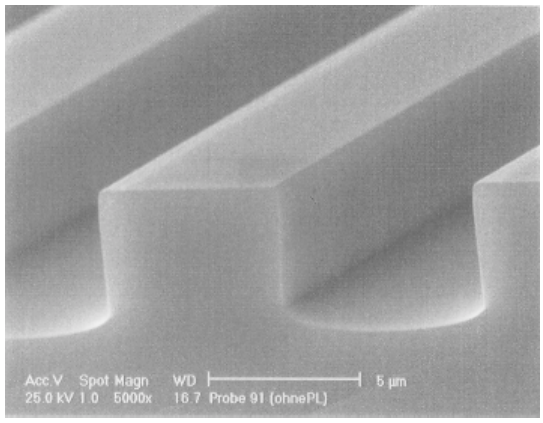

Fig. 4: SEM photograph of RIE etched GaAs (Photoresist removed)

Finally the vertical mirror facets have been coated with SiN and Au. SiN has been deposited by a PECVD-process, Fig. 5 shows a SiN-coating on GaAs, which has been deposited at a RF-power of 10 W, a pressure of 1 Torr at a background pressure of 25 mW, a substrate-temperature of 200 °C. The SiH_4- and NH_3-gas flows are 700 sccm and 18 sccm. The deposition rate is typically 13 nm/min. The final result of a high-reflecting SiN/Au-coating on a vertical laser mirror is shown in Fig. 6. The thickness of the SiN- and the Au-layer is 180 nm and 140 nm, respectively. The apparent thickness fluctuation in the Au-film thickness is due to the cleavage necessary for the SEM-inspection.

First InGaAs/GaAs-laser diodes fabricated with RIE-etching and mirror coatings show threshold-current densities of 1.5 kA/cm^2, which are close to the values achieved for a cleaved device. This demonstrates the excellent quality of the etching process and the subsequent deposition technique of the mirror-coatings.

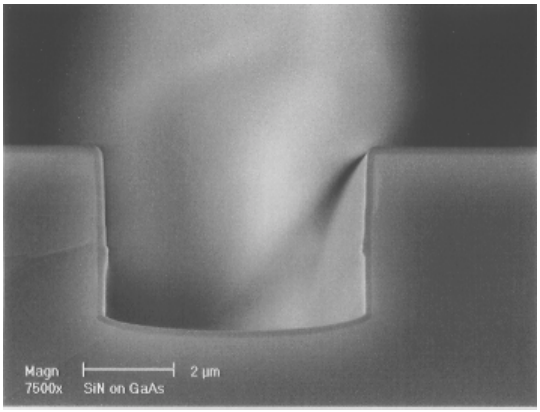

Fig. 5: SEM photograph of SiN-coating on GaAs

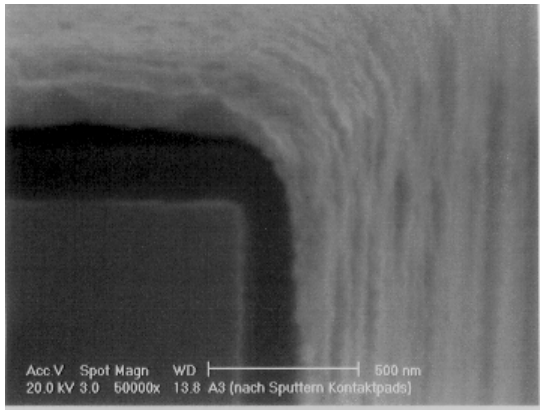

Fig. 6: SEM photograph of SiN/Au-coating on GaAs

2.2 Growth of III-V Materials

Since 1995 growth of epitaxial GaAs material and related compounds is done in the MISZ with a molecular beam epitaxy system (GEN II). A modular GEN II solid source MBE machine is a system specially designed for high quality growth of III-V materials. The controlled growth of single crystalline layers on an atomic scale makes it possible to design new materials with optimized electrical and optical characteristics.

A carbon dopant source was installed in the epitaxy system giving the possibility to grow p-type material with very low diffusion length of the dopant material and therefore very abrupt doping profiles.

2.2.1 Growth and Characterization of Modulation Doped High Mobility 2DEGs (G. Strasser, J. Smoliner, C. Eder, G. Ploner, L. Hvozdara)

Epitaxial growth of $Al_xGa_{1-x}As$ on GaAs gives a band discontinuity in the conduction and valence band. Intentional doping influences the Fermi levels and increases the band offset at the interface. Electrons move from the n-doped $Al_xGa_{1-x}As$ into the non-doped GaAs and form a two dimensional electron gas (2DEG). The offset and the bending of the bands prohibit the recombination of the carriers with the ionized impurities in the $Al_xGa_{1-x}As$. Impurity scattering is the most dominant scattering mechanism at low temperatures. In a 2DEG this scattering process is drastically reduced due to the separation of carriers and impurities (”remote impurities”). This leads to electron mobilities up to 10^7 cm^2/Vs (4.2 K).

Two-dimensional electron gases (GaAs/AlGaAs heterostructures) were grown with mobilities up to $1.8 \cdot 10^6$ cm^2/Vs at 4 K and $3.5 \cdot 10^6$ cm^2/Vs after exposure to red light. The sheet carrier concentrations vary from 0.5 to $5 \cdot 10^{11}$ cm^{-2}. Characterization was done via temperature dependent hall measurements (4 K to 300 K), SdH measurements, and cyclotron resonance absorption. Additional confinement by structuring and etching leads to quantum wire and quantum dot regimes. The optical and transport behavior of these low dimensional systems is investigated.

2.2.2 *Design, Growth and Characterization of RTDs and SLs (G. Strasser, C. Rauch, K. Unterrainer, W. Heiß, L. Hvozdara)*

The first working "three terminal devices" with electron injectors, drift regions and a "filter" to separate ballistic from thermal carriers were realized in December 1995. By the end of 1996 a big technological step further on was established by the first "four terminal device". Parallel to these activities, superlattice structures (GaAs/AlGaAs-superlattices with periods from 2 to 20 monolayers) were grown to investigate the doping behavior. Broken gap miniband structures and quantum cascade laser structures are designed, grown and measured. Aim of this work is the realization of terahertz detectors and emitters and the realization of an unipolar semiconductor laser in the infrared region. For a more detailed discussion of these projects see chapter 3.

2.2.3 *Design, Growth and Characterization of Epitaxial AlGaAs Bragg Mirrors (G. Strasser, T. Maier)*

The MBE-growth of AlGaAs Bragg mirrors was optimized to an extent that enables us to grow these mirrors with maximum reflectivity at a desired wavelength. The reflectivity of the mirrors was measured with a precision of 1% and compared to a theoretical model containing the thicknesses of the layers as input-parameters (Fig 7). From this comparison, the deviation of the thicknesses from the nominal values could be determined and a calibration performed. Bragg mirrors grown with this calibration show good agreement with the theoretical model (calculated with nominal thicknesses) and exhibit maximum reflectivity at the wavelength they were designed for.

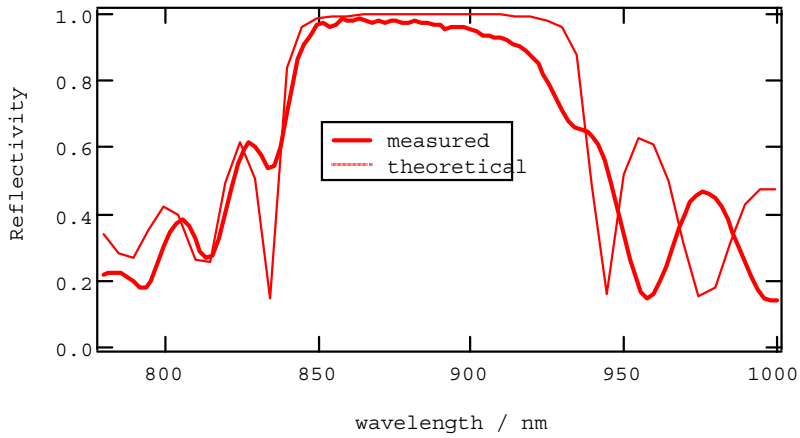

Fig. 7: Reflectivity vs. wavelength of a Bragg mirror consisting of 20 pairs $Al_{0.1}Ga_{0.9}As$/AlAs, designed for 880 nm.

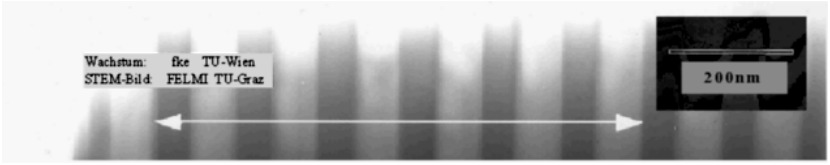

Fig. 8: TEM picture of AlAs/GaAs Bragg mirror (average thickness AlAs/GaAs: 133 nm)

3. Summary

In this summary a short description of running projects of the institute of solid state electronics (fke) are depicted which are not directly involved in the growth of semiconductor materials, but rely on III-V based samples and/or use devices patterned in the cleanroom (by optical, laser- or electron-beam lithography).

3.1 Fabrication, Characterization and Lithographic Structuring of Dielectric Bragg Mirrors (T. Maier)

Dielectric Bragg-mirrors for vertical-cavity surface emitting laser diodes offer an attractive alternative to MBE grown mirrors, allowing a greater flexibility to optimize important features of the laser such as threshold current, optical power and lasing wavelength by adjusting the mirror reflectivity and the resonator length to the MBE-grown structure.

We fabricated SiO_x/SiN_x-Bragg mirrors using PECVD and measured the spectral dependence of their reflectivity. The deposition was found to be very homogenous and highly reproducible, allowing the fabrication of tailor-made Bragg mirrors for a given wavelength. High-reflectivity mirrors ($R > 0.98$) were realized by deposition of 10 SiO_x/SiN_x-pairs (Fig. 9).

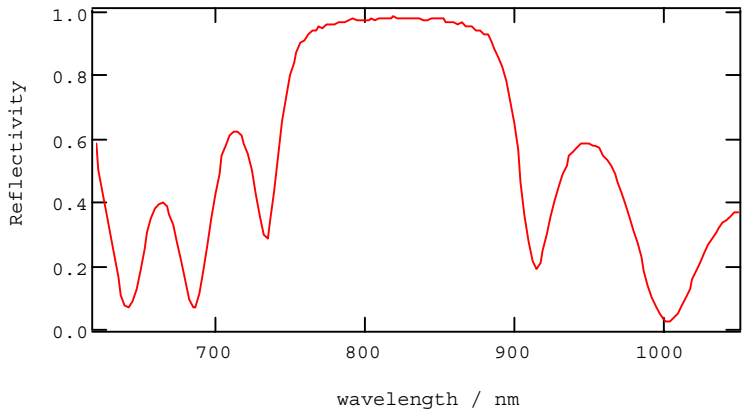

Fig. 9: Reflectivity vs. wavelength of 10 pairs SiO_x/SiN_x.

The SiO_x/SiN_x-layers were then patterned using standard photoresist masks. Etching was done in two steps: first by argon ion-milling, then in an SF_6-plasma for which the substrate (GaAs) serves as an etch stop layer, leaving SiO_x/SiN_x mesas on a clean GaAs-surface.

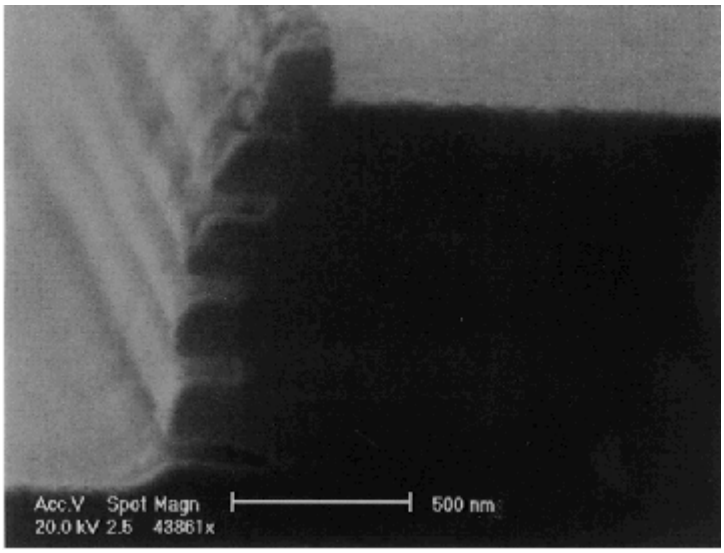

Fig. 10: SEM picture of a SiO_x/ SiN_x mesa (5 pairs)

3.2 Nanostructured Airbridges for THz Schottky Diodes (M. Hauser, E. Zottl, G. Strasser)

A new application of electron beam lithography (EBL) was the production of nanostructured metal airbridges, which are used to form ultrafast THz Schottky diodes. These devices operate at room temperature and can be used as detectors for far infrared radiation (FIR) or mixers for THz signals. New processes have been developed to reach the low capacitances necessary for diodes operating in the THz regime.

The diodes consist of n doped GaAs layers grown on a semiinsulating GaAs wafer. The diode is defined by proton implantation of the surrounding area. Therefore a mask covering only the active diode area is employed. It consists of a three layer stack of silicon nitride as a protective layer for the active diode area, a polyimide layer, and a thick layer of gold for masking of the implantation ions (Fig. 11).

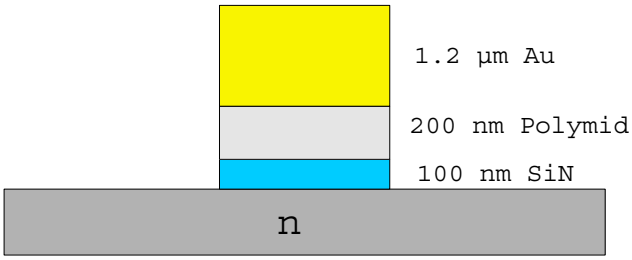

Fig. 11: Sketch of the ion implantation mask

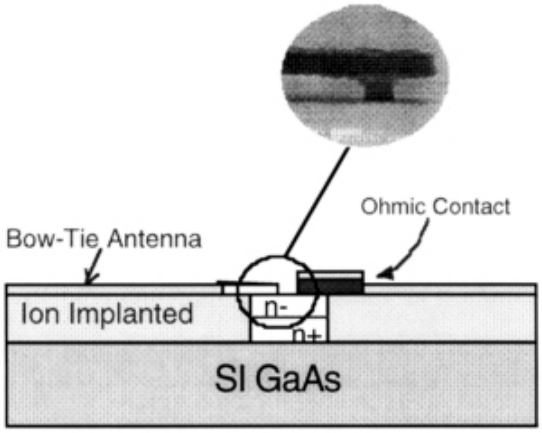

Fig. 12: Submicrometer Schottky diode design

A bowtie antenna is used to couple the FIR to the leads of the diode (Fig. 12). One lead connects the bowtie to the n-layer by an annealed ohmic contact. The Schottky contact forming the diode consists of a gold air bridge connecting the other end of the bowtie to the active diode area across the implanted region. A scanning electron microscope picture of this part of the device is shown in the insert. The airbridge is about 10 μm long, 200 nm wide and forms a Schottky contact with a diameter of less than 100 nm. The distance from the airbridge to the surface is about 250 nm. The capacitances of the leads are low enough to guarantee a cutoff frequency of more than 5 THz.

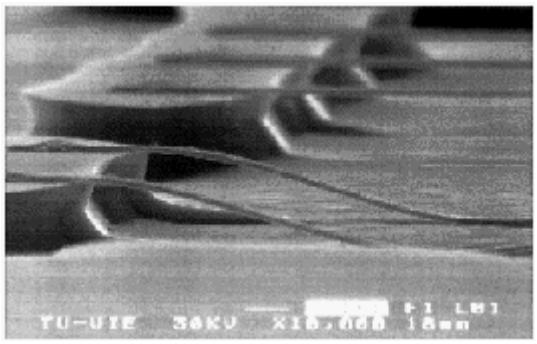

Fig. 13: SEM picture: airbridges.

3.3 BEEM Experiments on Quantum Wires (C. Eder, J. Smoliner)

In this project, a special scanning tunneling microscopy (STM) technique, the so-called "ballistic electron emission microscopy" (BEEM), is applied to quantum wires. For this purpose, the sample is covered with a thin Au-film (d < 100 Å) before the topography is measured with the STM. Because of the low thickness of the Au film, a part of the electrons passes the Au film ballistically and penetrates into the semiconductor. This ballistic electron current is measured simultaneously with the tunneling current via an additional backside electrode. In addition, the ballistic electron current can also be measured as a function of the applied bias voltage. Such a BEEM spectrum shows a diode-like behavior and is used to measure the barrier height at the Au-semiconductor interface.

In this project, BEEM measurements are applied to quantum wires, which are fabricated by laser holography on GaAs-AlGaAs heterostructures grown in the MBE system at the MISZ.

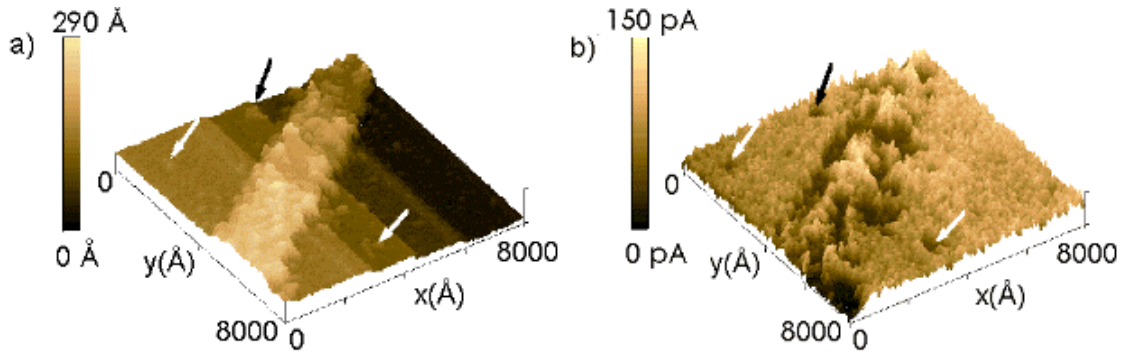

Fig. 14: (a) 3D image of a single quantum wire, (b) corresponding BEEM image. The arrows indicate Au clusters in the etched areas.

Figure 14 (a) shows the topography of a single quantum wire, Fig. 14 (b) the BEEM image, which was measured simultaneously. Two main details are evident: First, there are some Au-clusters accumulated on the wire, which are reflected as dark areas in the BEEM image. This cluster formation depends on sample preparation and was avoided in most recent measurements. Second, the BEEM current is slightly enhanced on the wire. This enhancement becomes clear if one looks at the bandstructure of the etched and non etched areas of the quantum wire sample. As one can see in Fig. 15 (a) the effective surface barrier height is higher in the etched areas, since here, the AlGaAs barrier under the surface is higher than the barrier of the Au-GaAs Schottky contact.. Thus, the corresponding BEEM current is lower than in the non etched areas on the quantum wire. To prove this experimentally, the barrier height was measured across the quantum wire and Fig. 15 (b) shows the experimental data. Detailed investigations on this topic are currently in progress.

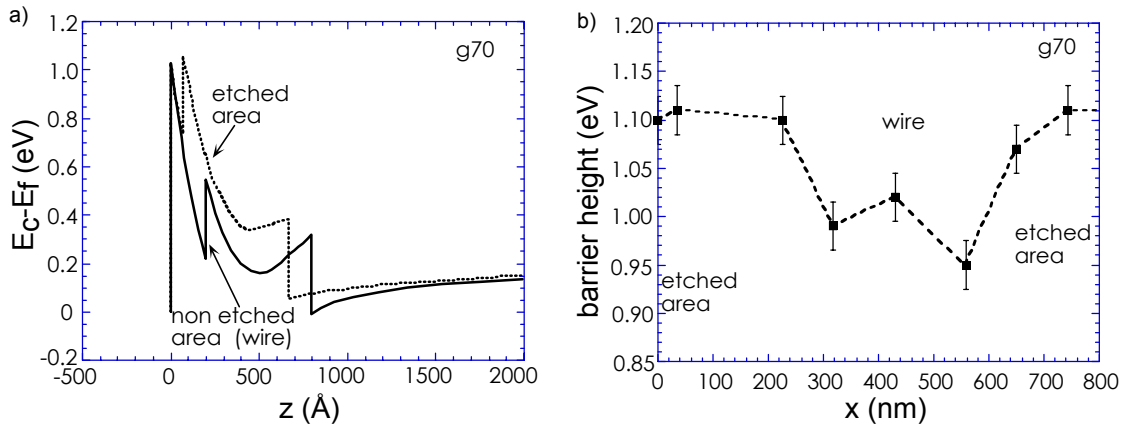

Fig. 15: (a) self consistently calculated bandstructure; (b) measured barrier height profile across a quantum wire.

3.4 Studies on the Lifetime of Intersubband Transitions in Semiconductor Superlattices (K. Unterrainer, R. Zobl, G. Strasser)

In unipolar semiconductors laser operation can only be achieved by a population inversion of charge carriers, which is governed by the lifetime of electrons (or holes) in excited states. In this work, the lifetime of electrons in excited states is investigated. In the last year pump and probe experiments on samples designed, grown, processed and tested in the MISZ were performed using the free electron laser "FELIX" in Nieuwegein (the Netherlands). The measured lifetimes of 400 ps in GaAs/AlGaAs are compared to calculated results of a theoretical model. This comparison shows that a combination of electron-electron scattering and optical and acoustical phonon scattering is limiting the electronic lifetime. In the running project asymmetric coupled quantum wells with a more sophisticated bandstructure and therefore a more complex level system are grown to test the possibility of subband inversion. Besides a deeper understanding of lifetimes in coupled wells a long-term goal is the development of an optically pumped FIR-semiconductor laser.

3.5 Ballistic Electron Spectroscopy of Biased Vertical Superlattices (C. Rauch, G. Strasser, K. Kempa, K. Unterrainer, W. Boxleitner)

The splitting of minibands in biased superlattices has direct consequences on the ballistic electron transport properties. Due to the localization of the electron wave function, the quasi-continuous miniband breaks up into a ladder of discrete Wannier-Stark states.

Using the concept of a hot electron transistor the transmittance of an undoped superlattice, grown in the drift region between base and collector, can be measured directly.

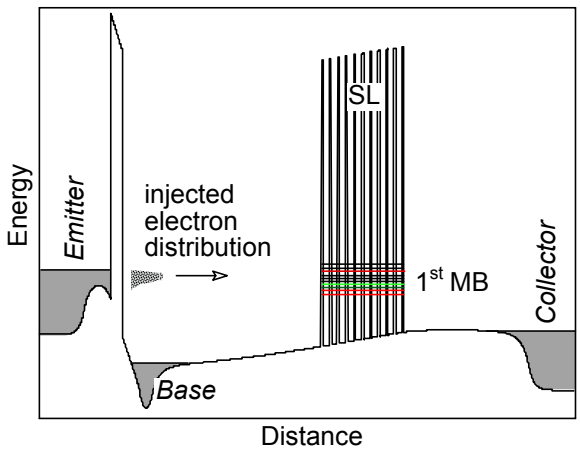

Fig. 16: Conduction band diagram of a three terminal device under typical bias conditions

An energy tunable electron beam is generated by a tunneling barrier and used to probe ballistic transport through the superlattice at given bias conditions (Fig. 16). The collector current is measured as a function of the injection energy. The probability for an injected hot electron to cross the superlattice reflects the transmittance of the discrete ladder of Stark states and can be considered to be proportional to the measured transfer ratio ($\alpha = I_C/I_E$).

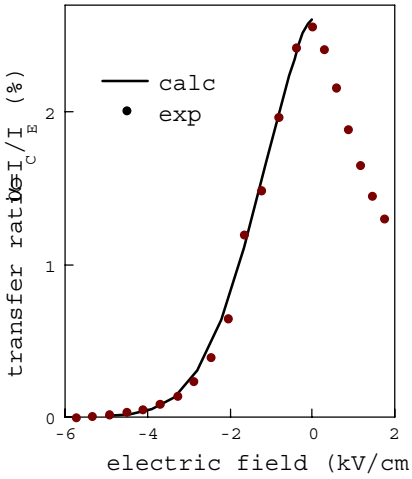

Fig. 17: Measured (dots) and calculated (line) transfer ratio vs. electric field

Figure 17 shows the transfer ratio of a ten period GaAs/AlGaAs superlattice versus electric field. The maximum transmission can be observed at zero bias voltage, since all superlattice states are extended over the whole superlattice dimension. Applying an electric field leads to a decrease of the transmission due to the localization of the lowest and uppermost superlattice states, i.e., these states do not contribute to the ballistic transport any more. The transfer ratio of the superlattice vanishes for an applied electric field of about 5 kV/cm. This is in good agreement with the simple estimate of the localization length $\lambda \approx \Delta/eF$ (Δ is the miniband width, and F the applied electric field) which decreases to about half of the total superlattice length at this bias.

In addition, we perform theoretical calculations based on a transfer matrix method using an envelope function approximation. The solid line in Fig. 17 shows the result of such a calculation for the measured structure. We find an excellent agreement between our experimental results and the quantitative theoretical prediction.

For the first time, the collapse of the superlattice states under electrical field can be observed directly using the technique of ballistic hot electron spectroscopy. To resolve the discrete Wannier Stark states, we designed a Four Terminal Device (FTD) including a resonant tunneling diode as an injector in order to decrease the width of the injected electron distribution.

3.6 Electron Transport Through a Combination of Different Superlattices (C. Rauch, G. Strasser, E. Gornik)

In this report we summarize the results obtained by hot electron spectroscopy of combinations of field free undoped superlattices. The study was carried out using a modified tunneling hot electron transfer amplifier, with an injector consisting of a tunneling barrier embedded within two highly doped GaAs contact layers. An energy tunable electron beam is injected into the structure under investigation. The measured static transfer ratio is defined by the ballistic electron current measured at the collector of the three terminal device divided by the emitter current ($\alpha = I_C/I_E$). Since the transfer ratio is proportional to the transmittance of the structure, which is grown between the base and the collector contact, we get important information of the transport mechanism in such sophisticated quantum mechanical systems.

The samples grown by Molecular Beam Epitaxy we have studied consist of the following common features: A highly doped n^+-GaAs collector contact layer ($n = 1x10^{18}$ cm^{-3}) is grown on a semiinsulating GaAs substrate. Followed by the heterostructure under investigation and the drift regions which are slightly n-doped ($\sim 5x10^{14}$ cm^{-3}), in order to avoid undesired band bending. These layers are followed by a highly doped ($2x10^{18}$ cm^{-3}) n^+-GaAs layer (base) of 13 nm width. On top of the base layer a 13 nm undoped $Ga_{0.7}Al_{0.3}As$ barrier is grown followed by a spacer and an n^+-GaAs layer, nominally doped to $n = 3x10^{17}$ cm^{-3}. Finally, a n^+-GaAs contact layer ($n = 1x10^{18}$ cm^{-3}) is grown on top of the heterostructure to form the emitter. The full width at half maximum (FWHM) of the injected energy distribution was measured to be 17 meV in width using a resonant tunneling diode in the drift region. It should be noted that the FWHM limits the energy resolution.

The fabrication (Fig. 18) of the three terminal device includes the following steps: $SiCl_4/SF_6$ reactive ion etching (RIE), unselective etching to the collector layer, metallization of the AuGeNi ohmic contacts, Si_3N_4 insulation of the emitter mesa (PECVD), and finally the metallization of the CrAu bonding pads.

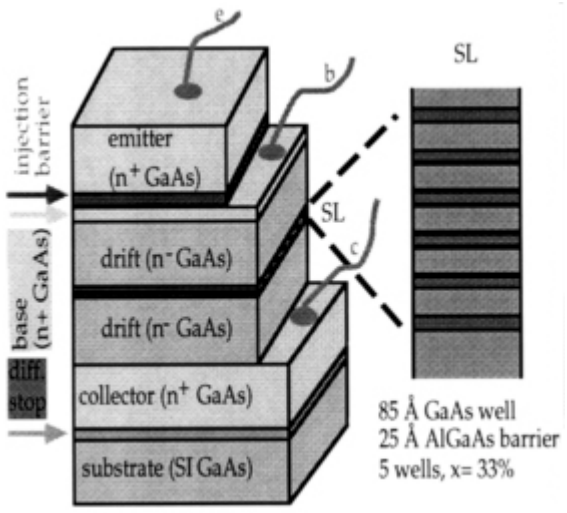

Fig. 18: Three terminal device

We have grown two samples with different combinations of five period superlattices. The superlattice growth parameters are given in the table below.

sample No.	superlattice 1		superlattice 2		superlattice 3	
	barrier (Å)	well (Å)	barrier (Å)	well (Å)	barrier (Å)	well (Å)
1	35	42.5	25	120		
2	35	42.5	25	120	15	85

Sample No. 1 consists of two superlattices. The parameters were chosen in such way that the lowest miniband of the first superlattice is aligned with the second miniband of the second superlattice. Injected electrons with energies high enough to traverse into the lower miniband of the first superlattice have two output channels. One channel is

defined by transport through the second miniband of the second superlattice without scattering. Electrons which are scattered in the second miniband can be collected via transport through the first miniband of the second superlattice.

Sample No. 2 consists of three different superlattices as noted in the table. The conduction band structure is sketched in Fig. 19. The first and the second superlattice have the same parameters as the superlattices in sample No. 1. The third superlattice is designed such that the minigap between the first and the second miniband is aligned with the second miniband of superlattice 2. The first minibands of superlattice two and three are aligned as well. Consequently only electrons which are scattered in the second superlattice can be collected and measured in the collector current. Electrons that are reflected by the minigap and not scattered into the first miniband will be bounced back and collected at the base layer.

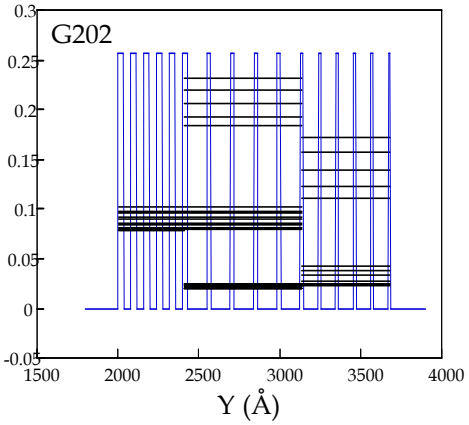

Fig. 19: Bandstructure of a combination of three different superlattices

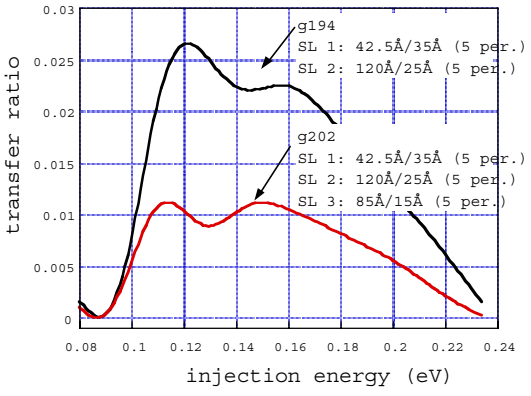

Fig. 20: Comparison of the transfer ratio of two different combinations of superlattices

In Fig. 20 the transfer ratio α versus injection energy is shown. A sharp increase of the transfer ratio is evident at about 90 meV which corresponds to the position of the first miniband of superlattice 1. It can be seen that the transfer ratio of sample No. 2 is about 50 % of the transfer ratio of sample No. 1. Consequently we assume that about half of

the electrons injected into the second miniband of the second superlattice are scattered into the first miniband. Since the energy gap between the second and the lowest miniband is of the order of an longitudinal optical (LO) phonon, we know that the interminiband transition is mainly governed by LO-phonon scattering which is the most effective scattering process at low temperatures. If the minigap is smaller than 36 meV one might achieve inversion and consequently a light emitting device. The design of such a structure is even more sophisticated. A prototype of a sample mentioned above is already grown and will be characterized soon.

3.7 Coherent Few-Cycle THz Emission from Plasmons in Bulk GaAs (R. Kersting, K. Unterrainer, G. Strasser, E. Gornik)

Femtosecond optical excitation of bulk semiconductors leads to the emission of coherent far infrared pulses. This emission results from instantaneous polarization, ballistic transport and drift of photogenerated carriers in the surface or built in fields of semiconductors. We have investigated the generation of few-cycle THz radiation from coherent plasmons in bulk GaAs.

For the first time our experimental data give direct insight into two distinctly different emission processes: THz generation by plasma oscillations of hot photogenerated carriers, and THz emission from coherent oscillations of cold extrinsic carriers.

The upper curve of Fig. 21 shows the autocorrelation of a THz pulse emitted from a p-i-n structure after femtosecond laser excitation. By increasing the excitation density, coherent emission can be found between 0.2 and 1.5 THz. The frequencies vary as the square root of the excitation density, as expected for plasmons. This proves that the THz emission results from the plasma oscillation of the photogenerated carriers. We find that the emitted THz radiation from the p-i-n diode is strongly damped. We attribute this to the fact that the photogenerated carriers are hot and thus subject to fast scattering processes.

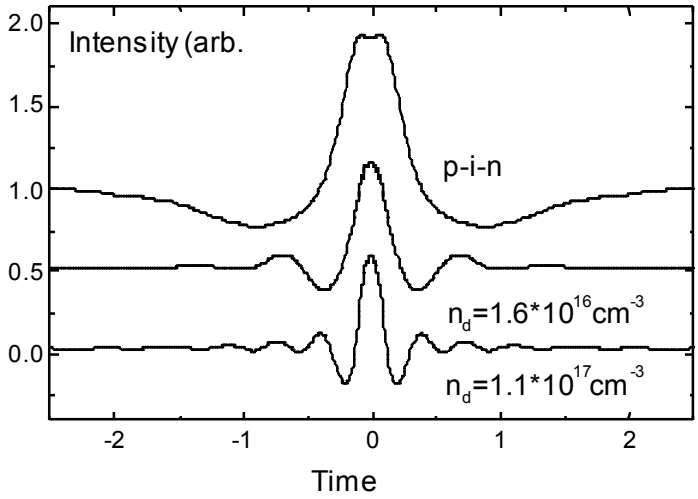

Fig. 21: Autocorrelation data recorded on the p-i-n structure and on two bulk GaAs structures with different doping concentrations.

A fundamentally new emission process is found in n-doped bulk GaAs. Here, the screening of the surface field by photogenerated carriers starts coherent oscillations of the extrinsic carriers in the GaAs bulk. Autocorrelation data are shown by the lower curves in Fig. 21. In contrast to the results on p-i-n structures the frequencies of these THz pulses depend on the doping concentration but not on the density of the photogenerated carriers. This shows that the THz radiation is emitted by the oscillation of the extrinsic electrons in the GaAs bulk. The damping times of these oscillations are much slower than in p-i-n structures which leads to multiple oscillations of the field. We show that the oscillations of the cold carrier plasma are limited to the center of the Brillouin zone and that the damping of the extrinsic plasma oscillations results mainly from optical phonon scattering.

Since the emitted power of the THz radiation strongly depends on the damping rate the cold plasma oscillation in bulk GaAs offer an attractive approach to generate intense THz pulses. Our experiments show that the emission power on n-doped structures is more than one order of magnitude higher than the power emitted from diode structures.

3.8 Photonic Bandgap Material Used as THz Resonators (K. Unterrainer, R. Kersting)

For the realization of a THz-laser an efficient coupling structure and resonator is needed. The resonator is defined by two photonic band gap mirrors which have been already developed at the institute (Fig. 22). Photonic band gap materials show high reflectivity in the THz range. Bow Tie antennas, connected via air bridges to the active mesa to avoid parasitic capacities will be used to couple out the emitted light. At the moment these new processes represent the main activities in this project.

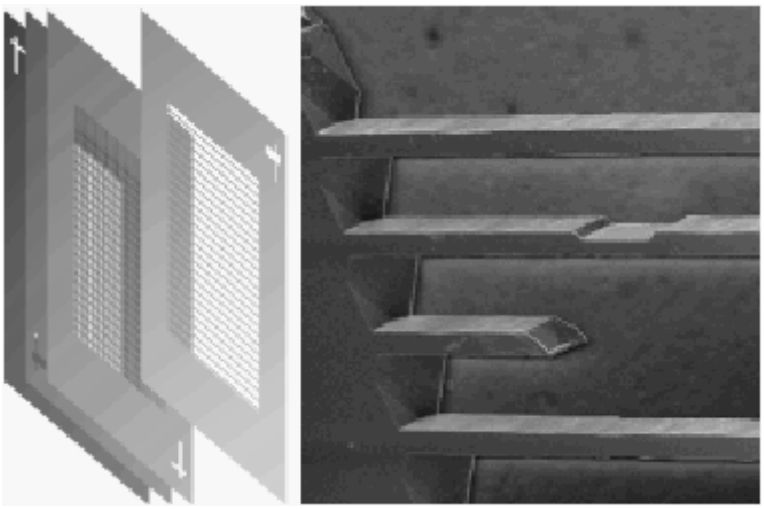

Fig. 22: Photonic band gap material.

3.9 Quantum Cascade Electroluminescence in GaAs/AlGaAs Structures (G. Strasser, M. Helm, L. Hvozdara, P. Kruck, E. Gornik)

The advent of a unipolar semiconductor laser based on intersubband transitions in quantum wells [1] in 1994 marked a breakthrough in the application of band-structure engineering. Since then, great progress concerning device operation and performance of

these so-called quantum cascade lasers has been achieved [2], however, these results were restricted to a single research laboratory and to a single material system, namely InGaAs/InAlAs lattice matched to InP.

We present here the design, growth and operation of an unipolar light emitting diode (LED) based on the material system GaAs/AlGaAs.

The structure essentially follows the design considerations given by Faist et al. [2], [3] with the modifications necessary due to the different material system. The diode (grown on a semi-insulating GaAs substrate) consists of 25 active periods of GaAs/ $Al_{0.45}Ga_{0.55}As$ coupled quantum well layers. The growth sequence of the active cell is 10 Å GaAs, 15 Å AlGaAs, 45 Å GaAs, 20 Å AlGaAs, and 45 Å GaAs (see also Fig. 23). The active cells are separated by miniband funnel injectors and the whole structure is embedded between two highly doped contact layers. The LED is designed for emission at about 6.5 µm, but longer or shorter wavelengths than this appear possible. The present choice was dictated by two considerations: on the one hand, shorter wavelength emission (or lasing) is generally easier to achieve due to the larger spontaneous emission rate and smaller losses. On the other hand we wanted to keep the Al content in the barriers below 45% in order to avoid effects related to the X-point.

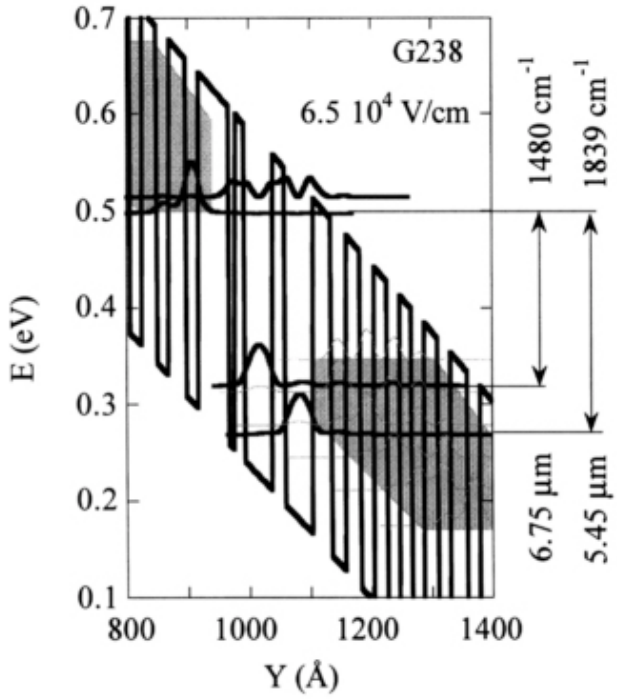

Fig. 23: Self-consistent calculations of the conduction band and the relevant wavefunctions (YY*) under bias

The structure was characterized by measuring the current-voltage characteristics as well as the intersubband absorption and photocurrent under near-zero bias.

Emission measurements were performed with a step-scan Fourier-transform spectrometer using lock-in techniques. 100 x 100 μm^2 size mesa structures were employed, which led to a current of the order of 100 mA under injection conditions (bias 8 V). Electrical pulses of typically 15 µs length with a 3 kHz repetition rate were applied to the sample

(5% duty cycle). The sample was kept at around 10 K in a LHe flow cryostate and the emission was detected with a LN_2 cooled HgCdTe detector.

A typical emission spectrum is shown in Fig. 24. The main emission peak (at 1450 cm^{-1}) is due to the 3-2 transition, but a second peak at higher energy resulting from the 3-1 transition is also visible. Figure 23 shows the calculated band structure under injection bias conditions, the energy-level line-up being in good agreement with the experimental results.

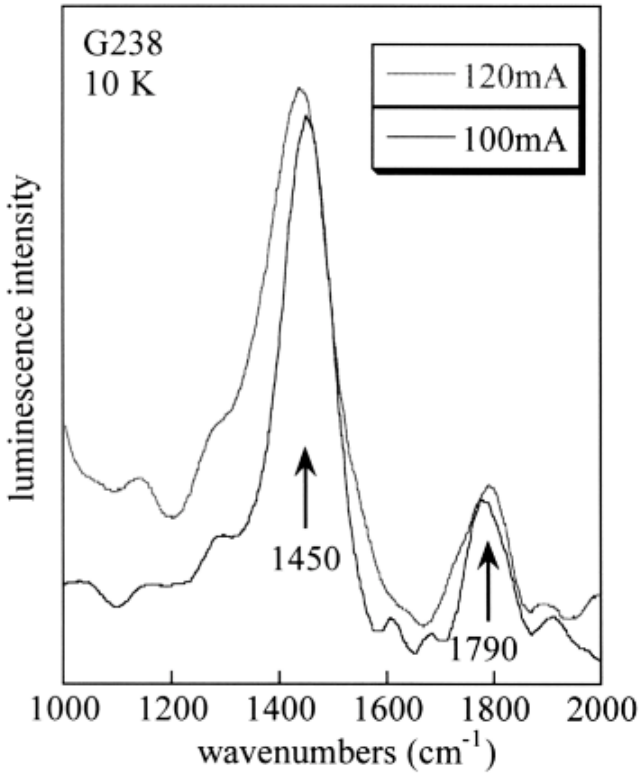

Fig. 24: Electroluminescence at 10 K

First attempts to fabricate a laser structure indicated difficulties with the electrical properties of the AlGaAs waveguide cladding layer. Thus most likely new concepts for optical mode confinement have to be developed in order to achieve a quantum cascade laser based on GaAs.

References

[1] J. Faist, F. Capasso, D. L. Sivco, C. Sirtori, A. L. Hutchinson, and A. Y Cho, Science **264**, 553 (1994)

[2] J. Faist, F. Capasso, C. Sirtori, D. L. Sivco, J. N. Baillargeon, A. L. Hutchinson, S.N.G. Chu, and A. Y. Cho, Appl. Phys. Lett. **68**, 3680 (1996)

[3] J. Faist, F. Capasso, C. Sirtori, D. L. Sivco, A. L. Hutchinson, S.-N. G. Chu, and A. Y. Cho, Appl. Phys. Lett. **64**, 1144 (1994)

Project Information

Project Manager

Univ.-Prof. Dr. Erich GORNIK

Institut für Festkörperelektronik, Technische Universität Wien, A-1040 Vienna

Project Group

Last Name	First Name	Status	Remarks
Auer	Peter	student	
Eder	Claudia	dissertation	
Finger	Norman	dissertation	
Fürböck	Christoph	dissertation	
Gianordoli	Stefan	student	
Golshani	Alireza	dissertation	
Gornik	Erich	Full Prof.	
Habas	Predrag	Post Doc	
Haider	Manfred	student	
Hainberger	Rainer	dissertation	
Hauser	Markus	Post Doc	50% GMe funding
Hvozdara	Lubos	dissertation	25% GMe
Kellermann	Peer Oliver	student	
Köck	Anton	Assistant Prof.	
Kröll	Peter	technician	
Langmann	Gottfried	technician	
Liu	Jian	student	
Ploner	Guido	dissertation	
Pogany	Dionyz	guest scientist	
Prinzinger	Johannes	technician	
Rauch	Christoph	dissertation	
Roßkopf	Valentin	dissertation	100% GMe
Schrenk	Werner	student	
Seliger	Norbert	dissertation	
Smoliner	Jürgen	Assistant Prof.	
Strasser	Gottfried	Assistant Prof.	
Unterrainer	Karl	Assistant Prof.	
Zobl	Reinhard	student	
Zotl	Ernst	student	

Publications in Reviewed Journals

1. A. Golshani, P.O. Kellermann, A. Koeck and E. Gornik and L. Korte, "Surface Emitting Laser Diode Array for Wavelength Division Multiplexing Based on Post Growth Adjustment of Surface Mode Emission", Submitted to *Appl. Phys. Lett*. Feb. 1997
2. P.O. Kellermann, A. Golshani, A. Koeck, E. Gornik, H.P.Gaugel, R. Winterhoff, J. Kuhn, "Single-mode and single-beam surface emission from visible red GaInP/AlGaInP laser diodes", to be published in *Appl. Phys. Lett*. 1997
3. A. Golshani, A. Koeck, S. Freisleben, C.Gmachl, E. Gornik, L. Korte, "Adjustable surface emission from AlGaAs/GaAs laser diodes based on first-order-grating-coupled surface mode emission", *Appl. Phys. Lett*. 69 (16), 2312 (1996)
4. A. Koeck, A. Golshani, R. Hainberger, E. Gornik; L. Korte, "Single-mode and single-beam emission from surface-emitting laser diodes based on surface mode emission", *Appl. Phys. Lett*, 69 (24), 3638 (1996)
5. C. Gmachl, A. Golshani, A. Koeck, E. Gornik; J.F. Walker, "Vertical-cavity surface-emitting lasers with monolithically integrated modulators" in *Microcavities and Photonic Bandgaps: Physics and Applications*; editted by John Rarity and Claud Weisbuch; Nato ASI Series vol. E 324; Kluwer Academic Publishers, Netherlands, p. 387 (1996)
6. C. Eder, J. Smoliner, "Local barrier heights on quantum wires determined by ballistic electron emission spectroscopy", *Appl. Phys. Lett.* 68, 2876 (1996)
7. J. Smoliner, C. Eder, G. Böhm, G. Weimann, "Low temperature current imaging spectroscopy on wet chemically etched quantum wires", *Appl. Phys. Lett.* 69, 52 (1996)
8. J. Smoliner, C. Eder, G. Strasser, G. Böhm, G. Weimann, "STM studies on quantum wire structures in air and liquid helium", *Superlattices and Microstruct*., Vol. 20, 261, (1996) (Proc. NANOMES 96 Symposium, SantaFe)
9. C. Eder, J. Smoliner, G. Strasser, "BEEM Studies on GaAs-AlGaAs quantum wire structures", *Superlattices and Microstruct*., Vol. 20, 357, (Proc. NANOMES 96 Symposium, SantaFe)
10. M. Hauser, J. Smoliner, C. Eder, G. Ploner, G. Strasser, E.Gornik, "Single Quantum Dots as Scanning Tunneling Microscope Tips", to be published in *Superlattices and Microstructures* (1996) (Proc. NANOMES 96 Symposium, SantaFe)
11. M. Hauser, J. Smoliner, C. Eder, G. Ploner, G. Strasser, E.Gornik, "Scanning Tunneling Microscopy with Single Quantum Dot Tips", *Phantoms Newsletter*, 12, 1 (1996)
12. C. Eder, J. Smoliner, G. Böhm, G. Weimann, "Room temperature current imaging tunneling spectroscopy of GaAs/AlGaAs quantum wires at ambient pressure", *Semicond. Sci. Technol*., 11, 1239, (1996)
13. C. Eder, J. Smoliner, G. Strasser and E. Gornik, "Ballistic electron emission microscopy in liquid helium using low dimensional collector electrodes", *Appl. Phys. Lett.* 69, 1725, (1996)

14. T.P. Sosin, W. Treciakowski, M. Leszczynski, G. Strasser,"Biaxial Deformation Effects in Quantum Wells", *Proc. ICPS23*, Berlin (1996)

15. W. Boxleitner, C. Rauch, G. Strasser, L. Hvozdara, E. Gornik, U. Meirav, V. Umansky, H. Shtrikman, "Electron Dynamics and Band Structure in high Quality GaAs/AlGaAs Superlattices", *Proc. ICPS23*, Berlin (1996)

16. W. Heiss, B.N. Murdin, C.J.G.M. Langerak, S.-C. Lee, G. Strasser, C.R. Pidgeon, I. Galbraith, E. Gornik, M. Helm, "The LO-phonon bottleneck in the intersubband cooling in wide quantum wells", *Proc. ICPS23*, Berlin (1996)

17. B.N. Murdin, W.Heiss, C.J.G.M. Langerak, S.-C. Lee, I. Galbraith, G. Strasser, E. Gornik, M. Helm, C.R. Pidgeon, "Direct observation of the LO phonon bottleneck in wide GaAs/AlGaAs quantum wells", *Phys. Rev. B* 55, 5171 (1997)

18. C. Rauch, G. Strasser, K. Unterrainer, L. Hvozdara, W. Boxleitner, E. Gornik, "Hot electron spectroscopy of undoped GaAs/GaAlAs superlattices", *Superlattices and Microstructures*, (to be published)

19. R. Kersting, K. Unterrainer, G. Strasser, E. Gornik, H.F. Kauffmann, "Coherent Few-Cycle THz Emission of cold plasmons", in Proc. *Gordon Research Conference on Laser Interactions with Materials* (extended abstract, to be published)

20. C. Rauch, G. Strasser, K. Unterrainer, B. Brill, E. Gornik, "Ballistic electron spectroscopy of vertical superlattice minibands", *Appl. Phys. Lett.*, 70, 649 (1997)

21. K.D. Maranowski, A.C. Gossard, K. Unterrainer, E. Gornik, "Far infrared emission from prabolically graded quantum wells", *Appl. Phys. Lett.*, 69, 3522 (1996)

22. R. Kersting, K. Unterrainer, G. Strasser, H.F. Kauffmann, E. Gornik, "Few-cycle THz emission from cold plasma oscillations", *Phys. Rev. Lett*. (submitted).

23. N. Seliger, P. Habas and E. Gornik, "A Study of Backside Laserprobe Signals in MOSFETs", *Microelectr. Eng.*, vol. 31, pp. 87 – 94, January 1996.

24. N. Seliger, P. Habas and E. Gornik, "Time-Domain Characterization of Lattice Heating in Power VDMOSFETs by Means of an Interferometric Laserprobe Technique", Digest to the *European Solid State Device Research Conference (ESSDERC´96)*, Bologna, Italy, 9 – 11 September 1996, p. 847

25. N. Seliger, P. Habas, A. Köck, D. Pogany and E. Gornik, "Backside Laserprobing of Transient Heating in Power VDMOSFETs", Digest to the *International Seminar on Power Semiconductors (ISPS´96)*, Prague, Czech Republic, 11 – 13 September 1996, p. 115

26. D. Pogany, N. Seliger, T. Lalinsky, J. Kuzmík, P. Habas, P. Hrkút and E. Gornik, "Study of Thermal Effects in GaAs Micromachined Power Sensor Microsystems by an Optical Interferometer Technique", Digest to the *International Workshop on Thermal Investigations of ICs and Microstructures (THERMINIC `96)*, Budapest, Hungary, 25 – 27 September 1996, p. 185

27. D. Pogany, T. Lalinsky, N. Seliger, J. Kuzmík, P. Habas, P. Hrkút and E. Gornik: "Power Sensor Microsystems Characterization Using a Contactless Optical Laser Method", Digest to the *International Conference of Advanced Semiconductor Devices and Microsystems (ASDAM´96)*, Smolenice, Slovakia, 20. – 24.October 1996, p. 201

28. D. Pogany, N. Seliger, T. Lalinsky, J. Kuzmík, P. Habas, P. Hrkút and E. Gornik, "Study of Thermal Effects in GaAs Micromachined Power Sensor Microsystems by an Optical Interferometric Technique", to be published in *Microelectronics Journal*, 1997

29. N. Seliger, P. Habas, D. Pogany and E. Gornik, "Time-Resolved Analysis of Self-Heating in Power VDMOSFETs using Backside Laserprobing", submitted to *Solid State Electronics*, October 1996

30. E. Burian, D. Pogany, T. Lalinsky, N. Seliger and E. Gornik, "Thermal Simulation and Characterization of GaAs Micromachined Power Sensor Microsystems", submitted to *EUROSENSORS XI* conference, February 1997

Presentations

1. C. Eder, J. Smoliner, G. Strasser, "Low temperature BEEM studies on quantum wires fabricated on GaAs-AlGaAs heterostructures", *ICPS23*, Berlin (1996)
2. M. Hauser, J. Smoliner, C. Eder, G. Ploner, G. Strasser, E.Gornik, "Single Quantum Dots as Scanning Tunneling Microscope Tips", *NANOMES 96 Symposium*, SantaFe
3. C. Eder, J. Smoliner, G. Strasser, "BEEM Studies on GaAs-AlGaAs quantum wire structures", *NANOMES 96 Symposium*, SantaFe
4. J. Smoliner, C. Eder, G. Strasser, G. Böhm, G. Weimann, "STM studies on quantum wire structures in air and liquid helium", *NANOMES 96 Symposium*, SantaFe
5. T.P. Sosin, W. Treciakowski, M. Leszczynski, G. Strasser, "Biaxial Deformation Effects in Quantum Wells", *Proc. ICPS23*, Berlin (1996)
6. C. Eder, J. Smoliner, G. Strasser, and E. Gornik, "Low Temperature Ballistic Electron Emission Microscopy Studies on GaAs/AlGaAs Heterostructures", *SXM2 Workshop*, Vienna (1996)
7. A. Köck, C. Gmachl, A. Golshani, S. Freisleben, E. Gornik, "Oberflächen-emittierende Laserdioden", *Mauterndorfer Laserseminar*, 20 – 23 March 1996, Mauterndorf
8. A. Koeck, A. Golshani, R. Hainberger, N. Finger, C. Gmachl, E. Gornik; L. Korte, "Quasi-single-mode surface-emitting laser diodes based on surface mode emission", *SPIE Proc.* Vol. 2682 "Laser Diodes and Applications II" of *Photonics West*, pp.169 – 175, OE/LASE'96, USA, SPIE Optical Engineering Press (1996)
9. A. Golshani, R. Hainberger, S. Freisleben, A. Koeck, E. Gornik; C. Gmachl; L. Korte, "Efficient surface emitting AlGaAs/GaAs laser diodes based on first-order-grating-coupled surface mode emission", *Proceedings of the "European Gallium Arsenide and related III-V compounds application symposium"*, 3B4; Paris 5 – 7 June, 1996
10. A. Koeck, N. Finger, C. Gmachl, A. Golshani, R. Hainberger, E. Gornik; L. Korte, "Single-beam and single-mode emission from surface-emitting laser diodes based on surface mode emission", *Int. Conf. on Solid State Devices and Materials*, Yokohama 26 – 29 August, 1996, *SSDM'96 Extended Abstracts* pp. 858, (1996)
11. A. Golshani, A. Koeck, R. Hainberger, E. Gornik; L. Korte, "Single-beam emission from surface emitting laser diodes based on surface mode emission", *Proceedings of*

the "Conference on Lasers and Electro-Optics (CLEO)/Europe", pp. 28; 8 – 13 September 1996, Hamburg, Germany, 1996

12. A. Koeck, A. Golshani, R. Hainberger, E. Gornik; L. Korte, "Single-beam and single-mode emission from surface emitting laser diodes based on surface mode emission", *Proceedings of the "26th European Solid State Device Research Conference"*; pp. 541; 9 – 11 September 1996, Bologna, Italy
13. R. Hainberger, N. Finger, A. Golshani, A. Koeck, E. Gornik; J.F. Walker "A new concept for a direct optical free-space interconnect without lenses", *Proceedings of the "26th European Solid State Device Research Conference"*; pp. 537; 9 – 11 September 1996, Bologna, Italy
14. A. Köck, "Oberflächenemittierende monomodige Laserdioden basierend auf dem Konzept der Oberflächenmodenkopplung", Preisträgervortrag, *46. Jahrestagung der Österreichischen Physikalischen Gesellschaft*, 23 – 27 September 1996, Linz
15. A. Köck, A. Golshani, N. Finger, E. Gornik; L. Korte, "Monomodige Einzelstrahlemission von oberflächenemittierenden Laserdioden basierend auf Oberflächenmodenkopplung (poster), *Photonik-Symposium der Volkswagen-Stiftung*, 7 – 9 October 1996, Schwäbisch Hall-Hessental, Germany
16. A. Koeck, A. Golshani, R. Hainberger, E. Gornik; L. Korte, "Single-beam and single mode emission from surface emitting laser diodes based on surface mode emission", *Proceedings of the "9th Annual Meeting IEEE Lasers and Electro-Optics Society"*; Vol. 1, pp. 125, 18 – 21 November 1996, Boston, MA, USA,
17. A. Koeck, A. Golshani, R. Hainberger, E. Gornik; L. Korte, "Digital beam steering from surface emitting laser diodes based on surface mode emission", *SPIE Proc*. Vol. 3001 "In-Plane Semiconductor: from Ultraviolet to Mid-infrared" of *Photonics West'97*, OE/LASE'97, USA, SPIE Optical Engineering Press (1997)
18. M. Hauser, J. Smoliner, C. Eder, G. Ploner, E. Gornik, "Single quantum dots as scanning tunneling microscope tips", *Superlatt.Microstruct*. 20, 623 (1996)
19. G. Ploner,J. Smoliner,G. Strasser,E. Gornik, "Transport characterization of quantum wires by magnetophonon and magnetic depopulation experiments", ICSMM-9 1996, to be published in *Superlatt. Microstructures*
20. G. Ploner, J. Smoliner, G. Strasser,E. Gornik, "Magnetophonon analysis of quantum wire systems", *Proceedings ICPS-23*, World Scientific 1996
21. G. Ploner, J. Smoliner, G. Strasser, E. Gornik, "Temperature dependent magnetotransport properties for systems of few quantum wires", *Physica B* 227, 24 (1996)
22. C. Rauch, G. Strasser, K. Unterrainer, L. Hvozdara, W. Boxleitner, E. Gornik, "Hot electron spectroscopy of undoped GaAs/GaAlAs superlattices", *9th Int. Conf. on Superlattices, Microstructures and Microdevices*, 14 – 19 July 1996, Liege, Belgium.
23. C. Rauch, G. Strasser, M. Heiblum, E. Gornik, "Ballistische Elektronen-Spektroskopie von Minibändern in GaAs/AlGaAs Übergittern", *ÖPG Jahrestagung*, 23 – 27 September1996, Linz

24. C. Rauch, G. Strasser, K. Unterrainer, E. Gornik, "Breakdown of the electron wave function in biased superlattices", *Workshop on Periodic Structures*, 27 – 31 January 1997, Les Houches, France
25. R. Kersting, K. Unterrainer, G. Strasser, E. Gornik, H.F. Kauffmann, "Coherent Few-Cycle THz Emission of cold plasmons", *Gordon Research Conference on Laser Interactions with Materials*, 9 – 14 June 1996, Holderness School, Plymouth, N.H., USA
26. K. Unterrainer, "Observation of Shapiro steps and direct evidence of Bloch oscillations in semiconductor superlattices", *9th Int. Conf. on Superlattices, Microstructures and Microdevices*, Liege, Belgium, 14 – 19 July 1996
27. K. Unterrainer, "Applications of FIR free electron lasers to non-linear spectroscopy", *15th General Conference of the Condensed Matter Division/EPS*, Baveno-Stresa, Italy, 22 – 25 April 1996
28. K. Unterrainer, "Intersubband Dynamics of Asymmetric Coupled Quantum Wells Studied by THz Optical Rectification", *9th International Winterschool on New Developments in Solid State Physics*, Mauterndorf, Austria, 19 – 23 February 1996
29. N. Seliger, "Backside-Laserprober zur Charakterisierung integrierter Halbleiterbauelemente", oral presentation at SIEMENS Munich, Germany, 7 February 1996
30. P. Habas, "Analyse thermischer Effekte an Leistungs-MOSFETs und SOI-Bauelementen", oral presentation at SIEMENS Munich, Germany, 7 February 1996
31. E. Gornik, P. Habas, N. Seliger, D. Pogany, and C. Fürböck: "Characterization of Silicon Devices by a Laser Probe Technique", *Jahrestagung Österreichische Physikalische Gesellschaft (ÖPG)*, Linz, Austria, 24 September 1996

Doctor's Theses

1. C. Gmachl, "Frequenzverstimmbare oberflächenemittierende Halbleiterlaserdioden mit vertikalem Resonator", TU Wien, 1996
2. W. Heiss, "Ferninfrarotspektroskopie an unipolaren Halbleitern — Relaxation und Emission", TU Wien, 1996
3. S. Michaelis, "Nichtlineare Spektroskopie an GaAlAs-Vielschichtstrukturen zur Bestimmung der optischen Eigenschaften im Bereich der Bandkante", TU Wien, 1996
4. V. Roßkopf, "Spektroskopie strukturierter Elektronengase", TU Wien, 1996
5. W. Boxleitner, "Untersuchungen der Smith-Purcell Emission in modulierten Halbleiterstrukturen", in progress
6. C. Eder, "Raster-Tunnelspektroskopie an Halbleiterstrukturen im Nanometer-bereich", in progress
7. N. Finger, "Herstellung von monomodigen oberflächenemittierenden Laserdioden im 1.5-Mikrometer Bereich", in progress
8. Ch. Fürböck, "Laserinterferometrie an Leistungsbauelementen", in progress

9. A. Golshani, “Herstellung von durchstimmbaren oberflächenemittierenden Halbleiterlasern”, in progress
10. R. Heer, “STM-Untersuchungen an Nanostrukturen”, in progress
11. Th. Maier, “Integration von VCSELs und Photodetektoren”, in progress
12. G. Ploner, “Temperaturabhängige Transport- und Tunnelspektroskopie an niedrigdimensionalen Elektronensystemen”, in progress
13. Ch. Rauch, “Emission von Halbleiterstrukturen”, in progress
14. N. Seliger, “Untersuchungen der Ladungsträgerdichte- und Wärmeverteilung in integrierten Halbleiterbauelementen mittels Laserinterferometrie”, in progress
15. S. Senkader, “Physikalische Modellierung und Simulation der Sauerstoffpräzipitation in CZ-Silizium”, in progress

Habilitations

1. K. Unterrainer, “Development of FIR (THz) radiation sources”, TU Wien, 1996
2. J. Smoliner, “Current Transport in Nanostructures”, TU Wien, 1996

Cooperations

1. Siemens AG, Dr. Bernd Borchert and Dr. Lutz Korte, Prof. E. Wolfgang, Dr. M. Stoisiek, Dr. G. Deboy, Dr. G. Sölkner; Dr. S. Görlich, Germany
2. Institut für Angewandte Chemie Berlin Adlershof e.V., Dr. K. Pfeiffer, Germany
3. Universität Stuttgart, 4. Physikalisches Institut, Prof. Dr. M.H. Pilkuhn, Germany
4. TU-München, Walter Schottky Institut, Prof. Weimann, Germany
5. TU München, Lehrstuhl für Techn. Elektrophysik, Prof. G. Wachutka, Germany
6. Universität Bremen, Inst. für Festkörperphysik, Prof. Dr. D. Hommel, Germany
7. RWTH Aachen, Inst. f. Halbleiterelektronik, Prof. H. Kurz, Germany
8. Centre National de la Recherche Scientific, Laboratoire de Microstructures edt de Microelectronique, B.Etienne, Cedex, France
9. Interuniversity Microelectronics Center (IMEC), Leuven, Belgium
10. University of Surrey, Physics Department, Dr. B.N.Murdin, UK
11. Herriot Watt University, Edinburgh, Prof. C. Pidgeon, UK
12. Ioffe Physico-Technical Institute, St. Petersburg, Prof. A.A. Andronov, Russia
13. Norwegian University of Science and Technology, Prof. K. Fossheim, Norwegen
14. Sub-Micron Center, Weizmann Institute, Rehovot, Prof. M. Heiblum, Israel
15. Academy of Sciences, High Pressure Research Center, Prof. Treciakowski Prof. Suski, Poland
16. Academy of Sciences, Institut of Physics, Dr. Bartos, Slowakia
17. Technische Universität Bratislava, Mikroelektronik, Prof. Csabay, Slowakia

18. Univ. of California, Lawrence Berkeley Laboratories, Prof. E.E. Haller, USA
19. University of California, Free-Electron-Laser, Santa Barbara, Prof. J. Allen, USA
20. Boston College, Dep. of Physics, Boston, Massachusetts, Prof. K. Kempa, USA
21. EPI MBE Components, St. Paul, Minnesota, USA
22. Universität Linz, Institut für Halbleiterphysik, Prof. G. Bauer, Doz. Dr. M. Helm
23. Universität Graz, Institut für Experimentalphysik, Prof. F. Aussenegg
24. Universität Innsbruck, Institut für Experimentalphysik, Doz. Dr. W. Seidenbusch
25. Siemens AG Villach, Dr. Prybil
26. Plansee AG, Reutte, Dr. Willhartitz
27. Universität Wien, Institut für Physikalische Chemie, Prof. Kauffmann
28. Universität Wien, Institut für Festkörperphysik, Doz. Dr. R. Höpfel
29. Universität Leoben, Institut für Physik, Prof. Kuchar
30. TU Wien, Institut für Angewandte u. Technische Physik, Prof. Ebel, Doz. Schattschneider, Doz. Pongratz
31. TU Wien, Atominstitut der österreichischen Universitäten,. Prof. Weber
32. TU Wien, Institut für Analytische Chemie, Prof. Robert Kellner

Backside-Laserprober Technique for Characterization of Semiconductor Power Devices

N. Seliger, C. Fürböck, P. Habaš, D. Pogany, E. Gornik

Institute of Solid State Electronics &
Center of Microstructure Research (MISZ),
TU Wien, A-1040 Vienna, Austria

An infrared laserprobe technique for the characterization of the self-heating in the μs range in power VDMOSFETs and IGBTs is presented. Based on the thermo-optical effect in silicon, this technique detects interferometrically the temperature induced changes of the silicon refractive index. The time evolution of the lattice temperature in the device active region is studied for the power devices biased under shorted load conditions. Optical experiments are combined with electro-thermal device modeling and electrical characterization. From the calculated phase modulation signals fitted to the experiments a value for temperature coefficient of the refractive index of $1.6 \cdot 10^{-4}$ K^{-1} is found which is in good agreement with the literature.

1. Introduction

The steady increase of the switching frequency of power semiconductor devices under high voltage and current conditions causes transient thermal effects to become a more severe and critical issue. Although much attention has been given to thermal effects in power devices, there are so far no experimental techniques available for a time-resolved analysis of destructive thermal effects in dynamic device operation. In this paper we present the application of the backside laserprobe technique [1] to analyze the transient heating in power Vertical Double-diffused (VD)MOSFETs and in Insulated Gate Bipolar Transistors (IGBTs) biased under shorted load conditions.

2. Optical Technique

The principle of the laserprober set-up is demonstrated in Fig. 1. An increase in the refractive index of silicon due to the lattice heating (thermo-optical effect) in dynamic device operation modulates the phase of the laser probing beam. The probing beam reflected from the gate and a reference beam reflected from the drain metallization interfere in a photodetector. The electrical signal at the detector corresponding to the thermally induced phase change is recorded and averaged by a digital oscilloscope. Since the photon energy of the laser beam ($\lambda = 1.3\mu m$) is below the energy gap of silicon, the optical measurements have no impact on the device electrical characteristics.

The laserprobe measurements were performed on commercially available VDMOSFETs of 150 V and 200 V breakdown voltage, and on IGBTs with 1200 V breakdown voltage. In VDMOSFETs, optical access through the drain contact is obtained after mechanical removal of the original contact metallization, polishing the substrate and evaporation of

a thin Ti-Au film leaving a small square window opened. This preparation does not change the device performance, but induces a small drain contact resistance. For measurements on IGBTs, the device preparation is different as mechanical contact removal would also destroy the p^+-anode layer of the IGBT. We have therefore developed a process technique which allows selective etching of the small window (100 µm x 100 µm) into the contact metallization. The etching stops just at the silicon surface (Fig. 1) which ensures the proper functionality of the device.

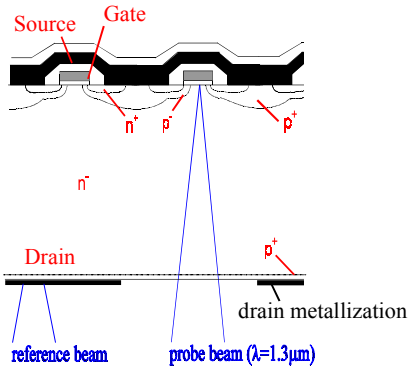

Fig. 1: Laserprobe method for the detection of the transient lattice heating in power devices. The probing laser beam (beam diameter of 8 µm) is focused through a small window in the drain contact on a single IGBT (or VDMOSFET) cell and is reflected from the polysilicon gate. The interferometer reference beam is placed at the metallization.

3. Experiments

In the experiments on VDMOSFETs, the amount of the transient lattice heating is controlled by applying pulses with different pulse levels from V_{GS} = 0 V to 8 V and 12 V and different pulse widths τ_H (5 µs to 60 µs) to the gate. The drain-to-source bias is held constant at V_{DS} = 15V. The transient drain current is monitored by a voltage drop across a resistor connected in series with the drain. The power dissipation in IGBTs is controlled by the drain-to-source voltage ranging from 50 V to 400 V. The device is switched by gate pulses of 15 V height and length of 10 µs. Here the transient current is measured inductively by means of a current probe. In both cases the pulse repetition frequency is chosen to 10 Hz, in order to enable total device cooling between subsequent pulses. Figure 2 shows typical results for the transient phase signal obtained from laserprobe experiments on VDMOSFET and IGBT. During the heating the phase signal increase is linear in time. After heating turn-off, the phase signal remains almost constant in the first 100 µs. In that case, the peak temperature decreases and simultaneously, the heat propagates into the silicon well. Therefore, the length where the temperature changes (the beam modulation length) increases. As the phase change is proportional to the integral of the temperature increase along the beam modulation length, the resulting phase signal is nearly constant.

Besides the thermo-optical effect, the phase of the laser beam is also modulated due to the free-carrier effect [2]. We have found that this effect can be neglected both in VDMOSFETs and IGBTs. Performing optical measurements on VDMOSFETs with

V_{DS} = 0 V and applying pulses to the gate (no device heating), the resulting phase signal is close to the detection limit of the measurement set-up. A similar experiment has been carried out on IGBT with a drain-to-source voltage of V_{DS} = 2 V. Even under this low power condition the thermally induced phase signal dominates and superimposes the free-carrier signal.

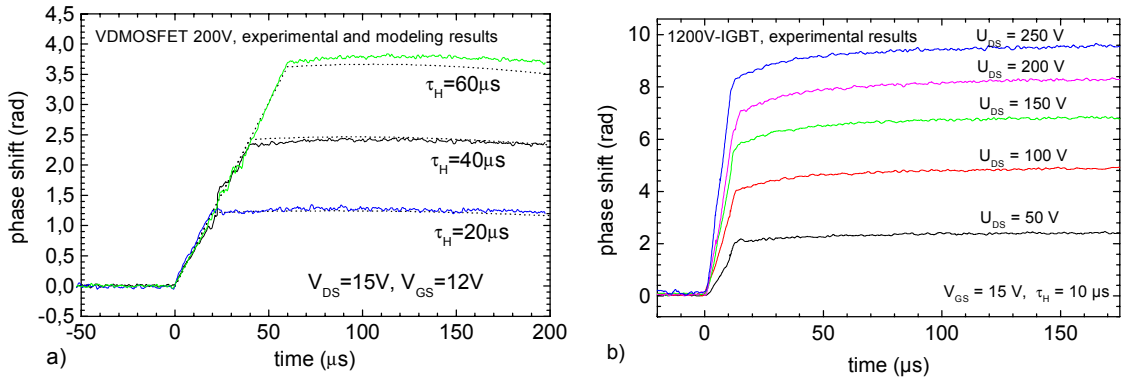

Fig. 2: Laser-probe measurement results for the time-resolved phase shift on a) 200V-VDMOSFET and b) 1200V-IGBT. Pulse widths t_H are indicated. The phase shift calculated for a value of the temperature coefficient of the refractive index of $dn/dT = 1.6 \cdot 10^{-4}\ K^{-1}$ of silicon is shown for VDMOSFET device (dotted line).

4. Numerical Modeling

The study of time dependence of the temperature in power devices requires modeling of the total chip consisting of several hundred cells including the chip package. To reduce the complexity of the model, we first analyzed the temperature distribution in a single VDMOSFET cell. The electrical characteristics of a single cell are calculated by a modified version of MINIMOS 6 [3]. The transient temperature profile is then obtained by numerically solving the 2-D heat conduction equation. The temperature distribution along the wafer depth (Fig. 3) at the center of the chip area is taken as input for modeling of the laser beam modulation.

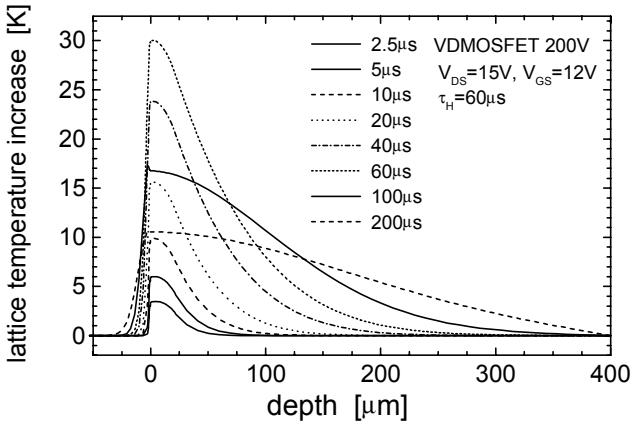

Fig. 3: Numerical modeling result of the transient temperature profile across the chip center (200V VDMOSFET).

The transient phase modulation signals are calculated by the application of the transmission-line model presented in [4], which has been extended including the lattice heating. The phase change obtained from the rigorous transmission line model is very close to that calculated from the temperature profile using a simple geometric optic approach. This implies that the geometric optic approach can be accurately used, which significantly reduces the complexity in the optical data interpretation. A direct comparison of the numerical modeling results and the phase shift from measurements is possible only if the exact value of the temperature coefficient of the refractive index of silicon (dn/dT) is known. On the other hand, assuming that accurate modeling results are provided, the dn/dT can be determined by the calibration of the experiments. For the purpose of the verification of numerical analysis, the channel temperature at various heating pulse widths τ_H is extracted from pulsed I-V measurements (Fig. 4).

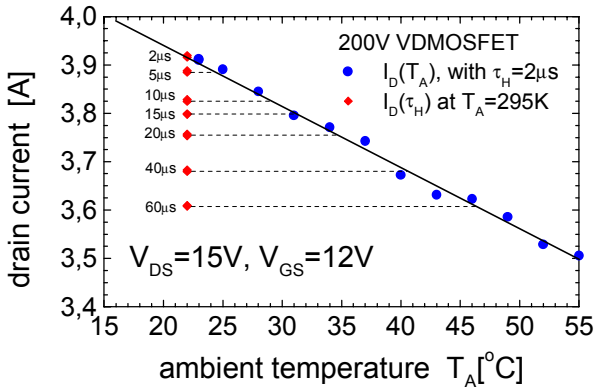

Fig. 4: Pulsed I-V measurements for the determination of the channel temperature for different heating pulse widths (200 V VDMOSFET). The channel heating at short pulses t_H = 2 µs (circles) at increased ambient temperature is used as a reference. From the decreased drain current due to self-heating with longer gate pulses (diamonds) the corresponding channel temperature is extracted.

The modeling results for the temperature close to the Si/SiO_2-interface correspond to the values obtained from the pulsed I-V measurements. As depicted in Fig. 4 for a heating

pulse width of τ_H = 60 µs, the temperature increase in the channel after 20 µs is extracted to ΔT = 12.5 K, in agreement with the calculated value of ΔT = 12 K. Quantitative matching of various modeling to measurement results of the transient phase shift at the end of the heating period results in a mean value across all samples of dn/dT = $1.6 \cdot 10^{-4}$ K^{-1}, where this result is very consistent with data from the literature [5]. Figure 2a shows a typical result for the calculated phase signal which is in good agreement with the experiment.

5. Conclusion

The backside laserprobe technique has been successfully applied to study the transient heating in power VDMOSFETs and IGBTs with a high temporal resolution. From the numerical analysis a 1-D thermal model combined with a geometric optic approach are found to be sufficient for the modeling of the phase modulation signals. From this study a value of dn/dT is obtained, which is the basis for quantitative studies of the critical thermal effects in such devices.

Acknowledgments

This work was partly supported by the "Bundesministerium für Wissenschaft und Forschung". The authors would like to thank Dr. G. Deboy (SIEMENS Munich) for providing IGBT samples and fruitful discussions.

References

[1] M. Goldstein, G. Sölkner and E. Gornik: "Heterodyne interferometer for the detection of electric and thermal signals in integrated circuits through the substrate", *Microelectr. Eng.*, Vol. 24, pp. 431 – 436, 1994.

[2] R. Soref and B. Benett: "Electrooptical effects in silicon", *IEEE J. Quantum Electr.,* Vol. QE-23, No. 1, pp.123 – 129, Jan. 1987.

[3] Group of authors: "MINIMOS 6 - User's guide", Institute for Microelectronics, TU Vienna, Austria, 1995.

[4] N. Seliger, P. Habaš and E. Gornik: "Modeling and measurements of backside laser-probe signals in MOSFETs", in *Proc. ESSDERC'95*, The Hague (NL), Sept. 1995, pp. 773 – 776.

[5] M. Bertolotti, V. Bogdanov, A. Ferrari, A. Jascow, N. Nazorova, A. Pikthin, L. Schirone, "Temperature dependence of the refractive index in semiconductors", *J. Opt. Soc. Am. B*., Vol. 7, No. 6, pp. 918 – 922, June 1990.

Project Information

Project Manager

Univ.-Prof. Dr. Erich GORNIK

Institut für Festkörperelektronik, Technische Universität Wien, A-1040 Vienna

Project Group

Last Name	First Name	Status	Remarks
Fürböck	Christoph	dissertation	
Gornik	Erich	university professor	
Habaš	Predrag	postdoc	
Pogany	Dionyz	guest scientist	
Seliger	Norbert	dissertation	

Publications in Reviewed Journals

1. N. Seliger, P. Habaš and E. Gornik: "A Study of Backside Laserprobe Signals in MOSFETs", *Microelectr. Eng.*, vol. 31, pp. 87 – 94, January 1996.
2. N. Seliger, P. Habaš and E. Gornik: "Time-Domain Characterization of Lattice Heating in Power VDMOSFETs by Means of an Interferometric Laserprobe Technique", Digest to the *European Solid State Device Research Conference (ESSDERC ´96)*, Bologna, Italy, 9 – 11 September 1996, p. 847.
3. N. Seliger, P. Habaš, A. Köck, D. Pogany and E. Gornik: "Backside Laserprobing of Transient Heating in Power VDMOSFETs", Digest to the *International Seminar on Power Semiconductors (ISPS ´96)*, Prague, Czech Republic, 11 – 13 September 1996, p. 115.
4. D. Pogany, N. Seliger, T. Lalinský, J. Kuzmík, P. Habaš, P. Hrkút and E. Gornik: "Study of Thermal Effects in GaAs Micromachined Power Sensor Microsystems by an Optical Interferometer Technique", Digest to the *International Workshop on Thermal Investigations of ICs and Microstructures (THERMINIC `96)*, Budapest, Hungary, 25 – 27 September 1996, p. 185.
5. D. Pogany, T. Lalinský, N. Seliger, J. Kuzmík, P. Habaš, P. Hrkút and E. Gornik: "Power Sensor Microsystems Characterization Using a Contactless Optical Laser Method", Digest to the *International Conference of Advanced Semiconductor Devices and Microsystems (ASDAM ´96)*, Smolenice, Slovakia, 20 – 24 October 1996, p. 201.
6. D. Pogany, N. Seliger, T. Lalinsky, J. Kuzmík, P. Habaš, P. Hrkút and E. Gornik: "Study of Thermal Effects in GaAs Micromachined Power Sensor Microsystems by

an Optical Interferometric Technique", to be published in *Microelectronics Journal*, 1997.

7. N. Seliger, P. Habaš, D. Pogany and E. Gornik: "Time-Resolved Analysis of Self-Heating in Power VDMOSFETs using Backside Laserprobing", submitted to *Solid State Electronics*, October 1996.
8. E. Burian, D. Pogany, T. Lalinský, N. Seliger and E. Gornik: "Thermal Simulation and Characterization of GaAs Micromachined Power Sensor Microsystems", submitted to *EUROSENSORS XI* conference, February 1997.

Presentations

1. N. Seliger: "Backside-Laserprober zur Charakterisierung integrierter Halbleiterbauelemente", oral presentation at SIEMENS Munich, Germany, 7.February 1996.
2. P. Habaš: "Analyse thermischer Effekte an Leistungs-MOSFETs und SOI-Bauelementen", oral presentation at SIEMENS Munich, Germany, 7 February 1996.
3. P. Habaš: "Characterisation of Semiconductor Devices by a Backside Laserprober Technique", oral presentation at TU Munich, Institute for Physics of Electrotechnology, Germany, 13 May 1996.
4. E. Gornik, P. Habaš, N. Seliger, D. Pogany, and C. Fürböck: "Characterization of Silicon Devices by a Laser Probe Technique", *Jahrestagung Österreichische Physikalische Gesellschaft (ÖPG)*, Linz, Austria, 24 September 1996.
5. P. Habaš: "Time-Resolved Characterisation of Semiconductor Devices by a Backside Laserprober Method", oral presentation at IMEC, Belgium, 25 November 1996.

Doctor's Theses

1. Norbert Seliger, "Backside-Laserprober zur Charakterisierung von Halbleiterbauelementen", in progress.
2. Christoph Fürböck, "Analyse kritischer thermischer Effekte in Leistungsbauelementen mittels Laserinterferometrie", in progress.

Cooperations

1. Siemens AG, Corporate Research and Development (ZFE T KM2), Munich, Germany, Prof. E. Wolfgang, Dr. M. Stoisiek, Dr. G. Deboy, Dr. G. Sölkner; Bereich Halbleiter Dr. S. Görlich.
2. Institute of Electrical Engineering, Slovak Academy of Sciences, Bratislava, Slovakia.
3. Lehrstuhl für Technische Elektrophysik, TU Munich, Germany, Prof. G. Wachutka.
4. Interuniversity Microelectronics Center (IMEC), Leuven, Belgium.

Single-Mode and Single-Beam Emission from Surface Emitting Laser Diodes Based on Surface Mode Emission

A. Köck, A. Golshani, R. Hainberger, P. O. Kellermann, E. Gornik
Institute of Solid State Electronics &
Center of Microstructure Research (MISZ), TU Wien,
A-1040 Vienna, Austria

L. Korte
Siemens AG, D-81730 München, Germany

Single-mode and single-beam emission has been achieved from surface emitting laser diodes based on the surface-mode-emission technique. By employing an optimized device design and a first-order grating coupler, the laser diodes show under pulsed operation condition a single-mode emission with a linewidth of 0.11 nm. A power up to 3.6 mW is emitted into a single, surface-emitted beam, which has a beam divergence of 0.20^{o}.

1. Introduction

The most important impact of laser diodes is the area of transmission systems for optical telecommunication, where single-longitudinal-mode (SLM) laser diodes are required to achieve a high transmission capacity and distance. Among the various types of single-mode laser diodes the distributed-Bragg-reflector (DBR) and the distributed-feedback (DFB) laser diodes are most commonly used and have been successfully employed in commercial transmission systems [1], [2]

By far most of the present SLM-laser diodes are conventional edge emitters, while many novel optoelectronic applications, like optical interconnects, optical computing and high power laser arrays, require surface emitting laser diodes. Various types of surface emitting laser diodes, like horizontal cavity lasers with 45°-mirrors, DBR and DFB-laser diodes with second order grating couplers, Master-Oscillator-Power-Amplifiers and Vertical Cavity Surface Emitting laser diodes have been developed so far [3] – [5].

We have presented a new concept based on the surface-mode-emission (SME) technique, which has been applied to realize a new type of surface emitting laser diode [6], [7]. In addition we have recently proposed this technique as flexible concept for a new type of SLM-laser diode [8]. A real single-mode emission from this type of laser diode, however, has not been achieved yet [9].

2. Experimental

We report on a single-mode and single-beam emission achieved from SME-laser diodes. Under pulsed operation condition a single-mode emission with a linewidth of 0.11 nm is achieved, while a power up to 3.6 mW is emitted into a single, surface-emitted beam with a beam divergence of 0.20^{o}. This has been achieved by an optimized device

geometry and by fabricating high-quality first-order gratings with an Ion-milling etching technique.

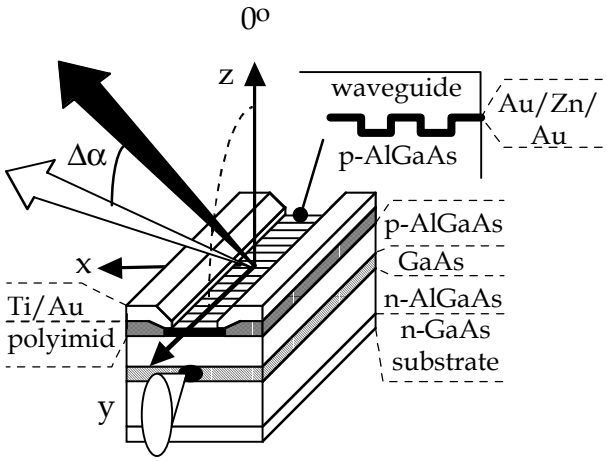

Fig. 1: Geometry of the SME-laser diodes. The surface grating is oriented in y-direction, while the laser stripe is oriented in x-direction. The window for the SME-coupling process has a width of 8 μm and extends over the whole length of the cavity.

The SME-technique is based on an interactive coupling between the laser light propagating in the active region of the laser diode and a transverse electrically polarized TE_0-surface mode propagating in a waveguide structure on top of the laser diode. This requires a special device geometry, which is shown in Fig. 1. The laser diode is a conventional GaAs/AlGaAs-double-hetero-structure grown by MOCVD. An n-AlGaAs cladding layer (thickness 1300 nm, 35% Al) is grown on a n-GaAs substrate followed by an undoped GaAs active region (thickness 90 nm). Next is a p-AlGaAs cladding layer (thickness 550 nm, 30% Al) with a highly doped p-GaAs cap layer (thickness 5 nm) on top. While in recent structures p-AlGaAs cladding layers with thickness of 700 nm and 900 nm were used, the thickness has been reduced to 550 nm in order to achieve an enhanced coupling between the laser light and the TE_0-surface mode. A first-order grating, which is holographically exposed in photoresist, is etched into the p-AlGaAs-top-cladding layer by ion-milling (grating period $\Lambda = 415$ nm, grating amplitude 100 nm). This etching technique has strongly improved the quality of the grating as compared to recent samples, where a wet-chemical etching process has been used. The evaporation of a semitransparent Au/Zn/Au metal stripe (50 Å/50 Å/200 Å) with a width of 12 μm oriented normal (x-direction) to the grating grooves (y-direction) defines the laser stripe. The single laser stripes are separated at a distance of 250 μm, the surface of the sample in between is isolated with polyimid. Ti-Au contact pads (500 Å/3000 Å), which overlap the laser stripe from both sides by 2 μm leaving a 8 μm wide window in the center of the laser stripe, are evaporated on the polyimid isolation. Next the laser stripe is spin-coated with photoresist (Hoechst AZ 6615, thickness 250 nm) forming a slab wave guide on top of the laser diode, which supports the TE_0-surface mode. Finally the laser bars are cleaved to a length between 400 μm and 600 μm.

Locally in the window the laser light is coupled to the TE_0-surface mode. In this experiment the window extends over the whole cavity length, while in recent experi-

ments the window (length 200 – 300 μm) was only a part of the cavity length. This increases the coupling efficiency from the laser light to the surface mode. Part of the laser light is scattered from the active region via the surface grating into the waveguide. The light is propagating in the waveguide as a zig-zag-wave, where part of the zig-zag-wave is scattered into air into the emission angle α resulting in efficient surface emission. In addition, part of the zig-zag-wave is scattered back into the active region providing a positive, wavelength selective feedback process, which can result in a single-mode emission. These coupling mechanisms have been discussed in detail in Ref. [8].

The corresponding far-field pattern in DC-operation is shown in Fig. 2. The farfield pattern is measured by scanning the laser diode along the laser stripe (x-direction) from one cleaved facet to the other. The sample emits the light into a single beam in an emission angle of -55.35°. The beam divergence in x-direction is less than 0.15°, while the beam divergence in the direction normal (y-direction) to the laser stripe is 8°. The intensity emitted per solid angle into the single beam is more than 15 times higher than the edge emitted intensity per solid angle, which demonstrates the high efficiency of the SME-technique. Presently a power up to 3.6 mW is emitted into the single beam, which is 15 % of the totally emitted power of 24 mW.

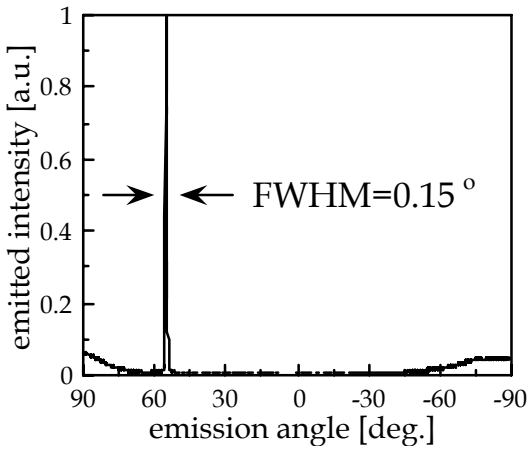

Fig. 2: The far-field pattern measured by scanning the laser diode along the laser stripe (x-direction) from one cleaved facet to the other. The SME-laser diode emits the light into a single beam in an emission angle of -55.35°. The beam divergence is less than 0.2o, a power up to 3.6 mW is emitted into this single, surface-emitted beam.

The SME-laser diodes show threshold current densities between 1.8 and 2 kA/cm^2. The wavelength emission spectrum of a SME-laser diode (threshold current I_{th} = 140 mA) in pulsed biased condition (pulse width 0.6 μsec, f = 40 kHz) at a current of 1.3 x I_{th} is shown in Fig. 3 (left). The sample shows a single-mode emission at λ = 874.08 nm with a full-width-half-maximum (FWHM) of 0.11 nm. The single-mode emission is maintained with increasing current, but the FWHM increases up to 0.17 nm at 1.6 x I_{th} and up to 0.27 nm at 1.8 x I_{th}. The right part of Fig. 3 shows the DC emission spectrum at a current of 205 mA. The laser diodes operates in a single-mode, the minimum linewidth achieved is 0.06 nm, the best side-mode-suppression-ratio is 24 dB.

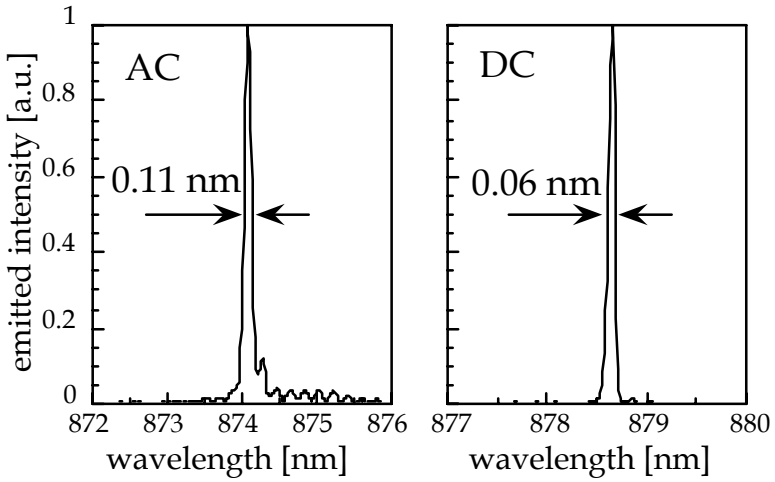

Fig. 3: Single-mode emission spectrum of a SME-laser diode in AC-condition (left) (pulse width 0.6 µsek, f = 40 kHz) at a current of 180 mA (= 1.3 x I_{th}) and in DC-operation at a current of 205 mA (right).

3. Discussion and Conclusion

The main advantage of the SME-type of laser diode as compared to surface emitting DBR- or DFB-laser diodes is a simple and flexible fabrication process. It utilizes the well-established technique of the conventional striped laser and requires no regrowth. The present performance of the SME-type of laser diode (relatively high threshold current densities (1.8 – 2 kA/cm^2), low output power) can be optimized by mirror-coatings: High-reflection mirrors on the cleaved facets will both decrease the threshold current density as well as increase the surface emitted power. The use of a quantum-well structure as active region instead of the double-hetero-structure should further decrease the threshold current density.

As has already been demonstrated [9], the emission wavelength (and so the emission angle) can be adjusted by the waveguide thickness and depends on the refractive index of the waveguide. This makes the SME-type of laser diode very suitable to be employed in practical applications: On one hand wavelength-division-multiplexing (WDM) techniques require on the transmitter side arrays of single-mode laser diodes, which emit at different, well-defined wavelengths. On the other hand WDM requires wavelength-tunable laser diodes on the receiver side for the heterodyne-detection-scheme [10]. The fabrication of laser bars containing laser diodes emitting at well-defined, different wavelengths (wavelength spacing $\Delta\lambda \sim 0.5 – 3$ nm) can be realized by processing adjacent SME-laser diodes with slightly different waveguide thickness ($\Delta d \sim 2 – 5$ nm). The use of an electro-optically active polymer, for example, as waveguide material will allow a continuous change of the waveguide's refractive index by applying an electric field across the waveguide. This would result in a continuous wavelength-tuning around a central wavelength primarily defined by the waveguide thickness. Thus SME-laser diodes have the potential to achieve both WDM-requirements. Therefore it is essential to apply the SME-technique to laser diodes operating in the 1.3 µm- and 1.5 µm-wavelength regime.

In addition due to their high beam quality, surface emitting SME-laser diodes can be employed as direct optical interconnects. For this specific application the steering of the surface emitted beam by tuning the emission wavelength is of high importance.

Acknowledgments

This work was also sponsored by the Stiftung Volkswagen, Hannover, Germany.

References

[1] J. Buus, "Single Frequency Semiconductor Lasers", Tutorial Texts in Optical Engineering, Vol. TT5, SPIE Optical Engineering Press (1991)

[2] T. Ikegama, in "Optoelectronic Technology and Lightwave Communications Systems", edited by C. Lin, Van Nostrand Reinhold, New York (1989)

[3] K. Iga and F. Koyama, in "Surface Emitting Semiconductor Lasers and Arrays", edited by G. A. Evans and J. M. Hammer, Academic Press, London (1993)

[4] D. Botez and D.R. Scifres, "Diode Laser Arrays", Cambridge University Press, New York (1994)

[5] N.W. Carlson, "Monolithic Diode-Laser-Arrays", Springer Verlag, Berlin, Heidelberg (1994)

[6] A. Köck, A. Seeberg, M. Rosenberger, E. Gornik, C. Thanner, L. Korte, Appl. Phys. Lett. 63, 1164 (1993)

[7] A. Köck, C. Gmachl, E. Gornik, M. Rosenberger, C. Thanner, and L. Korte, Appl. Phys. Lett. 64, 836 (1994)

[8] A. Köck, S. Freisleben, C. Gmachl, E. Gornik, M. Rosenberger, L. Korte, P. L. de Souza, Appl. Phys. Lett. 67, 452 (1995)

[9] A. Köck, A. Golshani, R. Hainberger, N. Finger, C. Gmachl, E. Gornik, L. Korte, Photonics West, OE/LASE'96, SPIE-Proceedings Vol. 2682, p. 169 (1996)

[10] J.E. Midwinter, Y.L. Guo, "Optoelectronics and Lightwave Technology", John Wiley & Sons, Chichester (1992)

Project Information

Project Manager

Dr. Anton KÖCK

Institut für Festkörperelektronik, Technische Universität Wien, A-1040 Vienna

Project Group

Last Name	First Name	Status	Remarks
Finger	Norman	dissertation	
Gianordoli	Stfan	student	
Golshani	Amir	dissertation	
Haider	Manfred	student	
Hainberger	Rainer	dissertation	
Kellermann	Peer Oliver	student	
Köck	Anton	assistent professor	
Maier	Thomas	dissertation	
Schrenk	Werner	student	

Publications in Reviewed Journals

1. C. Gmachl, A. Golshani, A. Koeck, E. Gornik; J.F. Walker, "Vertical-cavity surface-emitting lasers with monolithically integrated modulators" in *Microcavities and Photonic Bandgaps: Physics and Applications*; edited by John Rarity and Claud Weisbuch; *Nato ASI Series* vol. E 324; Kluwer Academic Publishers, Netherlands,p. 387 (1996)
2. A. Golshani, A. Koeck, S. Freisleben, C.Gmachl, E. Gornik, L. Korte, "Adjustable surface emission from AlGaAs/GaAs laser diodes based on first-order-grating-coupled surface mode emission", *Appl. Phys. Lett.* 69 (16), 2312 (1996)
3. A. Koeck, A. Golshani, R. Hainberger, E. Gornik; L. Korte, "Single-mode and single-beam emission from surface-emitting laser diodes based on surface mode emission", *Appl. Phys. Lett.*, 69 (24), 3638 (1996)
4. P.O.Kellermann, A. Golshani, A. Koeck, E. Gornik, H.P.Gaugel, R. Winterhoff, J. Kuhn, "Single-mode and single-beam surface emission from visible red GaInP/AlGaInP laser diodes'', to be published in *Appl. Phys. Lett*., 1997
5. A. Golshani, P.O. Kellermann, A. Koeck and E. Gornik and L. Korte, "Surface Emitting Laser Diode Array for Wavelength Division Multiplexing Based on Post Growth Adjustment of Surface Mode Emission", submitted to *Appl. Phys. Lett.* Feb. 1997

Presentations

1. A. Köck, C. Gmachl, A. Golshani, S. Freisleben, E. Gornik, "Oberflächen-emittierende Laserdioden", *Mauterndorfer Laserseminar*, 20 – 23 March 1996, Mauterndorf
2. A. Koeck, A. Golshani, R. Hainberger, N. Finger, C. Gmachl, E. Gornik; L. Korte, "Quasi-single-mode surface-emitting laser diodes based on surface mode emission", *SPIE Proc.* Vol. 2682 "Laser Diodes and Applications II" of *Photonics West*, pp.169 – 175, OE/LASE'96, USA, SPIE Optical Engineering Press (1996)
3. A. Golshani, R. Hainberger, S. Freisleben, A. Koeck, E. Gornik; C. Gmachl; L. Korte, "Efficient surface emitting AlGaAs/GaAs laser diodes based on first-order-grating-coupled surface mode emission", *Proceedings of the "European Gallium Arsenide and related III-V compounds application symposium"*, 3B4; Paris 5 – 7 June, 1996
4. A. Koeck, N. Finger, C. Gmachl, A. Golshani, R. Hainberger, E. Gornik; L. Korte, "Single-beam and single-mode emission from surface-emitting laser diodes based on surface mode emission", *Int. Conf. on Solid State Devices and Materials*, Yokohama 26-29 August, 1996 SSDM'96 Extended Abstracts pp. 858, (1996)
5. A. Golshani, A. Koeck, R. Hainberger, E. Gornik; L. Korte, "Single- beam emission from surface emitting laser diodes based on surface mode emission", *Proceedings of the "Conference on Lasers and Electro-Optics (CLEO)/Europe"*, pp. 28; 8 – 13 September 1996, Hamburg, Germany, 1996
6. A. Koeck, A. Golshani, R. Hainberger, E. Gornik; L. Korte, "Single- beam and single-mode emission from surface emitting laser diodes based on surface mode emission", *Proceedings of the "26th European Solid State Device Research Conference"*; pp. 541; 9 – 11 September 1996, Bologna, Italy
7. R. Hainberger, N. Finger, A. Golshani, A. Koeck, E. Gornik; J. F. Walker, "A new concept for a direct optical free-space interconnect without lenses", *Proceedings of the "26th European Solid State Device Research Conference"*; pp. 537; 9 – 11 September 1996, Bologna, Italy
8. A. Köck, "Oberflächenemittierende monomodige Laserdioden basierend auf dem Konzept der Oberflächenmodenkopplung", Preisträgervortrag, *46. Jahrestagung der Österreichischen Physikalischen Gesellschaft*, 23 – 27 September 1996, Linz
9. A. Köck, A. Golshani, N. Finger, E. Gornik; L. Korte, "Monomodige Einzelstrahlemission von oberflächenemittierenden Laserdioden basierend auf Oberflächenmodenkopplung (poster), *Photonik-Symposium der Volkswagen-Stiftung*, 7 – 9 October 1996, Schwäbisch Hall-Hessental, Germany
10. A. Koeck, A. Golshani, R. Hainberger, E. Gornik; L. Korte, "Single-beam and single mode emission from surface emitting laser diodes based on surface mode emission", *Proceedings of the "9th Annual Meeting IEEE Lasers and Electro-Optics Society"*; Vol. 1, pp. 125, 18 – 21 November 1996, Boston, MA, USA
11. A. Koeck, A. Golshani, R. Hainberger, E. Gornik; L. Korte, "Digital beam steering from surface emitting laser diodes based on surface mode emission", *SPIE Proc.* Vol. 3001 "In-Plane Semiconductor: from Ultraviolet to Mid-infrared" of *Photonics West '97*, OE/LASE'97, USA, SPIE Optical Engineering Press (1997)

Doctor's Theses

1. C. Gmachl, "Frequenzverstimmbare oberflächenemittierende Halbleiterlaserdioden mit vertikalem Resonator", TU Wien, 1996
2. N. Finger, "Herstellung von monomodigen oberflächenemittierenden Laserdioden im 1.5-Mikrometer Bereich", in progress
3. A. Golshani, "Herstellung von durchstimmbaren oberflächenemittierenden Halbleiterlasern", in progress
4. Th. Maier, "Integration von VCSELs und Photodetektoren", in progress

Cooperations

1. Siemens AG, Dr. Bernd Borchert and Dr. Lutz Korte, Otto Hahn Ring 6, 81739 Munich, Germany
2. Institut für Angewandte Chemie Berlin Adlershof e.V., Dr. Karl Pfeiffer, Rudower Chaussee, 12489 Berlin-Adlershof, Germany
3. Universität Stuttgart, 4. Physikalisches Institut, Pfaffenwaldring 57, Prof. Dr. M. H. Pilkuhn, 70569 Stuttgart, Germany
4. Universität Bremen, Institut für Festkörperphysik, Prof. Dr. D. Hommel, Bibliothekstraße, 28359 Bremen, Germany

Single Quantum Dots as Scanning Tunneling Microscope Tips

M. Hauser, J. Smoliner, C. Eder, G. Ploner, G. Strasser, E. Gornik

Institute of Solid State Electronics &
Center of Microstructure Research (MISZ)
TU Wien, A-1040 Vienna, Austria

We report the use of single quantum dot structures as tips on a scanning tunneling microscope (STM). A single quantum dot structure with a diameter of less than 200 nm and a height of 2 μm was fabricated by reactive ion etching. This dot was placed on a 40 μm high mesa and mounted on the tip of a STM. The topography of large structures such as quantum wires or gold test substrates is clearly resolved with such a tip. To check the transport properties of the tip, quantum dot arrays were fabricated on resonant tunneling double barrier structures using the same process parameters. Conventional tunneling spectroscopy clearly resolved the 0D states in our samples. Using a metal substrate as second electrode such STM tips can be used to perform high resolution energy spectroscopy on single dots and free standing wire structures.

1. Introduction

Recent advances in micro fabrication technology such as lithography, etching and epitaxial regrowth enabled a reduction of the dimensions of semiconductor devices in a way that tunneling processes in low dimensional systems (1D, 0D) can be studied. First experiments on 1D-1D and 1D-0D tunneling processes were carried out in ultra small, pillar shaped double barrier resonant tunneling diodes (DBRTDs) by Reed et al [1]. On such samples, the resonance structures in the tunneling current were assigned to resonant tunneling processes between 1D states in the emitter region and 0D states inside the quantum well defined by the two barriers [2]. In similar experiments, based on asymmetric DBRTDs, charging effects were also observed [3], [4]. Using a shallow etching process in combination with a side-gate, it was possible to adjust the 0D confinement by varying the gate voltage. The observed resonance structures in the tunneling current were assigned to Coulomb blockade effects [5], [6] as well as to ionized donor atoms [7]. Focused ion beam implantation can also be used to define structures containing quantum dots [8] . Using triple barrier RTDs as starting structure, tunneling processes in coupled quantum dot structures have also been investigated experimentally [9] and theoretically [10] – [12]. The fine structure of the current-voltage characteristic [13] in the above experiments can be explained by strong coupling between 1D subbands in the contact region and 0D states inside the quantum dots.

As main problem for all above sample structures, the formation of contacts to the quantum dots is difficult and requires planarization techniques and recess etching. Using the metal tip of a scanning tunneling microscope [14] as a mobile contact to single wires or quantum dots, however, this problem is overcome and even local tunneling spectroscopy on single wires can be performed [15], [16].

2. Experimental

In this paper we report an inverse approach to the above experiments and replace the metal tip of the STM by a single quantum dot on a high mesa. To test the resolution of such a tip, the topography of a gold substrate and also of a large quantum wire array was scanned. To check the electrical quality of the tip, conventional tunneling spectroscopy on double barrier resonant tunneling diodes was employed. The 0D states are clearly resolved in our samples demonstrating that such STM tips are an easy way to establish contacts to single dots and free standing wire structures.

To fabricate the tips, electron beam lithography on a double layer of PMMA / PMMA-MA copolymer resist, metallization and lift off were used to define a single gold dot on a GaAs substrate. Optical lithography and RIE (Ar, $SiCl_4$ and SF_6) was then used to define the mesa supporting the dot. Residual photoresist is also removed by this step. The mesa is then etched further by RIE (Ar, $SiCl_4$) processes using the small gold dot as etch mask to produce a thin pillar with 200 nm diameter and 2 μm height (Fig. 1).

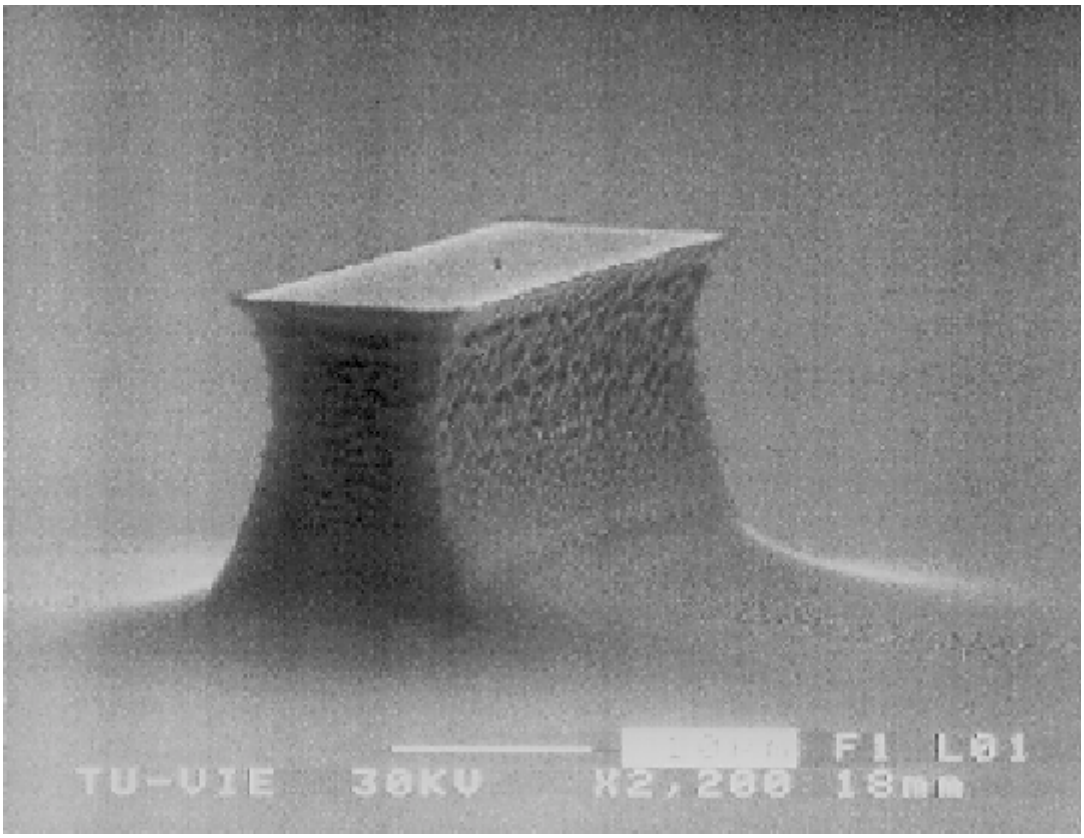

Fig. 1: The supporting mesa was defined by optical lithography and RIE. On top of it a single gold dot can be seen defined by electron beam lithography, metallization and lift off. The dot mask is etched into the mesa by further RIE processing to form a single quantum dot. This structure is then used to replace the metal tip of an STM.

This structure was mounted on the STM and used as a superfine STM tip to scan an array of wet chemically etched quantum wires. The result of this experiment is shown in Fig. 2.

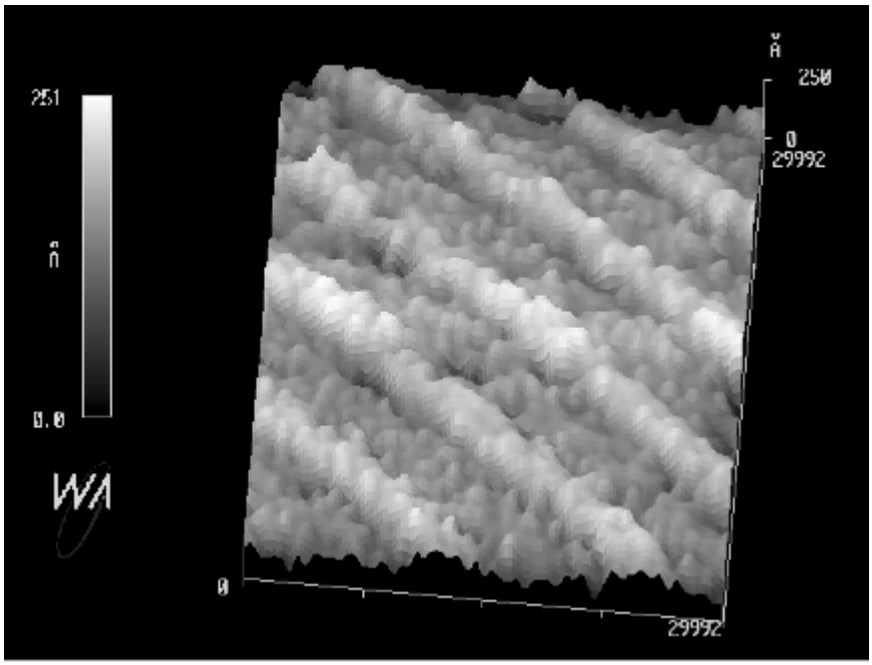

Fig. 2: Wet chemically etched quantum wires scanned with a STM. An etched quantum dot on a high supporting mesa was used as the tip of the STM.

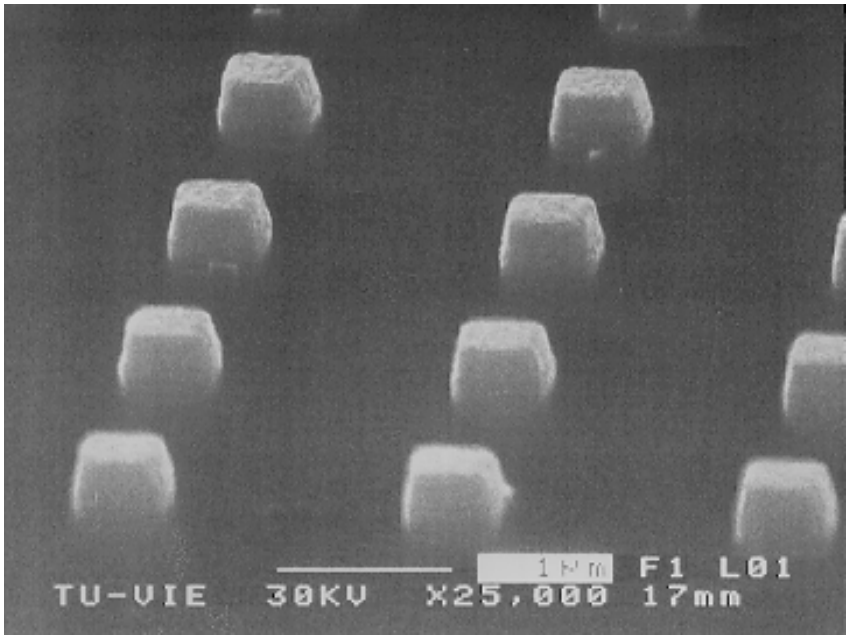

Fig. 3: Top contacts of quantum dots after planarization and recess etching by RIE. The metallized top contacts were used as an etch mask and form together with a second metallization a common top electrode for standard tunneling spectroscopy measurements.

To demonstrate that 0D levels are formed in the etched quantum dot we applied the same fabrication technology to standard RTD structures. An array of quantum dots planarized with resist, recess etched and metallized to form a top contact is shown in Fig. 3.

A bias voltage was applied to the quantum dots and the current through the dots was measured in liquid Helium by standard tunneling spectroscopy. Fig. 4 shows the obtained results. Resonant tunneling between 0D states and energy levels in the double barrier can clearly be seen in the current / voltage characteristic around -0.15 V, -0.35 V and -0.7 V. The resonances around -0.15 V are much better resolved in the derivative of the I/V characteristic.

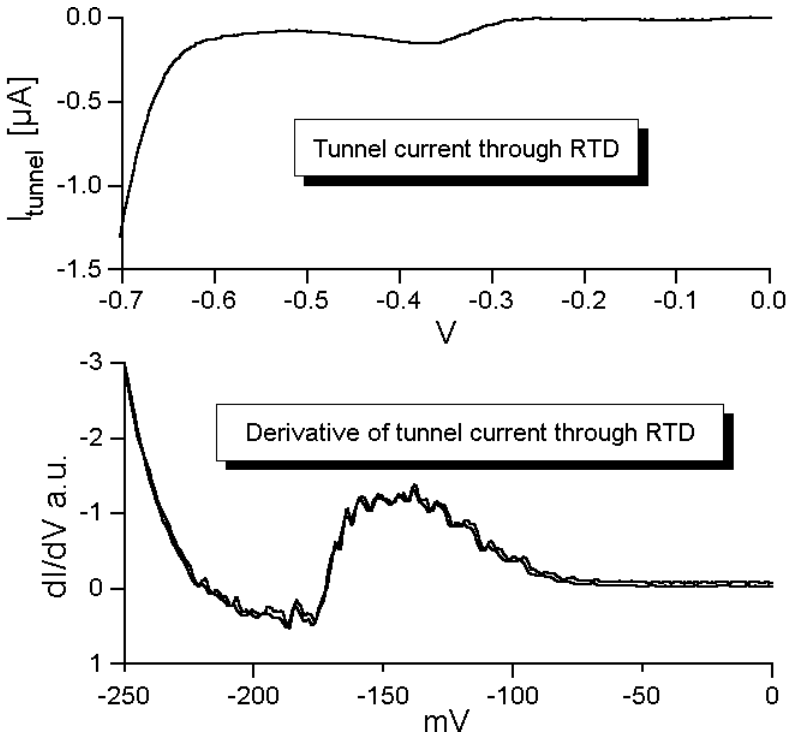

Fig. 4: Top image: IV characteristic of a RTD quantum dot array. Resonant tunneling through energy levels in the double barrier can be clearly resolved at bias voltages of 0.35 V and 0.7 V. Bottom image: Resonant tunneling through 0D energy levels can clearly be resolved in the derivative of the I/V characteristic around a bias voltage of 0.15 V. Similar resonances are also found at 0.35 V and -0.7 V.

3. Conclusion

In summary, we have used a single quantum dot structure as the tip of a STM. It was found that quantum dot structures with a diameter of less than 200 nm and a height of 2 µm form a very fine tip also suitable of scanning topographic profiles of other nanostructures such as quantum wires. Tunneling processes between low dimensional states on reference samples were also investigated in this configuration. For this purpose, quantum dot arrays were fabricated on resonant tunneling double barrier structures using the same process parameters than for the STM tips. In the RTD dot arrays, 0D states are clearly resolved by conventional tunneling spectroscopy. Thus, our method provides a simple way to for tunneling spectroscopy on single quantum dots, provided the STM is operated at low temperatures. As our STM can be operated in liquid helium [16], further experiments are in progress.

Acknowledgments

This work was also sponsored by Bundesministerium für Wissenschaft, Verkehr und Kunst and Jubiläumsfonds der Österreichischen Nationalbank).

References

[1] M.A. Reed, J.N. Randall, R.J. Aggarwal, R.J. Matyi, T.M. Moore, A.E. Wetsel, Phys. Rev. Lett. 60, 535 (1988).

[2] M. Boero, J.C.Inkson, Phys. Rev.B 50, 2479, (1994)

[3] Bu Su, V.J. Goldman, J.E. Cunningham, Science 255, 313 (1992)

[4] M.Tewordt, L. Martin-Moreno, J.T. Nichols, M. Pepper, M.J. Kelly, V.J. Law, D.A. Ritchie, J.E.F. Frost, G.C.A.Jones Rev. B 45, 14407, (1992)

[5] M. Tedwordt, L. Martin-Moreno, J.T. Nicholls, M. Pepper, M.J. Kelly, V.J. Law, D.A. Ritchie, J.E.F. Frost, G..A.C. Jones, Phys. Rev. B 45, 14407 (1992)

[6] P. Guéret, N. Blanc, R. Germann, H. Rothuizen, Phys. Rev. Lett. 68, 1896 (1992)

[7] M.W. Dellow, P.H. Beton, C.J.G.M. Langerak, T.J. Foster, P.C. Main, L. Eaves, M. Henini, S.P. Beaumont and C.W.D. Wilkinson, Phys. Rev. Lett. 68, 1754 (1992).

[8] S. Tarucha, J. Tokuta, Y. Hirayama, Rev. B 43, 9373, (1991)

[9] M. Tewordt, H. Asahi, V.J. Law, R.T. Syme, M.J. Kelly, D.A.Ritchie, A. Churchill, J.E.F. Frost, R.H. Huges, G.C.A. Josnes, Appl. Phys. Lett., 50, 413, (1987)

[10] C.Y. Fong, J.S. Nelson, L.A. Hemstreet, R.F. Gallup, L.L. Chang, L. Esaki, Phys. Rev. B 46, 9538 (1992)

[11] Zhen Li Ji, Phys. Rev.B 50, 4658 (1994)

[12] M. Tedword, R.J.F. Huges, L.M. Moreno, J.T. Nicholls, H. Asahi, M.J. Kelly, V.J. Law, D.A. Ritchie, J.E.F. Frost, G.A.C. Jones, M. Pepper, Phys. Rev. B 49, 8071, (1994)

[13] G.W. Bryant, Phys. Rev. B 44, 12838, (1991)

[14] G. Binnig, G. Rohrer, Ch. Gerber, E. Weibel, Phys. Rev. Lett. 49, 57 (1982)

[15] C. Eder, J. Smoliner, Appl. Phys. Lett. 68, 2876 (1996)

[16] J. Smoliner, C. Eder, G. Böhm, G. Weimann, Appl. Phys. Lett. 69, 52 (1996)

Project Information

Project Manager

Dr. Jürgen SMOLINER

Institut für Festkörperelektronik, Technische Universität Wien, A-1040 Vienna

Project Group

Last Name	First Name	Status	Remarks
Eder	Claudia	dissertation	
Hauser	Markus	postdoc	
Heer	Rudolf	dissertation	
Prinzinger	Johannes	technician	
Smoliner	Jürgen	assistant professor	

Publications in Reviewed Journals

1. C. Eder, J. Smoliner, "Local barrier heights on quantum wires determined by ballistic electron emission spectroscopy", *Appl. Phys. Lett.* 68, 2876 (1996)
2. J. Smoliner, C. Eder, G. Böhm, G. Weimann, "Low temperature current imaging spectroscopy on wet chemically etched quantum wires", *Appl. Phys. Lett.* 69, 52 (1996)
3. J. Smoliner, C. Eder, G. Strasser, G. Böhm, G. Weimann, "STM studies on quantum wire structures in air and liquid helium", *Superlattices and Microstruct.* Vol. 20, 261, (1996) (Proc. NANOMES 96 Symposium, SantaFe)
4. C. Eder, J. Smoliner, G. Strasser, "BEEM Studies on GaAs-AlGaAs quantum wire structures", *Superlattices and Microstruct.* Vol. 20, 357, (Proc. NANOMES 96 Symposium, SantaFe)
5. M. Hauser, J. Smoliner, C. Eder, G. Ploner, G. Strasser, E.Gornik, "Single Quantum Dots as Scanning Tunneling Microscope Tips", to be published in *Superlattices and Microstructures* (1996) (Proc. NANOMES 96 Symposium, SantaFe)
6. C. Eder, J. Smoliner, G. Böhm, G. Weimann, "Room temperature current imaging tunneling spectroscopy of GaAs/AlGaAs quantum wires at ambient pressure", *Semicond. Sci. Technol.* 11, 1239, (1996)
7. C. Eder, J. Smoliner, G. Strasser and E. Gornik, "Ballistic electron emission microscopy in liquid helium using low dimensional collector electrodes", *Appl. Phys. Lett.* 69, 1725, (1996)

Presentations

1. C. Eder, J. Smoliner, G. Strasser, “Low temperature BEEM studies on quantum wires fabricated on GaAs-AlGaAs heterostructures”, *ICPS23*, Berlin (1996)
2. M. Hauser, J. Smoliner, C. Eder, G. Ploner, G. Strasser, E.Gornik, “Single Quantum Dots as Scanning Tunneling Microscope Tips”, *NANOMES 96 Symposium*, SantaFe
3. C. Eder, J. Smoliner, G. Strasser, “BEEM Studies on GaAs-AlGaAs quantum wire structures”, *NANOMES 96 Symposium*, SantaFe
4. J. Smoliner, C. Eder, G. Strasser, G. Böhm, G. Weimann, “STM studies on quantum wire structures in air and liquid helium”, *NANOMES 96 Symposium*, SantaFe
5. C. Eder, J. Smoliner, G. Strasser, and E. Gornik, “Low Temperature Ballistic Electron Emission Microscopy Studies on GaAs/AlGaAs Heterostructures”, *SXM2 Workshop*, Vienna (1996)

Doctor’s Theses

1. C. Eder, “Raster-Tunnelspektroskopie an Halbleiterstrukturen im Nanometer-bereich”, in progress
2. R. Heer, “STM-Untersuchungen an Nanostrukturen”, in progress

Habilitations

1. J. Smoliner, “Current Transport in Nanostructures” , TU Wien, 1996

Cooperations

1. B. Etienne, Centre National de la Recherche Scientific, Laboratoire de Microstructures edt de Microelectronique (L2M), 196. av. H.Ravera, B.P.107, 92225 Bagneux, Cedex, France

Ballistic Electron Spectroscopy of Semiconductor Heterostructures

C. Rauch, G. Strasser, K. Unterrainer, E. Gornik

Institut für Festkörperelektronik, TU Wien
A-1040 Vienna, Austria

We present a study of ballistic electron transport in GaAs/GaAlAs with different well widths under given bias conditions. A three terminal device is used to inject an energy tunable electron beam via a tunneling barrier into an undoped superlattice and to collect the transmitted current as a function of the injection energy. Significant increase of the collector current is observed due to miniband conduction in the superlattice. Due to the localization of the electron wave function in biased superlattices, the quasi-continuous miniband breaks up into a ladder of discrete Wannier Stark states. The results are compared to calculations based on an envelope function approximation using a transfer matrix method. In order to resolve the discrete Wannier Stark states, a Four Terminal Device (FTD) is designed.

1. Introduction

Decreasing the barrier thickness of multiple quantum well structures leads to a stronger coupling between the degenerate eigenstates in the wells and thus to the formation of superlattice (SL) minibands. For these strongly coupled quantum wells the electronic states are extended. Applying an electric field in the direction perpendicular to the layer planes leads to a reduction of the interwell coupling and localizes the electronic states into a finite number of periods. This splitting of the quasi-continuous miniband into a ladder of discrete Wannier Stark states has direct consequences on the ballistic electron transport properties.

A hot electron transistor [1] is used to probe the superlattice transmittance. In such three terminal devices, an energy tunable electron beam is generated by a tunneling barrier, passes the superlattice after traversing a thin highly doped GaAs (base) and an undoped drift region. Having the possibility to drive the injected current and the electric field applied to the superlattice independently, the transmittance can be measured directly at given superlattice biases. The probability for an injected hot electron to cross the superlattice reflects the transmittance of the miniband and can be considered to be proportional to the measured transfer ratio $\alpha = I_C/I_E$.

2. Device Fabrication

Our samples, grown by molecular beam epitaxy (MBE), have the following common features: A highly doped n^+-GaAs collector contact layer ($n = 1x10^{18}$ cm^{-3}) is grown on a semiinsulating GaAs substrate. Followed by a superlattice and the drift regions which are slightly n-doped (~$5x10^{14}$ cm^{-3}), in order to avoid undesired band bending. To reduce quantum mechanical confining effects originating from the quantum well formed by the emitter barrier and the superlattice the drift region is chosen to be at least 200 nm

in width. This is followed by a highly doped ($2x10^{18}$ cm^{-3}) n^+-GaAs layer (base) of 13 nm width. As found in previous experiments [2], about 75% of the injected electrons traverse the base ballistically. On top of the base layer a 13 nm undoped $Ga_{0.7}Al_{0.3}As$ barrier is grown followed by a spacer and an n^+-GaAs layer, nominally doped to $n = 3x10^{17}$ cm^{-3}, in order to achieve an estimated normal energy distribution of injected electrons of about 15 meV [3]. It should be noted that the half width of the injected electron beam limits the energy resolution of the experiment. Finally, an n^+-GaAs contact layer ($n = 1x10^{18}$ cm^{-3}) is grown on top of the heterostructure to form the emitter. Four different superlattices have been studied with $Ga_{0.7}Al_{0.3}As$ barriers (2.5 nm) and GaAs wells, with varying widths (6.5 nm, 8.5 nm, and 15 nm) and periods (see table 1).

sample #	well (nm)	periods	Δ_{01}(meV)	Δ_{MB1}(meV)	Δ_{12}(meV)	Δ_{MB2}(meV)
1	6.5	5	46	22	114	94
2	8.5	5	33	13	85	53
3	15	5	14.5	3.5	40	14
4	6.5	10	46	22	114	94

Table 1: Summary of the superlattice tunneling structures investigated. Δ_{MB1} and Δ_{MB2} denote the widths of the first and of the second miniband, Δ_{01} the energy position of the first miniband with respect to the conduction band edge and Δ_{12} denotes the width of the minigap between the first and the second miniband.

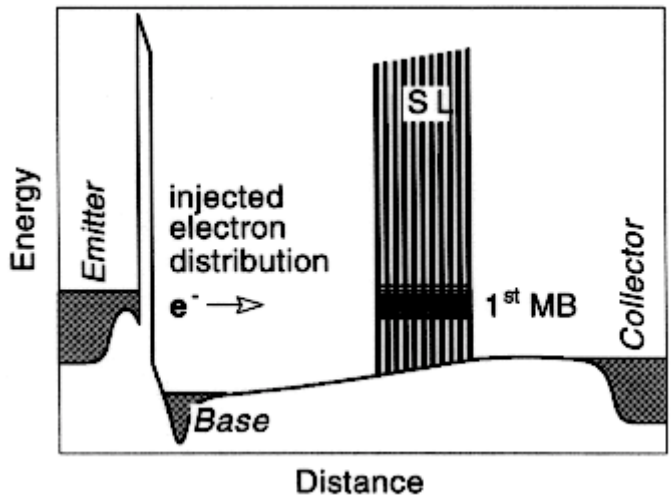

Fig. 1: Conduction band diagram under typical bias conditions.

The fabrication of the three terminal device includes the following steps: $SiCl_4/SF_6$ reactive ion etching (RIE), unselective etching to the collector layer, metallization of the AuGeNi ohmic contacts, Si_3N_4 isolation of the emitter mesa (PECVD), and finally the metallization of the CrAu bonding pads. More details can be found elsewhere [4].

The spatial profile of the bottom of the conduction band along the growth direction under typical bias conditions, as calculated by a Poisson solver, is shown in Fig. 1. All measurements are done in common base configuration at 4.2 K.

3. Results and Discussion

3.1 Unbiased Superlattices

Under flat band conditions the eigenstates of the periodic structure are expected to be extended over the entire length of the superlattice. Using the concept of a hot electron transistor the transmittance of an undoped field free superlattice, grown in the drift region between base and collector, is measured directly. To investigate the superlattice properties and to confirm the results of the measured transfer ratio $\alpha = I_C/I_E$, three superlattice structures with different well widths are measured.

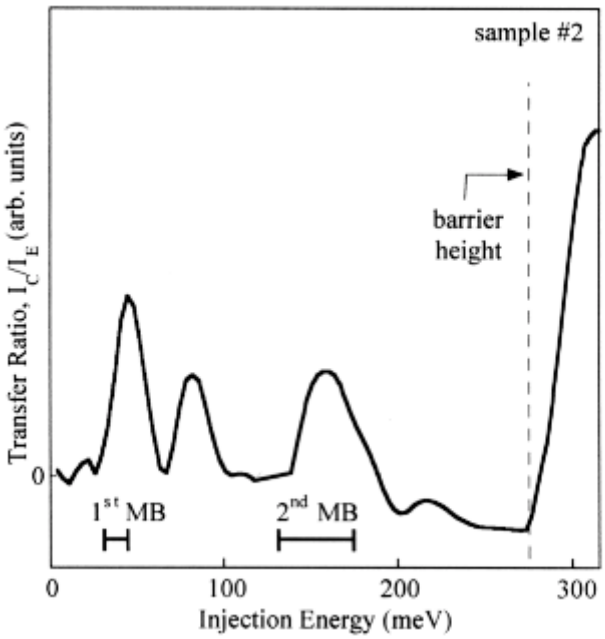

Fig. 2: The transfer ratio $\alpha = I_C/I_E$ versus injection energy ($\approx e.U_{EB}$) of sample #2. The calculated miniband positions are indicated by bars (├──┤).

The static transfer ratio of sample 2, $\alpha = I_C/I_E$, plotted in Fig. 2 as a function of the injection energy, shows several maxima and a sharp rise at 280 meV. No current is observed below the energy of the first peak. The position of the first peak coincides very well with the first miniband. Thus, we claim that the first peak is due to miniband transport through the lowest miniband. For energies higher than the first miniband the transfer ratio drops quite significantly since there is no transport possible through the forbidden minigap of the SL. The second observed peak is shifted 36 meV to higher injection energies and is ascribed to the first LO-phonon emission replica ($\hbar\omega_{LO}$ = 36 meV) of the injected electron distribution. The relative position in energy and width are equal to that of the first peak. The energy range of electrons injected at voltages corresponding to this second peak is in the forbidden band and no contribution is expected

from electrons which have not lost energy due to optical phonon emission. The peak at 150 meV represents transport through the second SL miniband. For an analysis of the observed features we compare the experimental data with the theoretically calculated miniband positions. The calculated positions and widths of the first and second miniband are indicated by bars. The sharp rise of the transfer ratio at 280 meV is due to the transition to continuum. This energy, which corresponds to the conduction band offset of the superlattice barriers, gives us a confirmation of the AlAs mole fraction of the AlGaAs compound.

In Fig. 3 we show the transfer ratio α as a function of the injection energy for three samples with different well widths at lower injection energies. There is a clear shift of the peaks to higher energies with decreasing superlattice well width. The calculated miniband positions are again indicated by bars as in Fig. 2. It can be seen that the tunneling data agree very well with the self constant solution of the Schroedinger equation. Note that it is possible to resolve even very narrow minibands at low energies as seen for sample 3.

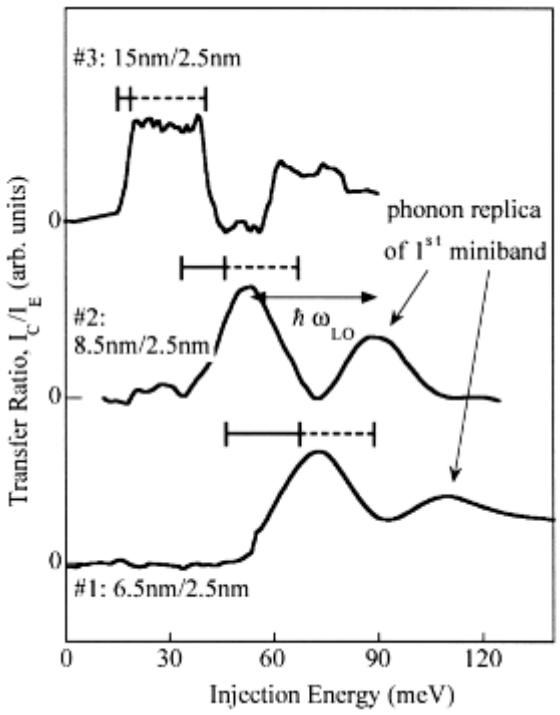

Fig. 3: Transfer ratio α versus injection energy for all three samples (├──┤ indicates the calculated miniband position, ├ ─ ┤ indicates the broadening due to the energy distribution of the injected electron beam). A double arrow represents the energy of a longitudinal optical phonon ($\hbar\omega_{LO}$ = 36 meV).

Due to the broadened energy distribution of the injected electrons, the peaks corresponding to ballistic transfer through the first miniband are broadened as well. The shape of the energy distribution is investigated using a three terminal device with a resonant tunneling diode grown in the drift region which acts as an energy filter of the injected electrons [5], [6]. Thus we are able to measure directly the injected normal energy distribution. It can be seen that this energy distribution is not symmetric and the

broadening takes place mainly at the low energy side. This low energy tail of the injected electron beam is indicated by dashed bars in Fig. 3.

3.2 Biased Superlattices — Breakdown of the Extended Electron Wave Function

The splitting of minibands in biased superlattices has direct consequences on the ballistic electron transport properties. Due to the localization of the electron wave function, the quasi-continuous miniband breaks up into a ladder of discrete Wannier-Stark states [7].

The transfer ratio of a biased 10 period superlattice (sample 4) was studied and compared with a theoretical transfer matrix calculation. The structure under investigation is except the number of periods similar to the structure described above.

The measured transfer ratio α as a function of the normal electron injection energy at different collector-base biases is shown in Fig. 4. It can be seen that the onset of the transfer ratio shifts with the applied collector-base bias since the lower edge of the first miniband shifts with the superlattice bias. The observed transfer ratio decreases quit dramatically with the applied electric field. Longitudinal optical phonon replicas, which are shifted 36 meV to higher injection energies, can be observed at all biases.

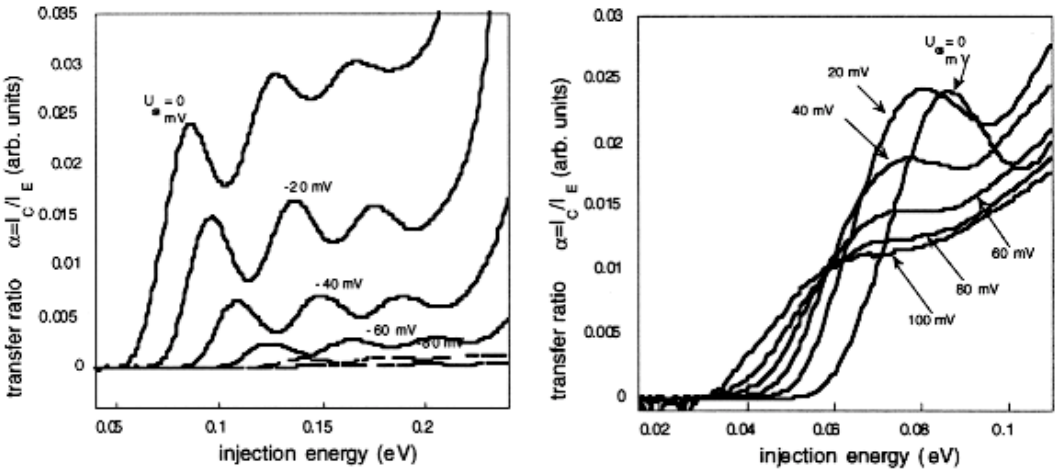

Fig. 4: Measured transfer ratios at different collector-base bias vs. injection energies

Figure 5 shows the transfer ratio at peak position of the investigated superlattice versus applied electric field. The maximum transmission can be observed at zero bias voltage, since all superlattice states are extended over the total superlattice dimension. Applying an electric field leads to a decrease of the transmission due to the localization of the lowest and uppermost superlattice states i.e. these states do not contribute to the ballistic transport any more. The transfer ratio of the superlattice vanishes for an applied electric field of about 5 kV/cm. This is in good agreement with the simple estimate of the localization length $\lambda \approx \Delta/eF$ (Δ is the miniband width, and F the applied electric field) which decreases to about half of the total superlattice length at this bias.

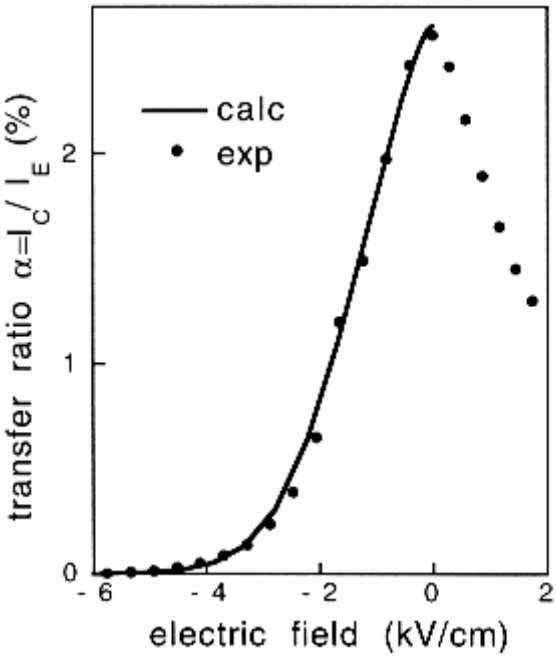

Fig. 5: Measured (dots) and calculated (line) transfer ratio vs. electric field.

In addition, we perform theoretical calculations based on a transfer matrix method using an envelope function approximation [8]. The solid line in Fig. 5 shows the result of such calculation for the measured structure. We find an excellent agreement between our experimental results and the quantitative theoretical prediction.

For the first time, the miniband positions, widths, and the collapse of the superlattice states under the influence of an applied electrical field using the technique of hot electron spectroscopy is observed directly.

3.3 Four Terminal Device (FTD)-Detection of Plasmon Emission

A new four terminal device is developed including a resonant tunneling diode as an injector in order to decrease the width of the injected electron distribution. As the resonant condition of the injector resonant tunneling diode is set, we are able to tune the injected sharp electron beam. This device is used to observe directly the relaxation of hot carriers via plasmon emission in a low doped ($n = 3x10^{17}$ cm^{-3}) GaAs drift region which is contacted to the ground in order to avoid undesired charging in this drift region.

In between this low doped drift region and the collector an analyzer resonant tunneling diode is grown. A SEM picture of the device is shown in Fig. 6. A schematic sketch of the band diagram is shown in the inset of the figure. The four terminal device is also being considered as a structure which allows the possibility to set up conditions for the beam plasma instability leading to local oscillations of charge densities and consequently to an emission of radiation in the THz range.

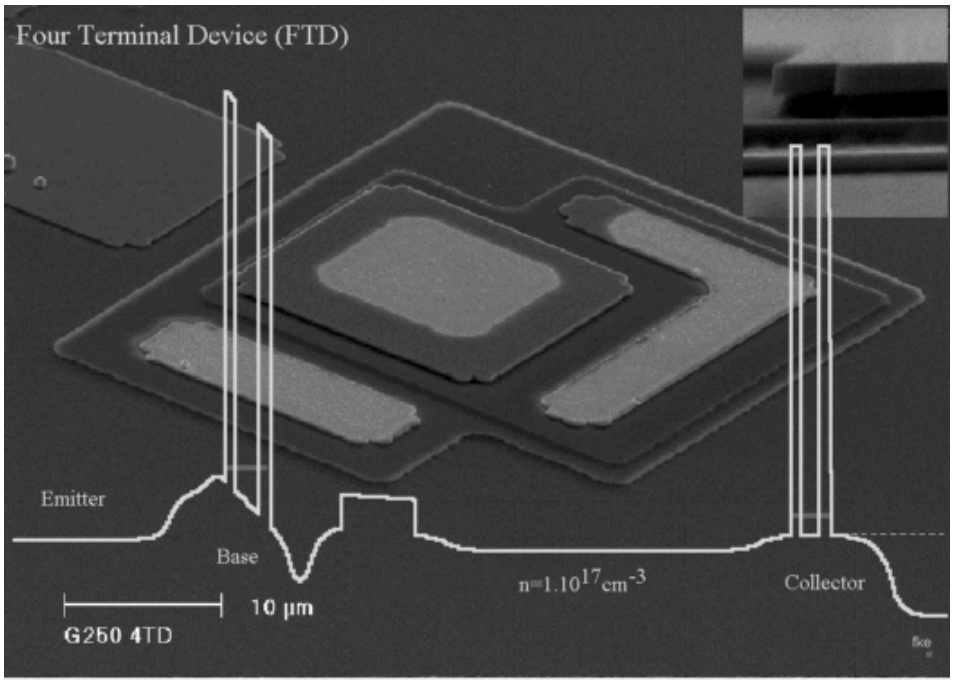

Fig. 6: SEM picture of the Four Terminal Device (FTD). The inset shows the conduction band structure.

In addition the four terminal device design is used to resolve the single Stark states of a short period superlattice, since the injected electron distribution is much narrower than the spacing between the single states.

4. Conclusion

In summary, direct experimental current spectroscopy of minibands in undoped superlattices is demonstrated using the technique of hot electron spectroscopy. Miniband widths and gaps of different unbiased superlattices are investigated and compared to the results of a self-consistent Schroedinger calculation. Applying an electric field to the superlattice the quasi-continuous miniband splits up into a discrete ladder of Stark states, and consequently the transmission of ballistic electrons decreases. The measured transfer ratio at different bias conditions is in excellent agreement to the theoretical calculation based on a transfer matrix method using an envelope function approximation. For the first time, the collapse of the superlattice electron states under the influence of an electrical field is observed directly in transport.

In order to increase the resolution of the experiment and in order to measure the relaxation of hot carriers via plasmon emission, a four terminal device (FTD) is designed and fabricated.

Acknowledgment

We are very grateful to K. Kempa for his calculations of the transmission of superlattices and for many helpful discussions. This work was partly supported by the Austrian Federal Ministry of Science, the Society for Microelectronics (GMe, Austria), and the European Research Office (project N68171-96).

References

[1] M. Heiblum, M.I. Nathan, D.C. Thomas, and C.M. Knoedler, Phys.Rev.Lett. **55,** 2200 (1985)

[2] B. Brill, to be published (1997).

[3] S. Bending, A. Peck, J. Leo, K.v. Klitzing, P. Gueret, and H.P. Meier, Solid-State Electronics **32**, 1161 (1989).

[4] C. Rauch, G. Strasser, K. Unterrainer, and E. Gornik, Appl. Phys. Lett. **70**, 649 (1997); B. Brill and M. Heiblum, Phys. Rev. B **49**, 14762 (1994)

[5] G. Strasser, C. Rauch, and E. Gornik, "Normal energy distribution of a tunneling injector", to be published

[6] M. Heiblum and M.V. Fischetti, IBM J. Res. Develop. **34**, 530 (1990).

[7] G.H. Wannier, Elements of Solid State Theory (Cambridge University Press, London, 1959), pp. 190-193.; L. Esaki, and R. Tsu, IBM J. Res. Dev. **14**, 61 (1970).

[8] G. Bastard, Phys. Rev. B **24**, 5693 (1983).

Project Information

Project Manager

Dr. Gottfried STRASSER

Institut für Festkörperelektronik, Technische Universität Wien, A-1040 Vienna

Project Group

Last Name	First Name	Status	Remarks
Hvozdara	Lubos	dissertation	25% GMe funding
Kröll	Peter	technician	
Rauch	Christoph	dissertation	
Strasser	Gottfried	assistant professor	

Publications in Reviewed Journals

1. T.P. Sosin, W. Treciakowski, M. Leszczynski, G. Strasser, "Biaxial Deformation Effects in Quantum Wells", *Proc. ICPS23*, Berlin (1996)
2. W. Boxleitner, C. Rauch, G. Strasser, L. Hvozdara, E. Gornik, U. Meirav, V. Umansky, H. Shtrikman, "Electron Dynamics and Band Structure in high Quality GaAs/AlGaAs Superlattices", *Proc. ICPS23*, Berlin (1996)
3. C. Rauch, G. Strasser, K. Unterrainer, L. Hvozdara, W. Boxleitner, E. Gornik, "Hot Electron Spectroscopy of undoped GaAs/GaAlAs superlattices", *Proc. ICSMM9*, Liege (1996); (to be published in Superlattices and Microstructures)
4. C. Rauch, G. Strasser, K. Unterrainer, B. Brill, E. Gornik, "Ballistic Electron Spectroscopy of Vertical Superlattice Minibands", *Appl. Phys. Lett.* 70 (5), 1997
5. W. Heiss, B.N. Murdin, C.J.G.M. Langerak, S.-C. Lee, G. Strasser, C.R. Pidgeon, I. Galbraith, E. Gornik, M. Helm, "The LO-phonon bottleneck in the intersubband cooling in wide quantum wells", *Proc. ICPS23*, Berlin (1996)
6. B.N. Murdin, W. Heiss, C.J.G.M. Langerak, S.-C. Lee, I. Galbraith, G. Strasser, E. Gornik, M. Helm, C.R. Pidgeon, "Direct observation of the LO phonon bottleneck in wide GaAs/AlGaAs quantum wells", *Phys. Rev. B* 55, 5171 (1997)

Presentations

1. C. Rauch, G. Strasser, K. Unterrainer, L. Hvozdara, W. Boxleitner, E. Gornik, "Hot electron spectroscopy of undoped GaAs/GaAlAs superlattices", *9th Int. Conf. on Superlattices, Microstructures and Microdevices*, 14 – 19 July 1996, Liege, Belgium

2. C. Rauch, G. Strasser, M. Heiblum, E. Gornik, “Ballistische Elektronen-Spektroskopie von Minibändern in GaAs/AlGaAs Übergittern”, *ÖPG Jahrestagung* 23 – 27 September 1996, Linz
3. C. Rauch, G. Strasser, K. Unterrainer, E. Gornik, “Breakdown of the electron wave function in biased superlattices”, *Workshop on Periodic Structures*, 27 – 31 January 1997, Les Houches, France
4. T.P. Sosin, W. Treciakowski, M. Leszczynski, G. Strasser, “Biaxial Deformation Effects in Quantum Wells”, *Proc. ICPS23*, Berlin (1996)

Doctor’s Theses

1. Ch. Rauch, “Emission von Halbleiterstrukturen”, in progress

Cooperations

1. Sub-Micron Center, Weizmann Institute, Rehovot, Prof. M. Heiblum
2. Plansee AG, Reutte, Dr. Willhartitz
3. EPI MBE Components, St. Pauls, Minnesota, USA
4. Boston College, Dep. of Physics, Boston, Massachusetts, USA, Prof. K.Kempa

Microelectronics Technology — Cleanroom Linz

Microstructure Research: Cleanroom Linz

G. Bauer, H. Heinrich, H. Thim

Institut für Halbleiterphysik, Abteilung Festkörperphysik des Instituts für Experimentalphysik, and Institut für Mikroelektronik, Johannes Kepler Universität Linz, A-4040 Linz, Austria

The main activities in the two cleanrooms in Linz supported by the GMe are described. The main research areas are the molecular beam epitaxy growth of Si based heterostructures, the MBE growth of selenides and of tellurides, as well as the MOCVD growth of GaAs based heterostructures for microwave device applications. Several in-situ as well as ex-situ characterization methods like reflection high energy electron diffraction, UHV scanning tunneling microscopy, Auger electron microscopy are used to establish the structural quality of the epitaxial layers. Lateral patterning by photolithography, electron beam lithography and reactive ion etching is used for the fabrication of low dimensional structures as well as for device research.

1. Nanofabrication of II-VI Heterostructures and of Si/SiGe Quantum Well Structures and Their Characterization

(G. Brunthaler, A.A. Darhuber, H. Straub, J. Stangl, Yan Zhuang, S. Zerlauth, T. Grill, G. Bauer)

Nanostructures defined by holographic lithography or by electron beam lithography were fabricated by reactive ion etching methods. In II-VI heterostructures like CdZnSe/ZnSe photoluminescence of periodic quantum wire and quantum dot patterns was observed down to feature sizes of about 40 nm and analyzed taking into account the elastic relaxation properties of strained nanostructures.

Periodic Si/SiGe structures were so far fabricated by holographic lithography and reactive ion etching and structurally characterized with respect to their elastic strain fields by x-ray diffraction methods.

Furthermore self-organized Ge islands (dots) grown by MBE as multilayers embedded in a Si matrix were studied with respect to their structural properties. For any kind of device application dot multilayers will be required in order to achieve a sufficiently high density in a given volume. The advantage of dots in comparison to two dimensional Si/SiGe structures is the fact that within the Ge dots a much higher strain status can be achieved in comparison to 2D SiGe layers, since the partial elastic relaxation in the three dimensional structures may inhibit the formation of misfit dislocations.

Selected references: [1] – [4]

2. Surface Analysis of II-VI Compounds by Auger Electron Spectroscopy

(E. Wirthl, M. Schmid, H. Sitter, H. Straub, G. Brunthaler)

Several II-VI compounds grown by molecular beam and by atomic layer epitaxy were investigated by quantitative Auger electron spectroscopy. Particularly for ternary and quaternary II-VI compounds, which are indispensable for any realization of a II-VI compounds based heterostructure laser, an exact control of chemical composition is required. Furthermore, in the fabrication process of such devices, reactive ion etch processes are required. In this context a study of the surface composition using depth profiling methods with compounds like ZnSe, CdSe, ZnTe and CdTe was performed, after reactive ion etching using a mixture of CH_4 and H_2. Furthermore the incorporation of oxygen as well as of carbon during these etching steps was studied.

Selected references: [5] – [9]

3. Intersubband Absorption in Quantum Wells and Superlattices

(M. Helm, P. Kruck, W. Hilber, T. Fromherz, V. Nikonorov)

Si/SiGe as well as GaAs/AlGaAs structures suitable for the investigation of intersubband absorption were fabricated using optical photolithography, reactive ion etching as well as the facilities for preparing contacts.

In p-doped Si/SiGe multi-quantum well structures, the polarization dependence of the intersubband absorption has been investigated theoretically as well as experimentally. A 6x6 Luttinger-Kohn band structure calculation was performed and the theoretical results were applied for the design of a mid-infrared quantum well photodetector (QWIP). The Si/SiGe detector characteristics were investigated and found to be not inferior to those reported previously for p-type GaAs/GaAlAs based QWIP's.

In asymmetric Si/SiGe MQW structures, the second harmonic frequency generation was studied. A frequency doubling of CO_2 laser radiation could be demonstrated. The optical nonlinearity is due to the asymmetry of the QW structure, which causes a non-linear susceptibility of second order.

In GaAs/GaAlAs superlattices the energy relaxation of hot carriers was investigated by comparing infrared absorption spectra taken at high electric fields at low temperatures with those recorded at different lattice temperatures.

Finally, GaAs/GaAlAs structures for the investigation of the Wannier-Stark effect were fabricated. In sufficiently large vertical electrical fields, minibands split into a ladder, a phenomenon which was studied by infrared absorption.

Selected references: [10] – [14]

4. Molecular Beam Epitaxy of Si-Based Heterostructures: Growth, Structural Characterization, and Electronic Properties

(Ch. Penn, F. Schäffler, S. Zerlauth; J. Stangl, A.A. Darhuber, G. Bauer)

Single and multiquantum well structures of $Si/Si_{1-y}C_y$, $Si/Si_{1-x}Ge_x$, $Si/Si_{1-x-y}Ge_xC_y$, $Si_{1-x}Ge_x/Si_{1-y}C_y/Si$ were grown by molecular beam epitaxy. Their structural properties were investigated by x-ray rocking curves and their electronic properties were assessed by photoluminescence. Optimum growth temperatures with respect to carbon incorporation and layer quality were found to be around 500 °C.

PL signals from single layers, single quantum wells and multi-quantum wells were observed for carbon contents up to 1.7%. Annealing experiments were performed at temperatures up to 850 °C in order to investigate the thermal stability of the carbon containing structures. Above this temperature the substitutional carbon concentration decreases as evidenced from x-ray diffraction data.

$Si_{1-x}Ge_x/Si_{1-y}C_y/Si$ multilayers were investigated with respect to their interface roughness using x-ray reflectivity measurements performed at the Optics Beamline of the ESRF, Grenoble. It turned out that the use of a antimony as a surfactant during growth appreciable decreases the interface roughness and results in a substantially longer vertical correlation length.

Selected references: [15] – [18]

5. Scanning Tunneling Microscopy Observation of Stress Driven Surface Diffusion due to Localized Strain Fields and of Initial Stages of Heteroepitaxial Growth

(G. Springholz, A.Y. Ueta, G. Bauer)

Using in-situ scanning tunneling microscopy the influence of localized strain fields of misfit dislocations on epitaxial growth has been studied in molecular beam epitaxy. Pronounced surface deformations caused by single dislocations and dislocation reactions were observed, in good agreement with calculations based on elasticity theory. Due to the local reduction of strain energy at the surface above the interfacial dislocations, ridgelike structures are formed, due to stress-driven surface diffusion during MBE growth. These observations prove the preferential epitaxial growth at surface sites above dislocations.

The initial stages of the MBE growth of PbTe on BaF_2 were studied using UHV-STM and atomic force microscopy. The PbTe growth is totally dominated by growth spirals formed around threading dislocations. With increasing layer thickness, due to dislocation annihilation, the threading dislocation density decreases substantially which results in a dramatic increase of the electron mobilities in the layers.

Selected references: [19] – [22]

Acknowledgments

The work in the clean rooms in Linz has been further supported by several projects from the FWF, Vienna, the Österreichische Nationalbank, the Projektforschung des BMfWVK, and a research fund from Daimler Benz Research Ulm.

References

[1] A.A. Darhuber, V. Holy, G. Bauer, P.D. Wang, Y.P. Song, C.M. Sotomayor Torres, M.C. Holland, "Quantitative analysis of elastic strains in GaAs/AlAs quantum dots", Physica B 227, 11 (1996).

[2] H. Straub, G. Brunthaler, W. Faschinger, G. Bauer, C. Vieu, "Photoluminescence of CdZnSe/ZnSe quantum well structures fabricated by reactive ion etching", J. Crystal Growth 159, 451 (1996).

[3] A.A. Darhuber, V. Holy, J. Stangl, G. Bauer, et al., "Lateral and vertical ordering in multilayered self-organized InGaAs quantum dots studied by high resolution x-ray diffraction", Appl.Phys.Lett., in print (Feb.1997).

[4] A.A. Darhuber, J. Stangl, G. Bauer, P. Schittenhelm, G. Abstreiter, "X-ray diffraction and reflection from self-assembled dots", Thin Solid Films, in print.

[5] E. Wirthl, H. Straub, M. Schmid, H. Sitter, P. Bauer, G. Brunthaler, "AES analysis of plasma-etched ZnSe", J.Cryst.Growth 159, 746 (1996).

[6] E. Wirthl, M. Schmid, D. Stifter, H. Sitter, P. Bauer, "Auger investigations on II-VI ternary compound semiconductors", J.Cryst.Res. and Technology 31, 297 (1996).

[7] E. Wirthl, H. Sitter, P. Bauer, "Determination of Auger-sensitivity factors in $Zn_{1-x}Mg_xTe$ for quantitative Surface analysis", Materials Science B, (1997), in print.

[8] E. Wirthl, H. Straub, H. Sitter, G. Brunthaler, M. Schmid, D. Stifter, P. Bauer, "AES investigations of plasma-etched II-VI binary compounds", Proc.Int.Symp. Blue Laser and Light emitting diodes, Chiba, Japan 1996, (Ohmsda Ltd IOS Press Inc.).

[9] S. Ferreira, H. Sitter, R. Krump, W. Faschinger, G. Brunthaler, "Room temperature blue electroluminescence from ZnMgCdSe quaternary system", J. Crystal Growth 159, 640 (1996).

[10] T. Fromherz, P. Kruck, M. Helm, G. Bauer, J.F. Nützel, G. Abstreiter, "TM and TE polarized intersubband absorption and photoconductivity in p-type SiGe quantum wells", Appl.Phys.Lett. 68, 3611 (1996).

[11] P. Kruck, M. Helm, T. Fromherz, G. Bauer, J.F. Nützel, G. Abstreiter, "Medium wavelength normal incidence p-type Si/SiGe quantum well infrared photodetector with background limited performance up to 85 K", Appl.Phys.Lett. 69, 3372 (1996).

[12] P. Kruck, M. Seto, M. Helm, Z. Moussa, P. Boucaud, F.-H. Julien, J.-M. Lourtioz, J.F. Nützel, G. Abstreiter, "Second order susceptibilities related to valence band

transitions in asymmetric Si/SiGe quantum wells" Solid State Electronics 40, 763 (1996).

[13] W. Hilber, M. Helm, K. Alavi, R.N. Pathak, "Hot-electron power loss in doped GaAs/GaAlAs superlattices measured by infrared differential spectroscopy", Appl.Phys.Lett. 69, 2528 (1996).

[14] W. Hilber, M. Helm, F.M. Peeters, K. Alavi, R.N. Pathak, "Impurity-band and magnetic-filed-induced metal-insulator-transition in a doped GaAs/GaAlAs superlattice", Phys.Rev.B 53, 6919 (1996).

[15] W. Faschinger, S. Zerlauth, G. Bauer, L. Palmetshofer, Appl.Phys.Lett. 67, 3933 (1995).

[16] S. Zerlauth, J. Stangl, A.A. Darhuber, V. Holy, G. Bauer; F. Schäffler, "MBE growth and structural characterization of $Si_{1-y}C_y/Si_{1-x}Ge_x$ superlattices", J.Cryst.Growth, in print.

[17] J. Stangl, S. Zerlauth, V. Holy, W. Faschinger, G. Bauer, "Reciprocal space mapping of $Si_{1-x}C_x$ epilayers and $Si_n/C/Si_n$ superlattices", Il Nuovo Cimento, in print.

[18] J. Stangl, A.A. Darhuber, V. Holy, S. Zerlauth, F. Schäffler, G. Bauer, "Interface roughness in pseudomorphic SiGe/SiC superlattices", Proc. Int. Conf. Phys. Semicond., Berlin 1996.

[19] G. Springholz, G. Bauer, V. Holy, Phys.Rev.B 54, 4500 (1996).

[20] G. Springholz, "Strain contrast in scanning tunneling microscopy imaging of surface dislocations in lattice mismatched heteroepitaxy", Applied Surface Science, in print.

[21] G. Springholz, A.Y. Ueta, N. Frank, G. Bauer, Appl.Phys.Lett. 69, 2822 (1996).

[22] G. Springholz, "Surface modifications due to strain relaxation in lattice mismatched heteroepitaxy", Festkörperprobleme, Vol. 35, ed. R. Helbig, Vieweg, Braunschweig/Wiesbaden) Vol.35, p.277 (1996).

Project Information

Project Manager

Univ.-Prof. Dr. Günther BAUER

Institut für Halbleiterphysik, Johannes Kepler Universität Linz, A-4040 Linz

Project Group

Last Name	First Name	Status	Remarks
Bonanni	Alberta	dissertation	
Brunthaler	Gerhard	Ph.D.	
Darhuber	Anton	dissertation	
Fünfstück	Britta	diploma student	
Helm	Manfred	assistant professor	
Hilber	Wolfgang	dissertation	
Kainz	Ursula	technician	
Köck	Franz	diploma student	
Kolmhofer	Gerald	diploma student	
Kruck	Peter	dissertation	
Li	Jianhua	Ph.D.	
Rabeder	Klaus	technician	
Schäffler	Friedrich	associate professor	
Schmid	Michael	diploma student	
Seyringer	Heinz	dissertation	
Sitter	Helmut	assistant professor	
Springholz	Gunther	Ph.D.	
Stangl	Julian	dissertation	
Steinbacher	Günther	diploma student	
Stifter	David	dissertation	
Straub	Hubert	dissertation	GMe funding
Ueta	Yukio	dissertation	
Wirtl	Elisabeth	technician	50 % GMe funding
Zerlauth	Stefan	dissertation	
Zhuang	Yan	dissertation	

Books and Contributions to Books

1. G. Bauer and W. Richter, "Optical characterization of epitaxial semiconductor layers", *Springer*, 1996.
2. M.A. Herman, H. Sitter: "Molecular beam epitaxy", 2nd revised and updated edition, *Springer Series in Mat. Sciences* Vol. 7, ed. M. B. Panish, Springer 1996.

Publications in Reviewed Journals

1. G. Brunthaler, F. Geist, H. Pascher, N. Frank, G. Bauer: "Interband magnetotransmission and coherent Raman spectroscopy of spin transitions in diluted magnetic $Pb_{1-x}Mn_xSe$", *Phys. Rev. B* 53, 3820 (1996).
2. G. Springholz: "Surface modifications due to strain relaxation in lattice-mismatched heteroepitaxy", in: *Festkörperprobleme / Advances in Solid State Physics* Vol. 35, ed. R. Helbig (Vieweg, Braunschweig/Wiesbaden), p. 277.
3. A.A. Darhuber, V. Holy, G. Bauer, P.D. Wang, Y.P. Song, C.M. Sotomayor Torres, M.C. Holland: "Quantitative analysis of elastic strains in GaAs/AlAs quantum dots", *Physica* B 227, 11(1996).
4. G. Hendorfer, W. Jantsch, W. Helzel, J.H. Li, Z. Wilamowski, T. Widmer, D. Schikora, K. Lischka: "Strain characterization of $HG_{1-x}Fe_xSe$-layers by electron spin resonance", *Mater. Sci. Forum*, in print.
5. M. Shima, L. Salamanca-Riba, G. Springholz, G. Bauer: "Double periodicity formation in EuTe/PbTe superlattices" *Mat. Res. Soc. Symp. Proc*. 399, 543 (1996)
6. G. Springholz, G. Bauer, V. Holy: "Local surface deformations induced by interfacial misfit dislocations in lattice-mismatched heteroepitaxy of EuTe on PbTe (111)", *Surface Science* 365, 453 (1996).
7. F. Geist, H. Pascher, M. Kriechbaum, N. Frank, G. Bauer: "Magneto-optical properties of diluted magnetic PbSe/$Pb_{1-x}Mn_xSe$ superlatttices", *Phys. Rev. B* 54, 4820 (1996).
8. G. Springholz, A.Y. Ueta, N. Frank, G. Bauer: "Spiral growth and threading dislocations for molecular beam epitaxy of PbTe on BaF_2 (111) studied by UHV-scanning tunneling microscopy", *Appl.Phys.Lett*. 69, 2822 (1996).
9. J. Stangl, A.A. Darhuber, V. Holy, S. Zerlauth, F. Schäffler, G. Bauer: "Interface roughness in pseudomorphic $Si_{1-x}Ge/Si_{1-y}C_y$ superlattices", *Proc. International Conference on the Physics of Semiconductors*, Berlin, Germany, July 21 – 26, 1996, to be published.
10. S. Zerlauth, J. Stangl, A.A. Darhuber, V. Holy, G. Bauer, F. Schäffler: "MBE growth and structural characterization of $Si_{1-y}C_y/Si_{1-x}Ge_x$ superlattices", *Proc. 9th International Conference on Molecular Beam Epitaxy*, August 5 – 9, 1996, Pepperdine University, Malibu, California, in print; J. Crystal Growth, submitted.
11. G. Springholz, G. Bauer, V. Holy: "Scanning-tunneling-microscopy observation of stress-driven surface diffusion due to localized strain fields of misfit dislocations in heteroepitaxy", *Phys. Rev. B* 54, 4500 (1996).

12. A.A. Darhuber, J. Stangl, V. Holy, G. Bauer, A. Krost, M. Grundmann, D. Bimberg, V.M. Ustinov, P.S. Kop'ev, A.O. Kosogov, P. Werne: "Structural characterization of self-assembled quantum dot structures by x-ray diffraction techniques", *Thin Solid Films*, submitted.

13. M. Holzmann, P. Baumgartner, C. Engel, J.F. Nützel, G. Abstreiter, F. Schäffler: "Fabrication of n- and p-channel in-plane-gate transistors from Si/SiGe/Ge heterostructures by focused laser beam writing", *Appl. Phys. Lett*. 68, 3025 (1996).

14. D. Stifter, H. Sitter: "Thickness correlated effects of the crystal and surface structure of C_{60} thin films grown on Mica by Hot Wall Epitaxy", *Thin Solid Films* 280, 83 (1996),

15. D. Stifter, H. Sitter: "Hot wall epitaxy of C_{60} thin films on Mica and their characterization", *Fullerene Science and Technol*. 4, 277 (1996).

16. M. A. Herman, H. Sitter: "MBE growth physics: Application to device technology", Microelectronics Journal 27, 257 (1996).

17. K. Wundke, U. Neukirch, J. Gutowski, D. Hommel, S. O. Ferreira, H. Sitter: "Coherent effects in nonlinear absorption of thin ZnSe layers and $Zn_{1-x}Cd_xSe$/ZnSe quantum wells under resonant excitation", *Proc. 10th Int. Conf. Dynamic Processes in the Excited States of Solids*, Palm Cove 1995, J.Luminescence 66, 65 (1996).

18. E. Wirthl, H. Straub, M. Schmid, H. Sitter, P. Bauer, G. Brunthaler: "AES analysis of plasma-etched ZnSe", *J. Crystal Growth* 159, 146 (1996).

19. S.O. Ferreira, H. Sitter, R. Krump, W. Faschinger, G. Brunthaler: "Room temperature blue electroluminescence from the ZnMgCdSe quaternary system", *J. Crystal Growth* 159, 640 (1996).

20. E. Belas, R. Grill, J. Fronc, A. Toth, P. Höschl, H. Sitter, P. Moravec: "Determination of migration energy of Hg interstitials in (HgCd)Te from ion milling experiments", *J. Crystal Growth* 159, 1117 (1996).

21. J. Hlavka, I. Ohlidal, F. Vizda, H. Sitter: "New technique of measurement of optical parameters of thin films", *Thin Solid Films* 279, 209 (1996).

22. E. Wirthl, M. Schmid, D. Stifter, H. Sitter, P. Bauer: "Auger investigations on II-VI ternary compound semiconductors", Proc. Int. Conf. on Ternary and Multinary Compounds, *J. Cryst. Res. and Technol.* 31, 297 (1996).

23. E. Belas, J. Franc, A. Toth, R. Grill, P. Höschl, H. Sitter, P. Moravec: "Type conversion of p-(HgCd)Te using H_2/CH_4 and Ar reactive ion etching", *Semicond. Sci. Technol*. 11, 1116 (1996).

24. T. Nguyen Manh, H. Sitter, D. Stifter: Preparation of Pristine and Ba-doped C_{60} films by hot-wall-epitaxy", in: *Fullerenes and Fullerene Nanostructures*, eds. H. Kuzmany et al., World Scientific 1996, p. 430 ff.

25. J. Hora, P. Panek, K. Navratil, B. Handlirova, J. Humlicek, H. Sitter, D. Stifter: "Optical response of C_{60} thin films and solutions", *Phys. Rev. B* 54, 5106 (1996).

26. I Hernandez-Calderon, J. Luyo, M. Melendez-Lira, M. Garcia-Rocha, O. de Melo, R. Leon, P. Diaz, L. Hernandez, J. Fuentes, H. Sitter: "Optical and structural properties of ZnSe/GaAs interfaces", *Appl. Surf. Sci*. 112, 1996.

27. J. Luyo, M. Melendez-Lira, M. Garcia-Rocha, O. de Melo, R. Leon, P. Diaz, L. Hernandez, J. Fuentes, H. Sitter, I. Hernandez-Calderon: "Optical and structural characterization of ZnSe/GaAs interfaces", in: *The Physics of Semiconductors*, ed. M. Scheffler and R. Zimmermann, World Scientific 1996, p. 1067-1070.

28. J. Luyo, E. Lopez-Luna, M. Melendez-Lira, I. Hernandez-Calderon, O. de Melo-Perciva, P. Diaz-Arencibia, R. Leon, J. Fuentes, H. Sitter: "Investigation of the optical and structural properties of MBE-grown ZnSe/GaAs heterostructures", *J. Cryst. Growth, Proc. MBE Conf.*, Malibu 1996.

Presentations

1. G. Brunthaler, H. Straub, G. Bauer, E. Wirthl and H. Sitter : "Nanostructuring in II-VI compounds by reactive ion etching", *International Symposium on II-VI compounds*, Würzburg, 28./29 Oct. 1996 (invited).
2. I. Gourgon, H. Mariette, Le Si Dang, N. Pelekanos, C. Vieu, H. Straub, D. Stifter, G. Brunthaler: "Strain Relaxation in CdTe-based Wires and Dots Studied by Photoluminescence" *Nanostructure Workshop*, Ioffe Institute, St. Petersburg, May 1996 (invited).
3. G. Springholz : "Molecular Beam Epitaxy of Lead Salt Compounds", International *Conference on Material Science and Materials Properties for Infrared Optoelectronics (SPIE)*, 30.9. – 2.10.1996, Uzghorod, Ukraine (invited).
4. G. Springholz: "Scanning Tunneling Microscopy on Semiconductor Heterostructures", *Annual Meeting of the Austrian Physical Society*, 23 – 27 September 1996, Linz, Austria (invited).
5. G. Springholz : "Misfit Dislocations and their Localized Strain Fields Studied by UHV-Scanning Tunneling Microscopy", *Workshop on Semiconductor Growth, Surface Morphology and Quantum Phenomena*, 19 – 21 February 1996, Rottach-Egern, Germany (invited).
6. V. Nunez, G. Springholz, T.M. Giebultowiecz, H. Kepa, K.I. Goldman, C.F. Majkrzak, G. Bauer: "Interlayer spin coherence in antiferromagnetic EuTe/PbTe superlattices observed byc polarized neutron diffraction", *9th International Conference on Superlattices and Microstructures*, 14 – 19 July 1996, Liège, Belgium.
7. F.Schäffler: "Si-Basierende Heterostrukturen: Grundlagen und Anwendungs-potential", *Jahrestagung der Österr. Physikal. Gesellschaft*, Linz, 23 – 27 September 1996.
8. G. Springholz, G. Bauer, V. Holy: "Einfluß der lokalen Gitterverzerrungen auf das MBE Wachstum von Epitaxieschichten", *Spring Meeting of the German Physical Society*, 19 – 23 March 1996, Regensburg , Germany.
9. G. Springholz: "Combined STM/AFM study of surface modifications due to misfit dislocation formation in lattice-mismatched heteroepitaxy", *4th European Park Scientific Instruments Users Meeting*, 18 – 20 September 1996, Paris, France.

10. G. Springholz, N. Frank, Y. Ueta, V. Holy, G. Bauer: "Misfit dislocation formation induced surface modifications studied by UHV-scanning tunneling microscopy", *Annual Meeting of the TMS Society*, February 4 – 9, 1996, Anaheim, CA, USA.
11. G. Springholz, F. Köck, Y. Ueta, G. Bauer: "The origin of spiral type growth mode in lattice-mismatched heteroepitaxy", *Fall Meeting of the Materials Research Society (MRS)*, Boston, MA, USA, December 2 – 6, 1996.
12. J. Stangl, S. Zerlauth, V. Holy, W. Faschinger, G. Bauer: "Hochauflösende Röntgenbeugung an $Si_{1-x}C_x$ Epitaxieschichten und $Si_n/C/Si_n$ Übergittern" (Poster), *Frühjahrstagung der Deutschen Physikalischen Gesellschaft*, 25 – 29 March 1996, Regensburg, Germany.
13. J. Stangl, S. Zerlauth, V. Holy, W. Faschinger, G. Bauer: "Reciprocal space mapping on $Si_{1-x}C_x$ epilayers and $Si_n/C/Si_n$ superlattices" (Poster), *3rd European Symposium on X-Ray Topography and High Resolution Diffraction (X-TOP '96)*, April 22 – 24 , 1996, Palermo, Italy.
14. J. Stangl, A.A. Darhuber, V. Holy, S. Zerlauth, F. Schäffler, G. Bauer: "Interface roughness in pseudomorphic $Si_{1-x}Ge_x/Si_{1-y}C_y$ superlattices" (Poster), *23rd International Coneference on the Physics of Semiconductors (ICPS XXII)*, July 21 – 26, 1996, Berlin, Germany.
15. J. Stangl, A.A. Darhuber, V. Holy, S. Zerlauth, G. Bauer: "Interface roughness in pseudomorphic $Si_{1-x}Ge_x/Si_{1-y}C_y$ superlattices from x-ray reflectivity" (Poster), *E-MRS Group IV "Heterostructures, Physics and Devices"*, June 4 – 7, Strasbourg, France.
16. H. Straub, G. Brunthaler, W. Faschinger, G. Bauer and C. Vieu: "Strain Relaxation induced Red Shift of the Photoluminescence of CdZnSe/ZnSe Quantum Wires", *XXV International School on Physics of Semiconducting Compounds*, Jaszowiec '96, Jaszowiec, Poland.
17. H. Straub, G. Brunthaler, W. Faschinger, G. Bauer, C. Vieu: "Photolumineszenz-Rotverschiebung durch Dehnungsrelaxation in CdZnSe/ZnSe Quantendrähten", *Frühjahrstagung der DPG*, Regensburg 1996.
18. Z. Wilamowski, W. Jantsch, M. Ludwig and G. Springholz: "Mesoscopic magnetism in short period semiconductor/antiferromagnet superlattices" (poster), *23rd International Conference on the Physics of Semiconductors*, 21 – 26 July 1996, Berlin, Germany.
19. E. Wirthl, H. Straub, H. Sitter, G. Brunthaler, M. Schmid, D. Stifter, P. Bauer: "AES-Investigation of Plasma-Etched II-VI Binary Compounds", Chiba, Japan, March 5 – 7, 1996.
20. A.Y. Ueta, G. Springholz, G. Bauer: "Spiral growth and improved nucleation PbTe on BaF_2 (111)" (poster), *9th International Conference on Molecular Beam Epitaxy*, August 3 - 7, 1996, Malibu, USA.
21. A.Y. Ueta, G. Springholz and G. Bauer: "Spiral growth and improved nucleation PbTe on BaF_2 (111)", *Jahrestagung der Österr. Physikal. Gesellschaft*, Sept. 23 – 27, 1996, Linz, Austria.

22. A.Y. Ueta, G. Springholz, G. Bauer: "Molecular beam epitaxy of PbTe and $Pb_{1-x}Eu_xTe$: Doping studies", *2nd International Workshop on MBE Growth Physics and Technology*, October 21 – 25, 1996, Warsaw, Poland.
23. A.Y. Ueta, G. Springholz, G. Bauer: "MBE growth and physical properties of PbEuTe", Frühjahrstagung der Deutschen Physikalischen Gesellschaft, 25 – 29 March 1996, Regensburg, Germany.

Doctor's Theses

1. A. Darhuber: "X-ray diffractometry of self-organized low-dimansional systems", in progress.
2. P. Kruck: "Infrared spectroscopy of semiconductor quantum well systems", in progress.
3. H. Seyringer: "Fabrication and characterization of Si based heterostructure devices", in progress.
4. J. Stangl: "X-ray diffraction and reflectivity from semiconductor heterostructures", in progress.
5. H. Straub: "Lateral patterning of II-VI compounds by holographic lithography and reactive ion etching", in progress.
6. S. Zerlauth: "Molecular beam epitaxy of SiGeC", in progress.
7. Y. Zhuang: "Fabrication of laterally structured semiconductor heterolayers", in progress.
8. A.Y. Ueta: "MBE growth and characterization of PbTe/PbEuTe epitaxial layers"
9. E. Wirthl: "Auger electron spectroscopy of RIE etched II-VI structures"
10. D. Stifter: "MBE growth of II-VI based heterostructures"

Cooperations

1. Walter Schottky Institut, TU München, Garching, Germany, Prof. Abstreiter
2. CEA-CNRS Microstructures de Semiconducteurs II-VI, Grenoble, Prof. Mariette
3. Institute of Physics, Polish Academy of Sciences, Warsaw, Poland
4. ESRF Grenoble, Optics Beamline, Dr. A. Freund, Dr. A. Souvorov
5. Institut für Festkörperelektronik,TU Wien
6. Daimler Benz Forschungslaboratorien Ulm, Dr. Presting, Dr. König
7. Universität Bayreuth, Experimentalphysik, Prof. Pascher
8. Nanoelectronics Research Centre, University of Glasgow, Prof. Sotomayor-Torres
9. Heriot Watt University, Department of Physics, Edinburgh, Scotland
10. NIST-Reactor Radiation Division, Gaithersburg, MD, USA
11. Department of Physics, Purdue University, west Lafayette, IN, USA

12. Department of Physics, Massachusetts Institute of Technology, Cambridge, MA, USA
13. Institut für Experimentalphysik, Ateilung Atom- und Kernphysik, Universität Linz
14. University of Warwick, Coventry, England
15. Fraunhofer Institut, Freiburg, Deutschland
16. IBM Watson Research Center, Yorktown Heights, USA
17. Fachbereich Physik, Universität Paderborn, Deutschland

Growth, Doping and Structuring of Si/SiGe/SiC

G. Brunthaler, A. Darhuber, T. Grill, Ch. Penn, F.Schäffler, J.Stangl, G. Steinbacher, H. Straub, S.Zerlauth, Y. Zhuang, G. Bauer

Institut für Halbleiterphysik, Johannes Kepler Universität, A-4040 Linz, Austria

We report on the structural and optical properties of silicon-based heterostructures containing ternary $Si_{1-x-y}Ge_xC_y$ alloys. Both single and multiple quantum wells were grown by molecular beam epitaxy and their quality was assessed by x-ray rocking analyses and by photoluminescence (PL) measurements. Optimum growth temperatures with respect to carbon incorporation and layer quality were found to be at around 500 °C. We observed well behaved PL signals from $Si_{1-y}C_y$ single layers and $Si/Si_{1-y}C_y$ multiple quantum wells as well as from $Si/Si_{1-y}C_y/Si_{1-x}Ge_x$ superlattices with carbon concentrations up to 1.7%. For an investigation of the thermal stability of these intrinsically metastable layers, ex-situ annealing experiments were conducted in the temperature range between 500 °C and 900 °C. Up to about 725 °C an improvement of the PL signals both with respect to intensity and linewidth is observed, whereas the amount of substitutional carbon remained unaffected. After annealing at 725 °C we observed the narrowest linewidth in a $Si_{1-y}C_y$ single layer reported so far in the literature. At higher annealing temperatures the PL signal decreases, but it takes more than 850 °C to observe a decrease of the substitutional carbon concentration in x-ray measurements. The results indicate that carbon containing epi-layers of high crystal quality can be grown by MBE, and that thermal stability is good enough to make the material interesting for device applications.

1. $Si_{1-x-y}Ge_xC_y$ Layers: Growth and Characterization

(F. Schäffler, S. Zerlauth, Ch. Penn)

It is the outstanding property of Si-based heterostructures to provide the application relevant combination of band structure engineering and silicon very-large-scale-integration (VLSI) compatibility. In the past few years most of the basic properties regarding the lattice mismatched $Si/Si_{1-x}Ge_x$ material combination, and especially the effects of strain on the band offsets and bandgaps, have been investigated. It has been found that the band offset at the interface between a pseudomorphic $Si_{1-x}Ge_x$ layer and a Si substrate occurs almost exclusively in the valence bands, whereas a tensilely strained Si layer is required for the implementation of useful conduction band offsets. By employing proper combinations of pseudomorphic and strain-relaxed epi-layers, both tensile and compressive strains can be custom designed, without sacrificing the important advantages of a Si substrate and the basic compatibility with Si technologies.

By exploiting *strain-engineering* as an additional degree of freedom, a wide variety of devices structures have been implemented in the $Si/Si_{1-x}Ge_x$ material system, reaching from heterobipolar transistors (HBT) over p- and n-type modulation-doped field effect transistors (MODFET) to optical detectors in the near infrared, and even light emitters. Nevertheless, so far only the pseudomorphic Si/SiGe HBT has reached production

status, whereas other devices with demonstrated superior properties, such as the n-type MODFET, are still restricted to test devices on a laboratory level. The main reason for the much slower development of the MODFET lies in the necessity for strain relaxed $Si_{1-x}Ge_x$ buffer layers. These have successfully been implemented by several research groups, but defect and morphology control still require further refinement to make them suited for a production environment.

Ternary $Si_{1-x-y}Ge_xC_y$ alloys offer an alternative route to strain-engineering in silicon-based heterostructures, which finally may overcome the problems imposed by relaxed buffer layers: Due to the covalent radii of C and Ge, which are smaller, and larger than that of Si, respectively, both compressively and tensilely strained, pseudomorphic layers can be implemented by proper adjustment of x and y in the active layers of a hetero-structure. However, in contrast to the binary $Si_{1-x}Ge_x$ alloys, which are thermodynamically stable for all compositions x, carbon has almost negligible solid solubility in both Si and Ge, but, on the other hand, tends to the formation of stoichiometric SiC. Since strain engineering requires C concentrations of a few percent to provide useful modifications of the band structure, non-equilibrium growth conditions at sufficiently low temperatures have to be established. This requires an optimization of the growth parameters to allow sufficiently high C incorporation without excessive degradation of the crystal quality through the undesirable generation of point defects. Also, the surface morphology has to be controlled in order to suppress strain-induced three-dimensional growth. In the following we report on the progress that has been made in Linz regarding the growth of heterostructures containing ternary $Si_{1-x-y}Ge_xC_y$ alloys. The main emphasis in 1996 has been put on the structural and optical qualities of these layer sequences, which are an essential prerequisite for any further assessment of the future role $Si_{1-x-y}Ge_xC_y$ alloys can play in the field of application-driven band structure engineering.

1.1 Sample Preparation and Characterization

The ternary $Si_{1-x-y}Ge_xC_y$ alloys were grown in a newly commissioned RIBER SIVA 45 MBE machine equipped with electron beam evaporators for Si, Ge, and C, and dopant effusion cells for Sb (n-type) and B (p-type). High-purity, single crystalline ingots are used for the Si and Ge sources, whereas pyrolytic graphite is used in the carbon evaporator. The fluxes of all three matrix materials are monitored, and feedback-controlled, by a quadrupole mass spectrometer with a cross-beam ion source and PID controllers. The mass spectrometer signals are calibrated by epitaxial growth of $Si_{1-x}Ge_x$ and $Si_{1-y}C_y$ reference layers, the compositions and layer thicknesses of which are determined by x-ray rocking analyses in combination with dynamic simulations. The flux stability, especially of the C source, which is the most critical one because of the small fluxes required, is occasionally checked by quantitative SIMS analysis.

High-resistivity (FZ, $\rho > 1000\ \Omega$cm) Si substrates of 100 mm diameter are chemically precleaned either by oxide removal in 5% HF or by a standard RCA cleaning procedure. Immediately after precleaning the wafers are mounted in 125 mm diameter, all-silicon adapters, a total of six of which can be introduced into the magazine of the load-lock chamber. After pump-down of the load-lock chamber into the 10^{-9} mbar range, the wafers are transferred into the growth chamber, where they are suspended by Mo-clamps underneath a radiative substrate heater made of pyrolytic graphite (PG). Prior to growth, which always commences with a Si buffer layer of 100 to 200 nm thickness, a thermal cleaning step is performed at 900 °C for typically 5 min to remove SiO_2 and

possible organic contaminations from the surface. This step can be controlled by in-situ reflection high energy electron diffraction (RHEED), which reveals a (2x1) reconstruction of the bare Si surface as soon as the amorphous oxide has been flashed off.

The heterostructures are routinely characterized by x-ray diffraction, which yields, as mentioned, in the case of single layers composition and layer thickness. In the case of multiple quantum wells and superlattices, the period length is the primary information derived from rocking measurements. The compositions and the thicknesses of the individual layers can also be extracted by fitting of dynamic simulation curves, however, a certain degree of ambiguity remains. For that reason additional information is useful, such as the composition determined by SIMS analysis, or Rutherford backscattering (RBS). The latter technique is not directly applicable to C, because of the minor backscattering yield from the light elements. Therefore, we are presently trying in collaboration with the University of Padua, to exploit a nuclear resonance with broad enough scattering cross section to enhance the back scattering yield to an extent that allows for an absolute, depth resolved evaluation of the carbon content.

For an investigation of the thermal stability of the strained $Si_{1-y}C_y$ layers annealing at temperatures between 500°C and 900°C was performed under vacuum either in a furnace or directly in the MBE growth chamber.

Photoluminescence (PL) spectroscopy is a versatile technique, which not only provides information on the band gaps and the band offsets, but is also a sensitive indicator of the overall crystal quality of the layers. This is of special interest for an optimization of the low temperature growth conditions required for the metastable incorporation of carbon, because the PL signal is strongly suppressed, once the density of growth-induced non-radiative recombination centers becomes too high. For our investigations, PL was excited by the 488 nm line of an Ar^+ laser, analyzed in a 0.32 m grating spectrometer and detected by a North Coast Ge detector in a standard lock-in technique. A temperature-variable He cryostat allowed for temperature dependent measurements in the range between 1.6 and 300 K.

1.2 Experimental Results

Three types of samples were grown for these studies, namely $Si_{1-y}C_y$ single layers, $Si/Si_{1-y}C_y$ multiple quantum wells, and strain compensated $Si/Si_{1-y}C_y/Si_{1-x}Ge_x$ superlattices. In the first two types of samples the band offset is almost exclusively restricted to the conduction band, which is energetically lower in the tensilely strained $Si_{1-y}C_y$ layers due to a strain splitting of the six-fold degenerate, Si-like conduction band. The situation is analogous to strained Si grown on a relaxed $Si_{1-x}Ge_x$ buffer layer and is therefore of special interest for the implementation of n-type MODFETs. Band alignment in the $Si/Si_{1-y}C_y/Si_{1-x}Ge_x$ superlattices, which are interesting for infrared detector applications because of the inherent strain compensation, is more complex: Since the $Si_{1-x}Ge_x$ layers introduce an additional valence band offset, carrier confinement is indirect both in k-space and in real space, with electrons being located in the $Si_{1-y}C_y$ layers and holes in the $Si_{1-x}Ge_x$ layers.

At growth temperatures of around 500 °C the as-grown samples of all three types showed well behaved PL signals. There is presently only one other group worldwide that has published comparable PL spectra from MBE-grown layers. As an example, Fig. 1 shows the spectrum of a ten-period $Si/Si_{0.989}C_{0.011}/Si_{0.9}Ge_{0.1}$ superlattice together with a schematic view of the strain-induced band alignment. Two distinct peaks are observed,

which originate from band edge recombination in the vicinity of the $Si_{1-y}C_y/Si_{1-x}Ge_x$ interface, where the wave functions of electrons and holes have finite overlap. The peak at higher energies, labeled SiC-NP, results from the no-phonon transition, whereas the other peak is its TO phonon replica. A NP transition in an indirect gap material is only possible if symmetry breaking mechanisms are present, such as the presence of a heterointerfaces and/or the statistical fluctuations in a random alloy, which is both the case in our layers. The relative strength of the superlattice related peaks can by judged by comparison with the TO replicas originating from the Si layers and from the substrate. Obviously, the quantum wells very efficiently collect electron-hole pairs from the several μm deep excitation volume, and also maintain long enough lifetimes to allow the observation of radiative recombination. The strength of the bandgap PL signal is therefore an important indicator of the crystal quality, since an excessive amount of defects in the layers and at the heterointerfaces associated with non-radiative recombination would quench the PL signal altogether. This is indeed the case, when growth temperatures below 450°C are employed.

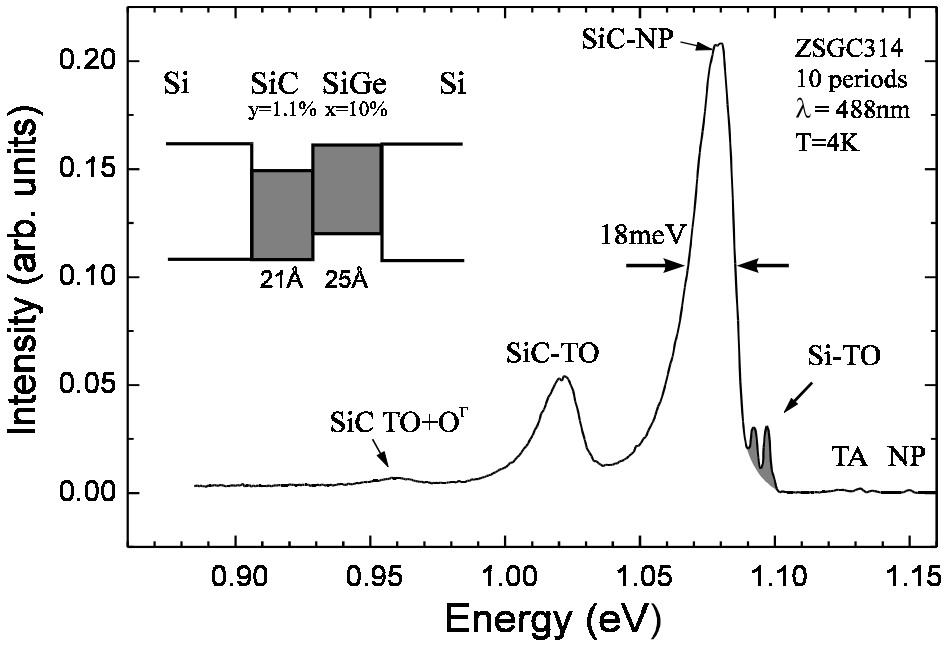

Fig. 1: PL spectrum of a ten-period $Si/Si_{0.989}C_{0.011}/Si_{0.9}Ge_{0.1}$ superlattice. The dominating signals are the no-phonon (NP) band edge recombination from the quantum well section and its TO-phonon replica. The shaded part of the spectrum results from the Si layers and the Si substrate.

Compared to the well established quantum well luminescence from single $Si_{1-x}Ge_x$ layers, the PL signal in Fig. 1 is almost a factor of six broader. Since close to a factor of ten higher Ge concentrations are required to induce the same amount of strain that is provided by a given carbon concentration, the statistical fluctuations of both the well width and the well depth are much more pronounced in the case of a $Si_{1-y}C_y$ layer of comparable average strain. In addition possible composition fluctuations from layer to layer may contribute to the line width from a superlattice. For the investigation of annealing effects we therefore mainly concentrated on single $Si_{1-y}C_y$ layers, which were grown thin enough to remain with the critical thickness limitations, but thick enough to suppress

quantum confinement effects. Save for the exciton binding energy, this way the true band gap recombination is measured without any necessity for the correction of confinement energies. In addition, cross checks with the multiple quantum well samples confirmed that the annealing behavior is qualitatively the same.

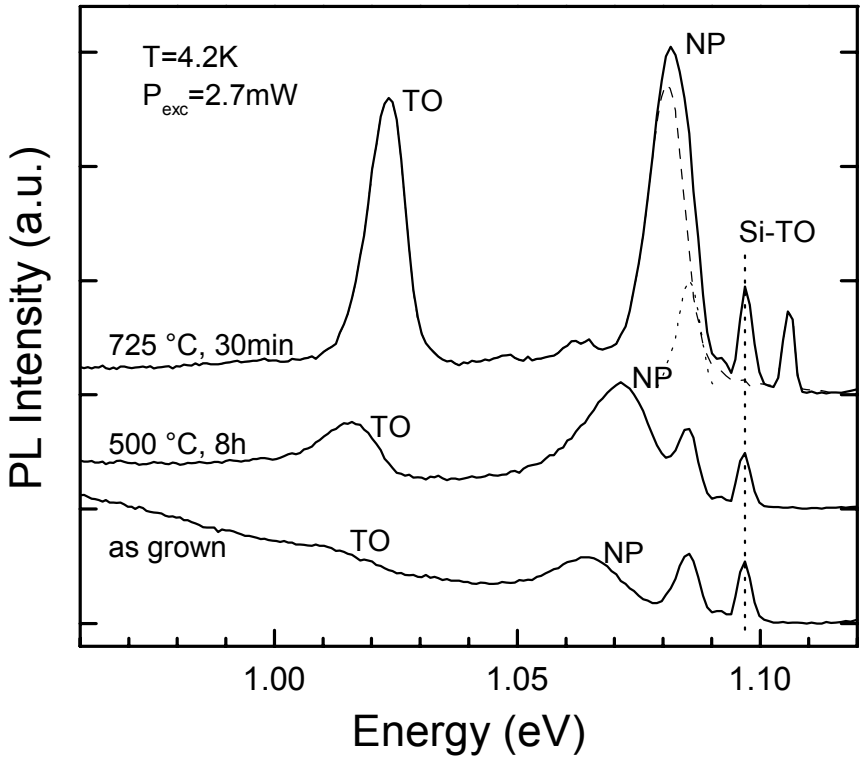

Fig. 2: Evolution of the PL signal of a single $Si_{1-y}C_y$ layer for increasing annealing temperatures. Note the blue shift and the line narrowing.

Figure 2 shows a series of PL measurements from a 100 nm thick $Si_{0.989}C_{0.011}$ layer, which underwent annealing at successively higher temperatures in the range between 500 and 725 °C. There are three main effects associated with annealing: (i) The intensity of the band gap PL signal increases significantly within the range of annealing temperatures shown here. (ii) There is a noticeable *blue shift* of the PL lines amounting to about 15 meV. (iii) The line width after background subtraction becomes much narrower as the annealing temperature is increased. In fact, the linewidth of 8.4 meV in the topmost curve of Fig. 2 is the narrowest observed to date in a $Si_{1-y}C_y$ layer.

Most interesting, the pronounced changes of the PL signal are not associated with a change of the substitutional carbon concentration, as has been checked by x-ray rocking analyses. Only at higher annealing temperatures of >850 °C a loss of substitutional carbon is observed, whereas the PL intensity starts decaying already at about 750 °C.

Since changes of the *average* C concentration can be ruled out, and quantum confinement effects through possible short range diffusion of substitutional carbon can be neglected in the thick layers used here, the development of the PL signal has to have other reasons. To further elucidate these mechanisms, PL measurements of the samples with the highest PL intensity were recorded as a function of the measurement temperature. This is shown in Fig. 3, where the TO-replica of the band gap recombination,

which is not affected by spurious signals from the Si substrate, is plotted for measurement temperatures in the range between 4.2 and 20 K. The most striking feature of these measurements, which was confirmed by experiments on the quantum well samples, is a *red shift* concomitant with a decay of the intensity as the temperature is increased.

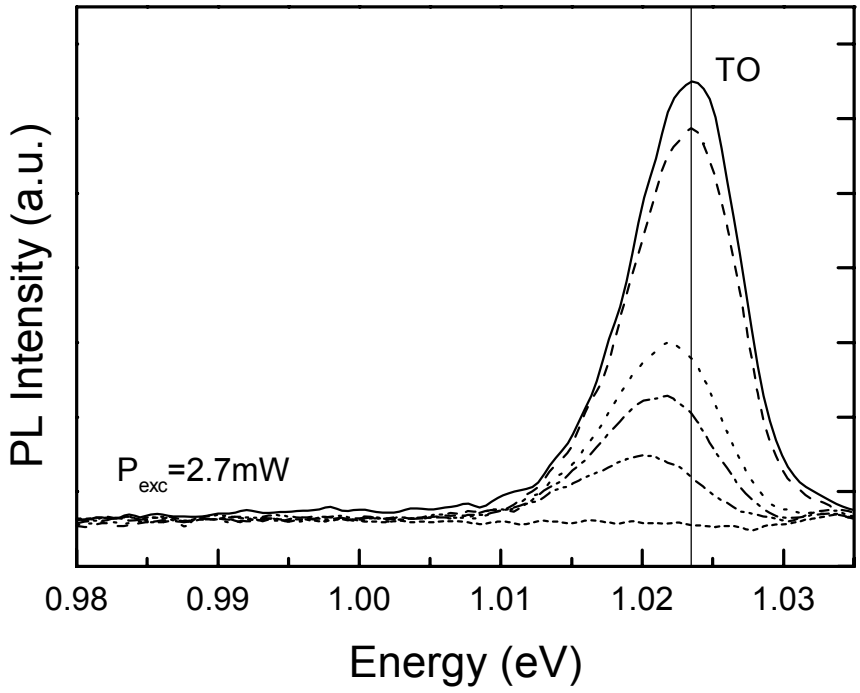

Fig. 3: Red shift of the PL signal with increasing measurement temperature. The TO-phonon replica is plotted here, because it is free of substrate-related signals.

1.3 Discussion

A consistent interpretation of the annealing effects and of the red shift with higher measurement temperature can be derived, when assuming that the as-grown samples contain non-radiative recombination centers as well as non-statistical fluctuations of the local, substitutional carbon concentration. The latter may be associated with C_2 and C_3 molecules, which are observed in the mass spectrum of the carbon molecular beam, and which are tentatively not completely dissociated at the low growth temperatures employed. Based on these assumptions the following effects will occur during annealing:

(i) At low annealing temperatures (middle curve in Fig. 2, 500 °C for 8 h), non-radiative recombination centers associated with growth defects begin to disappear. This leads to an increase of the PL intensity, but only to a minor decrease of the line width.

(ii) At higher annealing temperatures (upper curve in Fig. 2, 725 °C, 30 min) a redistribution of carbon on a local scale occurs, which leads to the dissolution of local carbon accumulations, introduced e.g. by molecular forms of evaporated C. The overall effect is a more homogeneous, statistical distribution of carbon, which causes two effects: First, the PL signal experiences a blue shift, because homogenization of the carbon concentration smears out the local band gap minima in regions of originally enhanced con-

centration. Second, the line width becomes narrower as the statistical fluctuations become smaller. This interpretation is corroborated by the fact that the ratio between NP signal and TO-replica decreases, which means a reduction of the symmetry-breaking alloy fluctuations.

(iii) Although the fluctuations of the carbon concentration become more homogeneous upon annealing, the remaining alloy is still random. This explains the red shift with increasing measurement temperature, which results from carriers bound to alloy fluctuations, as has been observed in $Si_{1-x}Ge_x$, too. With increasing temperature the electrons become mobile and establish an equilibrium distribution that preferentially fills the regions with the smallest band gaps.

(iv) The layers are thermally stable to beyond 850 °C, with no indications for a change of the average concentration of substitutional carbon. Thus noticeable diffusion of carbon or SiC precipitation requires higher temperatures and should not be a severe limitation for device processing.

1.4 Conclusions and Outlook

We have established MBE growth conditions for high-quality $Si/Si_{1-y}C_y$ and $Si/Si_{1-y}C_y/Si_{1-x}Ge_x$ samples with substitutional carbon concentrations of up to 1.7%. Well-behaved PL signals from band edge recombination in the $Si_{1-y}C_y$ layers, and at the $Si_{1-y}C_y/Si_{1-x}Ge_x$ interface, respectively, have been observed. The quality of the layers improves significantly upon annealing at moderate temperatures of about 725 °C, without affecting the substitutional carbon concentration. At these temperatures annealing mainly reduces the defect density in the layers and leads to a more homogeneous distribution of substitutional carbon. The layers are thermally stable to beyond 850 °C, where we observe first indications for a reduction of the substitutional carbon content.

Successful growth of carbon-containing, Si-based heterostructures is an important prerequisite for a future implementation of n-type MODFETs with tensilely strained $Si_{1-y}C_y$ quantum wells. In a next step growth conditions have to be adjusted to allow somewhat higher carbon concentrations of about 2 – 2.5%, which are necessary for the required conduction band offset of 130 to 160 meV. Such layers will allow the fabrication of MODFETs for an assessment of the electronic properties.

2. Nanostructuring of Semiconductors

(G. Brunthaler, H. Straub, A. Darhuber, T. Grill, Y. Zhuang, G. Bauer)

2.1 Introduction

The realization of semiconductor nanostructures is relevant for future electronic devices, optical emitters and the investigation of basic physical properties. In II-VI semiconductors the realization of wide band-gap blue-green diode lasers [13], [14] initiated the interest in light emitters from nanostructures. In such a nanostructure it is expected that low threshold laser structures can be realized.

In Si/SiGe heterostructures the investigation of nanostructures is driven by the miniaturization of today's integrated circuits and the potential of the Si/SiGe material system to increase the performance of such devices. Both material systems mentioned consist of

strained layers and the investigation of strain relaxation effects due to the formation of laterally patterned nanostructures is needed for practical implementations.

The purpose of our Si/SiGe study was to find a reliable etching procedure for the fabrication of Si/SiGe sub-micron structures. There are previous reports in the literature that in particular the sidewall steepness of SiGe embedded in Si is much worse than that of silicon. The etched Si/SiGe structures were than structurally characterized by x-ray diffraction.

2.2 Sample Preparation

The II-VI and Si/SiGe heterostructures were both grown by molecular beam epitaxy in Linz. The CdZnSe/ZnSe single quantum well (QW) heterostructures consist of a 1.1 μm thick, fully relaxed ZnSe buffer on top of the GaAs (001) substrate (grown by W. Faschinger). A 10 nm CdZnSe layer forms the QW and a 100 nm ZnSe layer acts as a cap. High density periodic patterns were defined either by holographic or electron beam lithography. In the case of e-beam lithography, well defined arrays of 40 x 40 μm^2 with wires and dots of different lateral size were written into a 150 nm thick polymethylmethacrylate (PMMA) resist layer. The lateral distance between individual pattern arrays is 150 μm. After deposition of a 40 nm thick titanium layer, a lift of process was used to produce the metallic structures on top of the sample with area filling factors between 0.5 and 0.15. These patterns were transferred into the QW structure by reactive ion etching (RIE).

During the RIE process the sample is exposed to a reactive gas plasma which contains active species that etch the material by chemical reactions. A CH_4/H_2 gas mixture (1:6 volume ratio) with a high frequency power of 90 W (corresponding to a DC bias of 450 V) at a pressure of 3.3 Pa (25 mTorr) is used for the II-VI compounds. The surface morphology and the lateral sizes of the etched structures were investigated by scanning electron microscopy (SEM). A typical SEM micrograph for small wires is shown in Fig. 4.

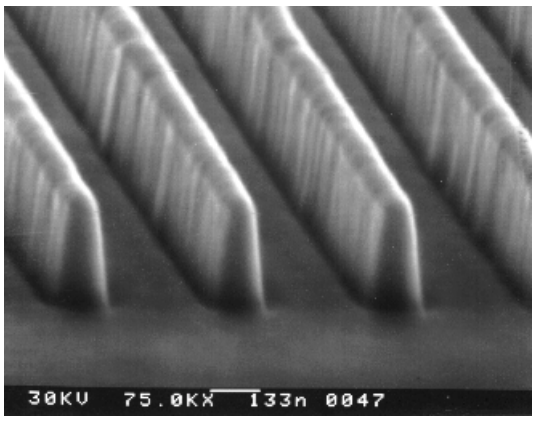

Fig. 4: Scanning electron microscopy image of CdZnSe/ZnSe wire structures defined by electron beam lithography and fabricated by reactive ion etching with a CH_4/H_2 gas mixture.

Si substrates and Si/SiGe multiquantum well layers (Ge-content: about 20%, 10 periods, Si layer width: 20.5 nm, and SiGe layer width of 1.8 nm) were laterally patterned using

holographic lithography (λ = 458 nm) by reactive ion etching. The period of the wires is about 400 nm, the wire width about 200 nm. The etching depth is about 200 nm. The etching gases consisted of a mixture of SF_6 and CH_4 (90%/10% mixing ratio) using the following parameters. The rf-power was 30 Watt, the pressure 40 mTorr, the flowrate of SF_6 was 50 sccm, and for CH_4 it was about 2.5 sccm. (The corresponding parameters for the Si/SiGe MQW samples were the same). The remaining photoresist was taken off by an oxygen plasma. The surface morphology of the samples was investigated by scanning electron microscopy. The structural parameters were studied by different x-ray diffraction techniques, as described below.

2.3 Optical Investigations

Low temperature (T = 1.9 K) PL measurements were performed with an x-y mapping set-up with a spatial resolution of 30 µm (determined by the laser spot diameter). The $Cd_{0.2}Zn_{0.8}Se$ QW embedded in ZnSe barriers (with a low temperature band gap E_g = 2.820 eV) was resonantly excited with an Ar^+ ion laser at an energy of 2.708 eV (457.9 nm) with about 100 W/cm^2. The PL spectra of the $Cd_{0.2}Zn_{0.8}Se$/ZnSe wires and dots with lateral dimensions between 80 and 1000 nm are shown in Fig. 5. The width of the PL emission line from the 2D reference mesa on the same sample is about 8 meV, a value which is essentially caused by alloy fluctuations in the ternary CdZnSe layer. Thus the splitting between free and bound excitons cannot be resolved.

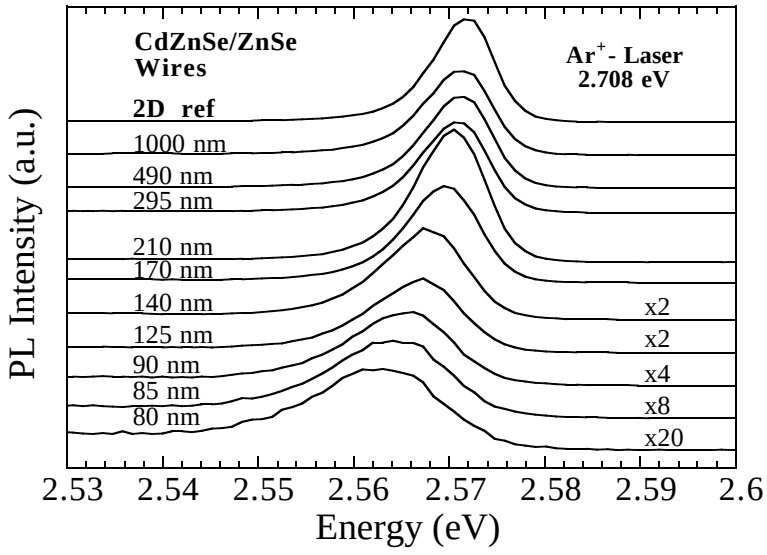

Fig. 5: Photoluminescence spectra of CdZnSe/ZnSe wire structures for lateral width of 80 to 1000 nm at 1.9 K. In addition the 2D quantum well reference spectrum on the same sample piece is shown.

Figure 6 shows the peak position of the PL line for wire and dot structures with lateral width between 80 and 1000 nm. A significant red shift occurs for wire sizes below 300 nm and dot sizes below 500 nm which is about 8 to 10 meV for the smallest wires and dots, respectively. The observed red shift will be discussed and compared with calculated band gap changes due to strain relaxation below.

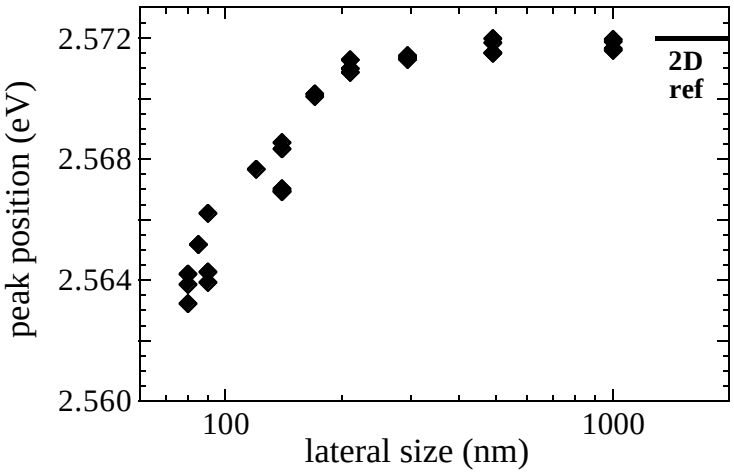

Fig. 6: Photoluminescence peak position of wire structures between 80 and 1000 nm for a resonant excitation energy of 2.708 eV (457.9 nm).

2.4 Strain Relaxation and Band-Gap Changes

Due to the formation of free perpendicular surfaces during the lateral patterning, the strained layers are able to relax partly. This is shown in Fig. 7 schematically for a thin wire structure. In order to calculate the detailed strain distribution of the wire structures, we follow an analytical method outlined by Faux and Haigh [15] but adopted it for our [110] oriented wires. This method solves the Airy stress equation by a Fourier series ansatz. The advantage of this method is that it is analytic, the disadvantage (as compared e.g. to finite element methods) is that only simple geometries can be treated with a restricted range of boundary conditions.

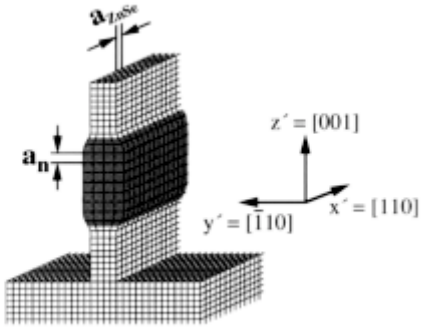

Fig. 7: Schematic strain relaxation of a laterally thin, partly relaxed CdZnSe/ZnSe wire.

Figure 8 shows the calculated strain distribution $\varepsilon_{y'y'}$, for a 80 nm wide wire of our CdZnSe/ZnSe structure, where the coordinate y´ in the epitaxial plane but perpendicular to the wires. The magnified displacements (by a factor 20) characterized by $\varepsilon_{y'y'}$ and ε_{zz} are shown in Fig. 9 for the wire cross section (the y´z-plane). It is clearly visible that the distortions are largest at the free surfaces. The shear component $\varepsilon_{y'z}$, which characterizes the deviations from a rectangular grid, is largest at the interface between the CdZnSe well and ZnSe barrier layers close to the free surface.

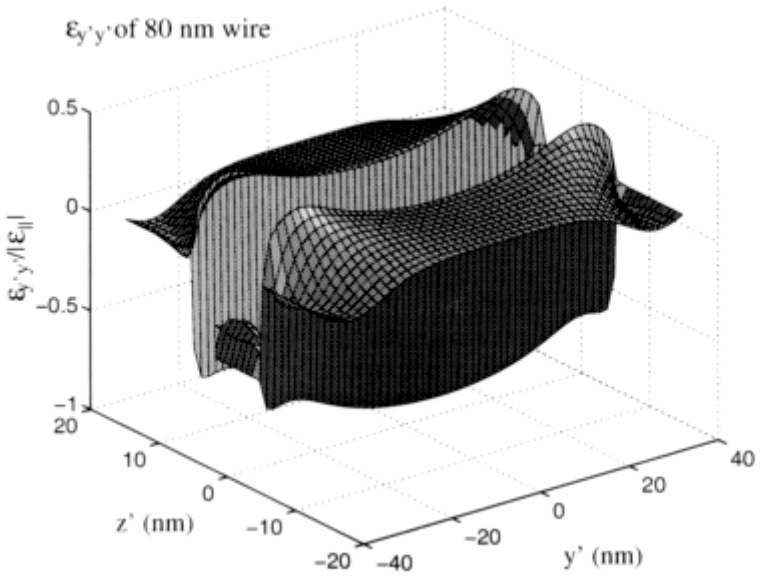

Fig. 8: Strain component $e_{y'y'}$ for the wire cross section y′z with the y′ direction in the quantum well plane but perpendicular to the wire and the z direction along the growth direction.

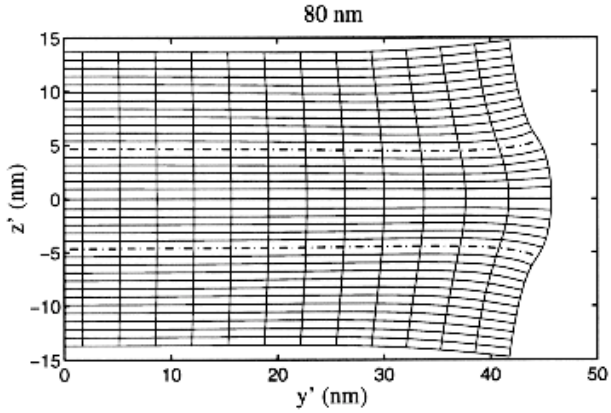

Fig. 9: The displacement, magnified by a factor 20, according to the strain components $e_{y'y'}$ and e_{zz} for the wire cross section (y′z-plane).

In <110> wires the non-uniform lattice deformation induces a piezoelectric polarization field [16], [17], [20]. The piezoelectric effect is directly connected with the shear components (shear strains ε_{jk}, $j \neq k$) as these describe the distortions of the cubic crystallographic cell. The potential distribution due to the piezoelectric were calculated accordingly for our wire structure with a width of 80 nm. The potential difference between upper and lower interface along the z-direction is about 12 meV. This bending of the quantum well potential and the associated electric field leads to a Stark effect which shifts the energy levels in the center of the well only by about 0.5 meV. Compared to the observed red shifts and the changes of the band gap due to deformation potential

coupling, the effects due to piezoelectric coupling will be only important at still smaller wire structures.

Due to the lateral wire confinement by RIE patterning in 80 nm structures, the eigenstate energies inside the CdZnSe well change by less than 0.5 meV for electrons and 0.4 meV for heavy holes. These additional lateral confinement energies (blue shifts) are much smaller than the experimentally observed red shifts and will not give a relevant contribution.

The band gap changes due to the elastic strain relaxation in the wire structures are much more important. For the conduction band, the strain induced energetic shifts are easily calculated as no splitting of degeneracies due to a tetragonal or orthorhombic distortion of the lattice occurs. Only the hydrostatic component of the lattice affects the position of the CB edge [18]. The situation for the VB is more complicated as even in the 2D QW system (tetragonal distortion without the presence of shear strain components), the four-fold degeneracy (Γ_8, including spin) of the cubic T_d crystal symmetry is removed. The energy levels of the valence band for cubic systems can be described by the k·p perturbation approach [19]. The effects of strain, confinement or other distortions can be included in the Hamiltonian of the system by using perturbation theory [22]. The deformation potential parameters a_v, b and d as introduced by Bir and Pikus [21] describe the energetic changes due to hydrostatic, tetragonal and shear deformations of the lattice, respectively. The solutions for the 6x6 Hamiltonian are obtained by numerical diagonalization for a given set of strain components which itself depends on the y′-z position inside the wire cross section. The resulting variation of the band gap over the cross section of the 80 nm wire is shown in Fig. 10.

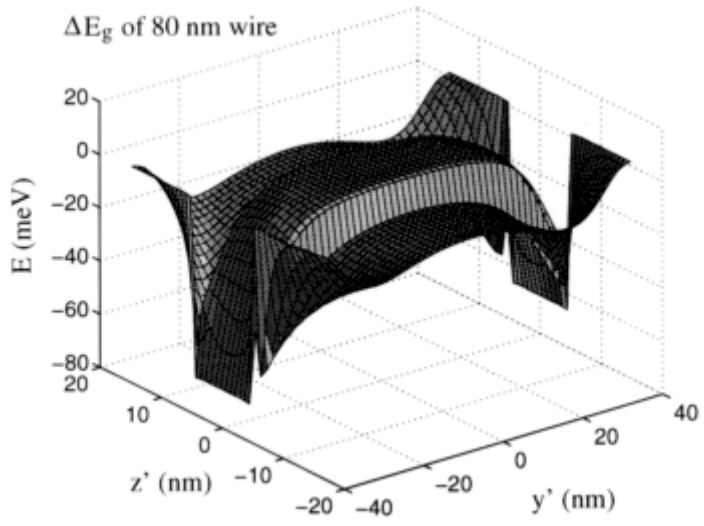

Fig. 10: Variation of the band-gap on the wire cross section (y′z-plane) for lateral wire width of 80 nm.

The calculated band gap changes of about 8 meV for the 80 nm wire structure are comparable with the experimentally observed PL line width of the 2D reference area on the sample. It is thus not expected to resolve any splitting of lines, but just a broadening and shift. It is also unknown how the PL emission efficiency is correlated with the spatial

position in the wire structure. This efficiency depends on the RIE induced damage near the free surfaces as well as on the carrier diffusion after generation by incident laser beam. In Fig. 11 the calculated averaged energetic band gap shift is compared with the experimentally observed spectral red shift of the PL emission and gives a quantitative agreement.

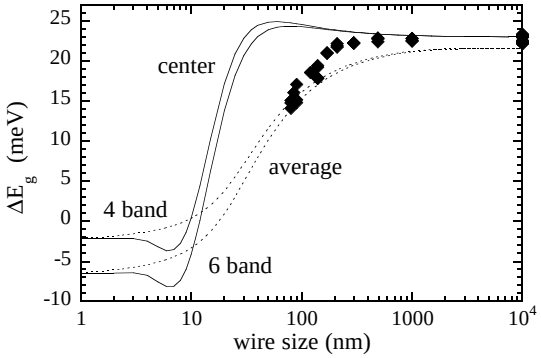

Fig. 11: Comparison of the calculated energy gap shift, averaged over the wire cross section, with the photoluminescence peak position for lateral wire width between 80 and 1000 nm. For comparison the gap in the center of the wire is shown for 6-band and 4-band calculation.

2.5 X-Ray Investigations

The structural parameters of the Si/SiGe multiquantum well layers were studied by employing x-ray diffraction techniques, like double and triple crystal diffractometry. In Figs. 12a and b (311) ω-scans are shown for two Si-wire samples, with identical period (glancing angle exit diffraction). For the sample shown in Fig. 12a, the etching time was 13 min, for the sample shown in Fig. 12b it was 17 min. Since the number of wire satellites in Fig. 12b is somewhat larger, the structural quality of the periodic wire structures has certainly been improved.

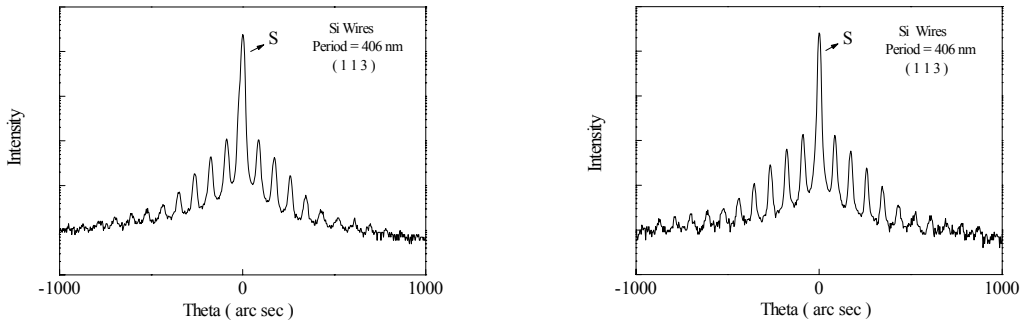

Fig. 12: ω-scans (113 reflection) of Si wire structures (area filling factor 0.5, period 406 nm) for RIE exposure times of 13 and 17 min, respectively)

Reciprocal spacemaps around the (004) and the (311) reflection were recorded for the etched Si/SiGe multilayer samples (sample code: SiGe 46, which was grown by Stefan Zerlauth in the SiGeC MBE apparatus in Linz) as shown in Figs. 13a and 13b. Not only

the MQW structure was etched through, but also part of the Si-buffer layer has been etched, as evidenced from the satellites accompanying the substrate peak marked by S. The MWQ structure gives rise to a superlattice peak (SL_O) which is accompanied along the q_x-direction by wire satellites. The period from the wire satellites is about 410 nm. A strain analysis based on these data will be performed.

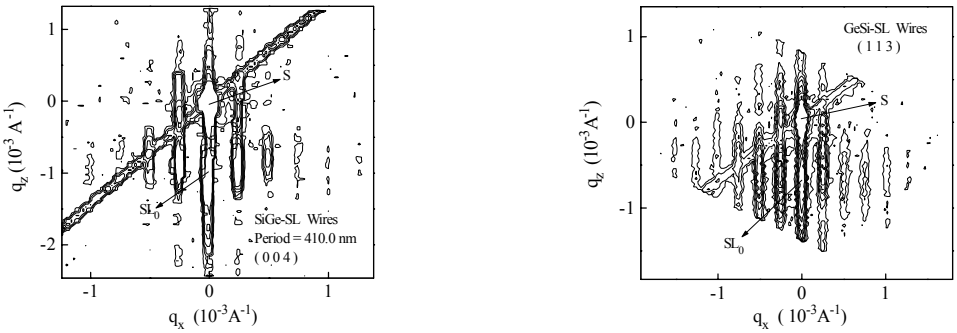

Fig. 13: (004) and (113) reciprocal space maps of a Si/SiGe wire structure (period 410 nm).

3. Silicon Technology

(F. Schäffler, G. Steinbacher)

For an implementation of Si-based device structures it is important to remain compatible with standard Si technologies as far as possible. Because the chemistry of $Si_{1-x}Ge_x$ and $Si_{1-y}C_y$ layers is very similar to that of Si, many process sequences can be utilized without modification. However, processes employing high temperatures, such as post-implantation annealing or high temperature thermal oxidation, have to be adjusted toward low thermal budgets to account for the metastability of most Si-based hetero-layer sequences. Thus heterodevices will have to utilize, and also may promote, a general trend toward lower processing temperatures, which is driven by leading-edge VLSI circuits, where the critical submicron feature sizes are jeopardized by thermal diffusion processes during high temperature steps.

For the development of Si-compatible, low-thermal-budget processing modules, as well as for a quick characterization of the electronic properties of epi-layer sequences, a versatile test layout with five mask layers was developed. The test elements reach from a simple transmission line arrangement for the assessment of the sheet and contact resistances of implanted and annealed ohmic contacts and variable-geometry Schottky diodes for an evaluation of Schottky barrier heights and periphery leakage currents, to gated multi-contact Hall bars and simple mesa-type FETs with variable gate lengths. The process sequence involves a self-aligned mesa etching step, which is essential for the gated Hall structures. All mask layers use a positive layout, which requires a image reversal photo resist (such as AZ5218) for the mesa process. Minimum feature sizes for optical contact lithography are 1μm, and additional marks for e-beam alignment are provided, which will allow the implementation of sub-micron gate lengths.

A complete processing sequence based on the five-layer layout was developed, which uses ion implantation and reactive ion etching for lateral structuring of the heterostruc-

tures, and — presently — lift-off processes for the metallization layer. Fig. 14 shows a cross-sectional view of an AZ5218 pattern with submicron feature size, which was achieved by controlled underexposure and appropriate development of the resist.

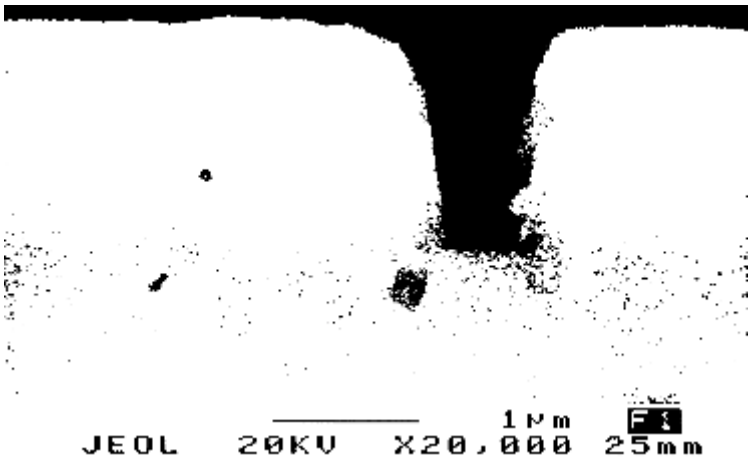

Fig. 14: Sub-micron resist pattern realized in image reversal resist AZ5218

4. X-Ray Diffractometry and Strain Analysis of Low-Dimensional Semiconductor Structures

(A.A. Darhuber, J. Stangl, S. Zerlauth, G. Bauer)

Strain relaxation in lattice mismatched systems has recently attracted a lot of attention with the increased application of strained layers in microelectronic and optoelectronic systems. There are in general two routes for strain relaxation: (i) plastic relaxation through misfit dislocation formation and (ii) elastic relaxation through a strain induced transition from a two dimensional planar growth mode to a three dimensional island morphology (as it is possible for compressively strained epilayers like Ge on Si or InAs on GaAs).

The strain induced islanding (Stranski-Krastanow growth mode) has found of lot of interest since it provides a possible mechanism for the formation of self-assembled quantum dots. Whereas changes of the surface morphology were already thoroughly studied and the conditions to control the size distribution and the self organizing behavior of the islands are rather well known, direct information on the strains and their relaxation is still lacking. These data are required for a proper interpretation of the electronic properties of such self-assembled dots. Therefore, we have been studying the structural properties of Ge dot multilayers embedded in Si (grown by MBE both at the Walter Schottky Institut as well as in Linz by S. Zerlauth) as well as of InAs dot multilayers in GaAs (grown at the Ioffe Institute St. Petersburg and at the Technical University Berlin) by x-ray diffraction techniques (reciprocal space mapping around symmetrical and asymmetrical reflections) and by x-ray reflectivity in Linz, at the ESRF Grenoble as well as at the Hasylab at DESY, Hamburg.

A typical cross sectional transmission electron microscopy micrograph of a SiGe dot multilayer is shown in Fig. 15, giving clear evidence for partial vertical ordering of the dots, as induced by strain fields. In addition to vertical ordering, lateral ordering in the (001) growth plane occurs as well, driven by the orientational dependence of the Young's modulus in this plane. For both Ge and InAs, the polar diagram of Young's moduli exhibit smaller values than that of the corresponding Si or GaAs matrix, with minima along the two orthogonal [100] and [010] directions.

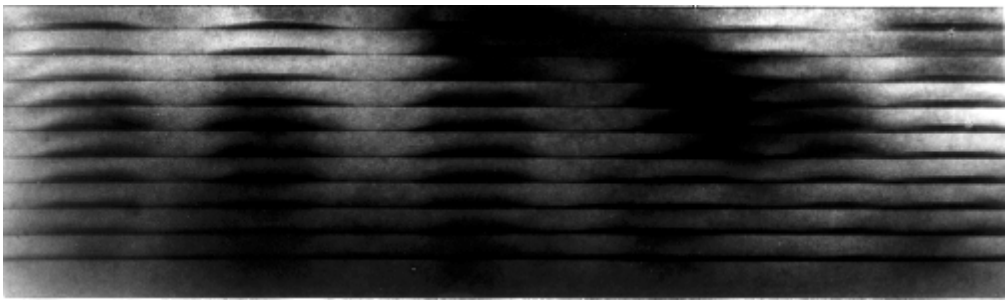

Fig. 15: Cross-sectional TEM, SiGe dot multilayer in Si (SiGe51).

So far from x-ray diffraction and reflectivity measurements the following information could be obtained:

(i) average values for the strain relaxation within the Ge dots in multilayers, as well as for the asymptotic strain in the Si matrix;

(ii) degree of vertical ordering of the dots in multilayers;

(iii) lateral ordering of the dots in the (001) plane in a square array along the [100] and [010] directions for Ge and InAs dots.

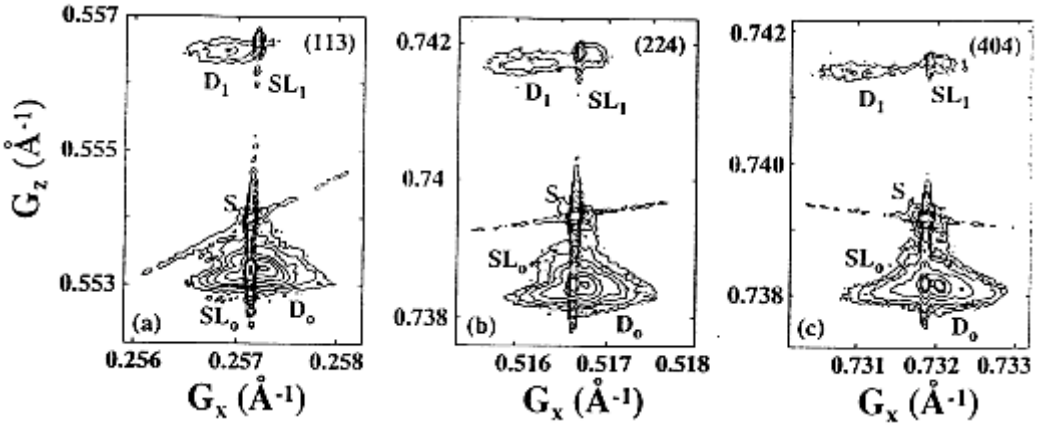

Fig. 16: Asymmetrical reciprocal space maps around the (113) (a), (224) (b), and (404) (c) reciprocal lattice points.

Figure 16 shows as an example the diffusely scattered intensity around (113), (224) and (404) reciprocal lattice points from a 19 period Ge dot multilayer sample (d = 30 nm). The diffusely scattered intensity comes from strained Si matrix regions (mainly around the central superlattice SL_0 peak) as well as from the dot region itself (SL_1).

More detailed investigations of the strain fields require:

(i) model calculations based on the finite element method or on the valence force model

(ii) grazing incidence diffraction measurements.

Acknowledgments

The investigations were further supported by several funding organizations like Fonds zur Förderung der wissenschaftlichen Forschung, Vienna, the Österreichische National-bank, the Projektforschung des BMWVK, and the Daimler Benz Research Organisation.

References

[1] for an overview see e.g. E. Kasper and F. Schäffler, Semiconductors and Semimetals Vol. 33, chapter 4, Academic Press, Boston 1991

[2] for an overview see e.g. A. Gruhle, Springer Series in Electronics and Photonics Vol. 52, chapter 4, Springer, Berlin 1994

[3] for an overview see e.g. U. König and F. Schäffler, Proc. Int. Conf. Solid State Devices and Materials (SSDM), Jap. Soc. Appl. Physics, Chiba 19993, p.201

[4] for an overview see e.g. H. Presting, H. Kibbel, M. Jaros, R.M. Turton, U. Menczigar, G. Abstreiter, and H.G. Grimmeiss, Semicond. Sci. Technol. 7, 1127 (1992)

[5] E.A.Fitzgerald, Y.-H. Xie, M.L. Green, D. Brasen, A.R. Kortan, J. Michel, Y.-J. Mii, and B.E. Weir, Appl. Phys. Lett. 59, 811 (1991)

[6] F.K. LeGoues, B.S. Meyerson, and J.F. Morar, Appl. Phys. Lett. 66, 2903 (1991)

[7] F. Schäffler, D. Többen, H.-J. Herzog, G. Abstreiter, and B. Holländer, Semiconductor Sci. Technol. 7, 260 (1992)

[8] K. Eberl, S.S. Iyer, and F.K. LeGoues, Appl. Phys. Lett. 64, 739 (1994)

[9] K. Brunner, K. Eberl, and W. Winter, Phys. Rev. Lett. 76, 303 (1996)

[10] K. Brunner, W. Winter, and K. Eberl, Appl. Phys. Lett. 69, 1279 (1996)

[11] F. Schäffler, M. Wachter, H.-J. Herzog, K. Thonke, and R. Sauer, J. Cryst. Growth 127, 411 (1993)

[12] L.P. Tilly, P.M. Mooney, J.O. Chu, F.K. LeGoues, Appl. Phys. Lett. 67, 2488 (1995)

[13] M.A. Haase, J. Qiu, J.M. DePuydt, H. Cheng, Appl. Phys. Lett. **59**, 1272 (1991).

[14] H. Jeon, J. Ding, W.R. Patterson, A.V. Nurmikko, W. Xie, D.C. Grillo, M. Kobayashi, R.L. Gunshor, Appl. Phys. Lett. **59**, 3619 (1991).

[15] D.A. Faux and J. Haigh , J. Phys.: Condens. Matter 2, 10289 (1990).

[16] M. Grundmann, O. Stier and D. Bimberg, Phys. Rev. B 50, 14187 (1994).

[17] L. De Caro and L. Tapfer, Phys. Rev. B 51, 4374 (1995).

[18] C.G. Van de Walle, Phys. Rev. B **39** 1871 (1989).

[19] E.O. Kane in *Semiconductors and Semimetals*, Ed. R.K. Willardson and A.C. Beer, Vol. 1, Academic Press, New York 1966.

[20] L. De Caro and L. Tapfer, Phys. Rev. B 51, 4381 (1995).

[21] G.L. Bir and G.E. Pikus, in "*Symmetry and strain induced effects in semiconductors"*, John Wiley, New York 1974.

[22] J. Singh, in Handbook on Semiconductors, Ed. T.S. Moss, Vol. 2 by M. Balkanski, (Elsevier Science, Amsterdam 1994), p. 235ff; J. Singh, in Physics of Semiconductors and their Heterostructures, Ed. Anne T. Brown, (McGraw-Hill, Amsterdam 1993), p. 218ff.

[23] A.A. Darhuber, V. Holy, J. Stangl,G. Bauer, P. Schittenhelm, G. Abstreiter: "Structural investigations for self assembled Ge dots by x-ray diffraction and reflection", Thin Solid Films, in print.

[24] A.A. Darhuber, V. Holy, J. Stangl,G. Bauer, P. Schittenhelm, G. Abstreiter: "Interface roughness in strained Si/SiGe multilayers", Materials Research Society, Boston , 1996, in print.

[25] A.A. Darhuber, V. Holy, J. Stangl, G. Bauer, A. Krost, F. Heinrichsdorff, M. Grundmann, D. Bimberg, V.M. Ustinov, P.S. Kopev, AS.O. Kosogov, P. Werner: "Lateral and vertical ordering in multilayered self-organized InGaAs quantum dots studied by high resolution x-ray diffraction", Appl.Phys.Lett., in print.

Project Information

Project Manager

Univ.-Prof. Dr. Günther BAUER

Institut für Halbleiterphysik, Johannes Kepler Universität Linz, A-4040 Linz

Project Group

Last Name	First Name	Status	Remarks
Brunthaler	Gerhard	Ph.D.	
Darhuber	Anton	dissertation	
Fünfstück	Britta	diploma student	
Grill	Thomas	diploma student	
Helm	Manfred	assistant professor	
Kruck	Peter	dissertation	
Li	Jianhua	Ph.D.	
Penn	Christian	dissertation	
Prinz	Adrian	dissertation	
Schäffler	Friedrich	associate professor	
Seyringer	Heinz	dissertation	
Stangl	Julian	dissertation	
Steinbacher	Günther	diploma student	
Straub	Hubert	dissertation	GMe funding
Zerlauth	Stefan	dissertation	
Zhuang	Yan	dissertation	

Books and Contributions to Books

1. G. Bauer and W. Richter, “Optical characterization of epitaxial semiconductor layers”, *Springer*, 1996.

Publications in Reviewed Journals

1. G. Brunthaler, G. Bauer, G. Braithwaite, N.L. Mattey, P. Philips, E.H.C. Parker, T.E. Whall : “Hot carrier transport in SiGe/Si two-dimensional hole gases”, *Proceedings of the International Conference on Hot Carriers in Semiconductors*, ed.: K. Hess et al., Plenum Press, New York 1996, p. 449.

2. H. Straub, G. Brunthaler, W. Faschinger, G. Bauer, C. Vieu: "Photoluminescence of CdZnSe/ZnSe quantum well structures fabricated by reactive ion etching", *J. Crystal Growth* 159, 451 (1996).

3. E. Wirthl, H. Straub, M. Schmid, H. Sitter, P. Bauer, G. Brunthaler: "AES analysis of plasma-etched ZnSe", *J. Crystal Growth* 159, 746 (1996).

4. J.H. Li, G. Bauer, L. Vanzetti, L. Sorba, A. Franciosi: "Strain and structural characterization of $Zn_{1-x}Cd_xSe$ laser structures grown on GaAs and InGaAs (001) substrates", *J. Appl. Phys*. 80, 81 (1996).

5. G. Bauer, J.H. Li, V. Holy: "High resolution x-ray reciprocal space mapping", *Acta Physica Polonica* A 89, 115 (1996).

6. G. Bauer, A. Darhuber, V. Holy: "Structural characterization of reactive ion etched semiconductor nanostructures using x-ray reciprocal space mapping", *Mat. Res. Soc. Symp. Proc.* 406, 457 (1996).

7. T. Fromherz, P. Kruck, M. Helm, G. Bauer, J.F. Nützel, G. Abstreiter: "Transverse magnetic and transverse electric polarized intersubband absorption and photoconductivity in p-type SiGe quantum wells", *Appl. Phys. Lett.* 68, 3611 (1996).

8. S. Yuan, H. Krenn, G. Springholz, Y. Ueta, G. Bauer, P.J. McCann: "Magnetoreflectivity of $Pb_{1-x}Eu_xTe$ epilayers and PbTe/$Pb_{1-x}Eu_xTe$ multi-quantum wells, *Phys. Rev. B,* in print.

9. W. Hilber, M. Helm, K. Alavi, R.N. Pathak: "Hot-electron power loss in a doped GaAs/AlGaAs superlattice at intermediate temperature studied by infrared differential spectroscopy", *Appl. Phys. Lett.* 69, 2528 (1996).

10. V. Holy, A.A. Darhuber, G. Bauer, P.D. Wang, Y.P. Song, C.M. Sotomayor Torres, M.C. Holland: "Elastic strains in GaAs/AlAs quantum dots studied by high resolution x-ray diffraction", *Solid State Electronics* 40, 373 (1996).

11. M. Helm, P. Kruck, T. Fromherz, A. Weichselbaum, M. Seto, G. Bauer, Z. Moussa, P. Boucaud, F.H. Julien, J.-M. Lourtioz, J.F. Nützel, G. Abstreiter: "Infrared studies of p-type Si/SiGe quantum wells: intersubband absorption, infrared detectors, and second harmonic generation", *Thin Solid Films*, in print.

12. P. Kruck, M. Helm, T. Fromherz, G. Bauer, J.F. Nützel, G. Abstreiter: "Medium-wavelength, normal incidence, p-type Si/SiGe quantum well infrared photodetector with background limited performance up to 85 K", *Appl. Phys. Lett.* 69, 3372 (1996).

13. W. Hilber, M. Helm, K. Alavi, R.N. Pathak: "Energy relaxation of hot electrons in GaAs/AlGaAs superlattices measured by infrared differential spectroscopy", *Superlattices and Microstructures* 21, 85 (1997).

14. A.A. Darhuber, V. Holy, J. Stangl, G. Bauer, A. Krost, M. Grundmann, D. Bimberg, V.M. Ustinov, P.S. Kop'ev, A.O. Kosogov, P. Werner: "High resolution x-ray diffraction and reflectivity studies of vertical and lateral ordering in multiple self-organized InGaAs quantum dots", *Jap. J. Appl. Phys.*, submitted.

15. M. Helm, P. Kruck, T. Fromherz, M. Seto, G. Bauer, J.F. Nützel, G. Abstreiter: "Intersubband transitions, infrared detectors and optical nonlinearities in SiGe multiquantum wells", *Mat. Res. Soc. Symp. Proc. 1997*, in print.

16. M. Wollitzer, J. Buechler, F. Schäffler, J.-F. Luy: "D-band Si-IMPATT diodes with 300mW CW output power at 140 GHz", *Electronics Lett*. 32, 122 (1996).

17. D. Többen, D.A. Wharam, G. Abstreiter, J.P. Kotthaus, F. Schäffler: "Quantized conductance in a $Si/Si_{0.7}Ge_{0.3}$ split-gate device and impurity related magnetotransport phenomena", *Solid State Electronics* 40, 405 (1996).

18. M. Holzmann, D. Többen, P. Baumgartner, G. Abstreiter, A. Kriele, H. Lorenz, F. Schäffler: "Magnetotransport of electrons in arrays of wires in $Si/Si_{0.7}Ge_{0.3}$ heterostructures", *Surf. Sci*. 361/362, 673 (1996).

Presentations

1. G. Brunthaler, T. Dietl, M. Sawicki, G. Stöger, J. Jaroszynski, A. Prinz, F. Schäffler, G. Bauer: "Metal-Insulator Transition in Sb-Doped Short Period Si/SiGe Superlattices", *9th International Winterschool on New Developments in Solid State Physics "Nanostructure Physics and Technology"*, Mauterndorf, Austria, Feb. 19 – 23, 1996 (invited).
2. G. Brunthaler, T. Dietl, A. Prinz, G. Stöger, M. Sawicki, J. Jaroszynski, F. Schäffler, G. Bauer: "Magnetic Field Induced Metal to Insulator Transition in Si/SiGe Short Period superlattices", *International Conference on the Application of High Magnetic Fields in Semiconductor Physics*, Würzburg, 28 July – 2 August 1996 (invited).
3. G. Brunthaler: "Localization in doped Si/SiGe heterostructures and superlattices", *International Conference on Electron Localization and Quantum Transport*, Jaszowiec, Poland, 3 – 6 Aug. 1996 (invited).
4. G. Brunthaler: "Können Halbleiter-Bauelemente mit einzelnen Elektronen funktionieren?", *ÖPG Jahrestagung*, Linz, 27. Sept. 1996 (invited).
5. A.A. Darhuber, J. Stangl, V. Holy, G. Bauer: "Structural investigation of quantum dot multilayers by x-ray diffraction", *2nd International Workshop on MBE Growth Physics and Technology*, 21 – 25 October 1996,Warsaw, Poland (invited).
6. M. Helm: "Intersubband transitions, infrared detectors, and optical nonlinearities in SiGe multiquantum wells", *Fall Meeting of the Materials Research Society (MRS)*, Boston, MA, USA, December 2 – 6, 1996 (invited).
7. M. Helm: "Infrared studies of p-type Si/SiGe quantum wells: intersubband absorption, infrared detectors, and second harmonic generation", *E-MRS Spring Meeting*, Strasbourg, France, June 1996 (invited).
8. G. Brunthaler, T. Dietl, G. Stöger, M. Sawicki, J. Jaroszynski, A. Prinz, F. Schäffler, G. Bauer: "Anderson-Mott Übergang in Si/SiGe:Sb Übergittern", *Frühjahrstagung der DPG*, Regensburg, 1996.
9. A.A. Darhuber, J. Stangl, G. Bauer, A. Krost, F. Heinrichsdorff, M. Grundmann, D. Bimberg: "Structural characterization of single and multiple layers of self assembled InGaAs quantum dots by high resolution x-ray diffraction and x-ray reflectivity", *23rd International Conference on the Physics of Semiconductors*, July 21 – 26, Berlin, Germany.
10. A.A. Darhuber, J. Stangl, V. Holy, G. Bauer, F. Heinrichsdorff, A. Krost, M. Grundmann, D. Bimberg, V.M. Ustinov, P.S. Kop'ev: "High resolution x-ray

diffraction and reflectivity studies of vertical and lateral ordering in multiple self assembled InGaAs quantum dots", *International Symposium on Formation, Physics and Device Application of Quantum Dot Structures*, Nov. 4 – 7, 1996, Hokkaido University, Sapporo, Japan.

11. A.A. Darhuber, V. Holy, J. Stangl, G. Bauer, J. Nützel, G. Abstreiter: "Interface roughness in strained Si/SiGe multilayers", *Materials Research Society Fall Meeting*, Boston, MA, USA, December 2 – 6, 1996.
12. A.A. Darhuber, V. Holy, J. Stangl, G. Bauer, P. Schittenhelm, G. Abstreiter: "Structural investigations of self-assembled quantum dots by x-ray diffraction and reflection", *Materials Research Society Fall Meeting*, Boston, MA, USA, December 2 – 6, 1996.
13. W. Heiss, B.N. Murdin, C.J.G.M. Langerak, S.-C. Lee, G. Strasser, C.R. Pidgeon, I. Galbraith, E. Gornik, M. Helm: "The LO-phonon bottleneck in the intersubband cooling in wide quantum wells", *23rd International Conference on the Physics of Semiconductors*, July 21 – 26, Berlin, Germany.
14. W. Hilber, M. Helm, K. Alavi, R.N. Pathak: "Energy relaxation of hot electrons in GaAs/AlGaAs superlattices measured by infrared differential spectroscopy", *9th International Conference on Superlattices and Microstructures*, 14 – 19 July 1996, Liège, Belgium.
15. P. Kruck, A. Weichselbaum, M. Helm, T. Fromherz, G. Bauer, J.F. Nützel, G. Abstreiter: "Polarization dependent intersubband absorption and normal-incidence infrared detection in p-type Si/SiGe quantum wells", *9th International Conference on Superlattices and Microstructures*, 14 – 19 July 1996, Liège, Belgium.
16. P. Kruck, T. Fromherz, M. Helm, G. Bauer, J.F. Nützel, G. Abstreiter: "p-typ Si/SiGe Quantentopf-Infrarotdetektoren: Untersuchung der polarisationsabhängigen Photoleitung und Absorption", *Frühjahrstagung der Deutschen Physikalischen Gesellschaft*, Regensburg, 1996.
17. J.H. Li, G. Springholz, F. Schäffler, G. Bauer: "Strain Status and Surface Morphology of SiGe Heterostructures", *MRS Spring Meeting*, San Francisco 8 – 12 April 1996.
18. S. Zerlauth: "MBE growth and structural characterization of $Si_{1-y}C_y/Si_{1-x}Ge_x$ superlattices", *Ninth International Conference on Molecular Beam Epitaxy*, August 5 – 9, Malibu, Kalifornien.
19. S. Zerlauth: "Grenzflächenrauhigkeit am System SiGeC", *MBE-Workshop in Frankfurt/Oder*, Sept. 15 – 17, 1996.
20. S. Zerlauth, W. Faschinger, G. Bauer, L. Palmetshofer: "Elektrische Eigenschaften von modulationsdotierten $Si/Si_{1-x}C_x/Si$-Strukturen" (Poster), *Frühjahrstagung der Deutschen Physikalischen Gesellschaft*, 25 – 29 March 1996, Regensburg, Germany.

Doctor's Theses

1. A. Darhuber: "X-ray diffractometry of self-organized low-dimensional systems", in progress.
2. P. Kruck: "Infrared spectroscopy of semiconductor quantum well systems", in progress.
3. C. Penn: "Electronic properties of $Si/Si_{1-y}C_y$ heterostructures", in progress.
4. H. Seyringer: "Fabrication and characterization of Si based heterostructure devices", in progress.
5. J. Stangl: "X-ray diffraction and reflectivity from semiconductor heterostructures", in progress.
6. H. Straub: "Lateral patterning of II-VI compounds by holographic lithography and reactive ion etching", in progress.
7. S. Zerlauth: "Molecular beam epitaxy of SiGeC", in progress.
8. Y. Zhuang: "Fabrication of laterally structured semiconductor heterolayers", in progress.
9. A. Prinz: "Carrier localization in Si/SiGe heterostructures", in progress

Cooperations

1. Walter Schottky Institut, TU München, Garching, Germany, Prof. Abstreiter
2. CEA-CNRS Microstructures de Semiconducteurs II-VI, Grenoble, Prof. Mariette
3. Universität Würzburg, Physikalisches Institut, Prof. Landwehr
4. ESRF Grenoble, Optics Beamline, Dr. A. Freund, Dr. A. Souvorov
5. DESY Hamburg, D6 Beamline, Prof. Materlik, Dr.H.Rhan
6. Daimler Benz Forschungslaboratorien Ulm, Dr. Presting, Dr. König
7. Universität Stuttgart, Prof. Kasper
8. Nanoelectronics Research Centre, University of Glasgow, Prof. Sotomayor-Torres
9. Institut für Festkörperelektronik, TU Wien

Characterization of Si-based Structures by Luminescence and ESR Experiments

W. Jantsch, S. Lanzerstorfer, M. Stepikhova, L. Palmetshofer

Institut für Halbleiterphysik, Johannes Kepler Universität, A-4040 Linz, Austria

Bulk Si, quantum-well structures of SiGe, and porous Si structures have been investigated by luminescence and electron-spin-resonance (ESR) methods. In luminescence we find after implantation and thermal treatment residual impurities with finger-print spectra and also dislocation related structures. The latter are distinguishable from other defects by their characteristic dependence on hydrostatic pressure and temperature. In ESR experiments, cyclotron resonance is clearly visible, which offers the possibility to detect free carriers without the need for contacts.

1. Introduction

Among the current problems in the technology of Si there is (i) the development and the integration of light emitting elements [1], [2] and (ii) the development of ultra-small ultra-fast devices. In both cases, small structures are used and effective characterization methods are needed to identify residual defects, carrier concentration and their mobility, dimensionality of the structure, etc. In many cases, electrical contacts impose substantial problems in such structures and therefore contactless methods are preferred if available. Among the standard methods for the characterization of defects is photo-luminescence which in high quality crystals can detect defect concentrations as low as 10^{10} cm^{-3}, in some cases sufficient also for low-dimensional samples. The spectra reveal their origin, however, only in rather specific cases. Electron spin resonance (ESR) in principle is more powerful since it yields information also on the chemical identity of the defect and its neighbors. On the other hand, ESR relies on the absorption of microwaves which penetrate the whole sample and thus its sensitivity is rather described by an absolute number of spins which for typical defects in Si is of the order of 10^{12}, too large for small structures. The sensitivity for free carriers in ESR can be much bigger, a few thousand electrons can be easily detected in cyclotron resonance if the mobility is high enough as it was demonstrated in the course of this project.

In this paper we concentrate on two examples of luminescence results. Some of the luminescence spectra seen exhibit sharp, characteristic patterns due to phonon replica and their isotope splittings, constituting a fingerprint of the defect species. Copper*, e.g.*, is clearly seen and detectable as a frequent contamination after even simple technological steps. Other luminescence spectra produce rather wide and less characteristic features and sometimes they are not clearly distinguishable from other luminescence centers. As an example, we present data obtained on Er-implanted samples which show, after specific treatment, meant for annealing of implantation defects, a strong emission [4] close to the technically interesting wavelength of 1.54 μm. We show that this emission at low temperature really is due to Er, but at temperatures above 150 K, luminescence due to dislocations prevails.

In part 3 we present photoluminescence data on porous Si which was doped electrolytically by Er. We observe emission of the characteristic 1.54 µm emission of Er even above room temperature although in bulk Si it is quenched already below 200 K.

2. Photoluminescence Due to Dislocations on Doped Si

Although Si plays the dominant role in microelectronics, it suffers for principle reasons in optoelectronic applications: Because of its indirect gap it does not permit the fabrications of band edge emitters in contrast to III-V and II-VI compounds. In the past few years, possibilities to overcome this shortcoming were investigated making use of luminescence due to localized states. One idea in this context was to utilize the intra-4f transitions of rare earth elements, and here in particular those of Er, whose lowest transition occurs at 1.54 µm, close to the damping minimum of silica fibers [4]. In the past few years, the weak luminescence yield was optimized but a principle problem still appears unsolved: the luminescence quenches at temperatures well below room temperatures, excluding technical application [3]. More recently, however, reports appeared, claiming electroluminescence also at room temperatures due to Er in Si. In order to clarify the origin of this luminescence we have investigated samples which show luminescence close to 1.5 µm also at 300 K.

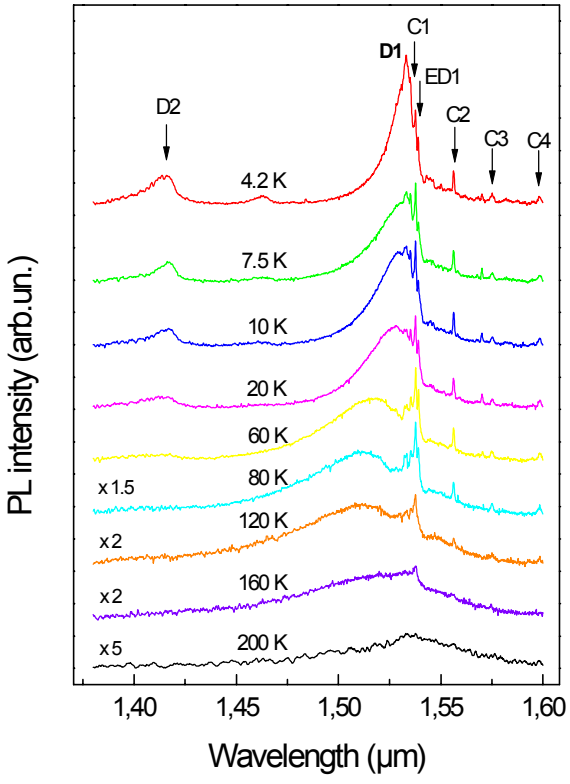

Fig. 1: Photoluminescence spectra of Er-implanted CZ-Si as a function of different temperatures.

The nature of this emission is more clearly seen in low temperature experiments. In Fig. 1, luminescence spectra are shown obtained in CZ-Si implanted with Er (2 MeV, $3 \cdot 10^{13}$ cm^{-2}) after annealing at 900 °C for 30 min. At low temperatures, the emission due

to interstitial (cubic) Er is seen (lines marked C1…C4) together with a line due to an Er complex [5]. In addition, a wide structure is seen close to 1.5 µm which, together with the line marked D2 is attributed to dislocations in the literature. The structure at 1.5 µm, known as D1 line in the literature [6], exhibits also a characteristic temperature shift — at low temperatures towards shorter, above 80 K towards longer wavelengths — whereas the Er line positions remain independent of temperature owing to the extremely localized nature of the 4f states.

Another characteristic feature of the Er lines is their independence on pressure which allows to distinguish them easily from the dislocation luminescence. This is shown in Fig. 2, where low temperature spectra are given for different hydrostatic pressure. It is clearly seen that the D-lines shift towards shorter wavelength whereas the Er lines remain independent of pressure. The pressure coefficient for the transition energy is evaluated to be -2.3 meV/kbar which may serve as an additional characteristic feature of the dislocation luminescence.

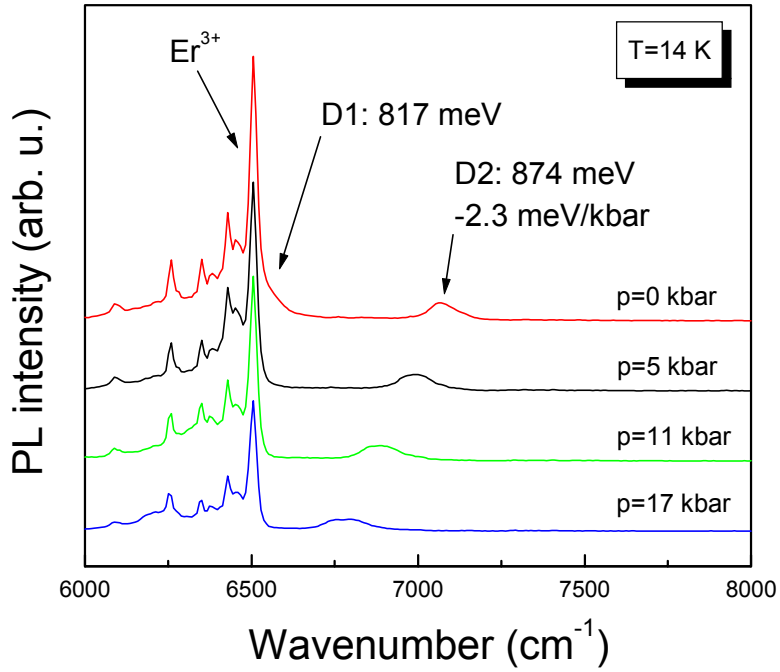

Fig. 2: Luminescence spectra of CZ Si:Er for pressures of 0, 5, 11, and 17 kbar, respectively. The highest pressure corresponds to the lowest D2 position.

The dislocation luminescence is seen also in electroluminescence devices designed for Er emission. Junctions prepared by implanting Er into p-type Si exhibit the same type of electroluminescence spectra when operated under forward bias condition as shown in Fig. 1, *i.e.*, they give strong Er luminescence at low temperature but above 150 – 180 K only the dislocation emission is seen.

3. Luminescence of Porous Si:Er

The temperature induced quenching of the Er luminescence in different host materials seems to correlate to the energy gap of the host: the bigger the energy gap, the higher the

critical temperature for quenching. Therefore, in order to improve the luminescence yield, any measure to increase the gap of Si based material should help. In order to test this hypothesis, we have produced porous Si by anodic etching. Porous Si consists of single crystal material with pores and columns of about 40 Å in diameter. Porous Si has been investigated in the last few years because of its bright visible photo- and electroluminescence which is interpreted in terms of the blue shift of the band edge emission due to electronic confinement in the small structures.

We introduced Er into po-Si electrolytically from $ErCl_3$ dissolved in ethanol. After annealing at 1000 °C for 10 s in an O_2/N_2 atmosphere the samples show sharp and intense Er-related emission which can be clearly demonstrated by excitation spectroscopy: The emission of the 1.54 µm can be excited resonantly both in the 870 and the 980 nm bands, which correspond to the transitions from the J=15/2 ground state of Er to the 9/2 and the 11/2 states, respectively. In bulk Si, these excitations are not detectable because of the strong competition of the interband transitions — these transitions are situated already above the gap of single crystal Si.

In Fig. 3 we show the temperature dependence of our po-Si:Er emission at 1.54 µm as a function of temperature in comparison to other Si-based host material. The dramatic improvement as compared to single crystal bulk Si is clearly seen which again demonstrates the empirical rule of Favennec [3].

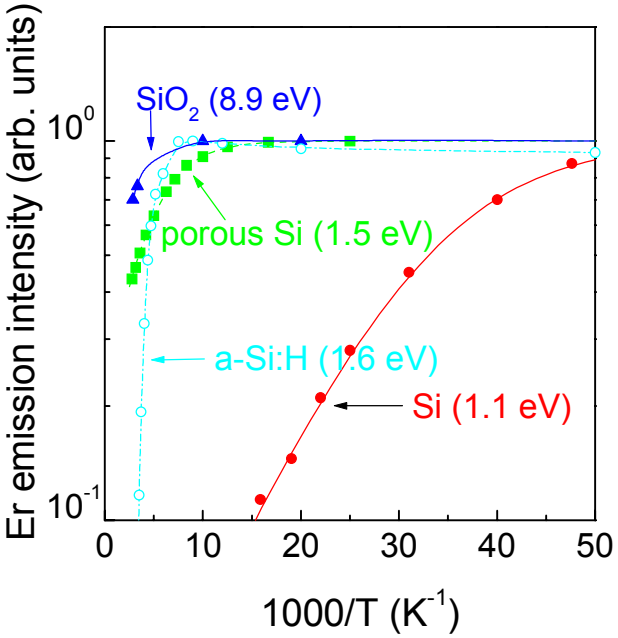

Fig. 3: Normalized luminescence yield of Er in Si-based material as a function of inverse temperature for bulk Si, amorphous Si, po-Si and SiO_2.

4. Conclusions

In this report we have shown that the technologically interesting luminescence of Er in Si can be improved dramatically at high temperatures by using Si-related material with larger energy gap: In agreement with the rule of Favennec, the thermal quenching of the

Er luminescence occurs at higher temperatures for material with higher energy gap. Porous Si provides one of very few possibilities so far to increase the gap of Si (the alloys of Si have a tendency for smaller gaps only). Reports in the literature on room temperature Er emission in electro-luminescence of forward biased p-n junctions should be reconsidered in view of our present results which show that the emission observed in our samples are due to dislocations at elevated temperature.

References

[1] W. Jantsch, H. Przybylinska, C. Skiebiszewski, S. Lanzerstorfer, L. Palmetshofer (invited): "Factors, governing the photoluminescence yield of Erbium implanted Silicon", *MRS proceedings* **422**, 101 (1996)

[2] W. Jantsch, H. Przybylinska (invited): "Rare Earth Luminescence in Semiconductors", *Proc. XXIII. Int. Conf. Phys. Semiconductors*, Berlin July 21-26, 1996*, in press*

[3] P.N. Favennec, H. l´Haridon, D. Moutonnet, M. Salvi, and M. Gauneau*, Mat. Res. Soc. Symp. Proc*. **301**, 181 (1993)

[4] H. Ennen, G. Pomrenke, A. Axmann, K. Eisele, W. Haydl, and J. Schneider, *Appl. Phys. Lett.* **46**, 381 (1985)

[5] H. Przybylinska, W. Jantsch, Yu. Suprun-Belevich, M. Stepikhova, L. Palmetshofer, G. Hendorfer, A. Kozanecki, R. J. Wilson, B. J. Sealy, "Optically active Erbium centers in Silicon", *Phys. Rev*. **B54,** 2532 (1996)

[6] R. Sauer, J. Weber, J. Stolz, E.R. Weber, K.-H. Küsters and H. Alexander, *Appl. Phys*. A**36**, 1 (1985)

Project Information

Project Manager

Prof. Wolfgang JANTSCH

Institut für Halbleiterphysik, Johannes-Kepler-Universität, A-4040 Linz

Project Group

Last Name	First Name	Status	Remarks
Jantsch	Wolfgang	university professor	
Lanzerstorfer	Sven	dissertation	15% GMe funding
Palmetshofer	Leopold	associate professor	
Wirtl	Elisabeth	technician	50% GMe funding

Publications in Reviewed Journals

1. W. Jantsch, H. Przybylinska, "Rare Earth Luminescence in Semiconductors", *Proc. XXIII. Int. Conf. Phys. Semicond.*, Berlin July 21 – 26, 1996
2. H. Przybylinska, W. Jantsch, S. Lanzerstorfer, C. Skierbiszewski, L. Palmetshofer, "High Pressure Studies of the Photoluminescence Yield of Erbium in Silicon", *Proc. XXIII. Int. Conf. Phys. Semicond.*, Berlin July 21 – 26, 1996
3. W. Jantsch, H. Przybylinska, "Erbium in Silicon: a Possible Light Source for 1.5 μm and a Challenge for Defect Physics", *Acta Physica Polon.* **90** (4), 623 (1996)
4. H. Przybylinska, W. Jantsch, L. Palmetshofer, "Erbium Luminescence in Silicon", *IInd International Winter Workshop on Spectroscopy and Structure of Rare Earth Systems (SSRES '96),* March 24 – 29, 1996
5. W. Jantsch, H. Przybylinska, C. Skiebiszewski, S. Lanzerstorfer, L. Palmetshofer, "Factors, governing the photoluminescence yield of Erbium implanted Silicon", *MRS proceedings* 422, 101 (1996)
6. H. Przybylinska,W. Jantsch, Yu. Suprun-Belevich, M. Stepikhova, L. Palmetshofer, G. Hendorfer, A. Kozanecki, R. J. Wilson, B. J. Sealy, "Optically active Erbium centers in Silicon", *Phys. Rev. B* **54,** 2532 (1996)

Presentations

1. W. Jantsch, H. Przybylinska, C. Skiebiszewski, S. Lanzerstorfer, L. Palmetshofer, "Factors, governing the photoluminescence yield of Erbium implanted Silicon" (invited), *MRS spring meeting 1996*, San Francisco, Ca

2. H. Przybylinska, W. Jantsch, L. Palmetshofer, “Erbium Luminescence in Silicon” (invited), *IInd International Winter Workshop on Spectroscopy and Structure of Rare Earth Systems (SSRES ‘96)*, March 24-29, 1996, Polanica Zdroj (Poland)
3. W. Jantsch, “Erbium in Silicon” (invited), *XXV International School on Physics of Semiconducting Compounds*, Jaszowiec ´96
4. W. Jantsch, H. Przybylinska, “Rare Earth Luminescence in Semiconductors” (invited), *XXIII. Int. Conf. Phys. Semicond.*, Berlin July 21 – 26, 1996
5. H. Przybylinska, W. Jantsch, S. Lanzerstorfer, C. Skierbiszewski, L. Palmetshofer, “High Pressure Studies of the Photoluminescence Yield of Erbium in Silicon”, *XXIII. Int. Conf. Phys. Semicond.*, Berlin July 21-26, 1996

Cooperations

1. Doc. Z. Wilamowski, Dr. H. Przybylinska, Institute of Physics, Polish Academy of Science, 02-668 Warsaw, Poland
2. Prof. A. Peaker, University of Manchester Institute of Science and Technology, Centre of Electronic Materials, Manchester, UK

Ge^+ Implantation into Silicon: Behavior of Deep Level Defects

L. Palmetshofer and Y. Suprun-Belevich

Institut für Halbleiterphysik, Johannes Kepler Universität Linz
A-4040 Linz, Austria

Implantation-induced defects and their annealing behavior in Si and SiGe have been investigated using deep-level transient spectroscopy. For Ge^+ implantation in silicon three types of defects have been observed: vacancy-related defects which anneal out during annealing up to 600 °C, Ge-related defects which are formed during annealing and disappear at 900 °C, and radiation defects which are generated during annealing and disappear also at 900 °C. For ion bombardment of strained SiGe layers we found a strong influence of the strain on the production, diffusion and annealing of implantation-induced defects.

1. Introduction

Strained Si/SiGe layers can be used to improve the performance of silicon based electronic devices such as heterobipolar transistors and modulation-doped field effect transistors [1]. The Si/SiGe heterostructures are usually grown on Si substrates by molecular beam epitaxy at relatively low temperatures (< 750 °C). However, during the fabrication of a device, a number of ion implantation and high temperature annealing steps would typically follow the epitaxial growth. These processing steps are known to introduce defects or to modify already existing defects and can cause strain relief in the strained layers. At present, the properties of implantation-induced defects and their high-temperature annealing behavior in SiGe layers remain largely unstudied. Implantation-induced defects are also important in the case of ion-beam-synthesized SiGe layers. It has been shown that simple SiGe/Si heterostructures can be fabricated by ion implantation and solid-phase epitaxial regrowth [2].

In the context of these problems, a program was started to investigate implantation induced defects and their annealing behavior by deep-level transient spectroscopy (DLTS). Two aspects have been treated so far. First, the formation and annealing behavior of deep level defects after implantation of Ge^+ into Si, and second, the influence of the mechanical strain on radiation defects.

2. Experimental

Phosphorus-doped CZ-grown Si wafers were implanted with 320 or 640 keV Ge^+ ions with doses up to $3x10^{16}$ cm^{-2} corresponding to a peak Ge concentration of about 3 at.%. Deep level defects were investigated after subsequent isochronal annealing steps in the temperature range 100 – 1100 °C. Rapid thermal annealing (RTA) of the samples was performed by halogen lamp irradiation with 20 s exposure in a nitrogen gas flow. Deep-level transient spectroscopy measurements [3] were carried out using a 1 MHz capacitance bridge, a pulse generator and a liquid-nitrogen-cooled cryostat (77 – 400 K). The

DLTS signal was obtained from the capacitance transient using the lock-in averaging method. Depth profiles of defects were obtained in double-pulse differential mode (DDLTS) [4].

Due to a 4% difference between the covalent radii of Si and Ge atoms the implantation of Ge into Si allowed us to vary the magnitude of the elastic misfit stress. The mechanical strain was investigated by high-resolution x-ray diffraction measurements using a four-crystal monochromator [5]. Some of the strained Ge^+ implanted samples (in the following designated as Si:Ge) were then irradiated with 24 or 70 keV H^+ ions at doses between $1x10^{10}$ and $1x10^{12}$ cm^{-2} to introduce radiation defects. The H^+ implantation energy was chosen such that the radiation defects were placed into the region of the maximum gradient of the Ge concentration. All the ion ranges were calculated with the TRIM code [6]. The radiation defects formed by H^+ irradiation were electrically characterized again by DLTS measurements.

3. Results and discussion

3.1 Deep level defects in Ge^+ implanted Si

Three groups of deep levels have been observed by DLTS in the implanted samples. The first group of defects is observed in as-implanted samples and in samples annealed at low temperatures. Figure 1(a) shows a typical DLTS spectrum of Si implanted with a low dose of Ge^+. The defects are labeled according to their energy position in the gap in eV. Three defects are detected in such samples: E(0.17), E(0.22) and E(0.41). Annealing experiments show that these defect levels are observed up to about 600 °C annealing temperature. The concentration of the defects decreases continuously with the annealing temperature.

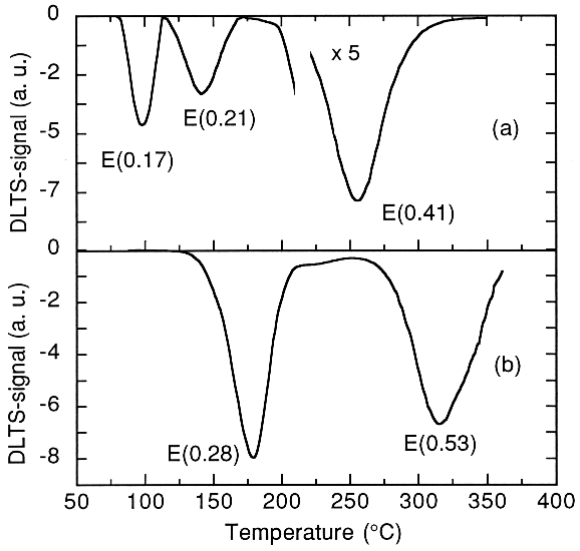

Fig. 1: DLTS spectra of Ge^+ implanted Si (640 keV): (a) dose 10^{11} cm^{-2}, annealing at 100°C; (b) dose 10^{12} cm^{-2}, annealing at 700 °C.

The second group of defect levels is observed after high temperature annealing. Figure 1(b) shows a typical DLTS spectrum of Ge^+ implanted Si after annealing at 700°C. Two new defect levels, E(0.28) and E(0.53), are observed instead of those in as-implanted silicon. The new levels show up at about 500 °C and disappear only after annealing at very high temperatures (> 900 °C). In samples implanted at doses above 10^{13} cm^{-2} an additional minority carrier trap E(+0.17) is observed after 700 °C annealing, which disappears also above 900 °C. The third group of defect levels — two less dominant levels at E(0.40) and E(0.15) — is also observed after high temperature annealing between 700 and 900 °C.

The three levels observed in as-implanted silicon can be attributed to vacancy-related defects: E(0.17): vacancy-oxygen pair, E(0.21): divacancy, and E(0.41): a mixture of the divacancy and the phosphorus-vacancy pair [7]. The position and shape of the defect profiles measured by DDLTS coincides very well with the vacancy distribution calculated by the TRIM code. The profiles are shifted towards the surface as compared with the ion distribution.

The levels E(0.28) and E(0.53) observed in the temperature region 500 – 900 °C can be attributed to defect complexes containing Ge atoms. The position and shape of the profiles of these levels coincide with the profile of the ion distribution according to TRIM. The Ge-related levels are not formed during ion implantation, they are created during the annealing as a result of the recrystallization of amorphous inclusions and the release of Ge atoms from them. This process is accompanied by a sharp decrease of the defect-related mechanical strain.

The levels E(0.15) and E(0.40) observed after high temperature annealing are not related to the implanted species. From the shape of the defect profiles and from the fact that similar levels were observed also in Si^+ implanted silicon it is concluded that the levels are related to radiation defects. The defects are generated during the recrystallization of amorphous inclusions and are not observed after implantation at doses above 10^{13} cm^{-2}.

The main message of our study of deep levels in Ge^+ implanted silicon together with strain measurements for the SiGe technology is that it is possible to obtain SiGe layers after implantation of Ge^+ into silicon and appropriate annealing. The radiation defects can be annealed out completely and the Ge atoms are introduced on regular lattice sites. So far experiments have been performed only with low Ge concentrations (up to 3 at%). Since for doses above the amorphization dose (about 10^{14} cm^{-2}) the annealing of the radiation defects occurs by solid state epitaxial regrowth, higher Ge concentrations are not expected to cause difficulties.

3.2 Influence of mechanical strain on radiation defects

The response to ion implantation is different for a strained SiGe layer and unstrained silicon. This has been found by investigating radiation defects after bombardment with H^+ ions. H^+ bombardment of Si introduces the vacancy-related defect levels E(0.17). E(0.21) and E(0.41) as described above, and in addition, a H-related level E(0.30) [7].

The production rates of these defects are essentially lower in strained Si:Ge samples. The decrease of the defect concentrations in Si:Ge as a function of the stress is shown in Fig. 2. The concentration of the defects was obtained from DLTS and DDLTS measurements, the stress was calculated from the strain in the implanted layer measured by x-ray diffraction [8]. DDLTS measurements have shown that defect profiles are signifi-

cantly broader in Si:Ge samples than in silicon. The annealing behavior of the deep levels is also different for Si and Si:Ge. The annealing of the vacancy-related defects generally takes place in two stages. In the Si:Ge samples the beginning of both stages is shifted towards lower temperatures. The onset for the annealing of the H-related level E(0.30) is also shifted to lower temperatures in the Si:Ge samples.

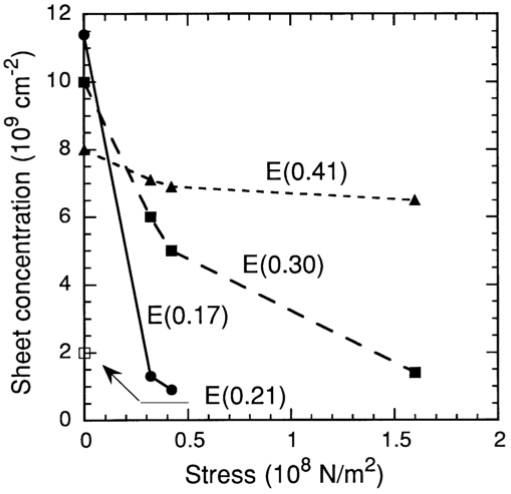

Fig. 2: Concentration of the defects in Si:Ge introduced by H+ bombardment (70 keV, $5x10^{10}$ cm^{-2}) versus the Ge-related stress calculated from the measured strain. Stress zero denotes the Si reference sample.

The behavior of the radiation defects in Si:Ge cannot be explained by changes in the primary defect production (vacancies and interstitials) during bombardment due to the slightly changed stoichiometry. It is concluded that the Ge-related misfit strain is responsible for the reduced production rates of the observed defects, broadening of the defect profiles and the shift of the annealing stages. The production of primary defects (vacancies and interstitials) during ion bombardment and their behavior afterwards (diffusion, annihilation, capture by impurities, etc.) takes place in a field of mechanical stress. Elastic energy can be transferred to primary defects, thus influencing their behavior and the formation of defect complexes observed by DLTS. A detailed discussion is given in refs. [8] and [9].

References

[1] F. Schäffler: in "*Grundlagen und Technologie elektronischer Bauelemente",* (Gesellschaft für Mikroelektronik,Wien, 1995), p. 93.

[2] F. Corni, S. Frabboni, G. Ottaviani, G. Queirolo, D. Bisero, C. Bresolin, R. Fabbri, M. Servidori: *J. Appl. Phys.* 71 (1992) 2644.

[3] D.V. Lang: *J. Appl. Phys.* 45 (1974) 3023.

[4] H. Lefevre, M. Schulz: *Appl. Phys.* 12 (1977) 45.

[5] A. Pesek, P. Kastler, K. Lischka, L. Palmetshofer: *Nucl. Instr. Meth. B* 80/81 (1993) 569.

[6] J.F. Ziegler, J.P. Biersack, U. Littmark: "*The Stopping and Range of Ions in Solids", Vol. 1* (Pergamon, New York, 1985).

[7] L. Palmetshofer, J. Reisinger: *J. Appl. Phys.* 72 (1992) 2167.

[8] Y. Suprun-Belevich, L. Palmetshofer: *Nucl. Instr. Meth. B* 115 (1996) 557.

[9] Y. Suprun-Belevich, L. Palmetshofer: *Nucl. Instr. Meth. B,* accepted.

Project Information

Project Manager

Univ.-Doz. Dr. Leopold PALMETSHOFER

Institut für Halbleiterphysik, Johannes Kepler Universität Linz, A-4040 Linz

Project Group

Last Name	First Name	Status	Remarks
Ablinger	Karlheinz	technician	
Palmetshofer	Leopold	associate professor	
Schmidt	Thomas	dissertation	
Suprun-Belevich	Yuri	postdoc	University Minsk
Wirtl	Elisabeth	technician	50% GMe funding

Publications in Reviewed Journals

1. T. Schmidt, L. Palmetshofer, "Defect Levels in H-Bombarded Gallium Arsenide", in *Ion Beam Modification of Materials,* eds. J. S. Williams, R. G. Elliman, M. C. Ridgeway, (Elsevier, 1996), p. 853.
2. Y. Suprun-Belevich, L.Palmetshofer, "Defect Production in Si by Ion Bombardment under the Influence of Internal Mechanical Strain", *Nucl. Instr. Methods B* 115, 557 (1996).
3. Y. Suprun-Belevich, L. Palmetshofer, "Behaviour of Radiation Defects under the Influence of Mechanical Strain in Ion-Implanted Silicon", *Nucl. Instr. Methods B* , accepted.

Presentations

1. L. Palmetshofer, Y. Suprun-Belevich, "Behaviour of Radiation Defects under the Influence of Mechanical Strain in Ion-Implanted Silicon", *10th International Conference on Ion Beam Modification of Materials*, Albuquerque, September1996.

Doctor's Theses

1. Th. Schmidt: Defekte in Galliumarsenid nach Bestrahlung mit leichten Ionen, Johannes Kepler Universität Linz, 1996.

Cooperations

1. Department of Semiconductor Physics, Belarusian State University, Minsk, Dr. Yu. Suprun-Belevich.

Surface Analysis by Auger Electron Spectroscopy

H. Sitter, E. Wirthl, P. Bauer

**Institut für Experimentalphysik,
Johannes Kepler Universität, A-4040 Linz, Austria**

We investigated the ternary II-VI compound semiconductors $Zn_{1-x}Mg_xTe$ $x \in [0, 1]$ by quantitative Auger Electron Spectroscopy. Emphasize was put on the behavior of the sensitivity factor s of the various constituents of the compound as a function of the composition of the ternary compounds. The sensitivity factors were calculated by a new formalism and showed a strong dependence on the compound composition. In the case of Te we found a change of the line shape and the appearance of Coster-Kronig transitions. Binary II-VI compounds like ZnSe, ZnTe, CdSe and CdTe were investigated with respect to their surface composition after reactive ion etching in CH_4/H_2 admixtures of different composition.

1. Introduction

The binary and ternary II-VI compound semiconductors are applicable to the production of blue light emitting diodes [1] – [3]. One of the main problems in these optoelectronic devices is the degradation, which is mainly caused by defects generated from strain and stress in the layers. A possibility to overcome that drawback is to fabricate lattice-matched multilayer structures. Since the lattice match is very sensitive to the composition of the compounds, an exact control during growth of the layers is indispensable. A method to control the composition is the Auger Electron Spectroscopy (AES). A main problem in quantitative AES (QAES) is that the sensitivity factors *s* of the constituents, which are equal to the probability of the occurrence of an Auger process [4] are only known for pure elements. Within this project we performed QAES on various compositions of $Zn_{1-x}Mg_xTe$ $x \in [0,1]$.

Parallel with the development of wide band gap II-VI blue-green diode lasers, the investigation of optical properties of quantum wires and dot structures has attained considerable interest [5] – [8]. An established method for the fabrication of lateral structures (e.g. quantum wires and dots) is the reactive ion etching (RIE) technique [9]. Most of the earlier studies of RIE on II-VI compounds used chlorine-containing gas mixtures [10]. In latter works a mixture of CH_4 and H_2 was used as etchant, which allows the fabrication of very small vertical structures with a minimal width of about 25 nm [11], [12]. In the literature a mixture between 1:6 and 1:8 for CH_4:H_2 ratio is reported to be an optimum etchant with respect to optical behavior of the fabricated nanostructures [5]. There are only few publications which are dealing with the chemical analysis of etched structures [13], [14].

We performed quantitative Auger electron spectroscopy (QAES) [15] analysis of ZnSe, ZnTe, CdSe and CdTe samples which were grown by molecular beam epitaxy (MBE) [16], and etched by RIE. In our analysis emphasize was given on the changes of the chemical composition of the etched samples due to the various ratios of CH_4:H_2 in the

etchant not only at the surface but also by depth profiling. In addition, the influence of oxygen as part of the etchant was investigated.

2. Results and Discussion

2.1 Sensitivity Factors

The sensitivity factors for Zn, Mg and Te as a function of the composition of the sample obtained with different primary electron energies were evaluated. A general trend could be seen that the sensitivity factors for all elements are increasing with increasing Mg content in the sample. Only the sensitivity factor of Te has a minimum in the range of x = 0.5. This is due to so-called Coster-Kronig transitions [16], which become dominant for samples with a composition around x = 0.5. The Auger spectra for $Zn_{1-x}Mg_xTe$ layers with different concentrations of Mg show beside the normal MNN Auger transitions also the MMN Coster-Kronig transitions. As a consequence the normal Auger transitions are decreased since the number of exciting primary electrons is constant in all the experiments.

2.2 Reactive Ion Etching

In the II-VI compounds ZnSe, ZnTe, CdSe and CdTe (i) the deviations from the stoichiometry, and the incorporation of (ii) oxygen and (iii) carbon were investigated as a function of the etching gas ratio in the RIE process.

(i) Down to a depth of about 20 Å the concentration of Zn and Se is lowered due to a large incorporation of carbon and some additional oxygen. The ratio of Zn to Se is nearly constant.

The lowest deviations from stoichiometry were found at CH_4:H_2 ratios of 1:6 and 1:7. Other CH_4:H_2 ratios showed large deviations from stoichiometry. For comparison, also as-grown samples were sputtered which showed no deviations from stoichiometry and indicate no effect due to preferential sputtering. Therefore we conclude, that deviations from stoichiometry which were investigated to a depth of 100 Å have their origin in the etching process.

(ii) The incorporation of oxygen into the samples could be clearly analyzed by QAES. In the case of Zn compounds the oxygen concentration is increasing with increasing hydrogen content in the etchant, whereas for the Cd compounds the oxygen content is decreasing. For a ratio of CH_4:H_2 of about 1:7 the incorporation of oxygen is low (between 1 and 2%) for all analyzed systems.

(iii) In contrast to oxygen, the carbon concentration decreases with sputter depth. The incorporation depth is between 20 and 80 Å. For Zn compounds, the C incorporation depth is lowest around a CH_4:H_2 ratio between 1:6 and 1:7, whereas for Cd compounds the depth is monotonically increasing with higher H_2 content. At a CH_4:H_2 ratio between 1:6 and 1:8, the incorporation depth is relatively low in all compounds.

3. Conclusion

The sensitivity factors for the constituent elements in the ternary II-VI compound $Zn_{1-x}Mg_xTe$ depend very strong on the composition of the compound.

For the investigated II-VI compounds (ZnSe, ZnTe, CdSe and CdTe) a relative small deviation from stoichiometry for a CH_4:H_2 etchant ratio around 1:7 is found as a common behavior. This is in agreement with literature, where an etchant with such a CH_4:H_2 ratio is used in order to give optimum optical behavior of the etched structures [5]. In addition, the incorporation of oxygen was detected over the whole investigated depth of 100 Å, whereas the carbon incorporation was limited to a depth between 20 and 80 Å.

References

[1] M.A. Haase, J. Qui, J. DePuydt, H. Cheng, *Appl. Phys. Lett.* **59**, 1272 (1991)

[2] J. Jeon, J. Ding, W. Patterson, A. Nurmikko, W. Xie, D. Grillo, M. Kobyashi, F.L. Gunshor, *Appl. Phys. Lett.* **59**, 3619 (1991)

[3] W. Faschinger, R. Krump, G. Brunthaler, S.O. Ferreira, H. Sitter, *Appl. Phys. Lett.* **65**, 3215 (1994)

[4] M.P. Auger, *Surf. Sci.* **48**, 1 (1975)

[5] M.A. Foad, M. Watt, A.P. Smart, C.M. Sotomayor Torres, C.D.W. Wilkinson, W. Kuhn, H.P. Wagner, S. Bauer, H. Leidererand, W. Gebhardt, *Semicond. Sci. Technol.* **6**, A115 (1991)

[6] H. Mariette, C. Gourgon, Le Si Dang, J. Cibert, C. Vieu, G. Brunthaler, H. Strau, W. Faschinger, N. Peekanos, W.W. Rühle, in *Proc. of Int. Conf. on Semicond. Heterostructures*, Montpellier, France, 1995, in print

[7] C. Ding, A.V. Nurmikko, D.C. Grillo, Li He, J. Han, R.L. Gunshor, *Appl. Phys. Lett.* **63**, 2254 (1993)

[8] C.M. Sotomayor Torres, A.P. Smart, M. Watt, K. Tsutsui, C.D.W. Wilkinson, *J. Electron. Mat.* **23**, 1 (1994)

[9] S.M. Rossnagel, J.J. Cuomo, W.D. Westwood, in *Handbook of Plasma Processing Technology - Fundamentals, Etching, Deposition and Surface Interactions*, Noyes Publications, Park Ridge, New Jersey (1990)

[10] T.R. Hayes, M.A. Dreisbach, P.M. Thomas, W.C. Dautremont-Smith, *J. Vac. Sci. Technol.* **B7**, 1130 (1989)

[11] D.E. Ibbotson, D.. Flamm, *Solid State Technol.* **31**, 77 (1988) and **31**, 105 (1988), and references therein.

[12] C.M. Sotomayor-Torres, A.P. Smart, M.A. foad, C.D.W. Wilkinson, in *Festkörperprobleme* **32**, Vieweg Verlag, Wien, 265 (1992)

[13] E. Wirthl, H. Straub, M. Schmid, H. Sitter, P. Bauer, G. Brunthaler, *J. Cryst. Growth* (1996) in print

[14] T.R. Hayes, U.K. Chakrabarti, F.A. Baiocchi, A.B. Emerson, H.S. Luftman, W.C. Dautremont-Smith, *J. Appl. Phys.* **68**, 785 (1990)

[15] M. Cailler, J.P. Ganachaud, D. Roptin, in *Advances in Electronic and Electron Physics* **61**, by P.W. Hawkes, Academic Press, New York, "Quantitative Auger Electron Spectroscopy", pp. 161-298 (1983)

[16] W. Bambynek, B. Crasemann, R.W. Fink, *Rev. Mod. Phys.* **44**, 716 (1972)

Project Information

Project Manager

Univ.-Doz. Dr. Helmut SITTER

Institut für Halbleiterphysik, Johannes Kepler Universität Linz, A-4040 Linz

Project Group

Last Name	First Name	Status	Remarks
Bauer	Peter	assistant professor	
Fuchs	Otmar	technician	
Sitter	Helmut	associate professor	
Straub	Hubert	dissertation	
Wirthl	Edwin	dissertation	

Publications in Reviewed Journals

1. E. Wirthl, H. Straub, M. Schmid, H. Sitter, P. Bauer, G. Brunthaler, "AES Analysis of Plasma-etched ZnSe", *J. Cryst. Growth* **159**, 746 (1996)
2. E. Wirthl, M. Schmid, D. Stifter, H. Sitter, P. Bauer, "Auger Investigations on II-VI Ternary Compound Semiconductors", *J. Cryst. Res. and Technol.* **31**, 297 (1996)
3. E. Belas, J. Franc, A. Toth, R. Gril, P. Höschl, H. Sitter, P. Moravec, "Type Conversion of p-(HgCd)Te Using H_2/CH_4 and Ar Reactive Ion Etching", *Semicond. Sci. and Technol.* **11**, 1116 (1996)
4. E. Wirthl, H. Straub, H. Sitter, G. Brunthaler, M. Schmid, D. Stifter, P. Bauer, "AES Investigations of Plasma-etched II-VI Binary Compounds", *Proc. Int. Symposium on Blue Laser and Light Emitting Diodes*, Chiba, Japan, 1996 (Ohmsda Ltd. IOS Press Inc.)
5. E. Wirthl, H. Sitter, P. Bauer, "Determination of Auger-Sensitivity Factors in $Zn_{1-x}Mg_xTe$ for Quantitative Surface Analysis", *Mat. Sci. B, Proc. EXMATEC*, Freiburg 1996

Presentations

1. E. Wirthl, H. Sitter, P. Bauer, "Determination of Auger Sensitivity Factors in ZnMgTe for Quantitative Surface Analysis", *EXMATEC*, Freiburg, Germany, 1996
2. E. Wirthl, M. Schmid, D. Stifter, H. Sitter, P. Bauer, "Auger Investigations of II-VI Ternary Compound Semiconductors", *10th Int. Conf. on Ternary and Multinary Compounds*, Strasbourg, France, 1996

3. E. Wirthl, H. Straub, M. Schmid, H. Sitter, P. Bauer, G. Brunthaler, “AES Analysis of Plasma-etched ZnSe”, *Int. Conf. on II-VI Compounds*, Edinburgh, UK, 1996
4. E. Wirthl, H. Straub, H. Sitter, G. Brunthaler, M. Schmid, D. Stifter, P. Bauer, “AES Investigation of Plasma-etched II-VI Binary Compounds”, *Int. Symposium on Blue Lasers and Light Emitting Diodes*, Chiba, Japan, 1996
5. H. Sitter, E. Wirthl, P. Bauer, “Quantitative Surface Analysis of II-VI Semiconductors by Auger Electron Spectroscopy”, *3rd Int. MBE Days*, Bratislava, Slovakia, 1996

Doctor's Theses

1. E. Wirthl, “Quantitative Auger-Analyse an binären und ternären II-VI-Verbindungs-halbleitern”, Universität Linz, 1996
2. H. Straub, “Photoluminescence and Strain Relaxation of CdZnSe/ZnSe Quantum Wires”, Universität Linz, 1997

Cooperations

1. Dr. Josef Liday, Technical University Bratislava, Institute of Electronics

Development of a 35 GHz Radar Sensor

A. Efanov, K. Lübke, Ch. Diskus, A. Springer, A. Stelzer, H.W. Thim

Institut für Mikroelektronik, Johannes Kepler Universität
A-4040 Linz, Austria

Experimental results with two different 35-GHz Doppler radar units are reported in this contribution. The system consists of a planar GaAs transferred electron oscillator and an InGaAs-mixer diode. The oscillator is a MESFET-like structure with a negatively biased Schottky-gate. A stationary high-field domain is formed underneath the gate and acts as a transit-time-independent broadband negative differential resistance. To achieve mixing with high sensitivity at zero bias the energy barrier of the diode must be made low. The mixer diode used in this module consists of 0.18 µm InGaAs with 38 % In content and $1 \cdot 10^{17}$ cm^{-3} Si n-type doping. This yields an energy barrier of 0.3 eV. With the first design a sensitivity of 1 mV/µW has been obtained.

1. Introduction

Millimeter-wave radar sensor systems especially suited for automotive applications were intensively developed during the last few years [1], [2]. Combination of a low-cost technology together with advanced electrical characteristics and high reliability is a cornerstone requirement for an application in the automotive industry [3], [4]. Since the microwave front-end unit is the key unit determining the system's performance and cost, it is the most crucial part of the whole system. Two different 35 GHz low-cost RF front-end Doppler units suited for automotive applications have been constructed. The homodyne unit consists of both receiving and transmitting corporate-fed microstrip patch array antennas, a microstrip directional coupler, a monolithic GaAs FECTED oscillator, and an integrated single Schottky diode mixer. The autodyne configuration uses only one antenna and the FECTED as a self-oscillating mixer. Inexpensive microstrip technology has been used, which yields a good compromise between cost factor and technical performance.

2. System Configuration

The block diagram of the front-end unit is shown in Fig. 1. The output power of the oscillator is fed into the transmitting antenna. At the mixer diode the reflected signal from the receiving antenna is combined with the LO signal provided by the 10 dB directional coupler. The amplified IF signal is fed into a signal processor. This configuration is suitable for both Doppler CW (continuous waveforms) as well as FM (frequency-modulated) CW radar systems.

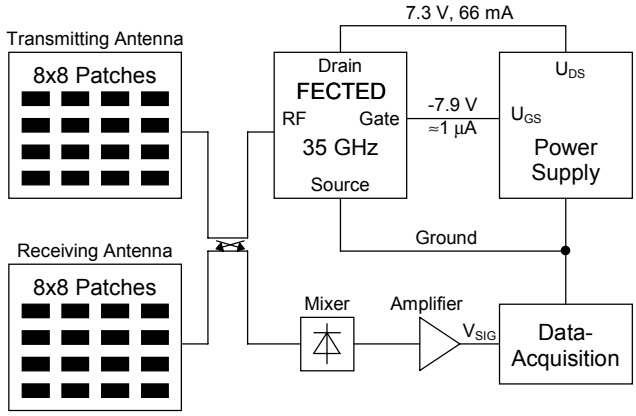

Fig. 1: Block diagram of the front-end unit using homodyne detection.

Further cost and size reductions of the module have been obtained with a simplified system configuration as shown in Fig. 2. In this design the FECTED (field effect controlled transferred electron device)-oscillator acts as a self-oscillating mixer [5] thereby sparing the mixer diode as well as the directional coupler and the second antenna. In this mode of operation the reflected signal received from the antenna changes the effective load impedance of the oscillator resulting in changes of both oscillator power and frequency which can be detected as bias current variations. A bandpass amplifier is used to separate the small bias current variations from the large DC current.

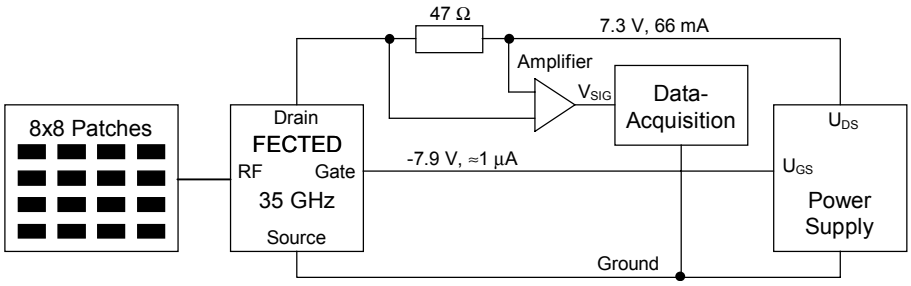

Fig. 2: Block diagram of the simplified front-end using autodyne detection.

3. Antennas

Two linearly-polarized corporate-fed microstrip patch array antennas have been designed for this system. The first one is a 4x4 array antenna with 16 degrees beamwidth and 17.5 dB (isotropic) power gain. The second one is a 8x8 array antenna with 8 degrees beamwidth and 21.5 dB (isotropic) power gain. The VSWR of both prototypes is below 2. A relatively inexpensive RT/duroid 5880 (a trademark of Rogers Corp.) substrate material of 0.254 mm thickness has been used for the fabrication of the antennas and the 10 dB directional coupler. The passive part has been made using standard photolithography and etching-technology, and has been covered by a gold film in order to minimize losses. A more detailed description of the antennas is given in [6]. Fig. 3 shows a photograph of the 8x8 array antenna module.

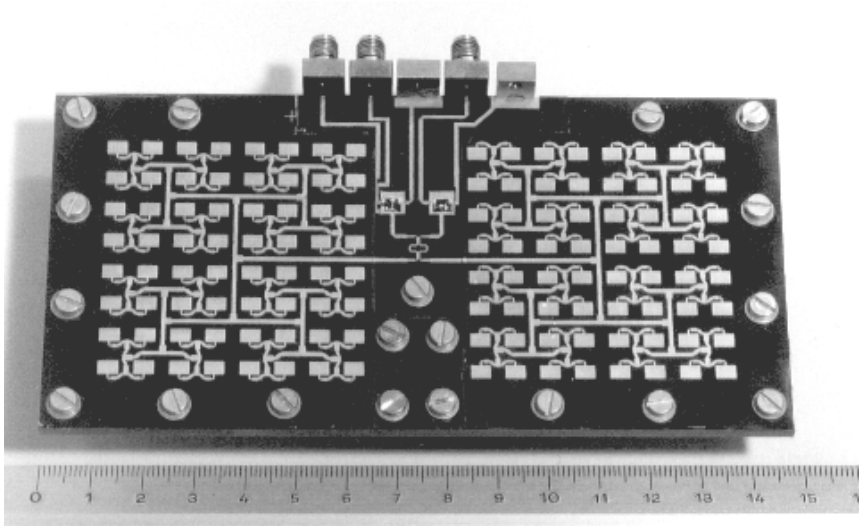

Fig. 3: Photograph of the front-end unit with 8x8 array antenna

4. Oscillator

In order to minimize costs a special planar Gunn diode has been used instead of a sophisticated transistor oscillator. This approach relaxes the demands on the resolution of the lithography. The device is called FECTED (Field Effect Controlled Transferred Electron Device) and is described elsewhere in this report. The device and the circuit have been fabricated on a 4x5 mm^2 GaAs chip with standard processing technologies. With the FECTED oscillator mounted in the sensor front-end an output power of about 4 mW at 34 GHz with an efficiency of 0.8 % has been measured. Further details of the FECTED have been published in [7].

5. Mixer Diode

5.1 Voltage sensitivity

The voltage sensitivity of a detector diode is defined as the output voltage generated by the diode into the load circuit divided by the RF-power absorbed in the diode. The goal of the optimization procedure is to make this sensitivity as large as possible [8].

The voltage sensitivity, β_v, of a circuit with load resistance R_L is given by

$$\beta_v = \frac{0.0005}{\left(I_s + I_0\right)\left(1 + R_j / R_L\right)\left[1 + \left(\omega C_j\right)^2 R_s R_j\right]} \left[\frac{\mathrm{mV}}{\mu\mathrm{W}}\right].$$

I_s ..... reverse saturation current
I_0 ..... bias current
C_j ..... junction capacitance of the diode
R_s ..... series resistance
R_j ..... dynamic resistance (= $q/nkT\,(I_s+I_0)$).

It is necessary to minimize both the junction capacitance and the series resistance. The capacitance of the diode can be decreased if the size of the junction diameter is reduced. To obtain low series resistance the conductivity of the bulk material should be as high as possible, the current path through the material should be as short as possible and a good ohmic contact (low resistivity) is needed.

It is well known that large LO power is needed to minimize conversion loss of a GaAs Schottky mixer diode. This is a consequence of the high barrier height of about 0.7 eV of GaAs Schottky diodes. For a typical set of parameters for 10 µm x 10 µm Schottky barrier diodes (f = 35 GHz, n = 1.4, R_s = 10 Ω, C_j = 70 fF, R_L = 1 MΩ) the maximum of the sensitivity β_v can be calculated from the above equation. If the detector should be used without bias current, which simplifies circuitry, then $I_0 = 0$ and the saturation current I_s has to be in the range of 10^{-6} A. This corresponds to a barrier height of approximately 0.22 – 0.25 eV. However, the barrier height can be reduced if $In_xGa_{1-x}As$ is used. With increasing x the energy gap of the semiconductor is lowered from 1.42 eV (x = 0; i.e. GaAs) to 0.33 eV for x = 1 (InAs). With decreasing energy gap the barrier height of the Schottky contact is also reduced. With $In_{0.38}Ga_{0.62}As$ the desired barrier height can be adjusted.

5.2 Diode fabrication

The diodes have been fabricated using epitaxial layers of $In_{0.38}Ga_{0.62}As$ grown by metal organic vapor deposition (MOCVD) on semi-insulating GaAs substrates. In order to grow good quality $In_{0.38}Ga_{0.62}As$ layers on GaAs a graded buffer layer is needed to compensate the difference in lattice constants between InGaAs and GaAs. The Indium content is increased from 0 to 38% in steps of 5% in this layer. The first active layer grown is an n^+-layer doped $6 \cdot 10^{18}$ cm^{-3} with a thickness of 0.8 µm. On top of this layer a 0.19 µm thick n-layer with $2 \cdot 10^{16}$ cm^{-3} doping concentration has been grown. The ohmic contact is recessed to the n^+-layer and the connection to the Schottky-contact on the top is led over a SiO_2-bridge.

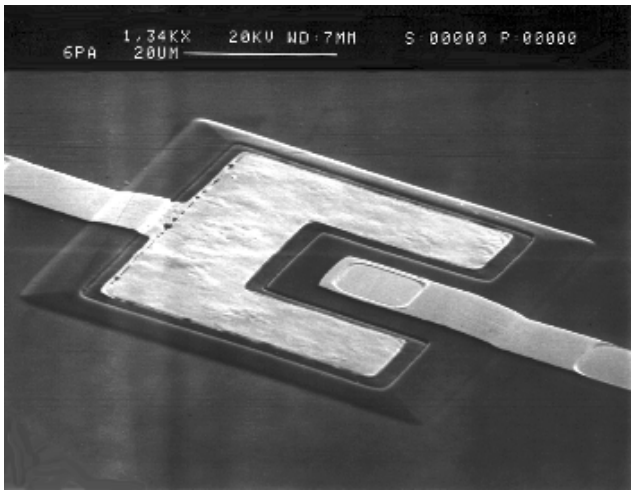

Fig. 4: SEM picture of the InGaAs Schottky diode

In Fig. 4, a SEM picture of the diode is shown. With the first design a sensitivity of 1 mV/µW has been obtained.

6. Results

Both front-end units have been tested with a target moving at a constant speed of 0.37 m/s from a distance of 2 meters towards the antenna. In the case of homodyne detection the amplified mixer signal V_{SIG} shown in Fig. 5 corresponds almost perfectly to the theoretic Doppler signal which is a harmonic function for constant target velocity. With a triangular corner reflector at a distance of 22 m, a signal amplitude of 100 mV after an amplification by a factor of 305 has been measured.

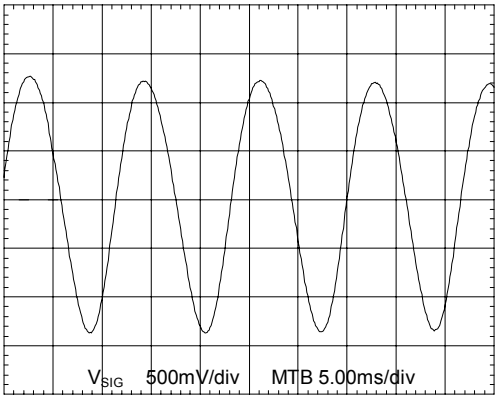

Fig. 5: Amplified (x 305) mixer signal from the homodyne configuration target velocity ... 0.37 m/s

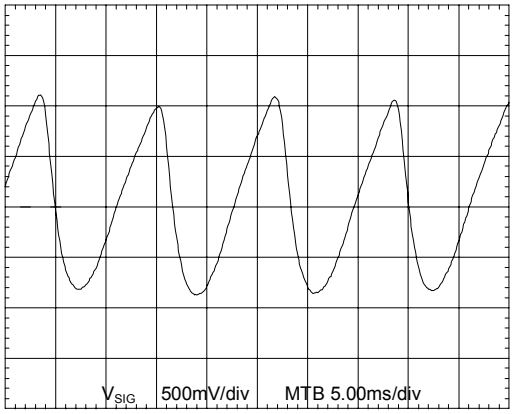

Fig. 6: Amplified (x 305) drain current modulation in the autodyne configuration, target velocity ... 0.37 m/s

For the autodyne configuration the detection range is much shorter because the reflected power received by the antenna must be sufficient to modulate the oscillator's output power. This modulation is highly nonlinear but periodical with half the wavelength as can be seen in Fig. 6 where the drain current modulation measured at a shunt and amplified is displayed.

7. Conclusion

Two different inexpensive configurations of the microwave part of a 35-GHz Doppler radar sensor system have been presented. The described approaches make it possible to achieve acceptable system performance with low-cost technology. The front-end with two antennas and the mixer diode has an operational range of at least 25 m. It is expected that this distance can be enhanced by optimizing the system components without increasing the transmitted power. A further cost reduction can be achieved by monolithically integrating the system on a single chip. The autodyne configuration has less sensitivity and higher noise level but it is the simplest and therefore cheapest approach.

Acknowledgments

The authors would like to thank G. Hinterberger, G. Hofmann and J. Katzenmayer for fabricating and testing the devices. This work was supported by the Austrian Science Foundation (FWF) under Contract number P8697-TEC.

References

[1] H.H. Meinel: "Commercial Applications of Millimeterwaves History, Present Status and Future Trends", IEEE Trans. on Microwave Theory and Techniques, (1995) 43, n° 7, pp. 1639 – 19.

[2] K.W. Chang, H. Wang, G. Shreve, J.G. Harrison, M. Core, A. Paxton, M. Yu, C.H. Chen, and G.S. Dow: "Forward-Looking Automotive Radar Using a W-band Single-Chip Transceiver", *IEEE Trans. on Microwave Theory and Techniques*, (1995) 43, n° 7, pp. 1659 – 1668.

[3] P. Heide, R. Schubert, V. Mágori, and R. Schwarte: "Coded 24 GHz Doppler Radar Sensors: A New Approach to High-Precision Vehicle Position and Ground-Speed Sensing in Railway and Automobile Applications", *IEEE MTT-S Digest,* International Microwave Symposium, Orlando, (1995), n°2, WE4D-4, pp. 965 – 968.

[4] J.-F. Luy, K.M. Strohm, H.-E. Sasse, A. Schüppen, J. Buechler, M. Wollitzer, A. Gruhle, F.Schäffler, U. Guettich, and A. Klaaßen: "Si/SiGe MMIC's", *IEEE Trans. on Microwave Theory and Techniques*, (1995) 43, n° 4, pp. 705 – 714.

[5] P.A. Jefford and M. J. Howes: "Modulation Schemes in Low-Cost Microwave Field Sensors", *IEEE Trans. on Microwave Theory and Techniques*, (1983) 31, n° 8, pp. 613 – 624.

[6] A. Efanov and H.W. Thim: "Corporate-Fed 2x2 Planar Microstrip Patch Sub-Array for the 35 GHz Band", *Antennas and Propagation Magazine*, (1995) 37, n° 5, pp. 49 – 51.

[7] K. Lübke, H.Scheiber, and H. Thim: "A Voltage Tunable 35 GHz Monolithic GaAs FECTED oscillator", *IEEE Microwave and Guided Wave Letters*, (1991) 1, n°2, pp. 35 – 37.

[8] I. Bahl, P. Bartia: *Microwave Solid State Curcuit Design*, Wiley, New York 1988.

Project Information

Project Manager

Univ. Prof. Dr. Hartwig THIM

Institut für Mikroelektronik, Kepler-Universität Linz, A-4040 Linz

Project Group

Last Name	First Name	Status	Remarks
Diskus	Christian	postdoc	
Efanov	Andrew	postdoc	Aerospace Monitoring Center, Lvov, Ukraine
Hilgarth	Thomas	student	
Hinterberger	Gabriele	technician	
Hofmann	Gerald	technician	
Katzenmayer	Hans	technician	
Lübke	Kurt	postdoc	
Springer	Andreas	dissertation	
Thim	Hartwig	university professor	

Books and Contributions to Books

1. C.G. Diskus, K. Luebke, A.L. Springer, H.W. Thim: "The Transferred Electron Effect", *Properties of Gallium Arsenide,* 3rd Edition, EMIS Datareview, Series.

Publications in Reviewed Journals

1. C.G. Diskus, "Mikrowellensensorik", Sonderheft "Mechatronik", *e&i*, 113. Jahrgang, H. 7/8, August 1996, pp. 500 – 512.
2. A.A. Efanov, C.G. Diskus, A. Stelzer, H.W. Thim, K.Lübke, A.L. Springer, "Development of a Low-Cost 35 GHz Radar Sensor", Digest to the 20th European *Workshop on Compound Semiconductor Devices and Integrated Circuits* (WOCSDICE '96), May 19 – 22, 1996, Vilnius, Lithuania
3. A.A. Efanov, Ch.G. Diskus, A. Stelzer, H. Thim, K. Lübke, and A.L. Springer, "Development of a Low-Cost 35 GHz Radar Sensor", Digest to the 1996 *International Workshop on Millimeter Waves,* organized by the IEEE-MTT, April 11-12, 1996, Orvieto, Italy, pp. 21 – 23, also published in *Annales of Telecomunications.*

Doctor's Theses

1. Andreas L. Springer: "Monolithisch integrierter V-Band Oszillator", Universität Linz, 1996.

Cooperations

1. VOEST-Alpine Stahl, Linz
2. Ferdinand Braun Institut Berlin
3. Fraunhofer Institut für Angewandte Festkörperphysik (IAF), Freiburg im Breisgau
4. GRAMES, École Polytechnique de Montrèal, Kanada
5. Institut für Hochfrequenztechnik, TU München
6. Institut für Feldtheorie und Höchstfrequenztechnik, ETH Zürich
7. Krohne Meßtechnik GmbH&Co.KG, Duisburg
8. Siemens AG, Zentralabteilung Forschung und Entwicklung, Komponenten und Module, München

UNICHIP

UNICHIP Vienna, a Technology Transfer Center for ASIC Design

N. Kerö[1], G.R. Cadek[1], W. Kausel, E. Kowarsch, P.C. Thorwartl
Institut für Allgemeine Elektrotechnik und Elektronik,
TU Wien, A-1040 Vienna, Austria

T. Sauter[1]
Institut für Computertechnik,
TU Wien, A-1040 Vienna, Austria

After a short description of the SME oriented work of UNICHIP a design of an analogue ASIC is presented. This project has been undertaken in close cooperation with and Austrian SME (Frequentis-Nachrichtentechnik) It serves perfectly well as an successful example of technology transfer of ASIC design and know-how.

1. Introduction

From its very beginning the work of the UNICHIP Wien design team was targeted towards technology transfer of ASIC design knowledge mainly to Austrian SMEs. Various measures were taken to achieve this goal. Firstly the undergraduate education of VLSI design methodologies has been intensified. Recently interesting diploma-theses have been completed such as a "Re-targetable VHDL-module for an SCSI-Controller" or "CULT – A new class of scaleable benchmark circuits for FPGAs".

For training and education focused directly towards SMEs we use various different approaches. Apart from front-end design courses which are held together with the University Extension Center, in-house training and consulting activities lasting between one and three days each have proved to be very successful. In the last two years more than 15 firms accepted this offer. Finally, projects performed in close cooperation with a partner from industry are by far the most effective way of technology transfer. In the remaining part of this report we shall describe such a transfer project.

2. Analog Headset Transceiver: A Technology Transfer Project

Together with Frequentis, an Austrian SME dealing with speech communication systems for air traffic control, an analogue headset transceiver ASIC was developed. Instead of focusing on design based training of Frequentis engineers, the authors tried to transfer knowledge on how to manage analogue IC design projects and to specify circuits to be developed and fabricated by sub-contractors. The cooperation started with a short product analysis study lasting no more than four weeks. As a result of this preliminary work, four areas suitable for replacing standard solutions with ASICs were spotted, one analogue and three digital designs of varying complexity. It was agreed to realize the analogue ASIC, this one being the most urgent.

[1] Member IEEE

The headset transceiver (HST) is basically the interface between the communication system and the air traffic controllers. Since each working place in a typical system has three sockets to which headsets can be connected, the first benefit expected from an integrated solution is a significant reduction of space on the printed circuit boards needed for the interfaces. Another advantage is the increased reliability. The third and somehow unusual benefit is a standardization aspect. Speech communication systems are unique solutions, and so far, despite a modular design of the digital parts of the system, the interface boards have been developed anew for each customer. An ASIC, however, is a fixed starting point for future designs and may thus help reduce also development costs.

2.1 Function of the HST

The basic function of the ASIC is the amplification and conditioning of the voice-band signals that come in from the headset's microphone or are applied to the earphones, respectively. In addition, the presence of a headset must be detected. If no headset, or more precisely, no microphone, is attached to the module, then a loop-back function is to be activated such that the speaker hears his own voice, signaling him that his partner does no longer exist. This function is also useful for testing purposes because the complete signal path through the system — including the CODECs and most of the analogue amplifiers — may be monitored.

Figure 1 shows a block diagram of one channel of the HST together with the specifications. The ASIC actually comprises two of them. Since there is only a single supply voltage available, the drivers for the loudspeakers need differential outputs to meet the specifications. To be independent of the dc levels of the signals generated by the CODEC, capacitive coupling is used. Thus the internal reference potential could be set to its optimum value, which is derived from the supply with a simple resistive divider. An optional external capacitor connected to the divider improves the PSRR, and this analogue ground is carefully buffered to minimize crosstalk between the signals.

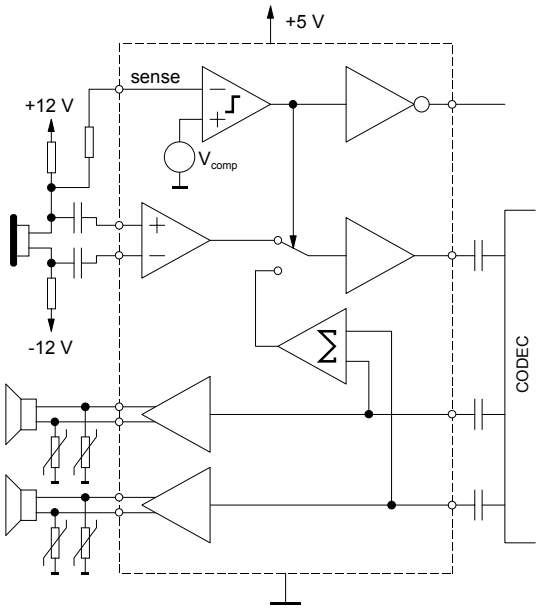

Power supply voltage	+5 V
Loudspeaker driver	
Output power	10 mW_{eff}
Load Impedance	150-600 Ω, 0,5-3 nF
Voltage gain	20 dB
Microphone amplifier	
Load impedance	20 kΩ, 15 pF
Voltage gain	0 dB
Summing amplifier	
Voltage gain	-20 dB
Harmonic distortion	< 1 %

Fig. 1: Block diagram of HST together with electrical specifications.

Like all circuits in air traffic control applications, the whole system must comply with IEC 801-2-91, which requires the circuitry to withstand ESD pulses of 8 kV applied to its ports. Therefore all connections to the headset are protected by additional transient voltage absorbers. Unfortunately, these devices impose a significant capacitive load on the output drivers of the HST. Another important requirement is that for reliability reasons the drivers must survive shorts between the output terminals as well as between the outputs and ground (a typical cause of such a short is a mechanical damage of the headset cable).

2.2 The Course of the Project

As a first step a three months' study was launched with the objective to evaluate the feasibility of this design from technical and economical points of view. As a result the following items could be delivered: an area estimation, design effort, possible ASIC manufacturers. It could be foreseen that the headset transceiver ASIC would be the only analogue integrated design effort for Frequentis for the next few years. Thus acquiring knowledge of the necessary design skills (CMOS amplifier design, analogue simulation, and analogue IC layout) would be of no use for the design engineers.

On the contrary, it turned out that correct (e.g. error free and complete) specification of integrated circuits to be designed by sub-contractors was the main knowledge for Frequentis to be gained from this collaboration. So far they had underestimated the constraints imposed by an ASIC design on internal project schedules. The design project was refined and launched. The very first task was the preparation of a detailed specification. This was done in close cooperation with design engineers of Frequentis who were used to working with discrete operational amplifiers. After the ASIC had been specified to a certain extent, the design work started.

The Mietec 2.0 μm CMOS process offered via EUROCHIP was selected for two good reasons. Firstly, there was an MPW run scheduled for mid-May, which perfectly fitted into the project timetable. Secondly, the process offered a wide range of supply voltages, which in turn was convenient for the designers at Frequentis in that they needed not specify critical design parameters like the required output power once and for all. If for example in later applications a higher output voltage swing was needed, the supply voltage could readily be increased to meet the changed requirements. Yet the primary goal was to use the 5 V supply already available in the system.

A few days before the submission to EUROCHIP, someone noticed that the external protection devices at the loudspeaker outputs had a huge parasitic capacitance, whereas all the time before a purely ohmic load had been assumed. This mistake stemmed from a simple misunderstanding. Our partners had thoroughly analyzed all headsets they used in their systems, but nobody had ever taken the true environment of the HST into account. As the designers were not familiar with analogue IC design, they did not know that 3 nF already mean a large capacitive load for a CMOS op-amp, and thus the protection devices had been neglected.

The fabrication phase of the prototypes unfortunately coincided with the summer holidays, and the ICs spent several weeks in different European countries waiting to be processed, packaged, or delivered to the customer. This was bad fortune indeed and no one had taken such a delay into consideration before, but when Frequentis eventually received the silicon, we were five weeks behind schedule.

In the meantime, the complete schedule had changed in that now a deadline for the availability of functioning prototypes in January had been set up. Although the problems with the first design had been spotted and the specification had reached a stable state, a second prototyping run via EUROCHIP with its eleven weeks turnaround time seemed impossible. The tight schedule and the fact that due to the unforeseen fabrication delay, Frequentis had partly lost their confidence in the EUROCHIP MPW services, led us to seek a purely commercial solution. For the new version, we selected AMS as manufacturer mostly because they are reachable from Vienna within two hours by car. The entire re-design on a 1.2 µm N-well process providing high ohmic poly (which had not been available in the processes offered via EUROCHIP) was then completed within two weeks. By the end of January 1997, Frequentis received the fully functioning engineering samples.

2.3 Implementation Details

While in the first version the chip size was about 8 mm², the final circuit after the re-design required only 4.7 mm². In the left and right columns of the core, one can see the amplifiers for the loudspeakers. Figure 2 shows the layout of the HST ASIC. The feed-back resistors have been placed in the pad ring. The low-noise microphone amplifiers occupy the top and bottom of the middle column in close proximity of the respective IO-pads. In the center of the core the summing amplifiers and the analogue ground buffer are located.

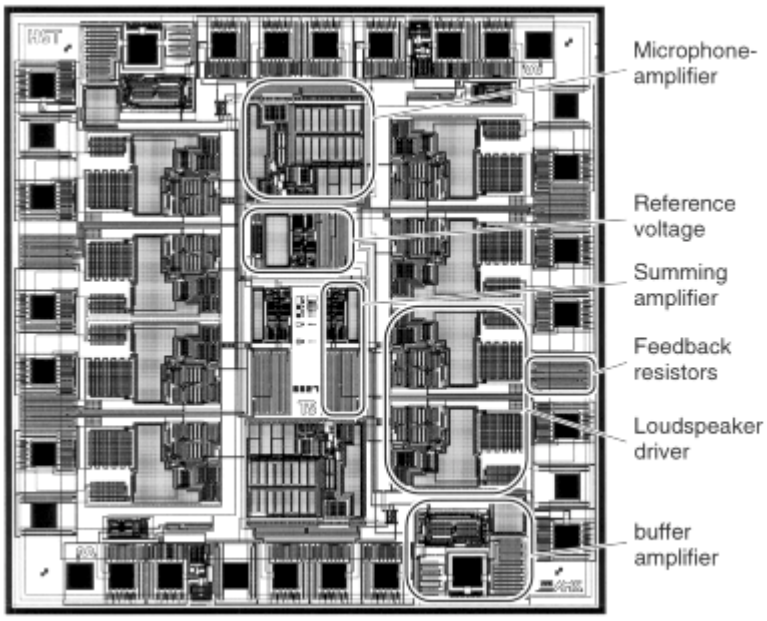

Fig. 2: Layout of the HST ASIC.

2.4 Conclusion

The development of an analogue ASIC helped the company to reduce the system costs, increase the reliability by implementing additional monitoring functions, and to a certain extent standardize their products. Prototyping services like those provided by EURO-PRACTICE proved to be very valuable, their cost-effectiveness being an essential

argument in easing the decision of an SME towards the use of new technologies. On the other hand, comparatively long turnaround times acceptable for universities may irritate industrial partners, and the consequences on project schedules have to be pointed out from the very beginning. In this sense both partners gained experience in managing projects including MPW prototyping.

References

[1] P.E. Allen and D.R. Holberg, *CMOS Analog Circuit Design*, Saunders College Publishing, 1987, p. 462.

[2] J.N. Babanezhad and R. Gregorian, "*A Programmable Gain/Loss Circuit*", *IEEE J. Solid State Circuits*, vol. SC-22, pp. 1082 – 1090, Dec. 1987.

[3] K.R. Laker and W.M.C. Sansen, "*Design of analog integrated circuits*", McGraw-Hill, 1994.

Project Information

Project Manager

Dipl.-Ing. Nikolaus KERÖ

Institut für Allgemeine Elektrotechnik und Elektronik, TU Wien, A-1040 Vienna

Project Group

Last Name	First Name	Status	Remarks
Cadek	Gerhard R.	dissertation	
Kausel	Wilfried	dissertation	
Kerö	Nikolaus	dissertation	
Kowarsch	Eduard	technician	
Sauter	Thilo	dissertation	
Thorwartl	Peter C.	dissertation	

Doctor's Theses

1. G.R. Cadek, "Entwurf und Realisierung eines integrierten Schaltkreises für die Sprachkomprimierung mit neuer Architektur", in progess.

Cooperations

1. AKG-Acoustics, Wien
2. Frequentis Nachrichtentechnik Ges.m.b.H, Wien
3. Semcotec, Wien
4. Institut für Computertechnik, TU-Wien, Austria
5. Institut für Technische Informatik, TU-Wien, Austria
6. Institut für Elektronik, TU-Graz, Austria
7. Institut für Angewandte Informationsverarbeitung, TU-Graz, Austria
8. Institut für Systemwissenschaften, Johannes Kepler-Universität Linz, Austria

ASICs in Electronic Instrumentation

H. Leopold, W. Meusburger, R. Röhrer, H. Senn, P. Söser

Institut für Elektronik, Technische Universität Graz
A-8010 Graz, Austria

Application Specific Integrated Circuits (ASICs) are used for various reasons in electronic instrumentation. The most significant advantages in industrial environment are obviously less power consumption and less space combined with a good possibility of signal conditioning for proper information transfer to a central processing unit. In laboratory equipment reliability and flexibility as well as the reduction of cost and space are the counting arguments for the use of ASICs. This paper will give a review on projects already worked out at the Department of Electronics and will then — as the annual report of UNICHIP Graz — focus on an ASIC devoted to highly accurate thermometric instrumentation.

1. Introduction

The Department of Electronics at the Technical University Graz started to design integrated circuits (IC) in 1988. Since then several systems have been developed in the department comprising ASICs devoted to electronic instrumentation. The methodology involved spans from gate-array to standard-cells if digital; in case of analog or mixed-mode the analog section is full-custom.

The systems under consideration are predominantly sensoric sensing physical properties of liquids (density, velocity of sound, and temperature) either in the harsh environment of industrial process control or in the clean laboratory with the highest level of accuracy.

2. Instrumentation in Industrial Environment

There are various reasons for the use of ASICs in electronic instruments for industrial environment. Our systems being in almost all cases instrumentation designed to support sensors the small size of the ASIC is very much appreciated as such systems fit directly into the probes. The small outline helps with respect to electromagnetic interference and to mechanical robustness. If power consumption is low the system can be supplied with a current loop (typically 4 – 20 mA), which is also used to carry information to the central processing unit. Both requirements (small, low power consumption) can be met with ASICs. Three ASICs of this kind have been developed at the department in the last years. They are briefly described in the following chapters.

2.1 GOETHE

This was the very first gate-array design [1] in the field of industrial instrumentation at our department. It was thought to replace a PCB system which was used to encode the temperature of a liquid into a bit-stream locked in frequency to the periodic signal coming from a mechanical oscillator carrying information on the density of said liquid. In other words, the temperature was measured using a platinum thermometer and a ref-

erence resistor in an integrating ratiometric Analog-to-Digital Converter (ADC). As the clock for the ADC was the mechanical oscillator, the resolution in temperature with respect to time was by far to low.

The ASIC (GOETHE) had an on-chip crystal oscillator to provide a fast clock signal for the ADCs. The control- and the quantization units for two of them were integrated in the gate-array. The resolution is 20 bit each. The analog sections of these ADCs are added off-chip. The results of the conversions are counted BCD numbers. They modulated the pulse width of the mechanical oscillator signal. The information was transferred by means of a binary current signal on a two-wire line also providing the power for the whole sensor system.

This ASIC brought the expected increase in performance and a significant decrease in space needed for the interface system.

2.2 ASTERIX

This ASIC was the first standard cell design at our department. It is used in a warm water boiler to periodically “wake up” a microcontroller which then takes measurements of temperatures and performs calculations on whether there is enough energy stored or not. The results are sent back to the ASIC which offers a multiplexed LCD driver circuit. The display shows status information.

The main advantage of this ASIC was an enormous reduction in the power needed to operate the control system as only a very small part was active all the time and the power consuming parts were activated for just a short period. With the multiplexed LCD driver in the ASIC a reduction of the package to a 28 pin type could be achieved. This saves extra cost for the PCB and the ASIC.

The development of ASTERIX was a cooperation of an Austrian enterprise, Joanneum Research and our department. ASTERIX is part of a product of this Austrian enterprise.

2.3 SUPERGOETHE

This ASIC is a more powerful version of GOETHE. Therefore a standard-cell approach was chosen in a 1.0 μm CMOS technology [2], [3]. The system was extended to be able to operate the analog sections of three 20-bit ADCs and to quantize up to three periodic signals (both density and velocity of sound are transferred to periodic electrical signals; the information is the length of the period) with selectable resolution. The problem with this quantization is the absolute accuracy, the long time- and the temperature stability of the crystal oscillator in the interface. To avoid this problem a method of counting multiple periods with no error and determining the length of these periods by counting a high frequency oscillator clock is used. If the rate for the information transfer and the oscillator clock have a fixed ratio the clock period can be measured in the central processing unit, where power consumption is no severe problem and therefore accurate and stable oscillators (e.g. heated crystal) can be used as reference. The time for the measurement is one second. The information gathered in this time is transferred in the following second. The supply current is periodically switched between two values. The information is encoded in the duty-cycle of this signal.

This ASIC is very flexible. It can be configured to many operational modes. It is used in two products so far. One is a two channel traceable thermometer with an accuracy of

0.01 °C. The second product is a modular sensor interface system for measuring density, temperature, pressure, and velocity of sound in industrial environment. This system is certified to be intrinsically safe.

2.4 Preworks on an ASIC for the Measurement of the Velocity of Sound

One method for measuring the velocity of sound in liquids is to determine the transit time for a known distance between the sender and the receiver of an ultrasonic pulse. This is done in electronic circuits on PCB level very well [4]. Some research activity was spent to find a way of integrating such a system on a single chip. Various input amplifiers have been designed but are not yet fully evaluated.

3. Instrumentation in Laboratory Equipment

To save space on the PCB and to increase reliability and functionality ASICs are put in electronic instruments for laboratories. Power consumption is normally no problem in this case except when the instrument is battery powered. Then of course this is a driving argument for the use of an ASIC. Two ASICs are presented here which were designed the years ago. Chapter 4 then covers a recently developed circuit in more detail.

3.1 ADONIS

Laboratory equipment often uses electromechanical components (pumps, transformers) which are dependent on the mains frequency. To eliminate the need of a switch to adapt the instrument to the right frequency these AC signals are often synthesized. A crystal oscillator is used together with H-bridge power switches to do this synthesis from a DC voltage. An ASIC (ADONIS) was developed using gate-array technology to get a 50 Hz and a 100 Hz signal to drive a transformer and a pump in a density meter [5]. All control signals for the power switches are generated in the ASIC. Overload switch-off and power-on-reset are available. The driving output signals can be turned on and off separately.

3.2 ENDOR

To minimize size and power consumption of a handheld battery powered density meter an ASIC (ENDOR) was designed [6]. It has a 8051-compatible microcontroller interface and consists of some glue logic, a unit to quantize and encode a Charge-Balance ADC and to measure the period of a signal. This signal comes from a mechanical oscillator, which is electrically brought to its resonance frequency. The period of this signal is used to calculate the density of the liquid. The ASIC works according to the specifications.

4. ENDEAVOR - An ASIC for a Highly Accurate Thermometer

As a result of the activities in research and development at the department a highly accurate thermometer was built [7], [8]. The accuracy is 0.001 K in the range from -200 °C to +800 °C. The thermometer offers two channels for measurement.

It uses a platinum resistor for sensing as this is the only type of temperature sensor with respect to this wide temperature range and this high accuracy [9]. The thermometer consists of two current sources, a voltage-to-current converter and of an ADC working

in current mode. There is also a microcomputer to select the channel, to set the right direction of the current, to control the ADC and to calculate the temperature.

Figure 1 shows the circuit diagram of the voltage-to-current converter. The currents I_P and I_N convert the unknown resistance of R_X and the resistance of R_0 (which is used as reference) to a voltage. The input current (I_E) of the ADC is the sum of an offset current (I_O) and the current, which comes from the voltage across R_X or R_0 (depending on the pairs of switches 3 and 4) and R_S. I_O makes I_E positive for all values of R_X and both currents I_N and I_P.

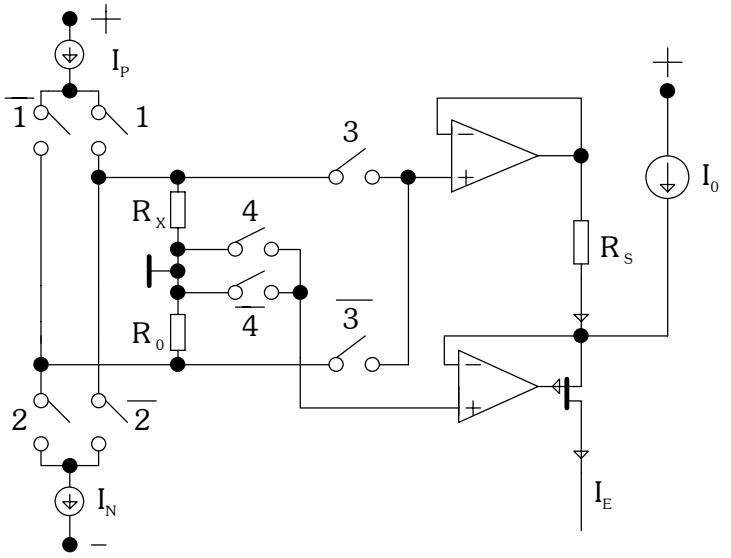

Fig. 1: Voltage-to-current converter

The control signals for the switches 1 to 4 are provided by the microcomputer. For one value of R_X we get four different currents I_E and therefore also four results of an analog-to-digital conversion. From these results we can get the ratio R_X/R_0 by subtraction and division without errors of the order zero (thermo- and offset voltages) and the order one (value of I_P, I_N and R_0).

Figure 2 shows the structure of the ADC [7], [10], [11]. The comparator S determines the discharge of capacitor C_i after the conversion. Comparator C is used to show that the voltage across C_i is lower than the voltage U_{Ref}. Switch 9 is used to start the conversion with the capacitor C_i discharged. The complementary pair of switches 6 can guide the current I_E either to the input or the output of the integrator. The same is done with the reference currents I_R and $I_R/256$ and the switches 7 and 8.

The current I_E is integrated for 0.1 s. The reference current I_R compensates I_E in this phase using a Charge-Balance method. The charge in C_i after this integration is determined with the help of $I_R/256$. The numeric result of this conversion is 256 times the number of clocks during the disintegration using I_R in addition to the number of clocks used for discharging with $I_R/256$.

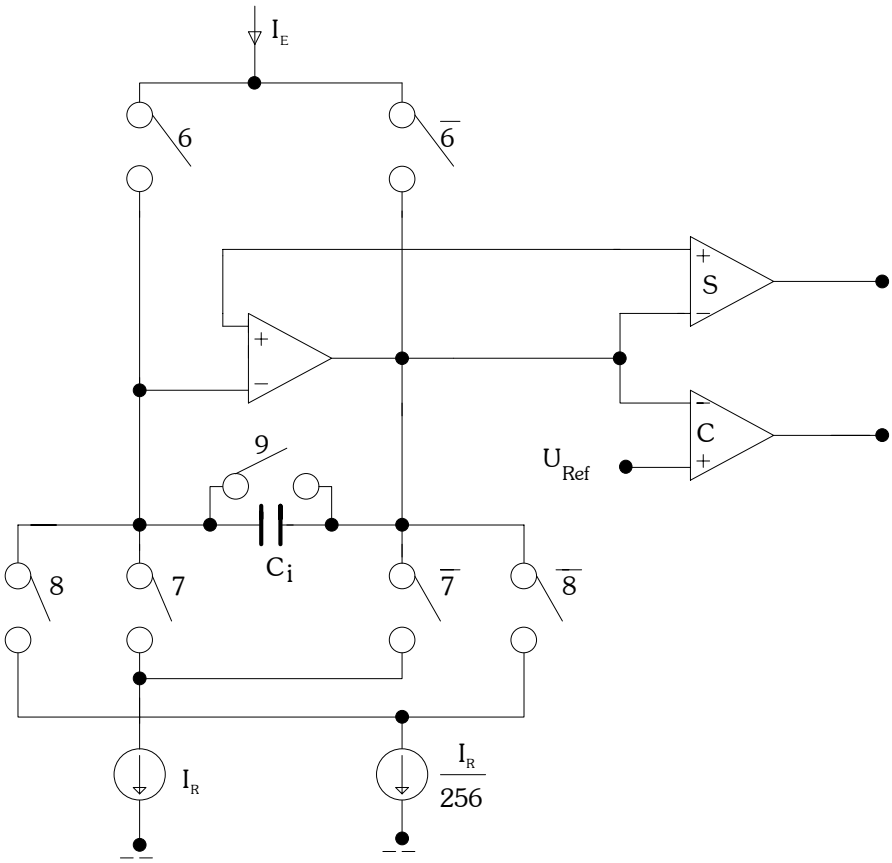

Fig. 2: Structure of the ADC

To control all the switches and to provide the time frame for the conversion a digital control unit is used. The number of clocks is counted by the microcomputer which also calculates the temperature either using IEC751 or ITS-90.

To be able to add more channels, to add more flexibility to the system of the thermometer and to overcome the electromagnetic compatibility (EMC) problems with digital signals on lines (between the comparators and the microcomputer) near a 23-bit ADC an ASIC (ENDEAVOR) was designed [12].

The number of channels was increased to eight. The counters for the clock pulses, which are the result of the analog-to-digital conversion, are added on-chip. There are no digital signals outside the ASIC when a conversion is made. On-chip counters have a low load capacitance on the clock line. Spikes in the power supply are therefore avoided. The information is serially transferred to the microcomputer at a time, when no conversion is going on. The digital signals then can cause no interference to the result of the conversion.

Figure 3 shows the block diagram of ENDEAVOR. A crystal oscillator provides the system clock of 1 MHz. Counters and decoders generate the control signals. A baudrate generator is implemented to provide a serial output signal of 9600 baud. The information has ASCII format, so a simple terminal program can be used to visualize the results of the conversions. The implementation of the original control unit guarantees compatibility to the existing system. The channels are periodically activated for measurement. The sequence can be set up with control signals.

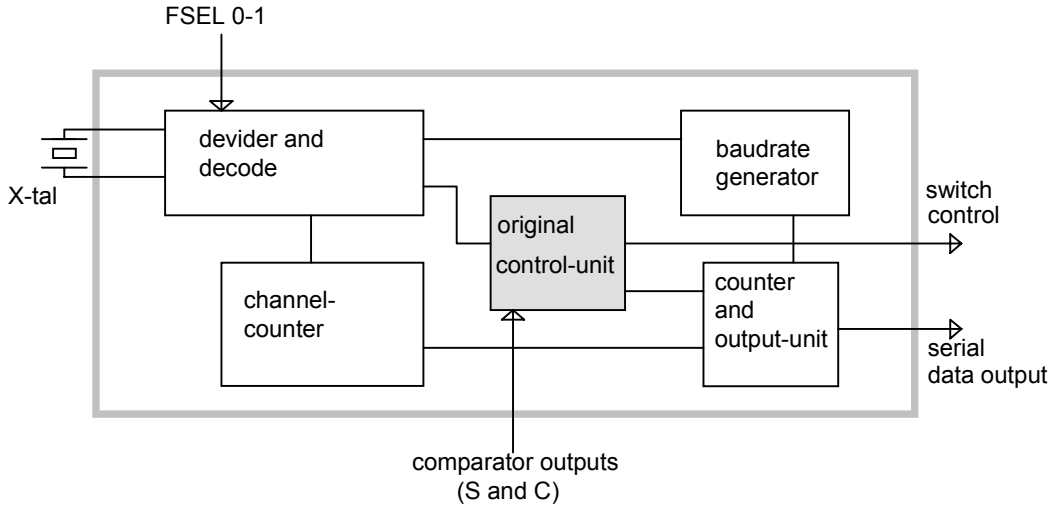

Fig. 3: Block diagram of the ASIC

The ASIC is in fabrication (0.8 µm AMS CMOS-process) at the moment. The transistor count is approximately 5500. The size is 1.9x1.9 mm^2. A 28 pin PLCC package is used. The first engineering samples are expected for the middle of March 1997. Then it will be seen if the selected targets could be reached:

- No digital signals outside the ASIC during conversion should bring a reduction of the system internal noise interference. The expected increase in the ADCs resolution is at least from 23 to 24 bits.
- 4 times more channels (8 instead of 2).
- More flexibility: a simple terminal program can be used to visualize the results of the conversation; the sequence of the active channel can be changed via control signals.
- Less power consumption and less space requirements for a smaller and cheaper thermometer.

5. Conclusion

The use of ASICs in electronic instrumentation offers a wide spectrum of advantages. Topics which lead to the decision to start the design of an ASIC are not only reduction of space and power consumption but are also sometimes problems of EMC. In most cases the functionality and reliability of the system can be raised as shown with the examples of the industrial instrumentation (multi-channel measurements and better overall performance). BiCMOS technology is supposed to bring new advantages in some critical analog integrated circuits.

Acknowledgment

The “Steiermärkische Landesregierung, Abteilung für Wirtschaftsförderung” is funding this project by carrying a substantial part of the cost for personnel. Without this support a continuous activity in the area of ASIC-Design at the Department of Electronics would not be possible.

References

[1] H. Leopold, M. Pacher, R. Röhrer, G. Winkler: "Monolithische integrierte Steuerschaltung für A/D-Umsetzer", *Arbeitsbericht der Informationstagung Mikroelektronik 1989*, 386 – 391

[2] P. Söser: "Ein höchstauflösendes Sensorinterface für die Abbildungsgrößen Spannungsverhältnis und Zeit", Dissertation, Institut für Elektronik, TU Graz. Eigenverlag, 1993

[3] H. Leopold, R. Röhrer, P. Söser: "Monolithischer Quantisierer und Kodierer für als Periode und Tastverhältnis dargestellte analoge Größen", *Tagungsbericht des Fortbildungsseminares der Gesellschaft für Mikroelektronik*, Großarl 1993, 121 – 127

[4] Österreichisches Patent 380339, 1986

[5] H. Leopold, P. Söser, W. Steiner, G. Winkler: "Eine monolithische Steuerschaltung für Leistungs-H-Brücken", *Arbeitsbericht der Informationstagung Mikroelektronik 1991*, 15 – 20

[6] W. Meusburger, R. Röhrer, H. Senn, P. Söser: "ENDOR — Ein ASIC für ein batteriebetriebenes Handdichtemeßgerät", in print, *Tagungsbericht AUSTROCHIP 97*, 1997

[7] H. Leopold: "An den Grenzen der Genauigkeit elektronischer Analogschaltungen", *Telematik* 1. 1995, 8 – 12

[8] H. Leopold, K. Schröcker: "Ein eichfähiges Millikelvinthermometer für -200 °C bis +800 °C", *Arbeitsbericht der Informationstagung Mikroelektronik 1987*, 219 – 223

[9] H. Preston-Thomas H.: "The international Temperature Scale of 1990 (ITS-90)", *Metrologia* 27, 1990, 3 – 10

[10] K. Schröcker: "A/D-Wandler für das Millikelvin-Thermometer", presentation on 5 October 1987, Institut für Elektronik, TU Graz.

[11] H. Leopold, K. Schröcker, M. Holzer: "Verifikation der Genauigkeit einer Analogschaltung im PPM-Bereich", *Arbeitsbericht der Informationstagung Mikroelektronik 1989*, 392 – 396

[12] H. Leopold, W. Meusburger, J. Pfeiffer, H. Senn, G. Winkler: "ENDEAVOR — Ein ASIC für ein hochgenaues Thermometer", in print, *Tagungsbericht AUSTROCHIP* 97, 1997

Project Information

Project Manager

Dipl.-Ing. Dr. Peter SÖSER

Institut für Elektronik, TU Graz, Graz, Austria

Project Group

Last Name	First Name	Status	Remarks
Drexel	Werner	student	Inst. f. Elektronik
Leopold	Hans	university professor	BMWFuK
Meusburger	Walter	assistant	BMWFuK
Röhrer	Robert	assistant professor	BMWFuK
Schatzberger	Gregor	student	Inst. f. Elektronik
Senn	Helmuth	researcher	Inst. f. Elektronik
Söser	Peter	assistant	BMWFuK

The salaries for H. Senn, G. Schatzberger and W. Drexel were refunded by Steiermärkische Landesregierung, Abteilung für Wirtschaftsförderung.

Publications in Reviewed Journals

1. V. Schindler, W. Mayerwieser, H. Bock, H. Senn: "A 180-MHz Two Phase Clocked Schift-Register Memory"; submitted for publication
2. W. Meusburger, H. Senn, P. Söser: "Development of Device Generators for the support of the analogue IC Design with Mentor V8", *Proceedings of the Mentor Graphics Alpine Local Users' Group Conference*; September 1996

Presentations

1. W. Meusburger: "Development of Device Generators for the support of the analogue IC Design with Mentor V8", *Mentor Graphics Alpine Local Users' Group Conference*, Chaumont/Switzerland, 27 September 1996

Cooperations

1. Institut für Angewandte Informationsverarbeitung und Kommunikationstechnologie; TU Graz, Prof. Dr. R. Posch
2. Forschungsgesellschaft Joanneum, Institut für Sensorik, Graz

3. Labor für Meßtechnik, Dr. H. Stabinger, Graz
4. Fa. Anton Paar GmbH, Graz
5. AMS, Austria Mikrosysteme International AG; Unterpremstätten
6. Entwicklungszentrum für Mikroelektronik; Siemens, Villach
7. MIKRON, Gratkorn

Microsensors

Miniaturized Sensor Systems

F. Kohl, P. Svasek, A. Jachimowicz, G. Jobst, F. Keplinger, G. Urban

Institut für allgemeine Elektrotechnik und Elektronik, TU Wien
L. Boltzmann Institut für biomedizinische Mikrotechnik
A-1040 Vienna, Austria

The acceptance of sensor concepts by industrial equipment producers requires an optimization of the sensor design for the specific application. We developed miniaturized thermal flow sensor designs for very different applications like a novel gas meter, for the investigation of the air intake of combustion engines and an extremely sensitive version for monitoring the flow of excess liquor cerebrospinalis during hydrocephalus treatment. In the field of biosensors, good sensor specifications are not sufficient for broad acceptance by the analytical equipment industry. The needs of a complete analytical process have to be considered by the sensor developer. For such purposes we established a cheap technology for the production of miniaturized fluid handling modules based on dry photoresists [1]. The flexibility of this technology allows the realization of complex structures needed for analyte preprocessing.

1. Introduction

Because of their inherent advantages as low analyte consumption, quick response, and cheapness, miniaturized sensors are very attractive for biomedical and many other applications. Sensors intended for example for the survey of industrial processes or for the monitoring of biomedical systems must fit perfectly into the specific system for doing their job as good as possible. These biosensor systems have to fulfill many different tasks as establishing the right environment for the sensor functioning, handling of the analytes, linking the sensor signal to the information processing equipment. Only a complete miniaturized sensor system will be acceptable for applications outside the research labs.

Beside such system aspects, the sensor element itself must match to the specific requirements of the intended use as good as possible. As a consequence, in some cases completely different manufacturing procedures have to be used even for sensors based on the very same technological concept. The presented examples of miniaturized thermal flow sensors are good examples to demonstrate this influence.

2. Experimental

2.1 Dry film resist technology for miniaturized analyte handling modules

Dry films resists are available as etching resists and for solder masks (i.e. VACREL®). The patterning of each resist layer is a three-step process: lamination, exposure, developing (Fig. 1). The achievable aspect ratio is approx. 0.5, e.g. grooves with a width of 100 µm can be formed if the layer thickness does not exceed 50 µm. The walls are not perpendicular to the surface but undercut at an angle of 15°. If structures higher

than 100 µm are desired, the process can be repeated using the same mask. We showed that three-dimensional structures can be realized without special bonding techniques. The complete process is illustrated in Fig. 1.

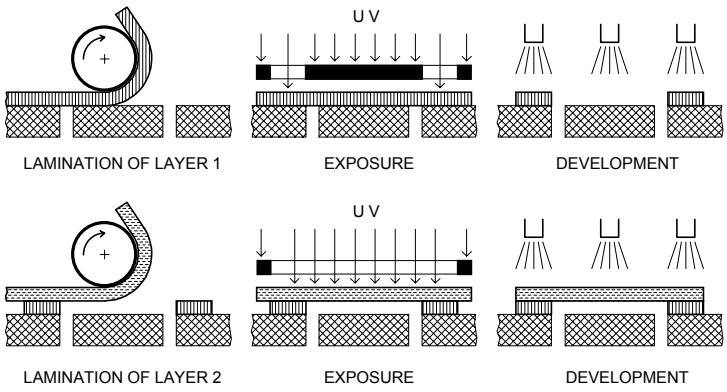

Fig. 1: Dry resist based manufacturing of a flow channel

The resist material must be cured after patterning of the last layer. This process consists of a temperature step and a final exposure to UV light.

Many biosensors require perfect mixing of the analyte and some added agents to produce accurate results. Miniaturized flow channels obstruct the mixing of fluids because of their inherent laminar flow profiles. We designed a miniaturized Moebius-type mixer [2] which on the one hand enhances the useful flow range and on the other hand reduces the required dead volume.

2.2 Miniaturized flow sensors

2.2.1 Micro Flow Sensor Treatment of Hydrocephalus

This sensor (Fig. 2) is a part of a miniaturized all-silicon device for the aid of patients suffering from hydrocephalus [3]. This device should measure the intracranial pressure and automatically opens a shunt for excessive liquor cerebrospinalis if required. The flow sensor serves for continuous monitoring and should detect reverse flow too. The flow sensor was placed on a thin film membrane borne by a micro-machined Si structure for highest flow sensitivity. A special mask alignment equipment that is capable for mask adjustment related to structures at the backside of the wafer is needed for the sensor manufacturing. This equipment is now available at MISZ laboratories. The desired flow detection limit for this application, namely 50µL/h was experimentally verified. It is planned to implement similar sensors in controlled drug delivery devices.

2.2.2 A sensor for the study of the air Intake of combustion engines

The air intake rate of a combustion engine is one of the key parameters needed for optimizing the combustion process. To investigate the dynamic behavior of a suction system, a useful flow sensor must offer quick response, high sensitivity, recognition of flow direction, and a wide dynamic range. Miniaturized thermal anemometers, based on thin film Ge thermistors, show a good compromise of the mentioned characteristics and changing of the direction of flow could be achieved using two temperature sensors

placed symmetrically to a thin film platinum resistor that represents the hot wire. Thanks to miniaturization a response to changes of flow within one ms was obtained. Prototypes of such flow sensors were successfully tested under simulated suction system conditions.

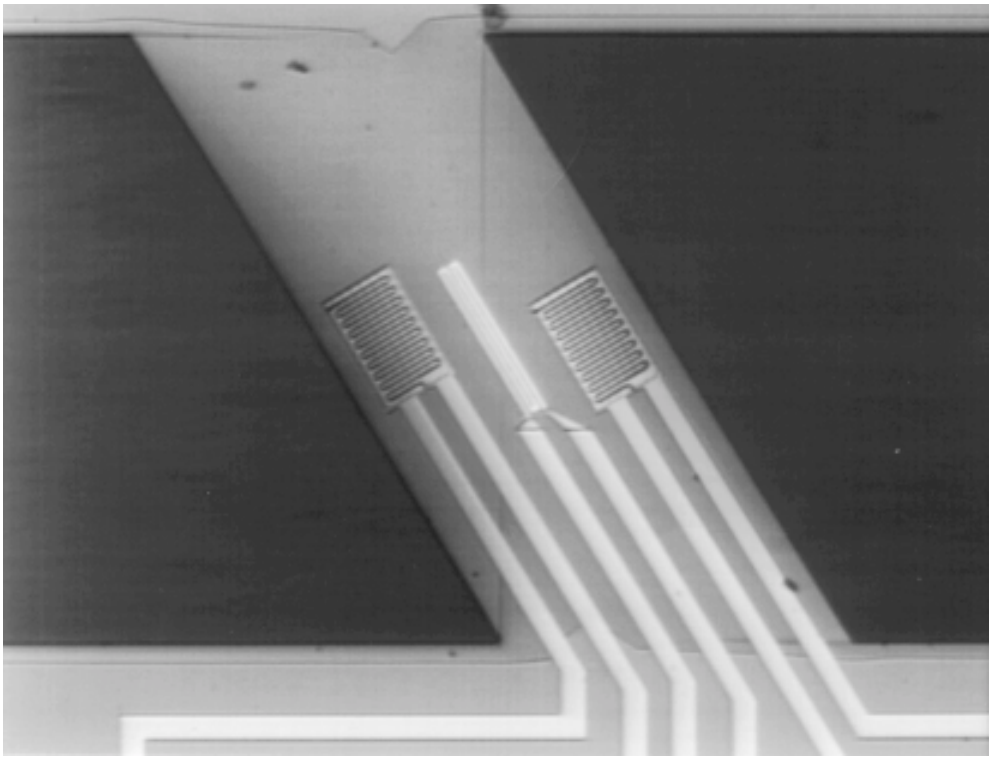

Fig. 2: A thermal flow sensor placed on a SiN_x micro bridge. Flow channel width measures 1 mm. A thin film platinum resistor of 750 W is located in the mid of two thin film Ge thermistors with a resistance of 56 kW.

2.2.3 Miniaturized thermal flow sensors for a novel gas meter

The gas meter concept uses the fluid oscillator principle, which is based on oscillations of the flow velocity field inside an especially shaped flow channel. The frequency of the oscillations increases in the range 0.1 to 100 Hz with increasing flow. The oscillation frequency can be measured best with a pair of thin film thermistors.

There are some remarkable requirements for this applications: high reliability for long term, service free operation (typical six to ten years), low power consumption for long term battery powered operation, high sensitivity at low gas velocities, miniaturized shape for undisturbed flow and simple incorporation, appropriate resistance values and good pairing tolerance for simple data acquisition circuits. On the other hand, there are no restrictions concerning the absolute accuracy and long term drift of the sensor elements. After an extensive evaluation of the technological alternatives the producer of the gas meter decided to use miniaturized self heated Ge thermistors placed on micro-machined membranes on silicon chips as the key element for flow detection. The design issues were minimum Si area and high thermal resistance for high flow sensitivity at low power consumption.

3. Conclusion

Miniaturized biosensors normally require an integrated analyte processing module to be an acceptable sensor system for utilization. Dry film photoresists offer the possibility to develop integrable fluid handling components in a very convenient way if modest miniaturization is sufficient. To optimize the design of a miniaturized sensor for integrability into a specific system is another successful way to make use of it. The presented miniaturized thermal flow sensors are examples for that concept.

References

[1] G. Urban, G. Jobst, P. Svasek, M. Varahram, I. Moser, E. Aschauer: "Development of a micro flow-system with integrated biosensor array", Micro Total Analysis Systems, Univ. Twente 1994, Kluwer Academic Publisher, ISBN 0-7923-3217-2, p.249.

[2] H. Mensinger, T. Richter, V. Hessel, J. Döpper, W. Ehrfeld: "Microreactor with integrated static mixer and analysis system", Micro Total Analysis Systems, Univ. Twente 1994,Kluwer Academic Publisher, ISBN 0-7923-3217-2, p.237.

[3] S. Seifert, G. Urban, J. Oswald, J. Joswig: "Mikrosystemtechnischer Volumensstrommesser für den Einsatz in der Medizin", Biomedizinische Technik, Band 41, Ergänzungsband 1, 1996, p. 278.

Project Information

Project Manager

Univ.-Doz. Dr. Gerald URBAN

Institut für Allgemeine Elektrotechnik und Elektronik, TU Wien, A-1040 Vienna

Project Group

Last Name	First Name	Status	Remarks
Biacovsky	Dalibor	dissertation	
Jachimowicz	Artur	assistant professor	
Keplinger	Franz	assistant professor	partially GMe funded
Kohl	Franz	assistant professor	
Steurer	Johannes	assistant professor	partially GMe funded
Urban	Gerald	associate professor	

Books and Contributions to Books

1. E. Aschauer, G. Jobst, R. Fasching, M. Varahram, P. Svasek, I. Moser, G. Urban, "Miniaturisierte integrierte Biosensoren für Glukose- und Laktatmonitoring", in *Multi-Sensor Praxis*, Springer Verlag 1997, p. 225 – 238.
2. G. Urban, "Microelectronic Biosensors for Clinical Applications", *Handbook of Biosensors, Food, and the environment*, CRC Press,1997 chapter 12, p. 257 – 279.
3. A. Urban, G. Jobst, "Biosensors with modified electrodes for in-vivo and ex-vivo applications", in *Frontiers in Biosensorics* (ed.: F.W.Scheller), Birkhäuser Verlag 1997, p. 161 – 173

Publications in Reviewed Journals

1. L. Yu, G. Jobst, I. Moser, G. Urban, H. Gruber, "Photolithographically patternable modified Poly(HEMA) hydrogel membrane", *Polymer Bulletin* 35 (1995), 759 – 765.
2. G. Jobst, I. Moser, G. Urban, Numerical simulation of multi-layered enzymatic sensors, *Biosensors & Bioelectronics*, 11, No 1-2 (1995), 111 – 117.
3. E. Aschauer, R. Fasching, M. Varahram, G. Urban, G. Nicolussi, W. Husinsky, G. Friedbacher, M. Grasserbauer, "Surface modification of platinum thin film electrodes towards a defined roughness and microporosity", *Journal of Electroanalytical Chemistry*, 1997 accepted

4. G. Jobst, M. Varahram, I. Moser, P. Svasek, E. Aschauer, Z. Trajanoski, P. Wach, P. Kotanko, F. Skrabal, G. Urban, "Thin-film Microbiosensors for Glucose-Lactate Monitoring", *Anal. Chem*., Vol. 68, 18 (1996), 3173 – 3179

Presentations

1. I. Moser, G. Jobst, P. Svasek, M. Varahram, A. Jachimowicz, F. Kohl, G. Urban, "Sensor-Mikrosysteme für klinische Monitoring-Anwendungen", *Biomedizinische Technik* Band 41, Ergänzungsband 1 (1996) 272 – 273

Doctor's Theses

1. D. Biacovsky, Micromachined flowsensors, in preparation.
2. R. Fasching, Development of an electrochemical CO_2-sensor, in preparation.
3. J. Kamper, Development of temperatur sensors for process control and monitoring, in preparation.
4. H. Penc, Treatment of esophageal veins by electrostimulation, in preparation.
5. A. Steinschaden, Detection of HIV-antibodies by impedance spectroscopy, in preparation.

Cooperations

1. Institut für Medizintechnik Dresden e.V., B. Voß-Straße 25–27, D-01445 Radebeul, Dr. S. Seifert
2. AVL List Gmbh, Kleisstr. 48, 8010 Graz, Dr. Schindler
3. Schlumberger Paris, Dr. D. Dominguez

Other Projects

High Precision Depth Profiles with SIMS

H. Hutter and K. Piplits

Institute of Analytical Chemistry, TU Wien
A-1060 Vienna, Austria

This paper demonstrates applications of surface analysis techniques for the investigation and characterization of materials and production processes. SIMS depth profile measurements of implanted erbium in silicon demonstrate that high precision measurements of low concentrations are necessary to assist implantation and simulation groups. Measurements of potassium profiles in fullerene films were performed to investigate diffusion processes in order to optimize material properties. Measurements of the three dimensional distribution of trace elements in high purity molybdenum points out the importance of distribution analysis of raw materials for microelectronics.

1. Introduction

Surface analysis techniques play an important role for supporting material development and process optimisation. One of the most common techniques is Secondary Ion Mass Spectrometry (SIMS). This is due to the high detection power of the method, the fact that all elements are detectable and the possibility of registering two- and three dimensional distributions of trace elements.

To support various investigations in the field of microelectronics, the performance of analytical methods has to be increased. The actual questions of technology demand a permanent development of the precision of measurements, especially at very low concentrations. The supervision of the implantation process stability by measurements of depth profiles for erbium demonstrates the support of optimizing production processes. Investigation of the implanted potassium distribution in C_{60} fullerenes supplies information for the development of new materials. It will be shown that the determination of trace element concentration is necessary for the development of high purity materials like molybdenum.

2. Results

2.1 Erbium in Silicon

The 4f shell of rare earth elements is well shielded by the outer shell electrons. Therefore these elements exhibit sharp and almost atom-like spectra when incorporated as dopants in semiconductors and isolators. The emitted wavelengths practically coincide with those observed for isolated atoms and depend only little on the host material. Erbium implanted into Si produces rich spectra of sharp lines in photo- and also in electroluminescence in a narrow spectral region close to 1,54 µm. This wavelength stimulates interest in Si:Er as a candidate for light emitting devices for fibreoptic communication systems and also for on-chip and inter-chip optical data transfer.

Investigations by high resolution photoluminescence and deep level transient spectroscopy of Er-implanted silicon were made by Dr. Palmetshofer [1].

The ion implantation of 320 keV (implanted by Dr. Palmetshofer, University Linz) and 2 MV (implanted in Guildford, UK) erbium in CZ and FZ silicon was performed at room temperature with doses of $3{,}13 \cdot 10^{13}$ and $8{,}13 \cdot 10^{13}$ cm^{-2}. To determine the diffusion coefficient of erbium in silicon, one series of the samples were tempered at 900 °C for 30 min in nitrogen.

The SIMS depth profiles of implanted erbium in silicon show no broadening of the erbium implantation profiles during the temperature treatment. The maximum concentration of erbium was about $2 \cdot 10^{18}$ atoms per cm^3, the profiles were Gaussian like. The detection limit was lower than $1 \cdot 10^{15}$ atoms per cm^3. This indicates that there is no significant diffusion of erbium at a temperature of 900 °C.

The profiles show no enrichment of Er at the surface, this indicates that Er does not segregate during the annealing in samples with implantation doses below 10^{14} cm^{-2}.

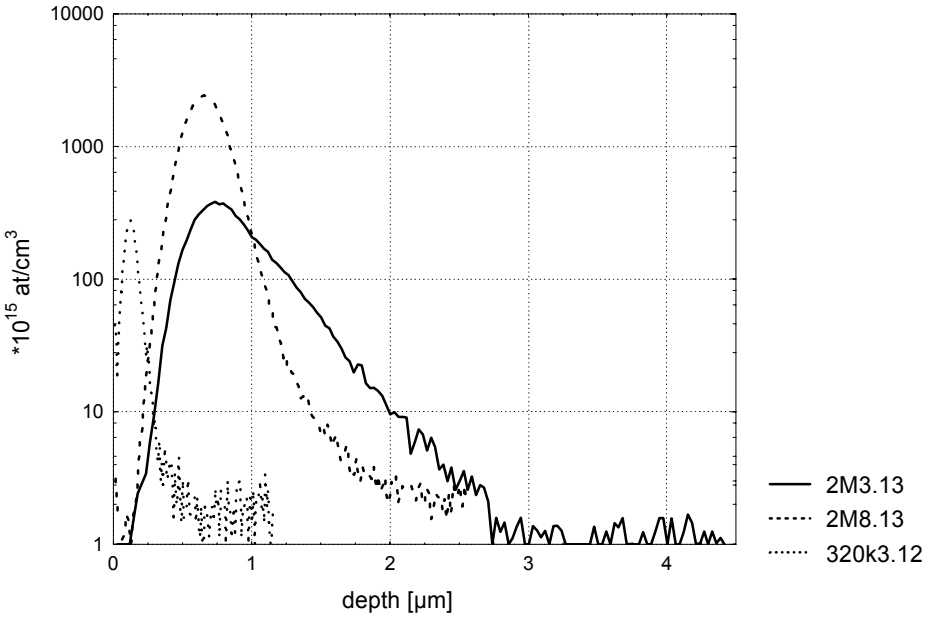

Fig. 1: SIMS erbium profiles of Si implanted with 2 MeV (2M3.13, 2M8.13) and 320 keV (320k3.12) Er^+ with doses of $3.13 \cdot 10^{13}$ cm^{-2} (2M3.13), $8.13 \cdot 10^{13}$ cm^{-2} (2M8.13) and 0.312·1013 cm^{-2} (320k3.12). All profiles show the expected gaussian distribution.

Contrary to all expectations the profiles of the first measured 2 MeV samples were channeling like. Further analysis shows that these profiles are not results of axial channeling in [100] direction but of planar channeling. Probably this is the result of an incorrect implantation process. Renewed implantations did not show this behavior.

2.2 K in Fullerens

Films of chromatographically purified C_{60} were prepared on silicon substrates by vacuum deposition. Ion implantation of 30 keV $^{39}K^+$ was performed at 300 °C in a vacuum better than 10^{-4} Pa. The depth profiles were measured using 5.5 keV O_2^+ primary ions.

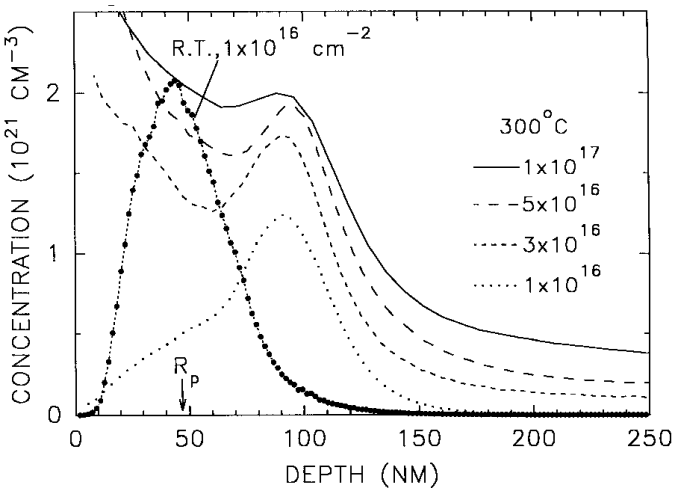

Fig. 2: SIMS potassium profiles for C_{60} films implanted with 30 keV K^+ at room temperature ($1 \cdot 10^{16}$) and at 300 °C (1, 3, 5 and $10 \cdot 10^{16}$ cm^{-2}).

Figure 2 shows the depth profile of $^{39}K^+$ for samples implanted with 30 keV at room temperature ($1 \cdot 10^{16}$ cm^{-2}) and at 300 °C (1, 3, 5 and $10 \cdot 10^{16}$ cm^{-2}). For room temperature implantation, the experimental profile is Gaussian-like with a weak diffusion induced tail at greater depths.

At 300 °C implantation temperature a peak appears in the tail region at about 100 nm, and the K-concentration within the theoretical ion range is strongly reduced. An increase of the dose leads to a subsequent increase of the peak at about 100 nm and to a slight shift of its maximum into the depth. However, with increasing dose the K-concentration in this region tends to saturate at a value of about $2 \cdot 10^{21}$ cm^{-3}. A certain amount of K diffuses out to the surface, but the diffusion into the depth is more pronounced. In all samples more than 70% of the implanted atoms are found underneath a 70 nm surface layer. Raman spectra indicate that there is a passivating a-C surface layer and the accumulation of K is at the a-C/C_{60} interface. These structures may have useful applications for new Tc superconducting devices on the basis of fullerenes which can be handled on air [2].

2.3 Ultra pure Molybdenum

Due to the high heat resistivity molybdenum is used as sample holder for the MBE process. During the MBE process trace elements with concentration below the ppm (part per million) level diffuse in the sample, this results in contamination of the devices. The use of ultra pure materials prevents this process. Not only the overall (bulk) concentration is decisive for this diffusion, also the distribution and the chemical state of the trace elements. Therefore the determination of the three dimensional distribution is necessary for the development of functional materials.

The material we investigated is 6N molybdenum, that means that the concentration of all trace elements together is below 1 ppm (part per million). This material is used for the production of MBE sample holders.

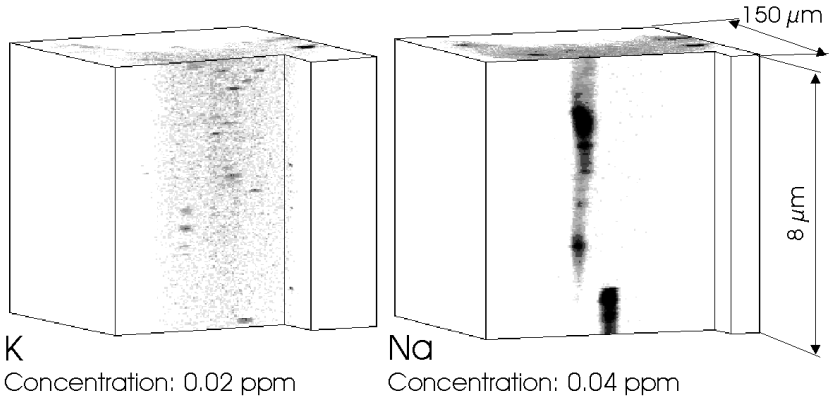

Fig. 3: 3D-distributions of K (left side) and Na (right side) in high purity molybdenum (6n purity). The K precipitates have diameters about 30 nm, the Na is concentrated in impurities with a diameter of about 1 µm.

The investigations indicates that the trace elements are concentrated in precipitates with diameters depending on the measured element. There is no correlation between the different species, this indicates that these elements are not present due to contamination during the production process.

3. Conclusion

Microelectronics is a continual challenge for modern material analysis. In many cases improvements of well established analytical methods, like SIMS, is necessary to obtain precise measurement results of the concentration of dopands and trace elements. This knowledge makes the development of new processes and materials possible.

References

[1] W. Jantsch, L. Palmetshofer: "Erbium Related Centres in Silicon", *Grundlagen und Technologic elektronischer Bauelemente*, Großarl 1995, ISBN 3-901578-01-3

[2] J. Kastner, H. Kuzmany, L. Palmetshofer, K. Piplits: "Formation of air stable buried K-fulleride layers by ion implantation", *Synthetic Metals* 70 (1995) 1469 – 1470

[3] L. Palmetshofer, M. Geretschläger, J. Kastner, H. Kutzmany, K. Piplits: "Characterization of K-fulleride layers formed by ion implantation", *J. Appl. Phys*. 77 (3), 1995

[4] H. Hutter, Ch. Brunner, St. Nikolov, Ch. Mittermayr, M. Grasserbauer: "Imaging surface spectrometry for two and three dimensional characterization of materials", *Fresenius J Anal Chem* (1996) 355:585 – 590

Project Information

Project Manager

Univ.-Ass. Dr. Herbert HUTTER

Institute of Analytical Chemistry, Vienna University of Technology, A-1040 Vienna,

Project Group

Last Name	First Name	Status	Remarks
Brunner	Christian	dissertation	
Fischer	Harald	diplom thesis	
Hutter	Herbert	Assistance Professor	
Piplits	Kurt	technician	partial GMe funding
Wolkenstein	Martin	dissertation	

Publications in Reviewed Journals

1. H. Hutter, C. Brunner, P. Wilhartitz, M. Grasserbauer: "Three Dimensional Characterization of Trace Element Distribution in High Purity Chromium", *Mikrochim. Acta* 122, 195 – 202 (1996)
2. H. Spicka, M. Griesser, H. Hutter, M. Grasserbauer, S. Bohr, R. Haubner, B. Lux, "Investigations of the Incorporation of B, P and N into CVD-Diamond Films by Secondary Ion Mass Spectrometry (SIMS)", *Diamond Related Mataterials* 5 (1996) 383 – 387
3. H. Hutter, Ch. Brunner, St. Nikolov, Ch. Mittermayr, M. Grasserbauer, "Imaging surface spectrometry for two and three dimensional characterization of materials", *Fresenius J Anal Chem* (1996) 355:585 – 590
4. S. Nikolov, H. Hutter, M. Grasserbauer, "De-noising of SIMS Images via Wavelet Shrinkage", *Chemometr. Intell. Lab. Syst*. 34 (1996) 263 – 273
5. Ch. Mittermayr, S. Nikolov, H. Hutter, M.Grasserbauer, "Wavelet Denoising of Gaussian Peaks: A Comparative Study", *Chemometr. Intell. Lab. Syst*. 34 (1996) 187 – 202

Presentations

1. H. Hutter, M. Wolkenstein, M. Grasserbauer, "Glättung analytischer Bilder mittels Waveletfilter", *AOFA 9*, 24 – 27 June 1996, Aachen, Germany

2. Ch. Brunner, H. Hutter, M. Grasserbauer, “Investigation of the synthesis of protective oxide layer on chromium with SIMS scanning techniques”, *AOFA 9*, 24 – 27 June 1996, Aachen, Germany
3. M. Wolkenstein, H. Hutter, M. Grasserbauer, “Improvement of Image Classification by Denoising”, *Chemometrics ´96*, September 9 – 11, 1996, Brno, Czech Republic
4. H. Hutter, M. Wolkenstein, M. Grasserbauer, “Wavelet Filtering for De-noising of Analytical Images”, *Euroanalysis IX*, September 3 – 7, 1996, Bologna, Italy
5. Ch. Brunner, H. Hutter, K. Piplits, P. Wilhartitz, R. Stroosnijder, M. Grasserbauer, “2D and 3D characterization of the trace element distribution by SIMS Imaging techniques”, *Euroanalysis IX*, September 3 – 7, 1996, Bologna, Italy

Cooperations

1. Institut für Experimentalphysik, Universität Linz, 1040 Linz, L. Palmetshofer
2. Insitut für Festkörperelektronik, TU Wien, 1040 Wien, G. Hobler
3. Institut für Allgemeine Elektrotechnik und Elektronik, TU Wien, 1040 Wien, F. Olcaytug
4. Metallwerk Plansee GmbH, 6600 Reutte Tirol, Dr. P. Wilhartitz

FTIR Measurements of the Hydrogen Concentration of SiN Layers

I. Jonak-Auer, R. Meisels, F. Kuchar

**Institute of Physics, University of Leoben,
A-8700 Leoben, Austria**

We report on new very accurate Fourier Transform Infrared (FTIR) measurements of the hydrogen content of amorphous silicon nitride (SiN) layers by evaluating the corresponding absorption lines with the help of polynomial fits. Our measurements show large differences in the hydrogen concentrations comparing layers which were deposited by plasma-enhanced chemical vapor deposition with layers deposited by thermal low-pressure chemical vapor deposition. The hydrogen content of the layers can be successfully reduced by applying various annealing procedures.

1. Introduction

Amorphous SiN layers are essential for the semiconductor industry as an encapsulant for silicon integrated circuits, as a diffusion barrier for H_2O and sodium ions [1], as passivation films, oxidation masks [2], gate insulators, and capacitor dielectrics [3]. Since the quality of SiN layers is highly dependent on the hydrogen content, the measurements we present are very important for the semiconductor industry. Hydrogen in SiN layers is chemically bound to Si and N, the source of hydrogen being the deposition reactants NH_3, SiH_4 and SiH_2Cl_2. If the hydrogen content in the layers is considerable, it will affect such properties as film structure, etch rate, stress and moisture permeability [4]. On the other hand, a certain amount of hydrogen in the films is desirable, because it reduces the trap density by passivating silicon dangling bonds which improves the device characteristics. Our measurements rely on the fact that the incoming IR radiation excites stretching vibrations of the Si-H and N-H bonds in the SiN layer, which leads to absorption lines in the MIR spectral region. The intensities of the absorption lines are directly related to the hydrogen content of the layer, thus providing a fast and non-destructive method of determining the hydrogen concentration. In this study we present a method of evaluating the N-H and Si-H absorption lines more accurately than it was possible up to now, we compare the hydrogen concentrations of SiN layers deposited by different processes and we also show how different annealing procedures influence the hydrogen concentration.

2. Experimental

Our experiments were performed using a Bruker Fourier Transform Spectrometer IFS 113v with a Globar source, a KBr beamsplitter and a DTGS detector. In order to determine the areas of the absorbance peaks as accurately as possible we first measure a transmission spectrum of the sample (SiN layer + Si substrate). To correct the data for errors due to the absorption of the Si substrate itself we subtract a transmission spectrum

of a pure Si wafer of the same thickness as the substrate of the coated wafer. From the resulting transmission spectrum the absorbance is calculated by:

$$\text{absorbance} = -\log(\text{transmission})$$

In contrast to commercially available FTIR software and recommended procedures in the literature [4], which in principle use linear baselines to evaluate the areas of the N-H and Si-H absorbance peaks at 3350 cm^{-1} and 2160 cm^{-1}, respectively, we do a polynomial fit of the spectral background outside the absorption lines. This yields a much higher accuracy in determining the areas of the absorbance peaks and therefore the hydrogen concentration. Both cases are illustrated in Fig. 1, which shows a Si-H absorbance line evaluated with the linear baseline method (a) and with a polynomial fit (b). While for the linear baseline method the areas are simply approximated by $(I-I')\cdot\Delta\nu$, we determine the areas between the absorbance line and the polynomial fit by integration. Comparisons between the two methods of evaluation yield differences of up to 30%.

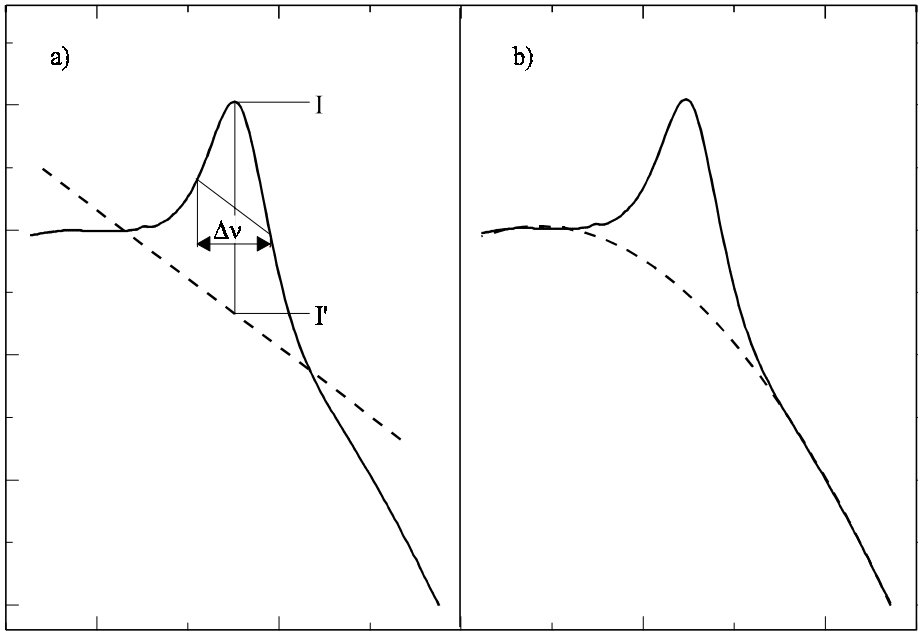

Fig. 1: a) Determination of absorbance area with the linear baseline method.
b) Determination of absorbance area with a polynomial fit.

In Fig. 2 the polynomial fit of Fig. 1 (b) is subtracted from the absorbance curve. The resultant line shape can very well be fitted by a Gaussian curve (dashed line), a fact which proves the high quality of the background fit.

SiN layers prepared both by plasma-enhanced chemical vapor deposition (PECVD) and thermal low-pressure chemical vapor deposition (LPCVD) with thicknesses between 1.5 μm and 10 nm were studied. For the thermally deposited SiN layers we also studied the influence of oxygen and nitrogen annealing procedures on the hydrogen concentration. Especially for the thinner thermal layers high intensity-resolution and stability of the measurement are essential since typical absorbance values correspond to changes in transmission of down to only 0.01%. Since absorptions due to CO_2 and water-vapor in the air also occur in the same spectral regions as the Si-H and N-H absorption lines, thorough evacuation of the spectrometer is essential for obtaining correct results.

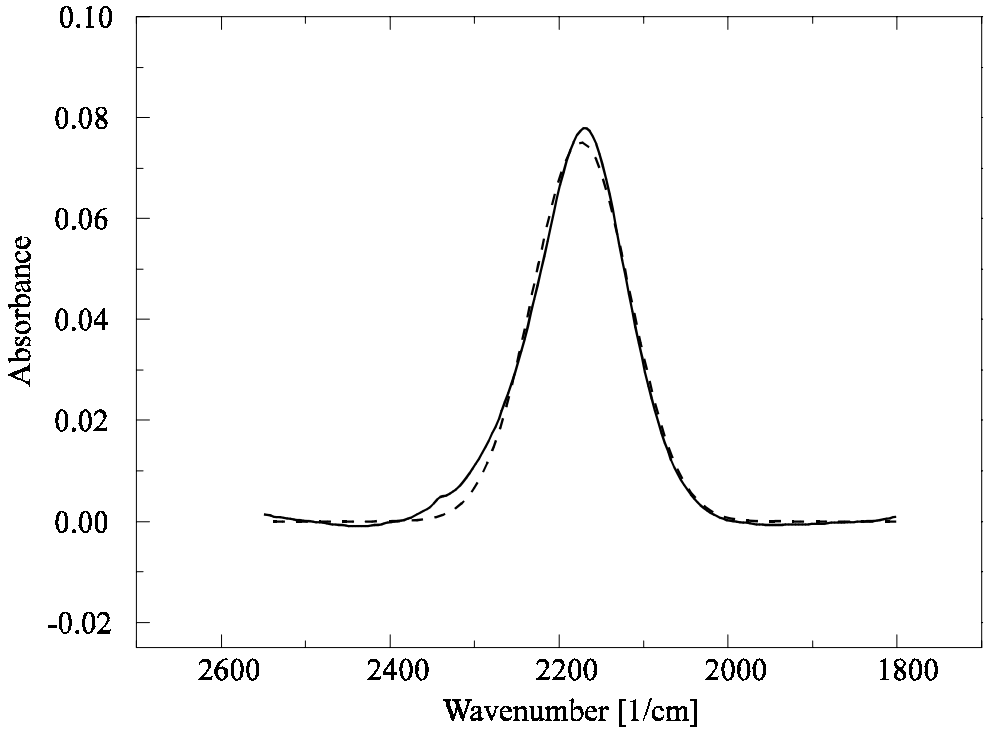

Fig. 2: Polynomial fit subtracted from absorbance curve (solid line) and appropriate Gaussian fit (dashed line).

In order to quantitatively determine the hydrogen concentration of SiN layers by FTIR it is necessary to have calibration factors which allow the conversion between the intensity of the absorption lines and the hydrogen concentration. One method of quantitative hydrogen concentration determination [4] is the resonant nuclear reaction

$$H + {}^{15}N \rightarrow {}^{12}C + {}^{4}He + \gamma.$$

A beam of accelerated $^{15}N^{++}$ ions impinges upon the SiN film and penetrates completely through to the Si substrate. There is appreciable probability for reaction only at the precise energy of 6.385 MeV. Thus, if the sample is bombarded with ions at this energy, the number of γ rays measured to come from the sample is proportional to the hydrogen concentration at the film surface. By increasing the energy of the ions a concentration profile of hydrogen versus depth can be determined and therefore the total hydrogen concentration can be measured. The total hydrogen concentration must then be apportioned properly between the Si-H and N-H bands which show different absorptivities (absorption per bond). The resulting equations, which relate the number of N-H and Si-H bonds per cm^2 to the areas of the N-H and Si-H absorbance lines, respectively, are [5]:

$$\frac{N-H}{cm^2} = \frac{Area_{N-H}}{5.3_x 10^{-18}} \qquad \text{and} \qquad \frac{Si-H}{cm^2} = \frac{Area_{Si-H}}{7.4_x 10^{-18}}$$

3. Conclusion

The total hydrogen concentration in our PECVD layers varies between $1.3 \cdot 10^{22}$ and $2.0 \cdot 10^{22}$ cm^{-3}, whereas the hydrogen concentration in the thermal LPCVD layers is much smaller and lies between $4.5 \cdot 10^{20}$ and $5.5 \cdot 10^{21}$ cm^{-3}. In PECVD layers the number of N-H bonds per cm^3 varies between $5.9 \cdot 10^{21}$ and $7.6 \cdot 10^{21}$, while the number of Si-H bonds per cm^3 is higher, namely between $5.8 \cdot 10^{21}$ and $1.4 \cdot 10^{22}$ .Thermal LPCVD layers on the other hand contain more N-H bonds than Si-H bonds: the number of N-H bonds per cm^3 varies between $4.5 \cdot 10^{20}$ and $5.8 \cdot 10^{21}$, the number of Si-H bonds is approximately an order of magnitude smaller than that of N-H bonds, but the Si-H lines are too weak to allow a reliable quantitative evaluation. The effects of different annealing procedures of thermal LPCVD layers on the hydrogen concentration are shown in Fig. 3: Oxygen annealing reduces the hydrogen concentration more than nitrogen annealing, the hydrogen concentration decreases from $5.9 \cdot 10^{21}$ cm^{-3} for the untreated layer to $1.0 \cdot 10^{21}$ cm^{-3} for the nitrogen annealed layer to $4.5 \cdot 10^{20}$ cm^{-3} for the oxygen annealed layer. With the presented FTIR method hydrogen concentrations of down to approximately $2 \cdot 10^{20}$ cm^{-3} can be measured if the layer thickness is about 100 nm. For very thin layers of the order of 10 nm the detection limit is somewhat higher and lies at approximately $1 \cdot 10^{21}$ cm^{-3}.

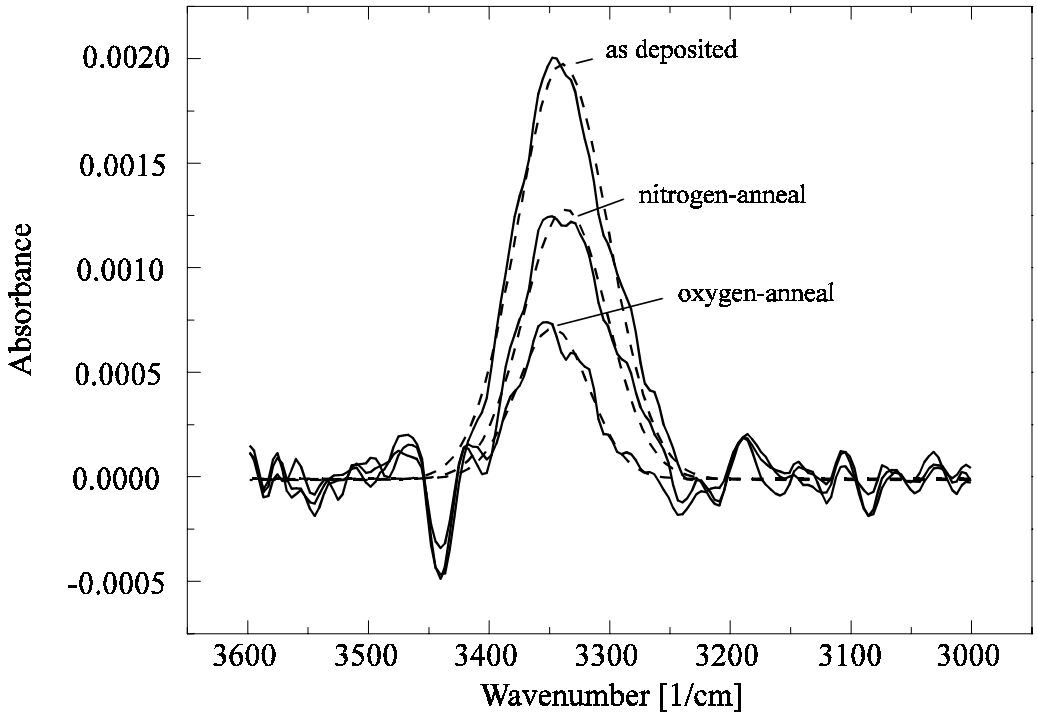

Fig. 3: Dependence of N-H absorbance lines (polynomial fits are already subtracted) on different annealing procedures for three samples (solid lines) and appropriate Gaussian fits (dashed lines).

Acknowledgments

Financial support for this work came from the *Steiermärkische Wissenschafts- und Forschungslandesfonds*, GZ AAW-12Ku24-93. All samples were prepared by *Austria Mikro Systeme International AG*.

References

[1] T.L. Chu: "Dielectric Materials in Semiconductor Devices", *J. Vac. Sci. Technol.,* Vol. 6, 1970, pp. 25 – 33.

[2] C.R.M. Grovenor, *Microelectronic Materials*, IOP Publishing Ltd., 1989, ISBN 0-85274-270-3.

[3] M. Ino, N. Inoue and M. Yoshimaru: "Silicon Nitride Thin-Film Deposition by LPCVD with In Situ Vapor Cleaning and its Application to Stacked DRAM Capacitor Fabrication", *IEEE Transaction on Electron Devices*, Vol 41, 1994, pp. 703 – 708.)

[4] W.A. Lanford and M.J. Rand: "The hydrogen content of plasma-deposited silicon nitride", *J. Electrochem. Soc*., Vol. 49, 1978, pp. 2473 – 2477.

[5] W.R. Knolle: "Characterization of Plasma-Deposited SiN", *Report AT&T Bell Laboratories*, Reading Pennsylvania 19607, unpublished.

Project Information

Project Manager

Univ.-Prof. Dr. Friedemar KUCHAR

Institut für Physik, Montanuniversität Leoben, A-8700 Leoben

Project Group

Last Name	First Name	Status	Remarks
Gold	Herbert	dissertation	
Jonak-Auer	Ingrid	dissertation	
Kuchar	Friedemar	university professor	
Lutz	Josef	assistant professor	

Publications in Reviewed Journals

1. I. Jonak-Auer, R. Meisels, F. Kuchar, B.D. McCombe, E. Elcess, C. Fonstad, "Magnetic field induced carrier-type inversion in an InGaAs/GaAs superlattice studied by cyclotron resonance", *Proc. of XXIII ICPS*, 21. - 26. 7. 1996, Berlin, Germany, World Scientific, pp. 2227 – 2230
2. I. Jonak-Auer, R. Meisels, F. Kuchar, "Determination of the hydrogen concentration of silicon nitride layers by fourier transform infrared spectroscopy", *Infrared Physics and Technology*, in print, 1997
3. I. Jonak-Auer, R. Meisels, F. Kuchar, "Fourier transform spectroscopy of silicon nitride layers: hydrogen concentration and thickness measurements", *Proc. of the 10th International Conference on Fourier Transform Spectroscopy*, 27. 8. – 1. 9. 1995, Budapest, Hungary, *Microchimica Acta*, in print
4. A. Pleschinger, J. Lutz, F. Kuchar, H. Noll, M. Pippan, "A structural and topographical study of low-pressure chemical-vapor-deposited polysilicon by scanning probe microscopy", *J. Appl. Phys*., in print, May 1997
5. A. Pleschinger, J. Lutz, F. Kuchar, H. Noll, M. Pippan, "A study of polycristalline and amorphous LPCVD-silicon films by atomic force microscopy", *Proc. of SXM2*, 16. - 18. 9. 1996, TU-Wien, Austria, *Surface and Interface Analysis*, in print

Presentations

1. A. Pleschinger, J. Lutz, F. Kuchar, H. Noll, M. Pippan, "A study of polycristalline and amorphous LPCVD-silicon films by atomic force microscopy", *SXM2 Workshop über methodische Entwicklungen und der industrielle Anwendungen der Nahfeld-Rastersondentechniken*, 16 – 18 September 1996, TU Wien, Austria

2. A. Pleschinger, J. Lutz, F. Kuchar, H. Noll, M. Pippan, “SPM-Untersuchungen von LPCVD-Polysilizium”, *Tagung der Österreichischen Physikalischen Gesellschaft*, 23 – 27 September1996, Universität Linz, Austria

3. I. Jonak-Auer, R. Meisels, F. Kuchar, B.D. McCombe, E. Elcess, C. Fonstad, “Magnetic field induced carrier-type inversion in an InGaAs/GaAs superlattice studied by cyclotron resonance”, *XXIII ICPS*, 21 – 26 July 1996, Berlin, Germany

Doctor’s Theses

1. I. Jonak-Auer, “Fourier-Spektroskopie an Halbleitermaterialien”, University of Leoben, Institute of Physics, 1996.

Cooperations

1. Austria Mikro Systeme International AG, Unterpremstätten, Dr. Noll

Pattern Transfer of Nanostructures

G. Stangl, P. Hudek[1], P. Hrkut[1], K. Riedling, W. Fallmann

**Institut für Allgemeine Elektrotechnik und Elektronik,
TU Wien, A-1040 Vienna, Austria**

The target of the investigations reported here was the patterning of relatively thick layers of sputtered carbon down to sub-µm structures by means of anisotropic reactive ion plasma etching. A process could be successfully developed which permits the preparation of carbon structures with an aspect ratio in excess of 1:4, using a thin poly-silicon layer as an etching mask.

1. Introduction

Thin layers of carbon exhibit a broad range of electrical and mechanical properties, depending on the processes used for their deposition. Their electrical resistivity may range between insulating and fairly well-conductive, and their hardness may lie anywhere between the hardnesses of graphite and diamond. Carbon films are chemically inert and therefore an excellent protective layer for surfaces that are subject to a corrosive environment or that must be biocompatible. All these properties make them an interesting material not only for sensors and related applications but also for a variety of purposes in some technological and micromachining processes. However, the preparation of small structures, particularly in thick carbon films, is not trivial: Wet-chemical techniques fail due to the chemical inertness of the carbon films, and the classic lift-off technique is hardly suitable for film thicknesses of the order of 1 µm or more. Therefore, plasma etching constitutes the only feasible ablative patterning method.

An obvious etching agent for carbon layers is oxygen plasma since the reaction products are gaseous and volatile; no re-deposition of etched material may therefore occur. However, conventional resist materials are subject to an etch rate in oxygen plasma that is by far greater than the etch rate of a dense carbon film. This prevents the preparation of structures with a high aspect ratio because it would require a resist thickness that significantly exceeds the thickness of the carbon film and therefore impedes the preparation of narrow lines. Hence, it is necessary to use a masking material for the etching process that is not or not significantly affected by the oxygen plasma.

An attractive candidate for such a masking material is poly-silicon. Although it is also oxidized by the oxygen plasma its masking properties do not deteriorate due to the oxidation because the oxygen plasma hardly attacks silicon dioxide. Patterning by reactive ion etching a thick carbon film down to sub-µm dimensions requires therefore a three-step approach: (1) Deposition of a poly-silicon layer atop of the carbon film; (2) structuring of the poly-silicon layer by a suitable lithographic process; and (3) transfer of the structures in the poly-silicon layer into the carbon film by reactive ion etching.

[1] Academy of Sciences, SK-84237 Bratislava, Slovakia

2. Experimental

The carbon films that were subjected to our etching experiments were generally very dense, electrically well conducting layers with thicknesses of 1 – 2 µm; they were prepared by means of RF sputtering at the Academy of Sciences in Bratislava. Conventional silicon wafers served as substrates. The poly-silicon etching mask film was also deposited by RF sputtering; a thickness of 0.2 µm proved to be sufficient for withstanding the etching of a 2 µm carbon layer. The poly-silicon mask was structured with a lift-off technique; the resist patterns were defined by E-beam lithography. The subsequent carbon etching took place in a Perkin-Elmer ECR-RIE-4000 plasma etcher at the *Institut für Allgemeine Elektrotechnik und Elektronik* in Vienna, using pure oxygen as an etching agent. In some experiments, the poly-silicon mask layer was subsequently removed in the same vacuum process by etching with $CF_4 + SF_6$ (Fig. 1).

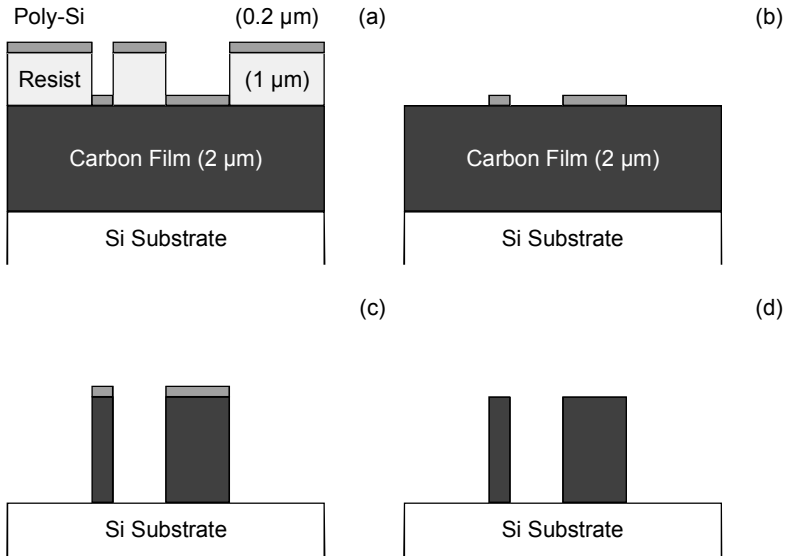

Fig. 1: Structuring of carbon films: (a) after deposition of the poly-Si mask layer; (b) after lift-off; (c) after anisotropic RIE-etching of the carbon film; (d) after removal of the poly-Si mask layer.

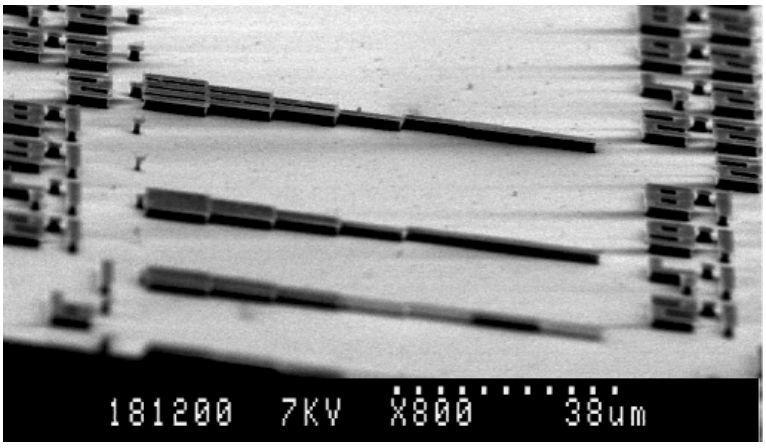

Fig. 2: Etched carbon structures on a silicon substrate.

By a proper choice of the process parameters, very steep sidewalls of the carbon structures could be obtained, with only a slight intentional underetching whose extent could be adjusted with the process parameters (Figs. 2 and 3).

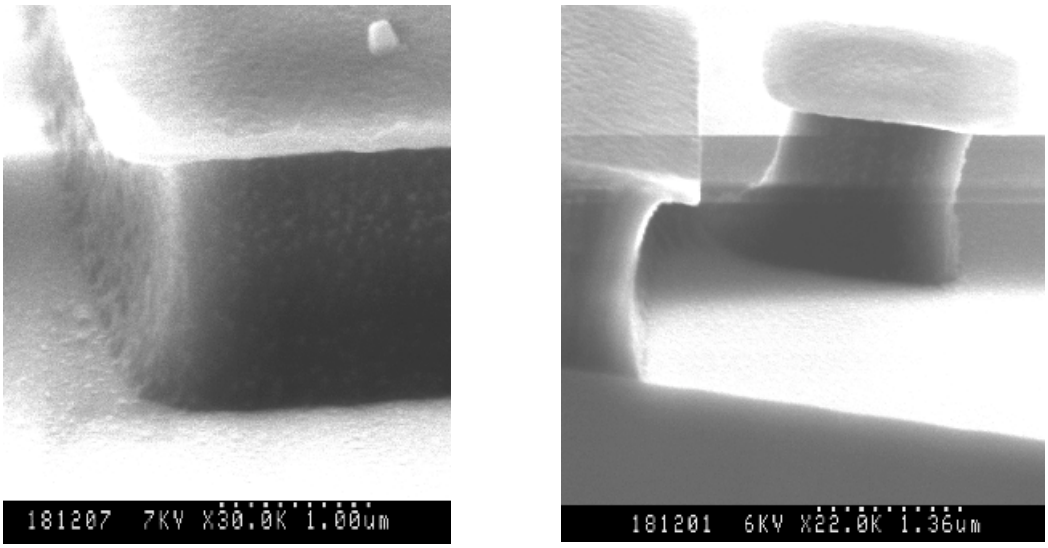

Fig. 3: Etched carbon structures with the poly-Si mask layer still on top.

Further optimization of the process permitted the preparation of structures with an exceedingly high aspect ratio, virtually vertical sidewalls, and a lateral resolution down to 0.2 µm or less (Fig. 4).

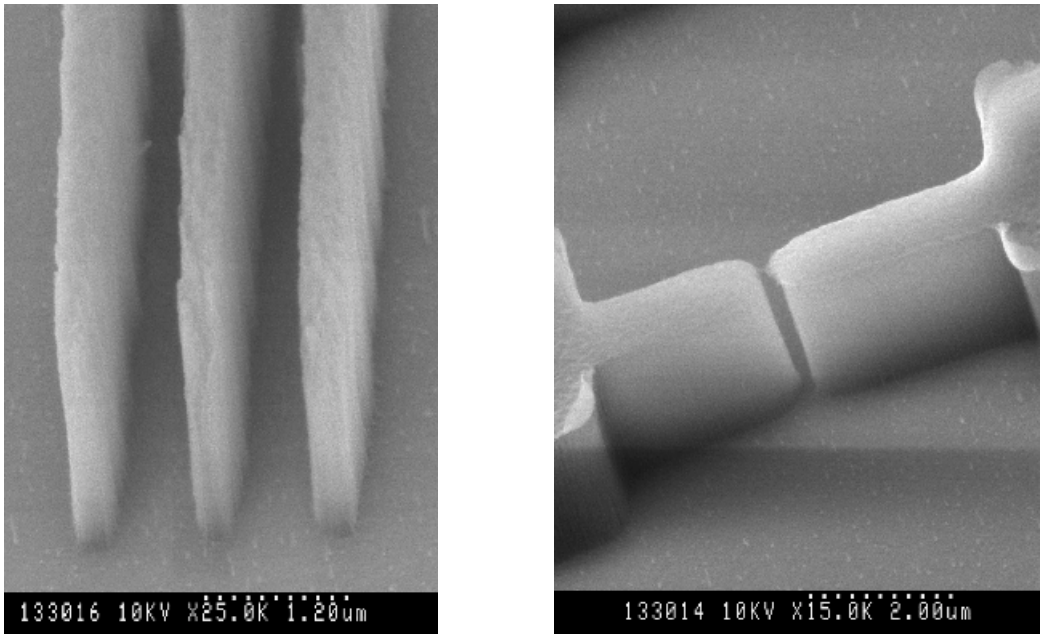

Fig. 4: High aspect ratio carbon structures after the removal of the poly-Si mask layer.

3. Conclusion

Our investigations show that sputtered carbon layers with thicknesses of several micrometers may be patterned down to a few tenths of a micrometer by reactive ion etching using a poly-silicon etching mask. The ratio between anisotropic and isotropic etching can be varied over a broad range by a variation of the process parameters. It is therefore possible to obtain a practically totally anisotropic etching behavior and very steep structures with an aspect ratio of up to 1:20. This permits the preparation of sub-µm carbon structures for a variety of electronic and micromechanical devices.

It should be noted that the deposition of the carbon films is crucial for the entire process: Special sputtering techniques are required to reduce the stress in the deposited layers that otherwise would lead to fractured edges of the etched structures and to the formation of residues where the film ought to be removed. Without stress reducing processing, such effects occur at or above a carbon film thickness of 1 µm. The deposition process developed at the Academy of Sciences in Bratislava currently guarantees stress-free deposition of 4 µm thick carbon films; it is planned to extend the feasible carbon film thickness range to 10 µm.

Acknowledgments

In addition to the Society for Microelectronics, the *Ost-West-Fonds* (project OWP 92) financially contributed to this work.

Project Information

Project Manager

Univ.-Doz. Dr. Karl RIEDLING

Institut für Allgemeine Elektrotechnik und Elektronik, TU Wien, A-1040 Vienna

Project Group

Last Name	First Name	Status	Remarks
Fallmann	Wolfgang	university professor	
Riedling	Karl	associate professor	
Schalko	Johannes	dissertation	partial GMe funding
Stangl	Günther	technician	

Publications in Reviewed Journals

1. D. Pum, G. Stangl, C. Sponer, K. Riedling, P. Hudek, W. Fallmann, U.B. Sleytr: "Patterning of Monolayers of Crystalline S-layer Proteins on a Silicon Surface by Deep Ultraviolet Radiation", Micro- and Nanoengineering 35, 1997, pp. 297 – 300.
2. D. Pum, G. Stangl, C. Sponer, W. Fallmann, U.B. Sleytr: "Deep Ultraviolet Patterning of Monolayers of Crystalline S-layer Protein on Silicon Surfaces", Colloides and Surfaces B: Biointerfaces, in print.
3. P. Hudek, W. Rangelow, I. Kostic, G. Stangl, Z. Borkowicz, R. Linnemann, L. Hadjiiski, T. Gotszalk: "Submicro- and Nanometer Structure Fabrication Using Direct Electron-Beam Writing and Reactive Ion Etching", Electron Technology, 28, 4, 1996, pp. 251 – 258.

Presentations

1. G. Stangl, D. Pum, C. Sponer, K. Riedling, W. Fallmann, P. Hudek, U.B. Sleytr: "Crystalline S-layer Protein as Resist Material on Silicon Surfaces, Patterned by DUV-Excimer-Laser-Radiation", ASDAM 96 (Advanced Semiconductor Devices and Microsystems), Smolenice Castle, Slovakia, October 1996.

Doctor's Theses

1. E. Cekan: "Ionen-Projektions-Lithographie: Aufbau, Anwendungstests und grundlegende Untersuchungen", TU Wien, 1996.

Cooperations

1. Academy of Sciences, Bratislava: Dr. P. Hudek
2. Fraunhofer Institut für Mikrostrukturierung, Berlin
3. IMS — Ionen Mikrofabrikations Systeme GmbH, Vienna: Dr. H. Löschner
4. ÖFZS Seibersdorf: Prof. Dr. Rüdenauer
5. Technics-Plasma, Munich
6. Shipley
7. DuPont, Frankfurt
8. Kalle-Höchst, Frankfurt

Recent Developments in Femtosecond Technology

M. Lenzner, S. Sartania, Z. Cheng, L. Xu, A. Poppe, Ch. Spielmann, F. Krausz, I.T. Sorokina, E. Sorokin, E. Wintner

Institut für Allgemeine Elektrotechnik und Elektronik, TU Wien, A-1040 Vienna, Austria

The availability of ultrabroad-band sub-10 fs optical pulses from Ti:sapphire laser oscillators allows 0.1 TW-scale pulse generation from compact kHz-rate amplifiers. The amplified sub-20 fs pulses can be compressed below 5 fs using novel techniques for self-phase modulation and dispersive compression. The resultant high-power light pulses comprising less than two oscillation cycles within their intensity-FWHM open up new possibilities in strong-field physics including the study of reversible nonlinear optical processes in solids beyond the 10^{14} W/cm^2 intensity level.

Despite the unmatched results in extreme ultrashort pulse generation with Ti:sapphire since a few years alternative laser materials are under investigation in order to achieve an all-solid-state laser design. The generation of 14 fs pulses from a KLM-modelocked Cr:LiSAF (60 mW average output power) and a similar Cr:LiSGaF laser (100 mW) is reported representing the shortest femtosecond pulses with the highest average power ever produced out of Cr-doped colquiriite laser crystal oscillators.

1. Introduction

The development of novel broadband solid-state laser materials along with concomitant advances in ultrafast all-optical amplitude modulation techniques has resulted in the emergence of a new generation of femtosecond sources over the last few years. Titanium-doped sapphire has been the most successful gain medium among a number of vibronic solid-state laser materials because of its broad bandwidth (approximately 200 nm FWHM centered at 800 nm) and excellent mechanical and thermal characteristics [1]. The discovery of Kerr-lens mode locking (KLM) [2] and novel means of intracavity dispersion control [3] have opened the way to an efficient exploitation of the enormous optical bandwidth of Ti:sapphire for ultrashort pulse generation.

Soon after the first dispersion-controlled KLM Ti:sapphire lasers had been put into operation it was recognized that system performance critically depends on the bandwidth $\Delta\nu_{GDD}$ over which the overall (negative) cavity group delay dispersion (GDD) is approximately constant [4], [5]. This finding led to the development of Ti:sappire oscillators using fused silica prisms [6] introducing the lowest cubic phase dispersion and allowing sechant-hyperbolic-shaped pulses down to 15 fs in duration. Further pulse shortening could be made possible by employing aperiodic (chirped) multilayer dielectric mirrors for intracavity dispersion control [3]. Specifically designed chirped mirrors have been capable of introducing a nearly constant negative GDD over a wavelength range significantly exceeding the largest $\Delta\nu_{GDD}$ achievable with prisms. As a result, mirror-dispersion-controlled (MDC) Ti:sapphire lasers can produce high-quality nearly-transform-limited pulses down to 7.5 fs in duration [7] (Fig. 1). The spectrum of these

pulses can be centered at 790 nm with a time-bandwidth product of ≈0,4. The use of dispersion engineered mirrors instead of prisms for GDD control also improves compactness and the reproducibility of system performance. This is because in MDC systems the net intracavity GDD (and hence pulse duration) is insensitive to resonator alignment, in strong contrast to prism-controlled systems.

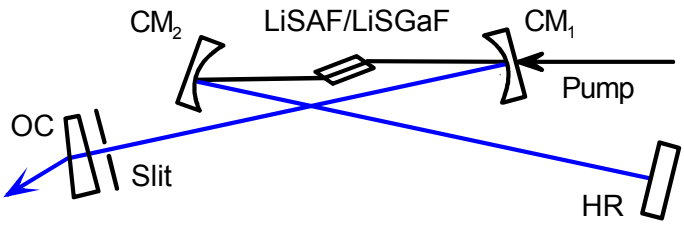

Fig. 1: Typical setup of a MDC femtosecond oscillator

When pursuing the ultimate goal of a really compact all-solid-state femtosecond laser system direct diode pumping of the laser material is a challenge. Thus, during the last years several Cr-doped colquiriite crystals like LiCAF, LiSAF, LiSGaF and others being known already since longer time [8], [9] have invoked new interest because of the availability of new red (670 nm) high power (~500 mW) laser diodes. The insights of optimum laser resonator design for the Ti:sapphire laser have been transferred successfully to the Cr-doped lasers by a number of authors [10] – [13] yielding so far only pulses in the 40-fs region as long as usable average output power is considered to be an essential feature (>50 mW).

Chirped mirrors as they have been developed for the Ti:sapphire laser proved to be too lossy for resonators containing the lower gain Cr-doped media. Hence, dielectric Gires-Tournois mirrors (GTM) have been developed causing lower losses due to a smaller penetration depth of the radiation within the structure. Their GDD is relatively high and adjustable but highly nonlinear hardly allowing to break the 40-fs pulse limit. Only recently, new dielectric materials and further optimized layer sequences allowed to create chirped mirrors which could be employed as straightforward as in the Ti:sapphire lasers [14] yielding pulse durations in the sub-20 fs regime at reasonable average powers as it will be reported later in more detail.

The present sub-10 fs MDC-KLM Ti:sapphire oscillators are ideally suited for seeding high-power femtosecond amplifier systems. The extremely broad bandwidth (≈120 nm) of the emitted sub-10 fs pulses centered at the gain peak of Ti:sapphire allows the implementation of chirped-pulse amplification (CPA) in a fairly simple and compact system. This is because, due to their ultrabroad bandwidth, the seed pulses can be substantially broadened by introducing a relatively small amount of GDD. In fact, the pulse duration increases to several picoseconds upon passage through the usual system components used for isolation and pulse selection. Additional broadening up to tens of picoseconds can be readily induced by introducing a piece of highly dispersive SF57 glass (Schott) without adding notable complexity. In the following, it will be depicted how 5 fs pulses could be generated by further amplification and an optimized pulse compression technique.

2. Sub-TW Pulse Generation

The pulse energy can be boosted beyond the millijoule level in a single-stage 8-pass "bow-tie" amplifier without excessive nonlinearities emerging in the amplifier crystal. Owing to the moderate amount of positive GDD to be compensated for, pulse recompression following amplification by a simple and high-throughput (≈80 %) double-prism sequence. The residual high-order phase dispersion of the system (up to fourth order) is eliminated by specially designed chirped mirrors. The absence of an extra pulse stretcher and lossy diffraction gratings significantly reduces system complexity and (indirectly) gain narrowing, respectively, as compared to conventional CPA systems. The described system currently produces 20 fs pulses beyond the millijoule level at a repetition rate of 1 kHz [15]. This performance comes in combination with excellent stability, pulse energy fluctuations are less than $\pm$3 %.

The high-power 20 fs pulses can be uniformly self-phase modulated across the beam profile in a microcapillary filled with some noble gas, as recently proposed and demonstrated (with 140 fs seed pulses) by M. Nisoli, S. DeSilvestri, and O. Svelto [16]. Suitable choice of the nonlinear medium (Kr, Ar, Ne, etc.), the channel diameter of the fused silica capillary, the length of the hollow waveguide, and the pressure of the noble gas allows controlling spectral broadening and the output beam profile. The pulses exiting the waveguide are propagated through an ultrabroad-band high-throughput dispersive system providing nearly optimum chirp compensation over the wavelength range of 650 – 950 nm [17]. Key components of the dispersive delay line include AR-coated thin fused silica wedged plates and chirped mirrors designed and manufactured by R. Szipöcs and K. Ferencz at the Research Institute for Solid State Physics in Budapest (Hungary). This compressor currently delivers 0.25 mJ, 5 fs pulses, which are focusable to intensities beyond 10^{17} W/cm^2 representing the world's shortest optical pulses.

The entire setup consisting of the MDC oscillator, multipass amplifier, recompression stage, and pump sources occupies an area of approximately 2 m^2 on the optical table. This compactness combined with the ruggedness and reliability of solid-state components make this system a versatile tool for a broad range of experiments in nonlinear optics and related fields. Furthermore, the unique performance described above holds out the promise of pushing the limits of nonlinear optics.

3. Prismless Cr:LiSAF and Cr:LiSGaF Lasers

It was a great challenge to improve the technology of dielectric chirped mirrors so as to make them suitable for LiSAF and LiSGaF lasers. New types of low loss chirped mirrors have been developed at the above mentioned Solid-State Physics Institute, Budapest, involving new dielectric layer materials with different steps of the index of refraction. New algorithms allowed further optimization of the dispersion properties, both aspects currently being filed for patent.

In this paper, we report the shortest, to our knowledge, pulses obtained in MDC-modelocked Cr:LiSAF and Cr:LiSGaF lasers of a duration of 14 fs at the substantial output power for Cr-lasers of 100 mW at 1.6 W incident 647 nm power.

Having optimized the net intracavity GDD by taking the measured dispersion data for LiSAF and LiSGaF crystals into account, a most simple and compact resonator design has been realized. The cavity is a standard X-cavity, consisting of only two curved (R =

100 mm) dispersive mirrors, the active medium, a high reflector end mirror and an output coupler varying from 0.4 to 2.3 %. The Cr:LiSAF crystal used had a length of 2.8 mm and 0.8 % Cr content, the Cr:LiSGaF crystal was 4 mm long with 0.75 % of Cr. The implemented dispersive mirrors exhibited a maximum GDD of ≈80 fs^2 (Fig. 2).

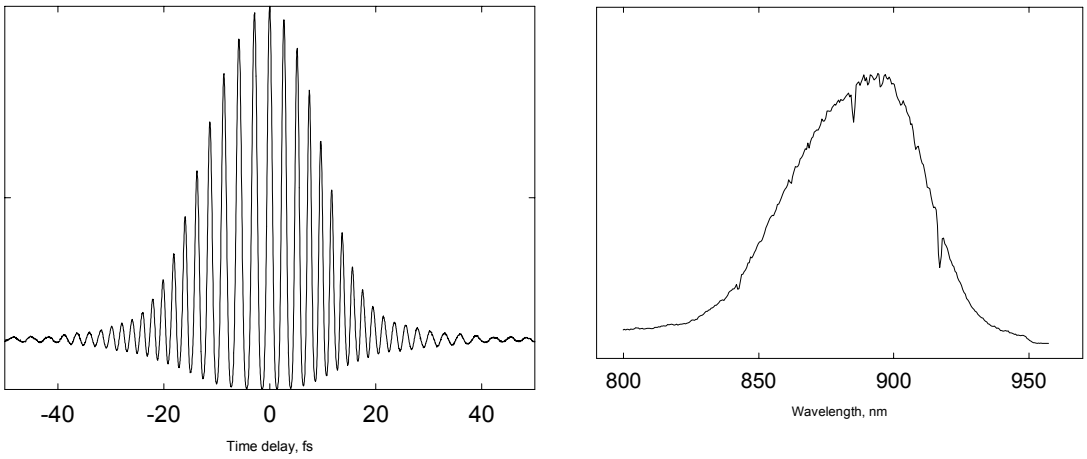

Fig. 2: Interferometric autocorrelation trace and spectrum of the shortest pulses out of a Cr-doped laser

The autocorrelation trace and the measured spectrum of the mode-locked laser pulses centered around λ = 880 nm and having a bandwidth FWHM of 70 nm allow to calculate a duration of 14 fs and a time-bandwidth product $\Delta\tau\Delta\nu$ = 0.32 using a $sech^2$ pulse shape fit indicating nearly transform limited pulse quality.

As a next step efficient diode pumping of this oscillator will be realized involving at least 4 of the presently available moderate power AlGaInAs array diodes emitting ~500 mW. After this is realized the Cr-doped colquiriite laser could be an interesting more compact alternative for some applications to the well established Ti:sappire femtosecond laser oscillator.

4. Conclusion

In conclusion, we demonstrated the first successful realization of 5 fs (< 2 optical cycles) laser pulses of 0.25 mJ energy via compression of amplified pulses originating from a MDC Ti:sappire oscillator and being self-phase modulated in a microcapillary. These pulses are focusable to intensities beyond 10^{17} W/m^2 and may be capable of pushing the current limit of coherent X-ray generation by laboratory scale experiments to shorter wavelengths than 6 nm reaching the important water window.

Furthermore, we showed what is to our knowledge the first generation of nearly transform-limited 14 fs pulses from prismless KLM Cr:LiSAF and Cr:LiSGaF lasers having average powers of up to 100 mW. The laser setup is characterized by extreme compactness, comprising only two dispersive mirrors, replacing conventional cavity mirrors, giving rise to high stability of the mode-locked operation.

Acknowledgment

This work was a joint project of two groups (F. Krausz and E. Wintner) at the above mentioned institute supported by the Austrian National Science Foundation Projects P 10409 and P 10733, the Austrian National Bank Projects No 6026 and 5847, and by the Gesellschaft für Mikroelektronik.

The 5 fs compression experiment has been performed in collaboration with M. Nisoli, S. DeSilvestri and O. Svelto from the Politechnico Milano (Italy). The cooperation with R. Szipöcs and K. Ferencz from the Research Institute for Solid-State Physics in Budapest (Hungary) for the development of the different versions of chirped mirrors is gratefully acknowledged. We also would like to thank the suppliers of the LiSAF and LiSGaF crystals, A. Cassanho of VLOC, Tarpon Springs, and H.P. Jenssen, University of Central Florida, Orlando, Florida for their support.

References

[1] P.F. Moulton: "Spectroscopic and laser characteristics of Ti:Al_2O_3", *J. Opt. Soc. Am.*, Vol. B4, pp 125 – 133, 1986.

[2] D.E. Spence, P.N. Kean and W. Sibbett: "60-fsec pulse generation from a self-mode-locked Ti:sapphire laser", *Opt. Lett.*, Vol. 16, pp 42 – 44, 1991.

[3] R. Szipöcs, K. Ferencz, Ch. Spielmann and F. Krausz: "Chirped multilayer coatings for broadband dispersion control in femtosecond lasers", *Opt. Lett*., Vol. 19, pp 201 – 203, 1994.

[4] C.P. Huang, H.C. Kapteyn, J.W. McIntosh, M.M. Murnane: "Generation of transform limited 32 fs pulses from a self-mode-locked Ti:sapphire laser", *Opt. Lett.*, Vol 17, pp 139 – 141, 1992

[5] F. Krausz, Ch. Spielmann, T. Brabec, E. Wintner, and A.J. Schmidt: "Generation of 33-fs optical pulses from a solid-state laser", *Opt. Lett.*, Vol 17, pp 204 – 206, 1992.

[6] Ch. Spielmann, P.F. Curley, T. Brabec, E. Wintner, and F. Krausz: "Generation of sub 20-fs mode locked pulses from a Ti:sapphire laser", *Electron. Lett.*, Vol. 28, pp 1532 – 1534, 1992.

[7] L. Xu, Ch. Spielmann, F. Krausz, and R. Szipöcs: "Ultrabroadband ring oscillator for sub-10 fs pulse generation", *Opt. Lett.*, Vol 21, pp 1259 – 1261, 1996.

[8] S.A. Payne, L.L. Chase, H.W. Newkirk, L.K. Smith, and W. Krupke: "LiCaAlF6:Cr3+: A promising new solid-state laser material", *IEEE J. Quantum Electron.*, Vol. 24, 2243 – 2252, 1988.

[9] L.K. Smith, S.A. Payne, W.L. Kway, and B.H.T. Chai: "Investigation of laser properties of Cr3+:LiSrGaF6", *IEEE J. Quantum Electron.*, Vol. 28, pp 2612 – 2618, 1992.

[10] M.J.P. Dymott and A.P. Ferguson:"Self-mode locked diode-pumped Cr:LiSAF laser producing 34-fs pulses at 42 mW average power", *Opt. Lett.*, Vol. 20, pp 1157 – 1159, 1995.

[11] D. Kopf, K.J. Weingarten, L.R. Brovelli, M. Kamp, and U. Keller: "Sub-50-fs diode-pumped mode-locked Cr:LiSgAf with an A-FPSA", *CLEO Techn. Digest* OSA, Vol. 8, p252, Washington D.C. 1995.

[12] I.T. Sorokina, E. Sorokin, E. Wintner, A. Cassanho, H.P. Jenssen, and R. Szipöcs: "47 fs pulse generation from a prismless self-mode-locked Cr:LiSGaF laser", *OSA Trends in Opt. and Photonics*, Eds. S.A. Payne, C.A. Pollock, Vol. 1, pp 258 – 260, 1996 (ASSL San Francisco).

[13] I.T. Sorokina, E. Sorokin, E. Wintner, A. Cassanho, H.P. Jenssen, and R. Szipöcs: "Prismless passively mode-locked femtosecond Cr:LiSGaF laser", *Opt. Lett*., Vol 21, pp 1165 – 1167, 1996.

[14] I.T. Sorokina, E. Sorokin, E. Wintner, A. Cassanho, H.P. Jenssen, and R. Szipöcs: "Femtosecond pulse generation from the novel low-loss chirped-mirror dispersion controlled Cr:LiSAF and Cr:LiSGaF lasers", *Technical Digest Advanced Solid-State Lasers Conference Orlando 1997*, OSA, paper MF2-1, p 129.

[15] A predecessor of this system has been reported by M. Lenzer, Ch. Spielmann, E. Wintner, F. Krausz, and A.J. Schmidt: "Sub-20-fs, kHz-repetition-rate Ti:sapphire amplifier", *Opt. Lett.*, Vol. 20, p. 1397 – 1399, 1995.

[16] M. Nisoli, S. De Silvestri, and O. Svelto: "Generation of high energy 10 fs pulses by a new pulse compression technique", *Appl. Phys. Lett*., Vol. 68, pp. 2793 – 2796, 1996.

[17] M. Nisoli, S. De Silvestri, O. Svelto, R. Szipöcs, K. Ferencz, Ch. Spielmann, S. Sartania and F. Krausz: "Compression of high-energy laser pulses below 5 fs.", *Opt. Lett.*, Vol. 22, accepted for publication.

Project Information

Project Manager

a.o. Prof. Dr. Ernst WINTNER

Institut für Allgemeine Elektrotechnik und Elektronik, TU Wien, A-1040 Vienna

Project Group

Last Name	First Name	Status	Remarks
Cheng	Zhou	dissertation	
Krausz	Ferenc	associate professor	
Lenzner	Mathias	postdoc	
Lin	Chang	dissertation	
Poppe	Andreas	dissertation	
Sorokin	Eugenii	postdoc	
Spielmann	Christian	postdoc	
Wintner	Ernst	associate professor	
Xu	Lin	dissertation	

Books and Contributions to Books

1. E. Wintner: "Semiconductor Lasers", Handbook of the Eurolaser Academy, Chapman & Hall, London, pp 125 – 146, 1996

Publications in Reviewed Journals

1. I.T. Sorokina, E. Sorokin and E. Wintner, A. Cassanho, H.P. Jenssen, M.A. Noginov: "Efficient cw TEM_{oo} and femtosecond Kerr-lens-modelocked Cr:LiSGaF laser", *Optics Letters* 21, 204 – 206, 1996.
2. I.T. Sorokina, E. Sorokin, and E. Wintner, A.C assanho, H.P. Jenssen, R. Szipöcs: "47fs pulse generation from a prismless self-mode-locked Cr:LiSGaF laser", *Trends in Optics and Photonics Series (Advanced Solid-State Lasers)* Volume 1, OSA, Washington, USA, pp 258 – 260, 1996.
3. I.T. Sorokina, E. Sorokin, E. Wintner, A. Cassanho, H.P. Jenssen, and R.Szipöcs: "Prismless passively modelocked femtosecond Cr: LiSGaF laser", *Optics Letters* 21, 1165 – 1167, 1996.
4. M. Lenzner, Ch. Spielmann, E. Wintner, F. Krausz, A.J. Schmidt: "Sub-20fs, kilohertz-repetition-rate Ti:sapphire amplifier", *Optics Letters* 20, 1397, 1996.

5. Ch. Spielmann, M. Lenzner, F. Krausz, R.S zipöcs: “Compact, high-throughput expansion-compression scheme for chirped pulse amplification in the 10fs range”, *Opt. Commun*. 120, 321, 1996.
6. Ch. Spielmann, L. Xu, F. Krausz: “Comment on the measurement of interferometric autocorrelations”, *Appl. Opt*. (in print).
7. L. Xu, Ch. Spielmann, R.Szipöcs, F. Krausz: “Mirror-dispersion-controlled Ti:sapphire ring oscillator”, *Opt. Lett*. 21, 1259, 1996.
8. L. Xu, Ch. Spielmann, A. Poppe, T. Brabec, F. Krausz, T.W. Hänsch: “Route to phase control of ultrashort light pulses”, *Opt. Lett*. 21, 2008, 1996.
9. W. Kautek, J. Krüger, M. Lenzner, S. Sartania, Ch. Spielmann, F. Krausz: “Laser ablation of dielectrics with pulse durations between 20fs and 3ps”, *Appl.Phys.Lett*. 69, 3146, 1996.
10. M. Nisoli, S. DeSilvestri, O. Svelto, R. Szipöcs, K. Ferencz, Ch. Spielmann, S. Sartania and F. Krausz: “Compression of high-energy laser pulse below 5 fs”, *Opt. Lett*. 22, (in print).
11. Ch. Spielmann, S. Sartania, F. Krausz, R. Szipöcs, K. Ferencz, M. Nisoli, S. DeSilvestri, and O. Svelto: “Intense sub-5s light pulses open the way to controlling atomic processes on the scale of the light oscillation period”, *Laser Focus World*, to be published Mai 1997.

Presentations

1. I.T. Sorokina, E. Sorokin, and E. Wintner, A. Cassanho, H.P. Jenssen, R. Szipöcs: “47 fs pulse generation from a prismless self-mode-locked Cr:LiSGaF laser”, *Advanced Solid-State Laser Conference* (paper WE6), San Francisco, February 1996.
2. E. Wintner, I.T. Sorokina, E. Sorokin, R. Szipöcs: “Prismenloser Cr:LiSGaF (40-) Femtosekunden-Laser”, *DPG-Frühjahrstagung Quantenoptik*, Jena, March 1996.
3. I.T. Sorokina, E. Sorokin, E. Wintner: “LiSGaF — interessantes Material für diodengepumpte cw- und fs-Festkörper-Laser”, *Laserseminar Mauterndorf*, Mauterndorf, Salzburg, March 1996.
4. I.T. Sorokina, E. Sorokin, E. Wintner: “Femtosecond pulses from novel solid-state laser sources”, *International Workshop on Laser Physics LPHYS’96*, Moscow, Russia, July 1996.
5. E. Sorokin, S. MacNamara, I.T. Sorokina and E. Wintner: “Multifocal resonator configurations for Kerr-lens mode-locking”, paper CWM2 *CLEO/Europe 96*, Hamburg, BRD, September 1996.
6. I.T. Sorokina, E. Sorokin, and E. Wintner, A. Cassanho, H.P. Jenssen, R. Szipöcs: “Prismless Kerr-lens mode-locked femtosecond Cr:LiSGaF laser”, invited paper CWA1, *CLEO/Europe 96*, Hamburg BRD, September 1996.
7. E. Wintner: “Semiconductor Lasers”, *Eurolaser Academy*, Vienna October 1996.

8. Ch. Spielmann, L. Xu, R. Szipöcs, F. Krausz: "Sub-10fs Ti:sapphire lasers", *Conference on Lasers and Electro-Optics*, Vol. 9, 1996 *OSA Technical Digest Series* (Optical Society of America, Washington, D.C., 1996), p. 28.
9. L. Xu, Ch. Spielmann, F. Krausz, and R. Szipöcs: "Ultrabroad-band ring oscillator for short pulse generation", in *Ultrafast Phenomena* Vol. 8, 1996 *OSA Technical Digest Series* (Optical Society of America, Washington, D.C., 1996), p. 2.
10. Ch. Spielmann, L. Xu, and F. Krausz: "Toward coherent control on a sub-10-fs time scale", in *Ultrafast Phenomena* Vol. 8, 1996 *OSA Technical Digest Series* (Optical Society of America, Washington, D.C., 1996), p. 315.
11. A. Stingl, Ch. Spielmann, R. Szipöcs, and F. Krausz: "Compact high-repetition-rate femtosecond lasers using chirped mirrors", *Conference on Lasers and Electro-Optics*, Vol. 9, 1996 *OSA Technical Digest Series* (Optical Society of America, Washington, D.C., 1996), p. 66.
12. L. Xu, A. Poppe, Ch. Spielmann, F. Krausz: "Phase control of sub-10fs pulses: is it feasible?", *European Quantum Electronic Conference*, Technical Digest, Paper QThI5.
13. M. Lenzner, S. Sartania, Ch. Spielmann, F. Krausz: "Sub-mJ, sub-20fs pulses from Ti-sapphire without using a pulse strecher", *Conference on Lasers and Electro-Optics Europe*, Technical Digest, Paper JThB3.

Doctor's Theses

1. L. Xu: "Entwicklung und Charakterisierung von sub-10fs Resonatoren", TU Wien, in progress
2. Z. Cheng: "Zerstörungen in Dielektrika mit Femtosekundenimpulsen", TU Wien, in progress
3. S. Sartania: "kHz Kompressionexperimente mit Femtosekundenimpulsen", TU Wien, in progress

Cooperations

1. Forschungsinstitut für Festkörperphysik der ungarischen Akademie der Wissenschaften, Budapest (Dr. R. Szipöcs)
2. Institut für Strahlwerkzeuge der Universität Stuttgart (Dr. A. Giesen)
3. Institut für Laserphysik der Universität Hamburg (Prof. G. Huber)
4. Institut für Allgemeine Physik der russischen Akademie der Wissenschaften, Moskau (Prof. I. Shcherbakov)
5. Physics Department, Alabama A&M University (Dr. M. Noginov)
6. CREOL, University of Central Florida (Prof. B. Chai, Prof. H. Jenssen)
7. Lightning Corp., Tampa, Florida (Dr. A. Cassanho)
8. Donezk Polytechnical Institute, Donezk (Dr. Nikolajew)

9. Lawrence Livermore Laboratory, Livermore, Kalifornien (Dr. W. Krupke, Dr. R. Solarz)
10. Sandia Laboratories, Livermore, Kalifornien (Dr. R. Trebino)

Appendix

The Society's Managing Committee and Address

President:

Univ.-Prof. Dr. Erich GORNIK
TU Wien, Institut für Festkörperelektronik

First Vice-President:

Dipl.-Ing. Gerhard KRAINZ
Wirtschaftskammer Österreich

Second Vice-President:

Univ.-Prof. Dr. Wolfgang FALLMANN
TU Wien, Institut für Allgemeine Elektrotechnik und Elektronik

Board:

Dr. Wolfgang ATTWENGER
ÖFZ Seibersdorf

Univ.-Prof. Dr. Günther BAUER
Universität Linz, Institut für Halbleiterphysik

Univ.-Prof. Dr. Helmut HEINRICH
Universität Linz, Institut für Experimentalphysik

Univ.-Prof. Dr. Hans LEOPOLD
TU Graz, Institut für Elektronik

Univ.-Prof. Dr. Fritz PASCHKE
TU Wien, Institut für Allgemeine Elektrotechnik und Elektronik

Mag. Miron PASSWEG
Bundesarbeitskammer

Dr. Robert SCHAWARZ
TU Wien, Institut für Allgemeine Elektrotechnik und Elektronik

Univ.-Prof. Dr. Arnold SCHMIDT
TU Wien, Institut für Allgemeine Elektrotechnik und Elektronik

Univ.-Prof. Dr. Siegfried SELBERHERR
TU Wien, Institut für Mikroelektronik

Secretary-General:

Univ.-Doz. Dr. Karl RIEDLING
TU Wien, Institut für Allgemeine Elektrotechnik und Elektronik

Administration:

Claudia RITTER

Address:

Gesellschaft für Mikroelektronik
c/o Technische Universität Wien
Institut für Allgemeine Elektrotechnik und Elektronik
Gußhausstraße 27-29/359, A-1040 Wien

Phone: +43-1-588 01-5223

Fax: +43-1-505 2666

Mail: gme@iaee.tuwien.ac.at

WWW: http://www.iaee.tuwien.ac.at/gme/